UNIVERSIDADE FEDERAL DO PARÁ
INSTITUTO DE GEOCIÊNCIAS
PROGRAMA DE PÓS-GRADUAÇÃO EM GEOLOGIA E GEOQUÍMICA

TESE DE DOUTORADO Nº 161

RECONSTITUIÇÃO PALEOAMBIENTAL E POTENCIAL PETROLÍFERO DA SUCESSÃO SILICICLÁSTICA-CARBONÁTICA PERMIANA DA BACIA DO PARANÁ

Tese apresentada por:

AILTON DA SILVA BRITO

Orientador: **Prof. Dr. Afonso César Rodrigues Nogueira (UFPA)**

BELÉM
2022

Dados Internacionais de Catalogação na Publicação (CIP) de acordo com ISBD
Sistema de Bibliotecas da Universidade Federal do Pará
Gerada automaticamente pelo módulo Ficat, mediante os dados fornecidos pelo(a) autor(a)

B862r Brito, Ailton S..
Reconstituição Paleoambiental e Potencial Petrolífero da Sucessão Siliciclástica-Carbonática Permiana da Bacia do Paraná / Ailton S. Brito. — 2022.
xxiii, 238 f. : il. color.

Orientador(a): Prof. Dr. Afonso C. R. Nogueira
Tese (Doutorado) - Universidade Federal do Pará, Instituto de Geociências, Programa de Pós-Graduação em Geologia e Geoquímica, Belém, 2022.

1. Sistema misto siliciclástico-carbonático. 2. rocha geradora. 3. geoquímica orgânica. 4. paleoambiente. 5. mar epicontinental. I. Título.

CDD 558.1

Universidade Federal do Pará
Instituto de Geociências
Programa de Pós-Graduação em Geologia e Geoquímica

RECONSTITUIÇÃO PALEOAMBIENTAL E POTENCIAL PETROLÍFERO DA SUCESSÃO SILICICLÁSTICA-CARBONÁTICA PERMIANA DA BACIA DO PARANÁ

Tese apresentada por

AILTON DA SILVA BRITO

Como requisito parcial à obtenção de Grau de Doutor em Ciências na Área de GEOLOGIA, Linha de Pesquisa Análise de Bacias Sedimentares.

Data de Aprovação: 15 / 02 / 2022

Banca Examinadora:

Prof. Dr. Afonso César Rodrigues Nogueira
(Orientador- UFPA)

Prof.ª Dr.ª Juliana Charão Marques
(Membro-UFRGS)

Prof. Dr. Alexandre de Andrade Ferreira
(Membro-PETROBRAS)

Prof. Dr. Joelson Lima Soares
(Membro-UFPA)

Prof. Dr. José Augusto Martins Corrêa
(Membro-UFPA)

Aos meus pais Valber e Maria Eunice.

AGRADECIMENTOS

À Universidade Federal do Pará (UFPA), ao Programa de Pós-Graduação em Geologia e Geoquímica e ao Conselho Nacional de Desenvolvimento Científico e Tecnológico pela oportunidade, apoio financeiro e concessão de bolsa de doutorado (CNPq - 140630/2019-8) e Coordenação de Aperfeiçoamento de Pessoal de Nível Superior - Brasil (CAPES) - Código de Financiamento 001.

À empresa Irati Petróleo e Energia LTDA e ao Marcelo Albuquerque pelos 163 furos de sondagens e mais de três mil análises geoquímicas cedidos para a realização dessa pesquisa.

À minha família: Valbe, Maria Eunice, Airton, Alessandro e Gildene, pelo incondicional apoio ao longo dos vários anos necessários para chegar até a conclusão desse doutorado.

Ao meu orientador Afonso Nogueira pela oportunidade de realização desse doutorado, pelo apoio, incentivos, paciência e valiosas críticas e sugestões. Sou grato ainda pelos ensinamentos técnico-científicos e conselhos que foram cruciais para minha evolução social e profissional.

Ao Prof. Dr. Sidney Lima da Universidade Federal do Piauí (UFPI) e ao Laboratório de Geoquímica Orgânica (LAGO) por todo suporte (técnico e financeiro) durante minha estadia na UFPI para realização das análises de biomarcadores.

Ao Prof. Dr. Joelson Soares pela atenção, paciência e valiosos ensinamentos ao longo desses 10 anos de academia. Obrigado pela amizade e por sempre está à disposição para dúvidas e discussões acerca da pesquisa.

Ao Prof. Dr. Roberto Vizeu pelos ensinamentos e produtivas discussões que foram fundamentais nesse trabalho.

À Lorena Tuane, doutoranda no Programa de Pós-graduação em Química (PPGQ-UFPI), pelo suporte na realização das análises de biomarcadores e interpretação dos cromatogramas. Agradeço ainda pela amizade e parceria desenvolvida ao longo desses anos.

Especial agradecimentos à Joelma Lobo e Bruno Veras, técnicos do Laboratório de Laminação do Instituto de Geociências da UFPA, não somente pela confecção das lâminas delgadas e polidas, mas principalmente pela amizade, atenção e apoio ao longo da pesquisa, em

especial nos últimos dois anos, que mesmo sob as restrições impostas pela pandemia Covid, se esforçaram para ajudar sempre que possível. As análises petrográficas só saíram no tempo previsto graças a incansável dedicação e comprometimento desses dois, muito obrigado!

Ao Dr. Marcelo Vasquez do Laboratório de Microscopia Eletrônica de Varredura (MEV-CPRM) pela disposição, gentileza e suporte na realização das análises de MEV/EDS. Ao Prof. Dr. Romulo Angélica e ao técnico Aldemir Sotero do Laboratório de Difração de Raios-X (DRX) pela realização das análises de DRX e auxílio nas interpretações.

Ao Dr. Artur Chahud pelo auxílio na identificação do conteúdo fossilífero.

Ao meu companheiro José Neto pela ajuda na elaboração das figuras, tabelas e análises estatísticas dos dados. Sou grato também pelo apoio, incentivo e por acreditar! Muito obrigado, te amo!

Ao Mcs. Renan Santos pela amizade e por todo apoio, sugestões, conselhos e troca de conhecimento durante o desenvolvimento desse trabalho.

Ao Mcs. Pabllo H. Santos, técnico do Museu de Geociências, pelo suporte e pelos longos anos de amizade.

Aos amigos do Grupo de Sedimentologia (GSED) e da pós-graduação: Bruna Nogueira, Renata veras, Luiz Saturnino, Fabio Domingos, Pedro Guilherme, Ivan Romero, Pedro Augusto, Walmir Lima, Alexandre Ribeiro pelo suporte, críticas, sugestões e trocas de conhecimento.

Agradeço a todos que contribuíram direta e indiretamente para o desenvolvimento da tese.

“A verdade pode sempre ser encontrada na simplicidade, e não na multiplicidade e confusão das coisas.”

— Isaac Newton

RESUMO

O Permiano foi marcado por extremas mudanças paleogeográficas e paleoclimáticas com predominância de condições áridas em todo o globo como consequência da queda eustática do final da glaciação carbonífera ao início do Permiano. As fases finais de aglutinação continental do supercontinente Pangeia proporcionaram soerguimentos acompanhados de sucessivas regressões dos mares epicontinentais culminando com a instalação de sistemas desérticos no final do Permiano. Durante a fase regressiva marinha o Pangeia Ocidental foi sítio deposicional de uma sucessão mista siliciclástica-carbonática de 50m de espessura sob condições paleoambientais restritas e rasas, amplamente distribuída na Bacia do Paraná, SE da América do Sul. A sucessão estudada inclui o topo da Formação Palermo, Formação Irati e a base da Formação Serra Alta, compreendendo um total de 120m. A Formação Irati é composta essencialmente por dolomito intercalado a folhelho cinza a negro rico em matéria orgânica, este considerado um importante gerador de hidrocarbonetos. Esta unidade recobre depósitos heterolíticos da Formação Palermo e é sobreposta pelos folhelhos da Formação Serra Alta. O alto teor e a boa qualidade da matéria orgânica presente nos folhelhos Irati despertaram interesse econômico desde o século XIX. Embora muitos trabalhos tenham contribuídos para o conhecimento do paleoambiente deposicional e potencial gerador dessa unidade, principalmente a partir de dados de geoquímica orgânica, ainda permanecem lacunas quanto o entendimento paleoambiental, previamente interpretado como mar restrito ou lacustre. Essa pesquisa foi realizada a partir de 125 testemunhos de sondagens distribuídos nas regiões centro-norte, centro-sul e extremo sul da bacia, cedidos pela empresa Irati Petróleo LTDA. complementados por afloramentos da região norte. Foram selecionados 23 testemunhos de sondagem para estudo sedimentólogico e estratigráfico a partir de análises de fácies/microfácies, auxiliadas por DRX, MEV-EDS e imagens de catodoluminescência. O teor de carbono orgânico total (COT) e análise de pirólise Rock-Eval e biomarcadores foram realizadas em amostras de 102 testemunhos. A integralização dos dados possibilitou: a correlação lateral da Formação Irati por mais de 2.000 km na direção SSW-NNE da bacia; a reconstituição paleoambiental; e caracterização lateral e vertical do potencial gerador. Vinte e uma fácies/microfácies foram identificadas, organizadas em cerca de 300 pares siliciclástico-carbonáticos que se agrupam em 59 ciclos de alta frequência representativos dos ambientes de *mid-outer ramp* e *offshore* dominado por sistemas de turbidez distais. A sucessão é constituída por quatro sequencias de terceira ordem (S1, S2, S3 e S4). Os limites de sequências são do tipo 2, sem evidência de erosão subaérea, marcados pela sobreposição de depósitos transgressivos de *offshore*. Os tratos de sistemas transgressivos são sucedidos por tratos de sistemas de mar alto definidos pela sobreposição dos folhelhos cinzas a negros por níveis de dolomito com tendência de espessamento ascendente, que indicam alta produtividade de carbonato sob condições normais a hipersalinas, evidenciado pela presença de gamacerano, cristais de halita e pseudomorfos de gipso. Os depósitos transgressivos das sequências S3 e S4 (Membro Assistência) formam os dois intervalos (*oil-shale*) com maior potencial gerador da Bacia do Paraná. O *oil-shale* S3 apresenta os maiores valores de carbono orgânico e potencial gerador. Os maiores picos de COT foram 19,40% para a região extremo sul, 22,23% para o centro-norte e 27,12% para o centro-sul da bacia. Quanto ao querogênio predomina tipo I e II, que também apresenta aumento da contribuição, principalmente do tipo I

convergindo para o centro-sul. *Oil-shale* S4 possue valores de COT inferiores para a região extremo sul (8,82%), centro-sul (21,7%) e centro-norte (14,61%). O tipo de querogênio nesse intervalo é semelhante ao *oil-shale* S3, predomina tipo II com alta contribuição do tipo I na região centro-sul e menores proporções do tipo III. A matéria orgânica da Formação Irati é dominantemente imatura, contudo, ocorrências de temperatura máxima de pirólise (Tmáx) igual ou superior a 440 ºC em amostras próximas das soleiras de diabásio mostram que houve maturação localizada de matéria orgânica, o que corrobora a ocorrência de um sistema gerador não-convencional para os depósitos mistos de folhelhos negros (geradores) - carbonatos (reservatórios) da Formação Irati. Em relação a quantidade e qualidade da rocha geradora presente na Formação Irati a porção centro-sul apresenta os maiores valores de carbono orgânico assim como potencial para geração de hidrocarbonetos. A análise dos padrões de empilhamento associada às idades prévias de SHRIMP U-Pb a partir de cinzas vulcânicas possibilitou a correlação da sucessão com a curva global do nível do mar, permitindo estimar uma idade de 8,0 Ma para o Mar Irati e de 2,7 Ma para as sequencias deposicionais de 3°ordem. Da mesma forma foram calculadas idades de 26,6 ka para os pares carbonáticos-siliciclásticos, 135,5 ka e 400 ka para os ciclos de alta frequência, cuja origem é aqui atribuída a ciclicidade climática induzida pela oscilação orbital terrestre, compatíveis com a ciclicidade Milankovitch. A caracterização dos ciclos com base nos dados faciológicos e de geoquímica orgânica também demostram um forte controle climático na geração dos intervalos ricos em matéria orgânica.

Palavras-chave: Sistema misto siliciclástico-carbonático, rocha geradora, geoquímica orgânica, paleoambiente, mar epicontinental

ABSTRACT

The Permian age was marked by extreme paleogeographic and paleoclimatic changes with predominances of arid conditions across the globe as a consequence of the eustatic sea-level fall from the end of the Carboniferous glaciation to the beginning of the Permian. The final phases of continental agglutination of the Pangea supercontinent caused uplifts accompanied by successive regressions of the epicontinental seas, culminating with the installation of desert systems at the end of the Permian. During the marine regressive phase, Western Pangea was the depositional site of a 50m thick mixed siliciclastic-carbonatic succession under restricted and shallow paleoenvironmental conditions, widely distributed in the Paraná Basin, SE of South America. The studied succession includes the top of the Palermo, Irati, and the base of the Serra Alta Formation, comprising a total of 120 m-thick. The Irati succession is essentially composed of dolomite intercalated with organic matter gray to black shale rich, which is considered an important source rock for hydrocarbons. This unit covers the heterolithic deposits from the Palermo Formation and is overlaid by shales from the Serra Alta Formation. The high content and good quality of organic matter present in Irati shales aroused economic interest since the 19th century. Although many works have contributed to the knowledge of the depositional paleoenvironment and generating potential of this unit, mainly from organic geochemical data, gaps remain regarding the paleoenvironmental understanding, previously interpreted as restricted sea or lacustrine. This research was carried out from 125 drill cores distributed in the center-north, center-south, and extreme south of the basin, provided by the company Irati Petróleo LTDA. complemented by outcrops from the northern region. Twenty-three drill cores were selected for sedimentological and stratigraphic study from facies/microfacies analyses, aided by XRD, SEM-EDS, and cathodoluminescence images. Total organic carbon (TOC), Rock-Eval pyrolysis, and biomarker analysis were performed on 102 cores. The integration of data allowed: the lateral correlation of the Irati Formation for more than 2,000 km in the SSW-NNE direction of the basin; the paleoenvironmental reconstitution; and lateral and vertical characterization of the generating potential. Twenty-one facies/microfacies were identified and organized into about 300 siliciclastic-carbonate couplet that are grouped into 59 high-frequency cycles representative of mid-outer ramp and offshore environments dominated by distal turbidity systems. The succession consists of four third-order sequences (S1, S2, S3, and S4). Sequence boundaries are type 2, with no evidence of subaerial erosion, marked by overlapping transgressive offshore deposits. Transgressive Systems Tracts are succeeded by Highstand Systems Tracts defined by the appearance of dolomite levels with a thickening upwards tendency, which indicates high carbonate productivity under normal to hypersaline conditions, evidenced by the presence of gammaceran, halite crystals. and pseudomorphs of gypsum. The transgressive deposits of sequences S3 and S4 (Assistance Member) form the two intervals (oil-shale) with the greatest generating potential in the Paraná Basin. Oil-shale S3 has the highest values of organic carbon and generating potential. The highest TOC peaks were 19.40% for the extreme south region, 22.23% for the center north, and 27.12% for the center-south of the basin. Kerogen predominates types I and II, which also presents an increased contribution, mainly from type I converging to the center-south. Oil-shale S4 presents lower TOC values for the extreme south region (8.82%), south-central (21.7%), and north-central (14.61%). The kerogen

type is similar to oil-shale S3, it predominates type II, with a high contribution of type I in the south-central region and smaller proportions of type III. The organic matter of the Irati Formation is predominantly immature, however, occurrences of maximum pyrolysis temperature (Tmax) equal to or greater than 440 ºC in samples close to diabase sills show that there was localized maturation of organic matter, which corroborates the occurrence of a non-conventional petroleum system for mixed deposits of black shales (generators) - carbonates (reservoirs) of the Irati Formation. Regarding the quantity and quality of the source rock present in the Irati Formation, the center-south portion presents the highest values of organic carbon as well as the potential for hydrocarbon generation. The analysis of the stacking patterns associated with the previous ages of SHRIMP U-Pb from volcanic ash allowed the correlation of the succession with the global sea-level curve, allowing to estimate an age of 8.0 Ma for the Irati Sea and of 2 .7 Ma for 3rd order depositional sequences. Likewise, ages of 26.6 ka were calculated for the carbonate-siliciclastic couplets, 135.5 ka and 400 ka for the high-frequency cycles, whose origin is here attributed to the climatic cyclicity induced by the terrestrial orbital oscillation, compatible with the Milankovitch cyclicity. The characterization of the cycles based on faciological and organic geochemical data also demonstrates a strong climate control in the generation of intervals rich in organic matter.

Keywords: mixed carbonate-siliciclastic system, source rocks, organic geochemistry, paleoenvironment, epicontinental sea

LISTA DE ILUSTRAÇÕES

CAPÍTULO VII

CAPÍTULO VIII

LISTA DE TABELAS

CAPÍTULO V

CAPÍTULO VI

CAPÍTULO VIII

CAPÍTULO IX

CAPÍTULO X

SUMÁRIO

CAPÍTULO I

1. INTRODUÇÃO

1.1. APRESENTAÇÃO

O Permiano é marcado por profundas mudanças paleogeográficas e paleoclimáticas influenciadas pelos pulsos terminais da glaciação carbonífera-permiana e pelas orogenias produzidas durante a aglutinação do supercontinente Pangeia. O Carbonífero-Permiano teve a mais longa idade do gelo do Fanerozóico a qual produziu variados avanços e recuos das geleiras no Gondwana em resposta aos *feedbacks* orbitais-climáticos de Milankovitch, especialmente quando modulados por ciclos de curta (100 ka) e longa (400 ka) excentricidade (Ogg *et al.*, 2016). Somada a esses acontecimentos tem-se as fases finais de colisão das massas continentais que levaram a formação do supercontinente Pangeia no Permiano. A convergência continental e formação de vastas cadeias de montanhas ao longo do supercontinente intensificou as condições áridas que perduraram ao longo do Permiano em todo o globo, culminando com a instalação de sistemas desérticos no final do período (Golonka & Ford 2000, Stanley 2009, Wicander & Monroe 2010). A sedimentação passou a ser fortemente influenciadas por regime de sazonalidade climática (Kutzbach & Gallimore 1989, Parrish 1993).

Os depósitos da sequência Gondwana I da Bacia do Paraná registram os últimos eventos da maior glaciação Paleozoica assim como o processo de continentalização da bacia devido a aglutinação das massas continentais e isolamento desta no continente. A desertificação é marcada pelas últimas incursões marinhas e subsequente dominância dos depósitos continentais eólicos. Durante a fase regressiva da sequência Gondwana I, no Cisuraliano, a limitada conexão com o oceano Panthalassa propiciou a instalação de um mar restrito e anóxico com predominância de condições rasas responsável pela implantação dos depósitos mistos siliciclásticos-carbonáticos amplamente distribuídos na Bacia Chaco-Paraná (América do Sul), e Bacia Caroo (África do Sul) denominado Mar Irati-Whitehill. Na Bacia do Paraná, Brasil, os depósitos demostram uma alta sensibilidade as oscilações orbitais-climáticas registradas pela ritmicidade de sua sedimentação mista. Nesta bacia os depósitos mistos siliciclásticos-carbonáticos estão concentrados na Formação Irati, com os últimos registros das camadas carbonáticas na base da Formação Serra Alta sobrepostos por espesso pacote pelítico desta unidade. São sotopostos pelos depósitos heterolíticos da Formação Palermo que registra a superfície transgressiva máxima da sequência Gondwana I.

As condições atípicas do mar Irati-Whitehill propiciaram a formação de folhelhos negros ricos em matéria orgânica intercalados as camadas carbonáticas e até mesmo formando intervalos de *oil-shale*. A grande relevância dessa unidade estimulou a execução de vários trabalhos de pesquisa tanto por setores privados como acadêmicos, principalmente focados nos dois intervalos de alto potencial gerador (Gilbert *et al.* 1975, Neto *et al.* 1978, Corrêa da Silva & Conford 1985, Afonso *et al.* 1991, 1994, Santos *et al.* 2009, Franco *et al.* 2010, Alferes *et al.* 2011, Ramos *et al*. 2015, Goldberg e Humayun 2016, Ribas *et al.* 2017, Reis *et al.* 2018). Apesar de muitos trabalhos terem contribuídos para o conhecimento do paleoambiente deposicional dos depósitos mistos ainda permanecem lacunas quanto ao seu entendimento. A alta contribuição de querogênio tipo I, variação de salinidade, presença de algas *Bothryococcus* ao longo da secção, ocorrência de fácies rítmicas ditas típicas de lagos e parâmetros moleculares levou muitos autores a atribuíram esses depósitos a ambiente lacustre (Amaral, 1971, Correa da Silva & Cornford 1985, Afonso *et al.* 1994). Atualmente há uma convergência na interpretação dessa unidade como formada em uma plataforma marinha rasa com base em conteúdo fossilífero e principalmente marcadores moleculares típicos desse ambiente (Oelofsen & Araújo 1983, Xavier *et al.* 2018, Cristiano *et al.* 2019, Martins *et al.* 2020). As poucas evidências paleontológicas na Formações Whitehill também promoveram divergências quando a interpretação do paleoambiente, especialmente no que tange as condições marinhas. Da mesma forma, o estudo do conteúdo palinológico em trabalhos acadêmicos na Formação Irati mostrou-se complexo devido ao baixo grau de preservação e diversidade palinológica (Lages 2014). Grãos de pólen, esporos, algas, principalmente *Bothryococcus* e acritarcas (Correa da Silva & Cornford 1985, Daemon *et al.* 1996, Araújo 2001).

O presente trabalho apresenta um estudo faciológico, estratigráfico e geoquímico da sucessão mista focado em 125 testemunhos de sondagens, apoiados por afloramentos que permitiu identificar os padrões cíclicos de empilhamentos e discutir os controles deposicionais. O refinamento do entendimento das condições deposicionais também permitiu compreender melhor a dualidade na sedimentação e influência marinha/continental na geração dos intervalos ricos em matéria orgânica. Da mesma forma, efetuar sua correlação com os eventos globais e calcular as idades dos padrões cíclicos e da vigência do Mar Irati. Assim como as variações laterais e verticais do potencial gerador dos folhelhos negros da Formação Irati ao longo da bacia.

1.2. ORGANIZAÇÃO DA TESE

A tese está organizada em onze capítulos com os resultados apresentados na forma de artigos científicos, submetidos em revistas internacionais e capítulos de livros de circulação nacional. O capítulo I apresenta a proposta dessa pesquisa com suas respectivas justificativas, objetivos e área de estudo. No capítulo II é feito a contextualização da geologia da Bacia do Paraná com ênfase na sequência Gondwana I. O capítulo III apresenta o contexto do sistema petrolífero não-convencional no qual os folhelhos geradores permianos estão inseridos. No capítulo IV são descritos os materiais e a metodologia utilizada nessa pesquisa. O capítulo V é composto pelo artigo intitulado "*Permian organic-rich shale within a mixed carbonate-siliciclastic system from an epicontinental sea in the West Gondwana, Paraná Basin, Southern Brazil: Paleoenvironmental and geochemical reconstruction"*. O artigo apresenta as discussões sobre os fatores controladores da sedimentação e paleoambiente deposicional. O capítulo VI apresenta o artigo científico intitulado "*High-Frequency cyclicity and organic matter distribution in Shallow Mixed Carbonate-Siliciclastic Ramp: a case of Irati Formation, Paraná Basin, Brazil"*, cujos objetivos principais foram caracterizar os padrões de empilhamentos deposicionais, discutir a relação da ciclicidade e a alta produção orgânica em um sistema misto e posicionar a sucessão em relação a curva global do nível do mar. O capítulo VII é composto pelo artigo científico denominado "*Biomarker Profile of Organic-Rich Shale from the Permian Irati Formation, Paraná Basin: Statistical and Paleoenvironment Implications of High Organic Matter Production within a Shallow and Cyclic Carbonate-Shale Sequence*". Este artigo é focado no detalhamento dos fósseis moleculares presentes nos folhelhos e margas da sucessão rítmica siliciclástica-carbonática presente na borda norte.

Os capítulos VIII, IX e X compõem capítulos de livros publicados na edição especial da editora Atena intitulada "Fósseis Moleculares e Aplicações em Geoquímica Orgânica". O capítulo VIII é denominado "Distribuição espacial dos intervalos *oil shale* permianos da bacia do paraná", o capítulo IX "Análise de biomarcadores neutros em sedimento da formação serra alta permiano (bacia do paraná)" e o capítulo x "preservação de geopolímeros no registro estratigráfico e suas implicações paleoambientais".

Os artigos apresentados nos capítulos V e VI e capítulos de livros em VIII e X tem o autor desta tese como primeiro autor. O Artigo em VII e o capítulo de livro IX têm o autor da tese como segundo autor. As considerações finais desta tese são apresentadas no capítulo XI. Os apêndices seguem após as referências ao final da tese. O Apêndice A e B compreendem materiais suplementares dos artigos que compõem o corpo desta tese.

1.3. JUSTIFICATIVA

O Potencial econômico dos folhelhos Irati vem sendo abordado desde os primeiros trabalhos sobre essa formação. Pádula (1968), Amaral (1971) e Mezzalira (1971) mostram que F. P. Oliveira (1889) já havia descrito os "schistos betuminosos" e Auguste Collen (1897) apresentou o primeiro estudo sobre os hidrocarbonetos da formação no estado de São Paulo, já I. C. White (1908) estudou a composição química da fração betuminosa ainda no início do século XX. O alto potencial dessa formação associado a necessidade energética no final do século passado levou a Petrobras implantar a primeira unidade para exploração do *Oil Shale* da Formação Irati em 1972 no Município de São Mateus do Sul (PR). Os folhelhos betuminosos representam um importante depósito de *Oil and Gas shale* amplamente distribuídos na porção sul do Brasil.

Contudo, os estudos sobre esses depósitos focados apenas nos intervalos geradores, principalmente a partir da geoquímica orgânica, dificultam uma compreensão ampla dos processos e controles deposicionais responsáveis pela geração de uma sucessão mista siliciclástica-carbonática rica em hidrocarbonetos. Da mesma Forma, o estudo limitado a amostragem em apenas um ou dois furos de sondagens limita a compreensão das variações espaciais do potencial gerador dos folhelhos. Como já foi colocado por alguns autores, esses folhelhos mostram variações nos parâmetros de controle deposicional, que se tornam mais evidentes quando se compara as sucessões correlatas nas porções norte e sul da bacia.

Atualmente há um consenso quanto a hierarquia litoestratigráfica, ampla continuidade, distribuição geográfica e a calmaria tectônica reinante durante a deposição da sucessão mista siliciclástica-carbonática que contém os folhelhos betuminosos. O mesmo não ocorre em relação ao ambiente deposicional. É unanime a interpretação das condições anóxicas necessária a geração dos folhelhos negros a betuminosos, apesar de seu mecanismo ainda não está totalmente compreendido. Apesar da vasta gama de trabalhos sobre a os folhelhos geradores, permanece dúvidas quando as condições climáticas, fatores controladores da deposição, ambiente deposicional e vigência do mar Irati. Ainda carecem estudos estratigráficos e sedimentológicos de detalhe, que permitam uma compreensão precisa dos processos controladores da sedimentação e geração dos intervalos ricos em matéria orgânica em um ambiente de sedimentação mista e considerado muito raso.

1.4. OBJETIVOS

O objetivo geral dessa tese de doutorado compreende na caracterização detalhada dos depósitos mistos siliciclásticos-carbonáticos para elucidar os fatores controladores da sedimentação e sua relação com os eventos globais do Permiano Inferior. Como etapas necessárias para o objetivo geral assim com complementares, foram cumpridos os seguintes objetivos específicos:

i) Definição de microfácies carbonáticas e siliciclásticas da sucessão mista e dos processos autóctones e alóctones responsáveis pela sedimentação;

ii) Identificação dos padrões de empilhamentos deposicionais para definir sua origem, duração, assim como duração do mar Irati;

iii) Caracterização da matéria orgânica e do potencial gerador, suas variações laterais e verticais nas porções sul, central e norte da Bacia do Paraná.

iv) Reconstrução paleoambiental da sucessão a partir de dados sedimentológicos, estratigráficos e geoquímicos mineral e orgânicos;

A integralização dos dados de geoquímica orgânica, sedimentológicos e estratigráficos com os já disponíveis na literatura, possibilitará a compreensão efetiva das variações organofaciológicas e do potencial petrolífero desses depósitos. A compreensão detalhada desses depósitos, suas variações laterais e verticais auxilia na identificação das áreas mais propícias a exploração comercial, assim como possibilitará uma compreensão ampla dos eventos paleoclimáticos e paleogeográficos do Permiano Inferior na Bacia do Paraná.

1.5. LOCALIZAÇÃO DA ÁREA DE ESTUDO

A sucessão estudada (figura 01) abrange furos de sondagem e seções aflorantes distribuídos nos estados de Santa Cataria (nos municípios de Papanduva e Três Barras), Paraná (município de São Mateus do Sul), Rio grande do Sul (município de Dom Pedrito e São Gabriel), Goiás (Pedreira Sucal, município de Perolândia) e São Paulo (Pedreira Partecal, município de Rio Claro). Para o estudo geoquímico foram coletado material em 125 poços, perfurados pela **IRATI PETROLEO E ENERGIA LTDA,** nos estados do Paraná, Santa Catarina e Rio Grande do Sul. Os furos foram realizados ao longo da faixa de afloramento das rochas da sequência Gondwana I onde as rochas da Formação Irati estão aflorando ou próxima a superfície.

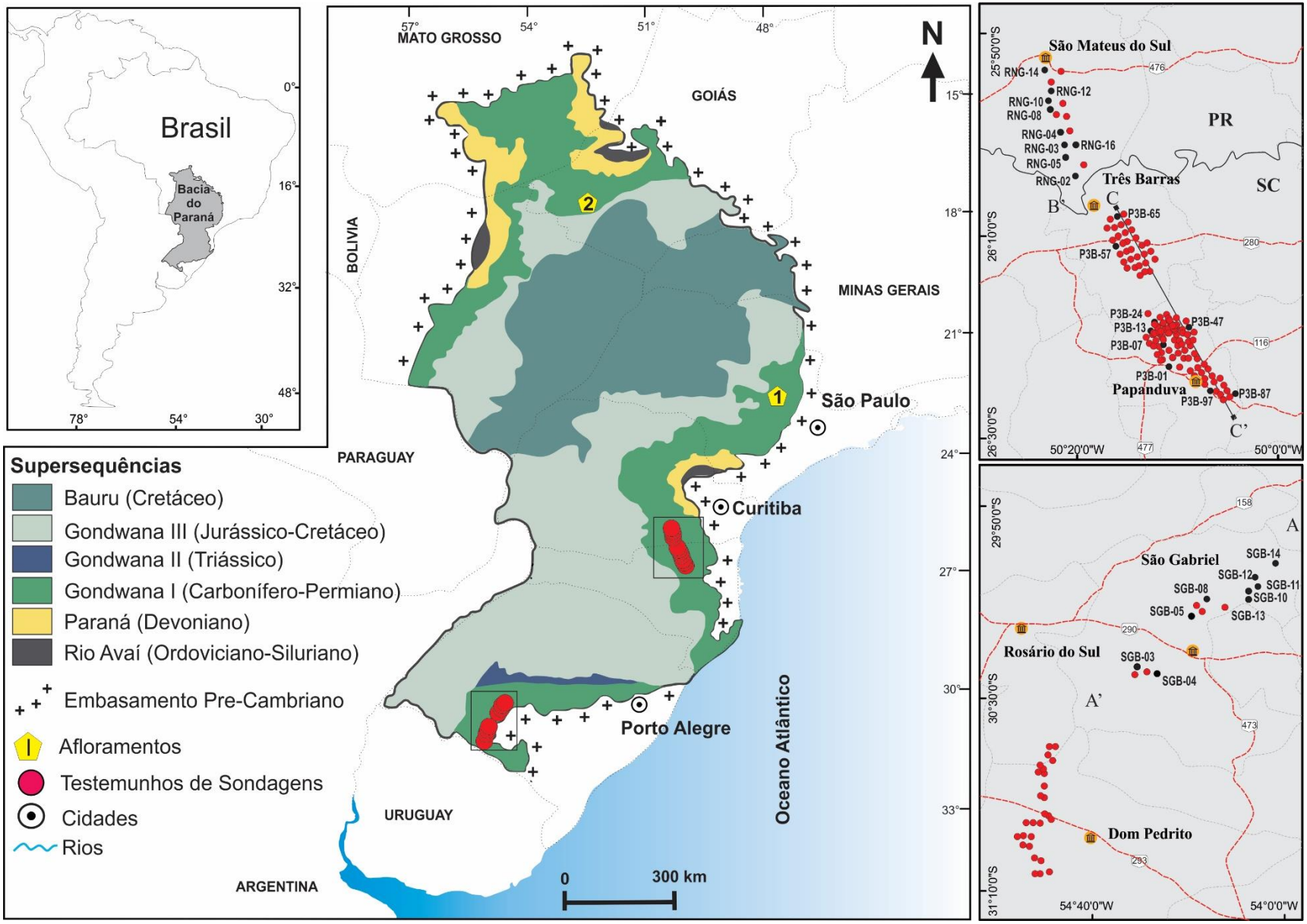

Figura 1.1. Mapa geológico simplificado da Bacia do Paraná e localização malhas de testemunhos de sondagens dos afloramentos e utilizadas nesse trabalho. Os 125 furos de sondagens cedidos pela empresa Irati Petróleo e Energia LTDA. estão distribuídos pelos estados do Rio Grande do Sul, Paraná e Santa Catarina

CAPÍTULO II

2. CONTEXTO GEOLÓGICO DA BACIA DO PARANÁ

A Bacia sedimentar intracratônica do Paraná possui forma ovalada com o eixo maior NNE-SSW e 1.750 km de extensão e o eixo menor com 900 km que acumulou sedimentos do Ordoviciano ao Cretáceo (Quintas *et al.* 1999, Milani *et al.* 1998, 2007). Encontra-se a sudeste no continente Sul-Americano em uma extensão territorial de aproximadamente 1.000.000 km^2 que abrange os estados do Rio Grande do Sul, Santa Cataria, Paraná, São Paulo, Mato Grosso, Mato Grosso do Sul e Goiás (figura 01). O preenchimento sedimentar se estende do sul e sudeste do Brasil para o nordeste da Argentina, leste do Paraguai e norte do Uruguai e perfaz uma área de cerca de 1.700.000 km^2 (Holz *et al.* 2010) integralizando a Bacia sedimentar do Chaco-Paraná (Milani *et al.* 1998). A Bacia do Paraná é limitada a oeste pelo Arco de Assunção, uma extensa flexura no embasamento, com direção N-S, que corta a porção leste do estado do Mato Grosso do Sul, no Brasil, atravessa o Paraguai e continua em subsuperfície pela Argentina até a região do Rio da Prata. O limite a Nordeste é estabelecido pela flexura de Goiânia, com direção NW-SE (Quintas *et al.* 1999).

A Bacia do Paraná jaz sobre rochas cristalinas de diferentes domínios geotectônicos pertencentes aos terrenos cratônicos Arqueanos, Paleoproterozoicos e cintões móveis Neoproterozoicos formados durante as orogenias Pan-Africana e Brasiliana relacionadas a formação do Gondwana Oeste (Holtz *et al.* 2010). É uma típica bacia intracratônica, cuja formação teve início no Siluriano e se desenvolveu no inteiro cratônico do Gondwana como resultado da flexura litosférica por sobrecarga associada a cinturões colisionais gerados pela convergência entre o Gondwana e a litosfera oceânica do Panthalassa ao longo do Fanerozoico (Milani *et al.* 1998). Milani *et al.* (2007b) coloca que a bacia nem sempre foi isolada no interior do continente, mas se originou como um golfo aberto para o Panthalassa, fechando sua margem sudeste ao longo do Fanerozoico com a convergência do paleocontinente e o assoalho oceânico. A bacia apresenta uma evolução estrutural complexa, classificada por Figueiredo & Gabaglia (1986) como uma bacia multicíclica iniciada por uma fase de fratura interior e seguida por várias fases de sinéclise interior. Devido a predominância desta última fase na bacia, Almeida (1980) a definiu como um sinéclise complexa desenvolvida ao longo do Paleozoico, que passa a anfíclise no Jurássico Superior devido intumescências provocadas por anomalias térmicas vulcânicas desse período.

O Período Permiano é marcado por ciclos de orogênese e subsidência crustal relacionados provavelmente a subsidência flexural cratônica devido a orogenia paleozoica na porção sul do Gondwana (Milani & Ramos 1998). Os depósitos permianos das bacias intracratônicas brasileiras registram as últimas incursões marinhas, características do Paleozoico, e a transição das condições de *icehouse* - residual da glaciação carbonífera - para *hothouse*, chegando a condições de superaquecimento (*extreme hothouse*) relacionada a maior extinção em massa do Fanerozoico, marcando o fim do Permiano (Hofmann 2016, Kiehl & Shields 2005, Meyer *et al.* 2008, Stanley 2009). No Eocretáceo se instalou na bacia uma densa atividade vulcânica que levou a formação de espessos derrames magmáticos de até 1.700 m de espessura, sills e diques que formam uma rede de intrusões ígneas formalizados na Formação Serra Geral (Araújo 2000). Esse mesmo autor mostra que o intenso magmatismo afetou a evolução térmica do Pacote sedimentar da bacia, por conseguinte, a geração de hidrocarboneto pelas rochas geradoras da Formação Irati, o que resultou na formação de um sistema petrolífero atípico. Santos *et al.* (2009) e Nomura *et al.* (2014) mostram que a influência térmica do evento magmático Serra Geral proporcionou a geração de óleo e gás nas bordas leste e sul da bacia no Cretáceo, mais precisamente entre 127 e 137 Ma, conforme Turner *et al.* (1994).

2.1. REGISTRO ESTRATIGRÁFICO

O registro estratigráfico da Bacia é representado por um pacote sedimentar com intercalação de rochas magmáticas de aproximadamente 7.000 metros (Milani *et al*. 2007), dividido em seis unidades aloestratigráficas de 2º Ordem ou supersequências (Figura 02), delimitadas por descontinuidades regionais descritas inicialmente por Milani (1997): Rio Ivaí (Ordoviciano-Siluriano), Paraná (Devoniano), Gondwana I (Pennsylvaniano-Eotriássico), Gondwana II (Meso a Neotriássico), Gondwana III (Neojurássico-Eocretáceo) e Bauru (Neocretáceo). As sucessões sedimentares das três primeiras supersequências registram ciclos transgressivo-regressivos completos, causados pela oscilação do nível relativo do Oceano Panthalassa que promoveu invasões do interior do Gondwana até o Eotriássico, enquanto as três últimas registram o processo de continentalização da bacia com intrusões de rochas ígneas relacionadas a abertura do Oceano Atlântico Sul (Milani *et al.* 1998).

A sedimentação na Bacia do Paraná iniciou no Meso-Ordoviciano com os conglomerados basais quartzosos com matriz arenosa feldspática, assentados diretamente sobre o embasamento cristalino pré-cambriano (Milani & Ramos 1998, Assine *et al.*1994). Sobre estes ocorrem arenitos conglomeráticos feldspáticos com estratificação cruzada e padrão

granodecrescente ascendente, predominando no topo arenitos finos a médios, totalizando um pacote da ordem de 300m, definidos como Formação Alto Garças (Milani *et al*. 1995, 1998, 2007). Esse pacote sedimentar é encerrado por diastemas, formados pela variação do nível de base durante o advento da glaciação Neo-Ordoviciana, que geraram um contato abrupto com os diamictitos sobrepostos da Formação Iapó que ocorrem em quase toda a bacia e registram a glaciação Neo-Ordoviciana do Gondwana. (Assine *et al.*1994, Milani *et al.* 1995, 2007). Os diamictidos foram sobrepostos pelos folhelhos fossilíferos transgressivo e arenitos finos, bem selecionados com estratificação cruzada, intercalados por siltitos com moldes de conchas depositados durante um evento regressivos que finalizam o primeiro ciclo transgressivo-regressivo da bacia denominado de **supersequência Rio Ivaí.** Essa unidade apresenta espessura variada, podendo chegar a 362 m no Brasil (Assine *et al.*1994), com tendência de espessamento para oeste em direção ao Paraguai onde são estimadas espessuras de até 1.000 m (Wiens 1990). Seu topo é encerrado pela discordância neosiluriana que possui abrangência regional (Milani *et al.* 2007).

A sedimentação na bacia é retomada no início do Devoniano pelos arenitos grossos, feldspáticos, por vezes conglomeráticos fluviais-costeiros da Formação Furnas (Milani *et al.* 2007). Esses arenitos foram depositados em sistema deltaico construídos por rios entrelaçados sob condições transgressivas com *onlap* costeiro de oeste para leste (Assine *et al.*1994). A rápida transgressão levou a deposição dos folhelhos marinhos da Formação Ponta Grossa de forma concordante sobre arenitos da Formação Furnas sem que ocorra interdigitações significativas (Assine *et al.*1994). A Formação Ponta Grossa é formada, da base para o topo, pelos membros Jaguariaíva, Tibagi e São Domingos. O Membro Jaguariaíva é constituído por folhelhos cinzas que ocorrem intercalados com arenitos finos retrabalhados por ondas em plataforma marinha rasa, representam o afogamento do sistema deltaico da Formação Furnas no Emsiano (Assine *et al.*1994). O Membro Tibaji, composto por arenitos e siltitos, reflete um momento regressivo com progradação de sistemas deltaicos (Milani *et al.* 2007). A sucessão deposicional é continuada por folhelhos cinza-escuros denominada de Membro São Domingos, interrompida no Eifeliano pelo avanço de um sistema deltaico, que produziu um padrão progradacional. A regressão instalada proporcionou a formação de duas Superfícies de Inundação Máxima (Emsiano e Givetiano) durante a transgressão devoniana (Assine *et al.*1994). A **supersequência Paraná** apresenta espessura máxima na ordem de 900 m (Milani *et al.* 1998). No final do Devoniano, eventos tectônicos deformacionais causam movimentações com reativação de estruturas rúpteis do embasamento, com consequente soerguimento de blocos e acentuada erosão dos sedimentos da Formação Ponta Grossa, finalizando a Sequência

Devoniana (Assine *et al.*1994). A Bacia do Paraná permaneceu como um golfo desde sua formação no Neo-Ordoviciano até o final da sequência Paraná no final do Devoniano com efetiva conexão com as áreas deposicionais da Bacia do Chaco-Paraná, com as quais compartilhou as incursões marinhas paleozoicas (Milani 2004).

No final do Devoniano houve o desenvolvimento de calotas de gelo nas proximidades e sobre a Bacia (Caputo & Crowell 1985, Caputo *et al.* 2008), promovendo o rebaixamento do nível do mar conforme o avanço das geleiras. A presença de geleiras foi fator inibidor a uma efetiva organização de sistemas deposicionais e à acumulação sedimentar expressiva (Milani *et al.* 2007). Durante o Mississipiano a região sudeste do Gondwana, que ainda estava próximo ao polo sul, encontrava-se a elevadas latitudes (Caputo & Crowell 1985). Somado as altas elevação da bacia, comumente atribuída a orogenia Herciniana (Zalán, 1991; López-Gamundí e Rossello 1993) promoveu profundas modificações tectônicas e climáticas que levaram a interrupção na deposição de sedimentos e formação de uma discordância regional que gerou um gap estratigráfico no Mississipiano de 70 Ma (Milani *et al.* 2007).

O início da deposição da **Sequência Gondwana I** registra o fim do degelo da calota polar, com a Formação Aquidauana ao norte e Grupo Itararé ao sul, relacionado a Glaciação Misssissipiana (Caputo & Crowell 1985). A Sequência Gondwana I é o registro do ciclo transgressivo-regressivo, que perdurou do Carbonífero Superior ao Eotriássico (Milani 1997). A sequência engloba o maior volume sedimentar da Bacia do Paraná, com uma espessura total na ordem de 2.500 m (Milani *et al.* 2007). A implantação desse espesso pacote sedimentar sucedeu a maior expansão e subsidência da sinéclise paleozoica com consideráveis alterações tectônicas e climáticas (Almeida 1980).

Superposta a Formação Aquidauana e Grupo Itararé, sob condições transgressivas pós-glacial, ocorre a deposição da Formação Palermo (Schneider *et al*. 1974). Esta Formação registra a Superfície Transgressiva Máxima (Milani *et al.* 1998). A regressão que se sucede é registrada pelas formações Irati, Serra Alta e Teresina (Milani 1997, Schneider *et al.* 1974).

A Supersequência Gondwana I registra o fim das incursões marinhas e o início da continentalização da Bacia, quando passa a predominar clima árido (Milani *et al.* 1998). Sob condições restritas e mar raso epicontinental ocorreu a deposição dos folhelhos, folhelhos betuminosos, margas e carbonatos da Formação Irati (Milani *et al.* 1998). Após a instalação de condições regressivas ocorreu a deposição dos folhelhos da Formação Corumbataí, ao norte, e da Formação Serra Alta, ao sul, superpostos pelos pelitos da Formação Terezinha, depositados sob ação de ondas e maré (Milani *et al*. 1998, 2007). A deposição dos arenitos, siltitos e folhelhos e da Formação Rio do Rastro finalizam a supersequência e registram o início das

condições áridas, no final do Permiano (Soares *et al.* 2014). Milani (2004) coloca que o arco magmático *Choiyoi*, implementado junto à calha de antepaís, foi importante elemento de restrição à comunicação do interior continental com o Panthalassa.

Quintas *et al.* (1999), a partir de dados geofísicos, identificaram três eventos distensivos principais para a Bacia do Paraná. O primeiro (há 440 Ma) responsável, provavelmente, pela deposição das sequências siluriana e devoniana, o segundo (há 296 Ma) relacionado a deposição das seqüências permo-carbonífera, triássica e eventualmente jurássica; o terceiro evento (144 Ma) associado à formação Serra Geral. Conforme Quintas *et al.* (1999) as maiores taxas de subsidência tectônica ocorreram no segundo evento no Permiano, relacionados as formações Palermo, Irati e Teresina e Rio do Rastro.

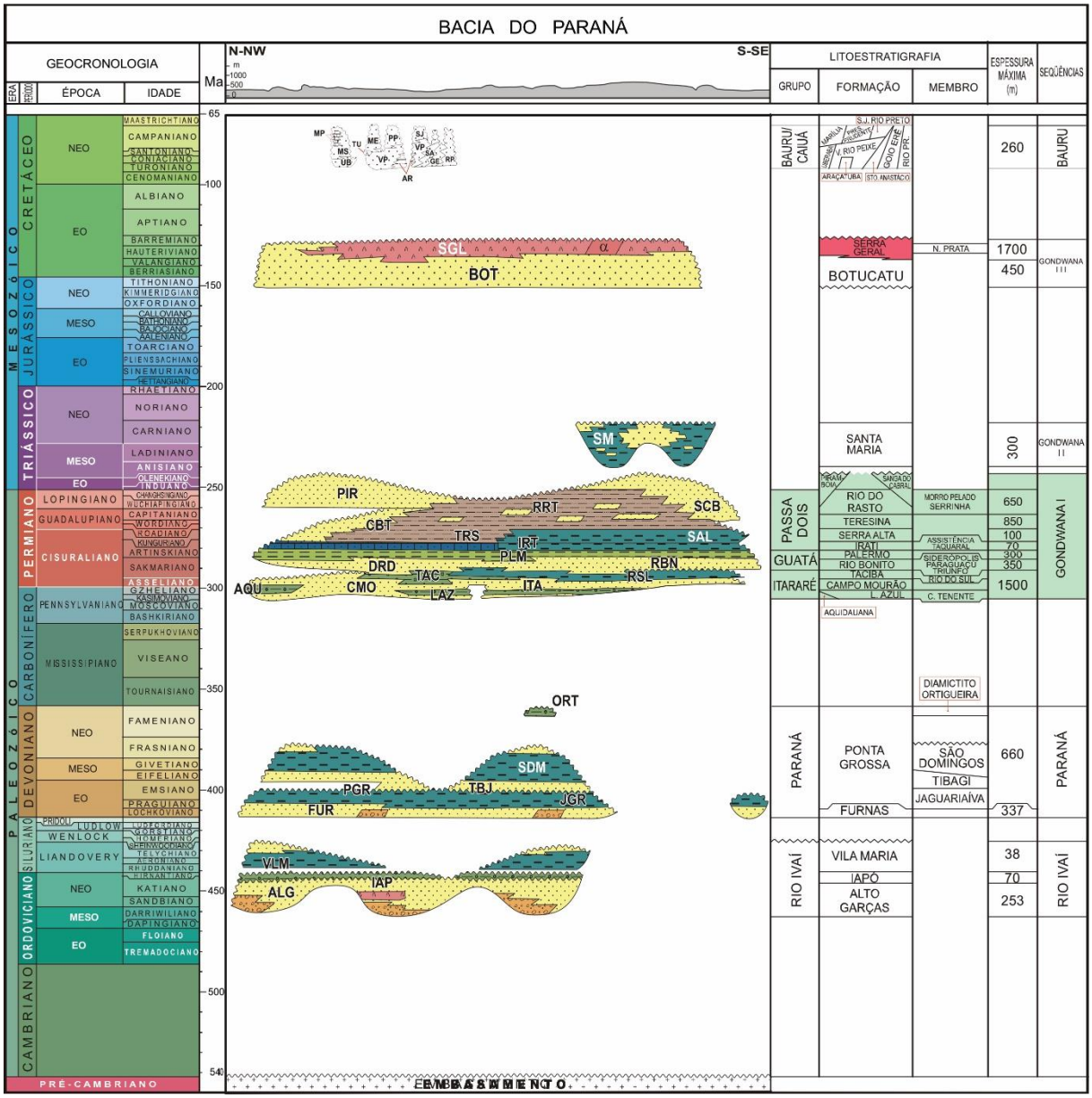

Figura 2.1. Carta estratigráfica da Bacia do Paraná com a relação cronoestratigráfica das seis sequências deposicionais e destaque para a Sequência Gondwana I, onde encontram-se as unidades que compõem a sucessão estudada neste trabalho (Formação Palermo, Irati e Serra Alta). Modificada de Milani *et al*. (2007).

2.2. SUCESSÃO MISTA SILICICLÁSTICA-CARBONÁTICA

A sucessão estudada inclui o topo da Formação Palermo, Formação Irati e a base da Formação Serra Alta, compreendendo um total de 120m. A Formação Palermo compõe uma sequência de terceira ordem onde o Trato de Sistema Transgressivo (TST), abaixo da superfície transgressiva máxima (STM) da sequência Gondwana I, é dominado por arenitos quartzosos finos a grossos com estratificação cruzadas com traços fósseis verticais, arenitos siltosos

altamente bioturbados e intercalação de pelitos e arenitos, gerando padrões de acamamento tipo *wavy* e lenticular, altamente bioturbados com fragmentos de carvão e marcas de raízes, folhelhos cinzas a negros e arenitos com estratificação cruzadas hummocky. O intervalo é encerrado por superfície de ravinamento por onda caracterizada por conglomerado arenoso ou ichnofácies *glossifungites* (Milani 1997, Netto 1994, Tognoli & Neto 2003). Esses autores descrevem o Trato de Sistema de Mar Alto (TSMA) como formado por acamamento tipo *wavy* e lenticular bioturbados em padrão agradacional.

A Formação Irati é bem conhecida devido seu alto potencial para *Oil Shale* e *Gas Shale* e pela ocorrência de fósseis bem preservados de *Mesosaurus brasiliensis*. A definição do nome Irati, que na língua tupi significa rio de mel, provém da cidade paranaense homônima, onde afloram os folhelhos betuminosos (Amaral 1971). Esta unidade foi designada por I. C. White em 1908 ao estudar as rochas gondwânicas em Santa Catarina (Amaral 1971). Santos *et al.* (2006) dataram a Formação Irati a partir de zircão SHRIMP presente em turfas de bentonitas, em 278.4±2.2 Ma, Kunguriano. A unidade apresenta espessura média de 40 m, podendo chegar a 70 m na porção Sul da Bacia (Holz *et al.* 2010). A pequena espessura, associada aos folhelhos negros característicos, com ampla distribuição na Bacia tornou a Formação Irati um estrato de referência bem conhecido para o Permiano (Xavier *et al*. 2018). Hachiro (1991) define essa unidade como uma sucessão de siltitos e argilitos cinzas a preto, intercalados por folhelhos negros, normalmente pirubetuminosos, lentes de rochas carbonáticas e lentes centimétricas de sílex nodular, registro de uma plataforma marinha rasa influenciada por tempestades em mar epírico restrito (Xavier *et al*. 2018). Dos Anjos *et al.* (2010) mostrou que os folhelhos são compostos por argilominerais ricos em Al na porção sul e central e Fe-Mg na porção norte da bacia, enquanto os folhelhos negros consistem em camadas mistas de saponita, talco, lagartita, nontronita e quartzo originados do intemperismo de rochas máficas-ultramáficas ou cinzas vulcânicas.

Os depósitos Irati apresentam uma distribuição espacial de mais de 1.000.000 km^2 que abrange os estados brasileiros de Mato Grosso, Goiás, Mato Grosso do Sul, São Paulo, Paraná, Santa Catarina e Rio Grande do Sul, chegando até ao Uruguai (Hachiro 1991). No estado de São Paulo a formação apresenta uma camada de dolomito na base ou próxima a ela de 2,5 a 4 m com uma sequência de folhelhos negros intercalados por calcários de 20 a 30 m, aumentando para 40 a 50 m em direção ao centro da bacia, chegando a 70 m no depocentro (Amaral 1971). Segundo esse mesmo autor, as camadas mergulham 1º20’ NW para o interior da bacia com direção N35ºE. No estado do Paraná as camadas estão dispostas com direção NW e mergulho <1º para SW, constituída por calcários na base e folhelhos negros intercalados por lentes de 5

a 20 cm de calcários perfazendo um empilhamento de 12 a 20 m. No estado de Santa Catarina as camadas apresentam direção N10ºE e mergulho <1º W, a formação inicia com pacote de calcários com 30 m. Putzer (1955) *apud* Amaral (1971) observou uma variação brusca no estado de Santa Catarina, onde ocorre um adelgaçamento de norte a sul, passando de 70 para 32 metros em menos de 40 km. No Rio Grande do Sul as camadas estão dispostas com direção NW e mergulho para Norte. Xavier *et al*. (2018) descreve perfis da base com a Formação Palermo ao topo da unidade, em contato com a Formação Serra Alta, com empilhamento de 40 e 60 m, onde identificou doze fácies com predominância de folhelhos intercalados a carbonatos centimétricas.

A formação foi subdividida por Barbosa & Gomes (1958) em membros Taquaral (Inferior) e Assistência (Superior). O **Membro Taquaral** é constituído por *mudstones* cinzas a negros e siltitos, pobre em carbono orgânico (Holz *et al.* 2010, Crivellani 2016). O **Membro Assistência** é formado por *mudstones* intercalados com folhelhos negros ricos em matéria orgânica (Holz *et al.* 2010, Xavier *et al*. 2018). O conteúdo paleontológico do Membro Assistência é representado por répteis mesosauridius, crustáceus pygocephalomorpha e peixes paleonisciformes desarticulados e em alta concentração, que segundo Xavier *et al*. (2018) ocorrem associados com estruturas típicas de ação de ondas de tempestades, como estratificação cruzada *hummocky*, além de conglomerados intraclastos e grainstones na região de São Gabriel no Rio Grande do Sul atribuído a este membro. Calças (2008) também registram estromatólitos e lenhos silicificados no estado de São Paulo.

Os depósitos basais da Formação Irati registram o início de uma transgressão marinha que se estabelece após a deposição dos pelitos de *shoreface* da Formação Palermo e o trato de sistema de mar alto da sucessão Tatuí a nordeste da bacia, separando-o do Membro Taquaral (Assine et al. 2003, Araújo 2001, Lages 2004, Holz *et al.* 2010). Para Rohn *et al*. (2007) e Holz *et al.* (2010) esse contato marca um limite de sequência de 3°ordem, enquanto Araújo, (2001) e Xavier *et al*. (2018) o considera um limite (SB1) de 4°ordem. A ausência de fácies representativas do TSMB sobre o SB1 torna esse limite coincidente com a Superfície Regressiva Máxima (SRM) (Xavier *et al*. 2018) que marca a base do TST (base do Membro Taquaral). Essa base é bem delimitada por *lags* conglomeráticos compostos de restos de peixes e tetrápodes na porção leste da bacia, passando para arenito conglomerático com abundantes fragmentos de vertebrados na região do Paraná (Castro *et al*. 1993, Chahud, 2007), delgados conglomerados descontínuos compostos por seixos de sílex e restos de peixes (Assine *et al*. 2003) brechas na porção sul da Bacia, no território brasileiro (Holz 1997, Holz *et al.* 2010). Para Araújo (2001) e Xavier *et al*. (2018) o Membro Taquaral coincide com uma sequência de

3°ordem (S1) formada pelos tratos de sistemas transgressivo e mar alto, cuja Superfície Transgressiva Máxima (STM) é marcado pela ocorrência de níveis de nódulos de sulfetos concentrados.

A passagem abrupta da sedimentação do Membro Taquaral para o Assistência é conhecida como uma superfície de 3°ordem (Goldberg 2001, Lages 2004, Rohn 2007, Xavier *et al*. 2018). Esse limite estratigráfico é assim interpretado devido marcar uma completa mudança nas condições paleoambientais da bacia, de plataforma siliciclástica marinha rasa com relativa boa circulação do meio, para rampa interna com sedimentação mista carbonática-siliciclástica com conexões mais restritas e condições anóxicas, representando assim uma abrupta queda relativa do nível do mar. A sedimentação do Membro Assistência inicia com brechas e conglomerados carbonáticas que passam progressivamente para folhelhos negros cinza-escuro intercalado com carbonatos de águas rasas em rampa interna, compondo um TSMB, *grainstones* em camadas tempestíticas em rampa intermediária, compondo o TST e folhelhos negros bituminosos de plataforma externa, compondo o TSMA (Xavier *et al*. 2018). O Membro Assistência é formado por duas sequências de 4°ordem, ambas constituídas por TSMB, TST e TSMA, depositado em rampa interna que passa progressivamente para rampa intermediária e rampa externa (Xavier *et al*. 2018).

CAPÍTULO III

3. SISTEMA PETROLÍFERO NÃO-CONVENCIONAL DA BACIA DO PARANÁ

Sistema Petrolífero compreende um conjunto de elementos e processos geológicos relacionados a geração, migração, acumulação e trapeamento do petróleo que se desenvolvem de forma síncrona no tempo e espaço (Magoon & Dow 1994). A geração ocorre com o soterramento efetivo da rocha geradora que leva a evolução térmica da matéria orgânica com consequente transformação desta em querogênio e este, por sua vez, em hidrocarboneto. No entanto, intrusões ígneas podem exercer significativo papel em um sistema petrolífero tanto na fase de geração como trapeamento. Intrusões ígneas podem promover o craqueamento térmico em um intervalo de tempo relativamente curto e os derrames ígneos podem funcionar como selante e/ou trapas. O fraturamento associado as intrusões podem gerar rotas de migração e reservatórios. Magoon & Dow (1994) definem um sistema petrolífero cuja maturação das rochas geradoras pelo efeito térmico de intrusões ígneas como um Sistema Petrolífero Não Convencional.

Os sistemas petrolíferos devoniano (Ponta Grossa-Itararé) e permiano (Irati-Rio Bonito/Pirambóia) da Bacia do Paraná obedecem ao conceito de sistema petrolífero não convencional. A atividade ígnea cretácea exerceu um forte impacto nos sistemas petrolíferos da bacia. O magmatismo básico toleíticas do Eocretáceo forneceu energia térmica que permitiu a maturação da matéria orgânica (Thomaz Filho *et al*. 2008), assim como favoreceu a migração e geração de reservatórios pelo fraturamento das rochas e formação de estruturas selantes. Contudo, as intrusões ígneas também tiveram aspectos negativos. O fraturamento das rochas também afetou as rochas selantes e promoveu o desmantelamento de estruturas trapeadoras (Artur e Soares 2002).

O sistema petrolífero não-convencional permiano da Bacia do Paraná tem como rochas geradoras os folhelhos negros da Formação Irati e reservatório os carbonatos da mesma unidade e os arenitos da Formação Rio Bonito, além dos arenitos eólicos/fluviais da Formação Pirambóia. O reservatório Rio Bonito é selado por rochas pelíticas enquanto o sistema Iratí-Pirambóbia é capeado pelas rochas basálticas do magmáticas cretáceo como é colocado por Milani & Zalán (1999). Outra peculiaridade do sistema petrolífero permiano da Bacia do Paraná está relacionada a rochas geradora (folhelhos negros) e reservatório (carbonatos) da Formação Irati. O maior potencial dessa unidade está relacionado aos *Oil/Gas shales deposits*, pois são folhelhos imaturos pirobetuminosos com teor de carbono orgânico que chegam a 27%. Esses

depósitos estão concentrados principalmente nos estados sulista do país (Paraná, Santa Catarina e Rio Grande Sul), onde *oil shale* ocorrem em dois níveis principais, pertencem ao Membro Assistência próximos a superfície, chegando a aflorar em algumas regiões ao longo do cinturão carbonífero. Neste trabalho esses intervalos são denominados organofácies B e E.

3.1. CARACTERIZAÇÃO GEOQUÍMICA DA ROCHA GERADORA

Os folhelhos da Formação Irati são ricos em matéria orgânica amorfa (Santos Neto 1993, Mendonça Filho 1994) que gerou querogênio tipo I e II de origem algálica e liptinítica (Neto 1983, Correa da Silva e Cornford 1985, Zálan *et al*., 1990, Afonso *et al.* 1994, Alferes *et al.* 2011). No município de São Mateus do Sul, estado do Paraná Alferes *et al.* (2011) verificou que esses folhelhos apresentam pouca evolução térmica, com *Tmax* normalmente abaixo de 440ºC e índice de vitrinita entre 0,34% e 0.40% (Correa da Silva e Cornford 1985). No entanto, no depocentro da bacia e regiões de influência das intrusões ígneas Goulart & Jardim (1982) sugerem que podem ter alcançado o início da janela de geração do óleo.

Os depósitos da Formação Irati apresentam uma estratificação com diferentes níveis de matéria orgânica, com intervalos com alto teor de COT (<1 a 20 %, com picos de 25%). Os folhelhos Irati contêm ~6,0 wt% de enxofre e ~5,1 wt% de ferro que ocorre na forma de pirita (Neto 1983). Afonso *et al.* (1991) classifica a Formação, com base na razão atômica $S_{(orgânico)}/C$ = (~0,003), como muito pobre em enxofre orgânico, com apenas 0.15 wt%.

Alferes *et al*. (2011) define para a Formação Irati no município de São Mateus do Sul (PR) sete unidades quimioestratigráficas com base em carbono orgânico total, enxofre total e resíduo insolúvel. Afonso *et al.* (1994) caracterizou os folhelhos Irati nesse município com base em biomarcadores, como imaturos e origem algal/microbial para a matéria orgânica.

3.2. ROCHA RESERVATÓRIO

O sistema misto siliciclástico-carbonático cisuraliano tem nos carbonatos da Formação Irati excelente reservatório de hidrocarbonetos. A rocha é dominantemente dolomito peloidal com baixa porosidade primária. Assim a geração de espaço poroso para acumulação de óleo é essencialmente diagenética. Apesar das propriedades do reservatório de baixa permeabilidade, fraturas, *vugs*, microfalhas, poros de dissolução e camadas deformadas de carbonatos são as principais estruturas que acumulam óleo. Em afloramentos e testemunhos de sondagens é comum a presença de fraturas, poros de dissolução e brechas preenchidos por óleo. Microfalhas normal e inversa também são comuns dentro das camadas de carbonatos deformadas. As

descontinuidades estruturais que cruzam as camadas dos folhelhos e carbonato são condutos naturais para a migração de fluido da rocha fonte para o reservatório. As propriedades naturais de baixa permeabilidade dessas rochas siliciclásticas-carbonáticas finas também atuam como um selante do reservatório carbonático subjacente. O comportamento reológico do sistema misto siliciclástico-carbonático resulta em uma deformação rúptil na rocha carbonática (mais competente) e deformação dúctil das camadas de folhelhos. Essa propriedade causa descontinuidade das estruturas lineares do carbonato, gerando condutos entre as camadas geradoras e os reservatórios. A presença persistente de óleo mesmo nas fraturas menos penetrantes demonstra que são suficientes para permitir a migração do óleo.

Os arenitos deltaicos da Formação Rio Bonito também apresentam excelente relação permo-porosidade, com boas condições de pressão e transmissibilidade, atingindo até 20% de porosidade em profundidades até 4.000 m (Milani et al. 1990). Óleo já identificado nesta unidade em poços perfurados no domínio sul da bacia possuem densidade API de 22 a 33, cuja correlação geoquímica é positiva com os extratos orgânicos da Formação Irati (Milani et al. 2007b). A Formação Rio Bonito compreende a unidade basal do Grupo Guatá e jaz diretamente sobre as sequencias glaciais do Grupo Itararé. É constituída por ortoconglomerados maciços na base seguido de pacotes de arenitos intercalados a pelitos de forma cíclica com ocorrências de calcários e camadas de carvão (Zacharias & Assine 2005) que permitiu a divisão da unidade nos membros Triunfo, Paraguaçu e Siderópolis (Schneider et al. 1974). Holz (1998) e Zacarias (2004) interpreta os depósitos da Formação Rio Bonito como o registro de uma sequência de terceira ordem constituída pelos tratos de sistema de mar baixo, tratos de sistema transgressivo e tratos de sistema mar alto, formados por preenchimento retrogradacional de um sistema deposicional estuarino-lagunar misto, dominado por ondas e marés em vales incisos num contexto de um trato de sistema transgressivo (Holz 2003, Zacharias & Assine 2005, Jasper *et al*. 2006). Para Milani *et al.* (2007b) a repetição cíclica é resultado da interação entre progradação dos lobos deltaicos e a variação do nível do mar, promovendo o retrabalhamento dos lobos arenosos por correntes de maré.

Os arenitos da Formação Rio Bonito são considerados bons reservatórios de hidrocarbonetos em virtude de suas propriedades permoporosas até mesmo em grandes profundidades (Bocardi *et al*. 2009). No trato de sistema de mar baixo o reservatório compreende arenitos subarcóseos finos a grossos de preenchimento de vales incisos, de leques aluviais e arenitos flúvio-deltáicos (Bocardi *et al.* 2009). Os reservatórios apresentam porosidade média é de 6,6% baixa a moderada qualidade devido a pobre a moderada seleção intercalações de camadas pelíticas e baixa continuidade lateral das camadas. Na porção superior

os arenitos são médios a muito grossos com clastos de argila e pirita com porosidade média nesse intervalo é de 2,73%, a qualidade do reservatório é comprometida pelas frequentes intercalações de camadas pelíticas. No trato de sistema transgressivo os reservatórios são caracterizados por arenitos subarcóseos finos a grossos com níveis de conglomerado maciços que ocorrem intercalados com camadas de pelitos de canal fluvial canais de maré, de ilhas barreiras, de barras de desembocadura e deltas de maré de enchente. com porosidade média de 12,7%, com porções de constituída por siltitos e arenitos finos a muito finos intercalados com camadas de calcário argiloso com porosidade média de 3,2%. Os arenitos do trato de sistema de mar alto são subarcóseos a quatzoarenitos médios a finos, bem selecionados com baixo teor de argila com elevados valores de porosidade média de 18,6%, evidenciados em perfil sônico (Bocardi *et al.* 2009).

CAPÍTULO IV

4. MATERIAIS E MÉTODOS

4.1. ANÁLISE DE FÁCIES E MICROFÁCIES

A análise de fácies sedimentares seguiu a metodologia clássica proposta por Walker (1992) que consiste no reconhecimento de fácies sedimentares, caracterizando a composição, geometria, texturas, estruturas sedimentares, padrões de paleocorrente, conteúdo fossilífero e compreensão dos processos sedimentares responsáveis pela geração de cada fácies. O agrupamento das fácies cogenéticas e contemporâneas permite inferir seus respectivos paleoambientes deposicionais. Por se tratar da identificação de litofácies essencialmente em rochas siliciclásticas e carbonáticas finas, com predominância de contados graduais foram coletadas amostras de forma sistemática em função das diferentes fácies para análise petrográfica e identificação de microfácies.

Devido a dominância de fácies de granulação fina ricas em matéria orgânica, com uma variação complexa da estrutura sedimentar em escala milimétrica, aqui é proposto uma classificação de microfácies das rochas siliciclásticas e mistas de granulação fina com base em Bennett *et al.* (1991) e Stow & Pipe (1984), proporcionando precisão adicional nas interpretações paleoambientais. As microestruturas das rochas siliciclásticas finas têm sido amplamente ignoradas como diagnósticas de ambiente deposicional, possivelmente devido à única estrutura macroscópica primária comum observada em *mudrock* ser a laminação plana (Potter *et al.* 1980, Kuehl *et al.* 1991). No entanto, as análises de seção delgada revelam uma variedade de microestruturas indicativas de condições ambientais particulares (por exemplo, Kuehl *et al.* 1991, Schieber *et al.* 2007, 2010, Schieber 2011). A correta interpretação dos processos sedimentares permite identificar associações de fácies cogenéticas que somadas as interpretações da dinâmica de fácies, geometria e suas interrelações permite diferenciar os ambientes e subambientes deposicionais. A definição de microfácies carbonáticas segundo Flügel (2004) foram realizadas a partir da descrição de lâminas delgadas com a nomenclatura baseada em Dunham (1962) e Embry & Klovan (1971). Lâminas representativas foram selecionadas para tingimento com Alizarina vermelho S para diferenciar as fases dolomíticas e calcíticas conforme Dickson (1966)

4.2. ANÁLISE DOS CICLOS DE ALTA FREQUÊNCIA

O estudo dos padrões cíclicos presentes na sucessão do Permiano Inferior da Bacia do Paraná tomou como base as proposições de Schwarzacher (2000) e Strasser *et al.* (2006). O primeiro autor colocar que as seções estratigráficas são compostas por padrões de repetições regulares da sedimentação em todas as escalas. Essas repetições cíclicas, de milímetros a centenas de metros, representam intervalos de tempo relacionados a periodicidade diária a variações orbitais de milhares a milhões de anos e são denominados ciclos. Goldhammer *et al.* (1993) complementa a definição colocando os ciclos deposicionais como as menores unidades deposicionais alocíclicas ou autocíclicas reconhecíveis com padrões progradacionais e/ou agradacionais. A aplicação dos conceitos de ciclos deposicionais de 3ª ordem como ciclos de baixa frequência (0,5 - 3 Ma) formado por ciclos de 4ª ordem (0,1 a 0,5 Ma) e 5ª (0,01-0,1), denominados de alta frequência seguem Goldhammer *et al.* (1990) e Schwarzacher (2000).

A caracterização dos padrões cíclicos e identificação das repetições foi auxiliada pela definição dos padrões faciológicos, tendencias de espessamento e afinamento, padrões retrogradacionais, agradacionais e progradacionais, assim como definição de superfícies-chaves como as superfícies de inundação, similar a uma parasequencia (Catuneanu *et al.* 2009). A avaliação dos padrões de variações cíclicos foi auxiliada por gráfico de Fisher. O método é usado para ilustrar a variação da espessura dos ciclos, definindo as superfícies-chaves e correlação estratigráfica em daquelas em subsuperfície. O gráfico de Fisher compara o desvio cumulativo da espessura média do ciclo e o número do ciclo para estimar a taxa de criação de espaço de acomodação relacionada às variações de nível do mar (Sadler *et al.* 1993, Husinec *et al.* 2008).

4.3. ANÁLISE DO CARBONO ORGÂNICO

A análise de Carbono Orgânico Total (COT) quantifica o carbono orgânico contido nas rochas sedimentares, tanto a fração da matéria orgânica solúvel (betume) quanto insolúvel (querogênio). O resultato é expressa como a porcentagem em peso relativo de carbono orgânico (Jarvie 1991). O processo de análise consiste na pesagem de cerca de 0,25g de material pulverizado e peneiramento em malha de 80 mesh, o qual é acidificado com HCl numa razão de 1:1 para eliminar os constituintes carbonáticos. A metodologia padrão sugere a permanência do material na solução ácida por 24h, sendo esta podendo sofrer alterações em função do teor de carbonato presente quando previamente determinado. A remoção do ácido é realizado lavando com água destilada e posterior secagem à 70º C por 10hs. O resíduo insolúvel é então submetido

à combustão num analisador de carbono (LECO WR-12) a temperaturas de até 1.300ºC para liberação do dióxido de carbono (CO_2) e do enxofre que é medido usando-se um detector de condutividade térmica. As análises de COT assim com de Pirólise *Rock-Eval* descritas a seguir foram efetuadas em de 3.123 amostras coletadas com intervalo de 0,5 a m em 102 poços ao longo dos estados do Paraná, Santa Cataria e Rio Grande do Sul. As análises foram realizadas no Weatherford Laboratórios Brasil, Rio de Janeiro seguindo a medodologia padrão. as modificações acime descritas foram realiadas nas análises de controle efetuadas no laboratório de geoquímica da Universiade Estadual do Rio de Janeiro (UERJ). As demais análises, totalizando 3.123 amostras.

4.4. PIRÓLISE DE ROCK-EVAL

Pirólise *Rock Eval* é uma técnica apresentada por Espitalié *et al*. (1977) que simula em laboratório o processo de maturação da matéria orgânica e degradação térmica do querogênio, submetendo cerca de 100 mg de amostra a temperaturas de 300° a 600°C com a taxa de aumento de 25°C/min em um micro forno com atmosfera inerte, utilizando o hélio como gás carreador. Durante o processo de aquecimento são liberados os hidrocarbonetos livres presentes na amostra (S1 a 300°C), os hidrocarbonetos gerados durante craqueamento térmico (S2 entre 300 a 600°C) e o gás carbônico (S3 entre 300 e 390°C) gerado pelo craqueamento térmico do querogênio. Os hidrocarbonetos e o CO_2 liberados durante o processo são medidos respectivamente, por um detector de ionização de chama (FID) e de condutividade térmica. Os resultados são expressos em mg de hidrocarbonetos (HC)/grama de rocha ou miligrama de CO_2/grama de rocha. A **Tmax** (Temperatura Máxima de Pirólise) é dada pela temperatura mostrada pelo pico S2 e demonstra a temperatura máxima na qual a matéria orgânica foi submetida para a geração de hidrocarboneto. O tipo de matéria orgânica pode ser determinado pelo Índice de Hidrogênio (IH) e Índice de Oxigênio (IO), obtidos associando esses picos com o teor de carbono orgânico total (COT). A integração de dados de IH e IO em diagramas do tipo van Krevelen permite identificar os quatro tipos básicos de querogênio (Espitalié *et al.* 1977), também permite definir a evolução térmica. A relação S1/S1+S2 (denominada Índice de produção - IP) é utilizada como um indicador do avanço do processo de geração e do nível de maturação da rocha geradora (Lisboa 2006). As análises foram realizadas no Weatherford Laboratórios Brasil, Rio de Janeiro.

4.5. BIOMARCADORES

4.5.1. Extração em Soxhlet e Cromatografia em Coluna Aberta

O processo de extração do betume da rocha total pode ser realizando utilizando extrator Soxhlet ou banho de ultrassom. Inicialmente três amostras de folhelhos negros que registram os picos de maior teor de carbono orgânico nos três estados do sul do país foram submetidas a extração via Soxhlet. Os rendimentos das respectivas frações (P1, P2 e P3) são apresentados na figura 3. Essas análises preliminares objetivaram compreender o espectro de marcadores moleculares presentes nos depósitos Irati e a partir delas determinar os parâmetros mais adequados para a análise em ampla escala dos depósitos. Da mesma forma, foi constatando o alto rendimento das amostras. Assim, visando otimizar o processo e reduzir o tempo de análise, as demais amostras foram extraídas via banho de ultrassom.

Para a extração em sistema tipo Soxhlet as amostras pulverizadas foram mantidas em dessecador com $CaCl_2$ e Pentóxido de Fosfóro (P_2O_5) para retirada do excesso de umidade durante 24 horas antes da extração. Para a obtenção do extrato orgânico a rocha pulverizada foi submetida a partir de mistura azeotrópica de diclorometano/metanol 12% (v/v) por 24 h. Foi adicionado ao extrato cerca de 500 mg de cobre metálico em pó para a retirada do enxofre, o extrato foi filtrado, evaporado sob pressão reduzida e acomodado em frasco de vidro. Para a extração por sistema de ultrassom foram utilizados 50 ml de diclorometato/metanol (88:12 v/v), três vezes. 500 mg de cobre metálico em pó foram adicionados ao extrato para remoção do enxofre usando ultrassom por 30 min sob aquecimento a 60 ° C. Os extratos foram filtrados e o solvente evaporado em evaporador rotativo. Os extratos foram fracionados por coluna cromatográfica (figura 04a) utilizando sílica como fase estacionária e o sistema eluente foi n-hexano, hexano / acetato de etila 12% (v / v), acetato de etila / metanol 5% (v / v).

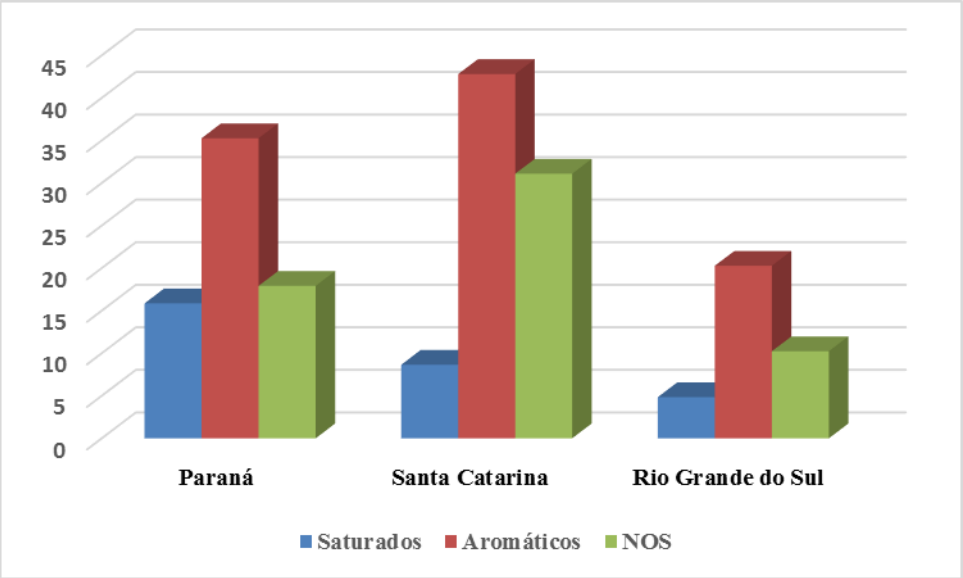

Figura 4.1. Fração do betume extraido em folhelhos negros da oil-shale S3 B em subsuperfíce nos estres estados do sul do país.

4.5.2. Cromatografia Gasosa Acoplada à Espectrômetro de Massa (GC-MS)

As análises por CG-EM das frações saturadas foram realizadas em um cromatógrafo da Shimadzu, modelo GCMS-QP2010 SE, equipado com auto injetor AOC-5000 (figura 04), seguindo as seguintes condições de análise: injetor 290 °C, razão split de 1:10, temperatura inicial do forno de 60 °C (1 min), apresentando duas rampas de aquecimento, a primeira de 6 °C/min até 280 °C permanecendo por 5 minutos, a segunda 1 °C/min até 315 °C durante 15 minutos. Para cromatografia dos componentes foi empregada uma coluna SLB-5MS, 30 m × 0,25 mm, espessura do filme interno de 0,25, usou-se He como gás de arraste com fluxo de 1,0 mL/min. A temperatura de interface e da fonte de íons foram 300 °C e 260 °C, respectivamente. O analisador de massas utilizado foi do tipo quadrupolo operando por impacto eletrônico (70 eV) e os fragmentos detectados na faixa de 47 a 650 Da. A identificação dos biomarcadores foi feita por comparação das ordens de eluição, tempos de retenção e espectros de massas com dados da literatura.

Figura 4.2. Análises de biomarcadores. Em (A) imagem mostra o processo de separação das frações em uma coluna cromatográfica com a fração P1 sendo coletada no frasco de vidro. Em (B) cromatógrafo da Shimadzu, modelo GCMS-QP2010 SE, equipado com auto injetor AOC-5000.

4.6. DIFRATOMETRIA DE RAIOS-X (DRX)

Amostras representativas das fácies/microfácies foram selecionadas para análise por difração de raios-X visando a caracterização das fases minerais presentes. A análise de DRX foi realizada no Laboratório de Caracterização Mineral da UFPA do Instituto de Geociências (LCM-UFPA) através do método do pó. As amostras pulverizadas em graal de ágata até a fração argila foram analisadas em Difratômetro de Raios-X Empyrean, da PANalytical, com Goniômetro θ-θ, tubo de raios-x cerâmico de anodo de Co ($K\alpha_1$ = 1, 78901 Å), foco fino longo de 1800W e filtro kβ de Fe. O detector utilizado é de área, do tipo PIXel^{3D} 2 x 2, com *scanning* em modo linear (1D), *active length* 3,3473° 2θ. A aquisição de dados foi feita com o software X'Pert Data Collector, versão 5.1, e o tratamento dos dados com o software X´Pert HighScore Plus (HSP), versão 4.9. A identificação mineralógica foi realizada através da comparação dos difratogramas obtidos com padrões (fichas) tanto no banco de dados do ICDD-PDF (International Center for Diffraction Data – Powder Diffraction File) como no COD (Crystallography Open Database).

4.7. MICROSCOSCOPIA ELETRÔNICA DE VARREDURA (MEV/EDS)

A caracterização textural e mineralógica das rochas finas foi auxiliada por análise de Elétrons Secundários, Retroespalhados e EDS. As análises foram realizadas em um microscópio modelo LS15 da Zeiss no laboratório de análise mineral (LAMIN-BE) da

Superintendência Regional de Belém do Serviço Geológico do Brasil—CPRM. As lâminas polidas das rochas carbonáticas e dos folhelhos foram metalizadas em alto vácuo com película de 20 µm de espessura de ouro (Au). As imagens de elétron retroespalhado (Backscattering Electron—BSE) foram obtidas com voltagem de 20 kV, corrente de chegada de 45 a 60 pA, distância de trabalho de 8,5 mm e ampliação entre 55 e 4000 vezes. As análises da composição química mineral foram por espectrometria de dispersão de energia (Energy Dispersive Spectrometry—EDS) de raios-X em um detector X-Act SSD 10 mm2 da Oxford Instruments. O filamento de emissão utilizado é de tungstênio e foi usado o modo de alto vácuo (3,0–1,5 10–5 mPa). Os resultados obtidos foram padronizados por espectros de energia de padrões do programa AZTec da Oxford Instruments. Resultados com desvio padrão acima de 10% da concentração do elemento foram descartados do cálculo da composição dos minerais, podendo esses estar presentes nos minerais em baixas concentrações como impurezas aprisionadas no retículo cristalino ou marcar incipiente alteração secundária dos minerais analisados.

4.8. CATODOLUMINESCÊNCIA

Análises de catodoluminescência foram realizadas nas rochas carbonáticas com o intuído de identificar microporosidade, as diferentes fases de cimentação carbonáticas e a relação textural com as fases siliciclásticas presentes. As análises foram realizadas no Laboratório de Catodoluminescência do Instituto de Geociências (UFPA), utilizando lâminas delgadas polidas em um microscópio óptico Leica, modelo DM 4500 P LED acoplado ao aparelho Optical cathodoluminescence CL 8200 MK5-2.s.

CAPÍTULO V

5. Permian organic-rich shale within a mixed siliciclastic- carbonate system from an epicontinental sea in the West Gondwana, Paraná Basin, Southern Brazil: Paleoenvironmental and geochemical reconstruction

Ailton da Silva Brito[1], Afonso César Rodrigues Nogueira[1], René Rodrigues[2], Renan Fernandes dos Santos[1], Rômulo Simões Angélica[1]

[1]*Programa de Pós-Graduação em Geologia e Geoquímica, Instituto de Geociências, Universidade Federal do Pará, Rua Augusto Corrêa s/no, 66075-110, Belém, PA, Brazil, R. Augusto Corrêa 01, Belém 66075-110, Brazil*

[2]*Chemostratigraphy and Organic Geochemistry Laboratory, Rio de Janeiro State University, São Francisco Xavier street, 524, 4°floor - Maracana, Rio de Janeiro, RJ 20550-900, Brazil*

ABSTRACT

The Permian was marked by the transition from icehouse conditions to extreme greenhouse phases that reached the Triassic during the Pangea Supercontinent assembly. Siliciclastic-carbonate shallow seas with massive organic matter accumulation dominated the Lower Permian West Gondwana, succeeded by extreme continentalization during the Upper Permian. The 50 m-thick organic matter-bearing succession of Paraná Basin represents a singular record of the Lower Permian, exposed in the southeastern Brazil. Previous paleoenvironmental reconstructions are focused mainly on geochemical data, and their laterally tabular beds continuous for hundreds of kilometers have been interpreted as platform or lake deposits. The outcrop and drill cores measured sections of the mixed succession revealed finely-laminated to graded organic-rich shales, wavy-crinkle lamination, massive to graded marlstone, heterolithic beds (evaporite and carbonate), finely-laminated to massive dolomudstone, carbonate breccia, peloidal dolopackstone, and wackestone. Detailed facies and microfacies analysis in the southeastern basin has confirmed the previous epicontinental ramp interpretation marked by freshwater input. The dolostone-shale rhythmite indicates an cyclic freshwater inflow in the marine realm reflected in the organic matter accumulation (kerogen type I and II). The bituminous shale intervals have high organic carbon values (5 to 25.7 wt.%). These organic-rich shale facies were produced widely in the ramp, suggesting that the Irati Sea served as a significant sink of atmospheric CO_2. Futhermore, the widespread dolostone beds formation was due to hypersaline conditions inducing dolomite precipitation and locally early dolomitization. Also, the Irati deposits provide a window of opportunity to study large-scale architectural strata related to a Permian mixed anoxic epicontinental sea of the West Gondwana.

Keywords: Organic matter, Lower Permian, Irati Formation, Shallow marine ramp, carbonate-shale microfacies.

5.1. INTRODUCTION

Permian epicontinental seas were widespread developed during the Paleozoic age, related to the Pangaea closure in the Permian-Triassic limit (Laporte 1969; Mazzullo & Reid, 1989; Borer & Harris, 1991; Lankarani *et al*., 2009; De Medeiros *et al*., 2019). Since current analogous models are absent, reconstructing ancient mixed siliciclastic-carbonate systems represents a considerable challenge for geoscientists. The recognition and details of the sedimentary processes in these Permian successions are hampered by the unusual rhythmic and monotonous deposition of organic matter-rich shale interbedded with carbonate rocks. These siliciclastic-carbonate pairs can be individualized in macro- (stratal distribution), meso- (bed), and microscale (lamina), indicating carbonate precipitation alternate with continental input on the shallow marine environment. The autogenic control in carbonate production implies the absence or low terrestrial sedimentation flow (Tucker & Wright, 1990). Despite the inhibitory effect of siliciclastic sediments, they coexist with micrite precipitation. In previous works, mixed siliciclastic-carbonate deposits have been documented throughout the geological record (e.g. Barnaby & Ward, 2007; Hender & Dix, 2008; Brandano *et al*., 2010; Longhitano *et al*., 2010; Zecchin & Caffau, 2011; Braga *et al*., 2012; Chiarella & Longhitano, 2012; Gramigna *et al*., 2012; Myrow *et al*., 2012; Zeller *et al*., 2015; Chiarella *et al*., 2017). Despite the abundant information about the origin of these deposits, understanding how cyclic sedimentation occurs is debatable. The Cisuralian succession exposed in the Paraná Basin, southeastern Brazil, is the object of this study and represents the unique record that allows the observation of these events in South America.

During the Lower Permian, vast, shallow, and restricted sea was developed in West Gondwana. The Permian Whitehill-Irati Sea reached 5.000.000 km^2 covering the central portion south of Brazil, northern Argentina, Uruguay, and Paraguay countries registered by the Irati and Mangrullo formations, as well as in South Africa, with extension in the Huab and Karoo basins as recorded by the Whitehill Formation (Branch *et al*., 2007; Xavier *et al*., 2018; Conti *et al*., 2019; Bastos *et al*., 2021). The last marine incursion is recorded in Permian deposits of the Paraná Basin and occurred after the Carboniferous glaciation during the establishment of greenhouse conditions coeval with the greater Phanerozoic mass extinction in the limit Permian-Triassic (Hofmann, 2016; Kiehl & Shields, 2005; Meyer *et al*., 2008; Stanley, 2009). The mixed siliciclastic-carbonate succession was deposited during the Lower Permian long-term (2nd order) regression associated with the continentalization of the West Gondwana (Milani, 1997; Milani *et al*., 1998).

The succession has been studied since the 1960s. However, despite a large amount of research on this unit, they are mainly focused on the source rock that comprises the organic-rich shales of the Assistência Member (Araújo, 2001; Anjos & Guimarães, 2008; Santos, 2009; Franco *et al*., 2010; Alferes *et al*., 2011; Maraschin & Ramos, 2015; Reis *et al*., 2018). Previous works based on (i) high contribution of type I kerogen, (ii) salinity variation, (iii) distribution of *Bothryococcus* algae along the section, (iv) occurrence of so-called rhythmic facies typical of lakes, and (v) molecular parameters suggest lacustrine conditions for the mixed deposits (e.g. Amaral, 1971; Correa da Silva & Cornford, 1985; Afonso *et al*., 1994). On the other hand, the more than 1.000.000 km^2 of depositional site, fossil assembly, molecular parameters of marine conditions are the primary evidence to support the shallow marine platform interpretation (e.g. Oelofsen & Araújo, 1983; Holz *et al*., 2010; Xavier *et al*., 2018; Ng *et al*., 2019).

The fossil content of Irati Formation comprises foraminifera, paleonisciform fish, brachiopod, ostracode, *pygocephalomorpha*, *Liocaris mesosauridius Mesosaurus*, *Stereosternum*, and *Brazilosaurus* crustaceans correlated with Whitehill and Huab formations, respectively from the Karoo and Huab basins, Africa (Oelofsen & Araújo, 1983; Hachiro & Coimbra, 1992; Soares, 2003; Xavier *et al*., 2018; Ng *et al*., 2019). The palynomorphs content has a low degree of preservation. It comprises pollen grains, spores, algae (mainly *Bothryococcus*), acritarchs, and a high quantity of amorphous organic matter (Correa da Silva & Cornford, 1985; Daemon *et al*. 1996; Araújo, 2001; Lages, 2014). The genus *Michrystridium* of acritarchs was identified only on the basal Irati Formation (Taquaral Member), with sporadic recurrences in this unit (Araújo 2001). On the other hand, *Bothryococcus* algae are frequent in entire succession.

New exploration fronts developed by private companies throughout the Parana Basin allowed many drill cores from these Permian mixed deposits described in detail and combined with previous and outcrop data. This procedure improved the facies and microfacies analysis allowing the lateral and vertical variations mapping. This work proposes a palaeoenvironmental reconstruction discussing the allogenic and autogenic controls for these cyclic deposits and the influence of siliciclastic input on the carbonate factory. Also, the paleogeography of these deposits is tentatively reconstructed, improving the geologic understanding of the Permian shallow seas from the West Gondwana.

5.2. GEOLOGICAL SETTING

The Paraná Intracratonic Basin (Fig. 01) is the largest Paleozoic-Mesozoic basin in Gondwana on the South American platform (Limarino & Spalletti, 2006). It has an oval shape with 1,750 km in length on the central axis (NNE-SSW) and the minor axis with 900 km that accumulated sediments from the Ordovician to the Cretaceous (Quintas *et al*., 1999; Milani *et al*., 1998; 2007). The basin fill extends from southeast to south of Brazil to the northeast of Argentina, east of Paraguay, and north of Uruguay, covering an area of about 1,700,000 km^2 (Holz *et al*., 2010) integrating the sedimentary basin of Chaco- Paraná (Milani *et al*., 1998). The Paraná Basin was not always isolated inland but originated as an open gulf for the Panthalassa (Zalán *et al*., 1990), closing its southeast margin along the Phanerozoic with the convergence of the paleocontinent and the ocean floor (Milani & Ramos, 1998; Milani *et al*., 2007). Considered a multicyclic basin initiated by an interior fracture phase and followed by several stages of interior syneclysis (De Figueiredo & Gabaglia (1986). Due to the predominance of this last phase, Almeida (1980) defined it as a complex syneclysis developed along the Paleozoic, which passes to amphiclysis in the Upper Jurassic due to swelling caused by volcanic thermal anomalies of that period. The ~7km-thick sedimentary rocks interbedded with magmatic rocks comprise six 2nd order sequences separated by regional unconformities (Milani, 1997; Milani *et al*., 2007). Private companies have prospected along the Basin, providing many drill cores. The subsurface information has complemented the outcrop data, allowing a better microfacies description and lateral and vertical correlation.

The mixed carbonate–siliciclastic deposits represent an early regressive interval from the Pennsylvanian-Eotriassic Supersequence, called the Gondwana I Sequence. This sequence marks the last marine incursion events preceding the continentalization of Gondwana (Milani, 1997; Milani *et al*., 1998; Milani *et al*., 2007). The dark-grey bituminous shale, marl, and carbonate from the Irati Formation were deposited under restricted conditions and shallow epicontinental sea. The thicker grey to black shales deposits of the overlying Serra Alta Formation recorded a more oxygenated and offshore condition. The shales of the Irati Formation are well known in the literature due to their high potential as Oil-shale and occurrences of well-preserved fossils of *Mesosaurus brasiliensis*. They are dated by Santos *et al*. (2006) from SHRIMP zircon present in bentonite peat in 278.4 ± 2.2 Ma, Kungurian age.

The mixed carbonate – siliciclastic deposits of Irati have an average thickness of 50 m, reaching 70 m in the southern portion of the basin (Holz *et al*., 2010). The small thickness, associated with the characteristic black shales, with wide distribution in the Basin, made the

Irati Formation a well-known reference stratum for the Permian (Xavier *et al*., 2018). The Irati deposits occupy an area of more than 1,000,000 km^2 that covers the central-west, southeast, and southern regions of Brazil until Uruguay. The Permian Rio do Rastro Formation comprises sandstone, siltstone, and shale, forming the last deposits in the upper supersequence under arid conditions, typical of terminal Permian (Soares *et al*., 2014). The Choiyoi magmatic arc rose marginal to the foreland basin and was a significant structural barrier between the inland portion of the continent and the Panthalassa Ocean to the west (Milani, 2004). The Choiyoi arc was a detrital sediment source to the basin, mainly in the upper Permian Rio Bonito Formation (Canile *et al*., 2016). The tectonic stability occurred during the deposition of the Irati and Teresina formations indicated by the concentric contours of the isopach maps coincident with the elliptical shape of the basin (Zálan *et al*., 1990; Milani 2004).

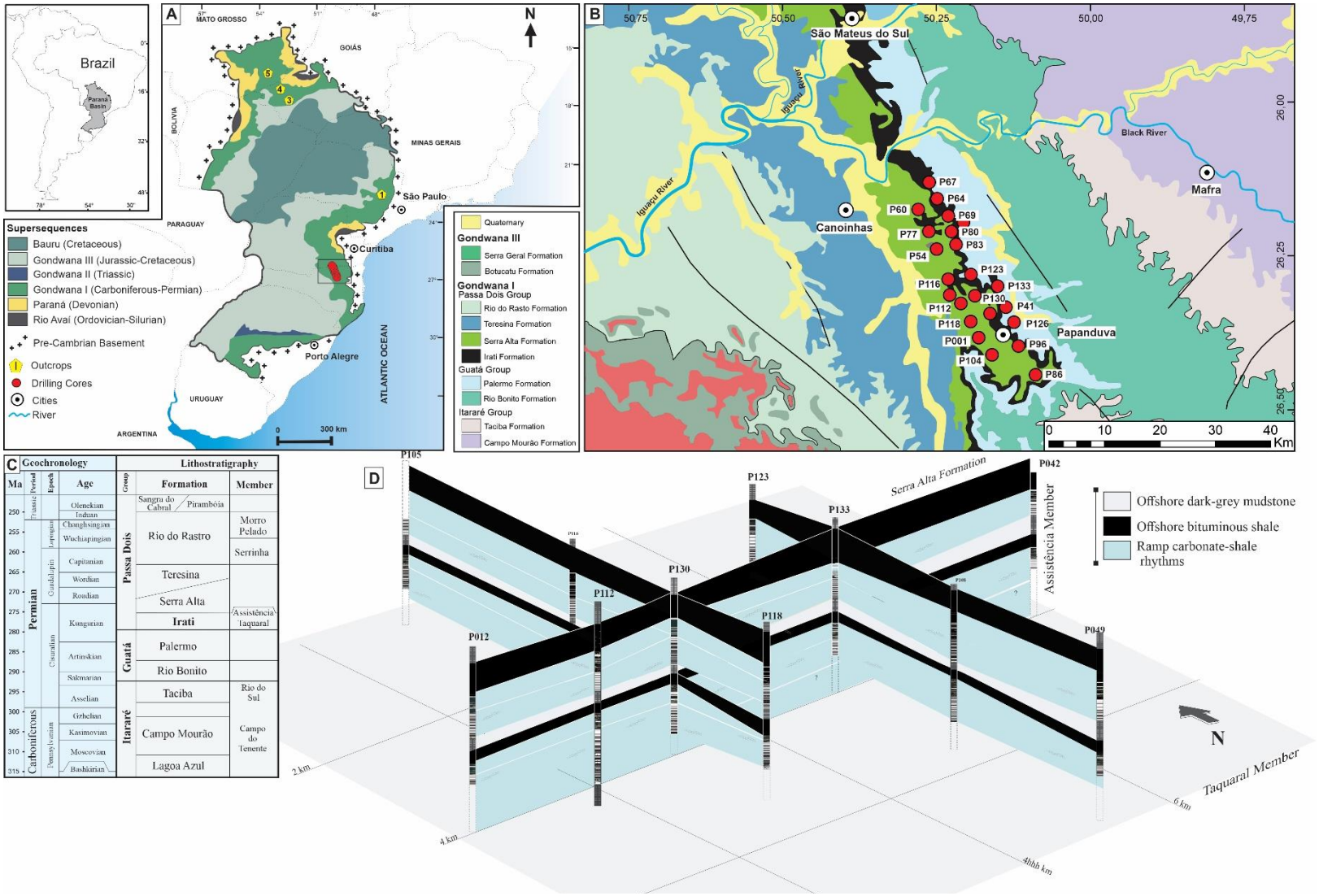

Fig. 1. The Paraná Basin in the Southeastern Brazil. A) Geologic map and general lithostratigraphy. B) Location of the studied drill cores and outcrops. C) Lithostratigraphy (Modified from Milani et al., 2007). D) Three-dimensional diagram of the Irati facies association showing the tabular geometry laterally continuous for hundreds of kilometers along the basin.

5.3. METHODOLOGY

The facies analysis was carried out in 23 wells drilled by the Irati Petróleo e Energia LTDA covering a maximum observation of 720m of rocks. Outcrop-base facies analysis complemented the drill core description and was used for paleoenvironmental reconstructions following the modeling technics of Tucker and Wright (1990), Walker (1992), Walker and James (1992), and Reading (1996). The classification of carbonate rocks and microfacies definition was after Wright (1992). Here is proposed a microfacies classification of the mixed and fine-grained siliciclastic rocks based on Bennett *et al*. (1991) and Stow and Pipe (1984), because the dominance of fine-grained and organic-rich facies with a complex variation of the millimeter-scale sedimentary structure, providing additional accuracy in the paleoenvironmental interpretations. Microstructures of the fine siliciclastic rocks have been largely ignored as diagnostic of depositional environment, possibly due to the only common primary macroscopic structure observed in mudrock is planar lamination (Potter *et al*., 1980; Kuehl *et al*., 1991). Nevertheless, thin section analyzes reveal a variety of microstructures indicative of particular environmental conditions (e.g. Kuehl *et al*., 1991; Schieber *et al*., 2007; 2010; Schieber, 2011).

Two hundred samples were systematically collected according to facies/microfacies analysis. One hundred twenty thin sections were analyzed under an optical microscope of transmitted and reflected light. The mineralogy identification was improved by cathodoluminescence (CL), scanning electron microscopy, energy dispersive spectroscopy (SEM/EDS), and X-ray diffraction (XRD). Thin sections were stained with Alizarin Red S and potassium ferricyanide mixture to differentiate calcite and dolomite crystals following Dickson's (1966) methodology. Total Organic Carbon (TOC) and mineralogy were additional criteria used to characterize fine lithofacies. Kerogen type and quality (Rock-Eval Pyrolysis), as well as TOC, were used in the correlation of facies and depositional environments.

5.4. SEDIMENTARY FACIES AND MICROFACIES ANALYSIS

5.4.1. General Aspects

Twenty-one facies and microfacies were recognized in the studied succession summarized in Table 1. It comprises basically fine-grained siliciclastic rocks (less than 33% of carbonate), organic-rich shale (> 5 wt%), carbonate breccia, marlstone (between 33% and 66% of carbonate), evaporites, rhythmite composed of shale-carbonate and peloidal carbonate (> 66

% of carbonate). The most prominent feature of these deposits is the rhythmical intercalation of carbonate and black shales beds throughout the basin, continuously observed for hundred kilometers (Fig. 2). 50 m-thick mixed siliciclastic-carbonate Irati succession overlies siliciclastic deposits from the Palermo Formation and is overlaid by dark grey shales of the Serra Alta Formation. The first 10 m of the Serra Alta Formation exhibits the last carbonate laminae interbedded with the shale and complement the studied succession. From south to north of the Paraná Basin, the succession shows a lateral variation of the carbonate/terrigenous relationship. The carbonate/terrigenous ratio increases gradually northward of the basin. The gamma-ray profiles for the southernmost basin corroborate the siliciclastic facies over carbonate rocks (e.g. Xavier *et al*., 2018). In the central portion of the basin, this ratio is 1:2.5 to the Assistência Member while in the northernmost border occur mainly carbonate-rich lithotypes, reaching 15-50 m. it is particularly observed in open-pit of quarries and road cuts and is poor in fossil content, despite the Assistência Member hosting abundant mesosaurid reptile bodies fossil. Few fish bones, *Chondrichthyes* tooth, ostracods, and bryozoan fragments are found sporadically.

The sedimentary facies were grouped in three associations that indicate deposition in a homoclinal shallow marine unrimmed platform (Tables 1, 2, Fig. 3). The mixed carbonate-siliciclastic facies of Irati can be individualized in the outer-mid ramp and offshore, according to Burchette & Wright (1992).

5.4.1.1. Post-depositional Features

Carbonate breccia (Fig. 5A) forms a conspicuous horizon (0.3 to 6 m) at the base of Assistência Member (Fig. 03). They have a highly complex fabric varying from matrix-, clast-support to fractured- and undisturbed beds. The breccia is composed of (i) dolostone clast with submillimeter lamination (~50 µm), and micro dome features similar to the underlying finely-laminated dolomudstone microfabric; (ii) intraclasts with identical texture and structure described for the laminate fenestral carbonate facies; (iii) intraclast of peloidal packstone with macro- (100 a 50 µm) and micropeloids (~10 µm); (iv) dolomudstone intraclasts and; (vi) silicified clasts. Besides the pervasive calcite and pyrite cementation, length-slow chalcedony is also present. Plus, the breccias interval are rich in vugs, commonly filled with oil. A common feature observed within the breccias clast are V-shaped fractures infilling by booklet kaolinite, insoluble residue, or cemented by calcite. Carbonate nodules are commonly observed over the

breccias layers with dissolution channels and sometimes with geopetal structure, represented by polymict rounded clasts.

The dolostone layers are rich in nodular chert and elongate chert lenses, mainly concentrated at the base of the succession. Oriented nodular chert or silex lenses also are replacing carbonate clast in the breccias. The concentration of yellow nodular chert forming layers with grading from clast- to matrix-support (~40 cm) are common in the siltstone/mudrock rhythmite (Fig. 5B). Nodular cherts have a rounded shape with variated sizes. It occurs within or bordered by siltstone lamination which disrupted the original shale fabric. Some nodules show pyritized border similar to micritization of carbonate grains. Also, silica lenses oriented to the shale lamination can reach up to 5 cm.

Black shale with 5 cm to 3 meters presents massive to cubic pyrite (Fig. 2), reaching six centimeters oriented parallel to the lamination. Pyrite is a common mineral in this succession, but centimeter pyrite occurs within fractures, breccia, and shale. The fractures and pores within the carbonate layers are filled by oil or cemented by pyrite, calcite, dolomite, and chalcedony. The centimetric pyrite is generally associated with sills of basalt related to the thermal effect of the Serra Geral Formation commonly associated with upper Assistência Member (Fig. 2). Local tectonic deformation is indicated by smooth and drag folds with flanks reaching one meter of length, bounded by normal faults with centimetric to metric displacement, modifying the primary bedding.

Sedimentary dikes including the small ptygmatically folded dykes occur crosscutting the carbonate-shale layers. centimeter dykes have v-shape with eroded borders and filling of structureless siliciclastic or carbonate material. The carbonate infill also can have a brecciated internal structure. In the ptygmatically folded dykes is possible to observe the source bed. They are common in the micro-scale interbedded carbonate-shale with variable organic matter content. Most commonly, the dykes are isolated filled by siliciclastic, but mostly of micrite, according to the source bed. Dikes are associated in the same interval with the synsedimentary and soft-sedimentary structures.

Cone-in-cone structures forming layers of 10 to 30 cm is observed within the shales of Taquaral Member. They occur punctuated with thin lenses of grey to black claystone, just below the layers of carbonate breccias. Unlike the breccias, the distribution of these structures is not continuous in the section. The vertical and inclined growth of the crystals generated stacked cone-like structures that encompass shale fragments, forming discontinuous and deformed lenses between the growth planes. Calcite 'beef' comprises thin layers of fibrous calcite with fibers oriented perpendicular to the flat bedding, conformable and interspersed with the organic-

rich shales, distributed at various levels in the Assistência Member and Serra Alta Formation. Bedding-parallel fibrous calcite veins are common in fractures across the succession.

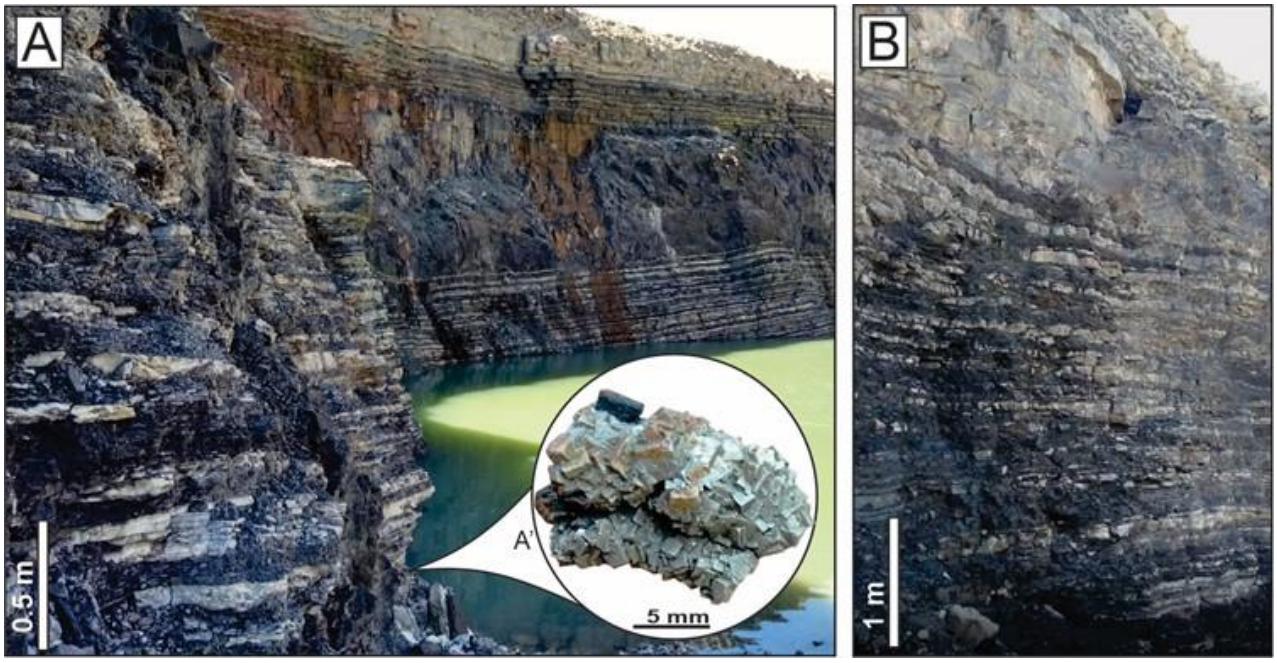

Fig. 2. The mixed deposits from Irati Formation in the Partecal quarry, in the northeastern Paraná Basin. A) The rhythmic interbedded fine siliciclastic/carbonate deposits are organized in laterally continuous tabular layers related to the Assistência Member, with euhedral pyrite crystals in A'. B) Detail of organic-rich shale alternating with dolostone.

Table 1. Summary of the facies and microfacies descriptions followed by the depositional process of Irati Formation.

Facies / Microfacies	TOC (wt%)	Description	Sedimentary process
Mudrocks			
Finely-laminated kerogen shale	**10-27**	Well-developed parallel-orientated homogenous fabric with fragmented phosphatic fishbones, kerogen, and oriented pyrite crystals.	Organic and silty clay decanted in an anoxic environment. Granulometric segregation due turbidity.
Graded kerogen shale		Even parallel lamination with a normal gradation from silt-rich, clay- to thinner organic-rich triplets or siltstone/claystone couple laminae	
Wavy-crinkly laminate shale	**2-10**	Interbedded siltstone and mudstone in an undulate pattern with discontinuous or isolated silt-rich lenses	Induced microbial activity with trapping and bind of silt and flocculated muds during growing of mats.
Laminated silt-shale		Even parallel lamination exhibit lateral pinch and swell geometry downlapping in low-angle siltstone laminae forming kerogen- to clay-rich couplets.	Bedload transport of silt and flocculated muds by weak currents
Dark-grey mudstone	**< 2**	Dominated by oriented clay minerals (>95%) with homogenous fabric or fainting laminated	Suspension fall-out of mud within dysoxic to anoxic conditions.
Massive to laminated siltstone		Centimeter lenses of bioturbed grey siltstone	Fall-out of fine sediment followed by infaunal colonization.
Heterolithic sandstone/mudstone		Light grey and grey-greenish fine sandstone to siltstone forming ripples with cross-lamination interbedded with dark-grey mudstone. Highly bioturbed	Oscillatory dominated flow with alternating traction and suspension. Episodic bioturbation
Mixing lithologies			
Graded sandy shale	**2-10**	Upward gradation of 1 to 4 mm-thick of wavy, cross-lamination to even parallel laminae, and diffuse bedding composed of fine sand, silt, and clay particles.	Grading generated by low-density turbidity flow.
Siltstone/mudrock rhythmite		Thin interbedded grading laminae of siltstone/claystone/OM and carbonaceous shale, separated by quartz-rich siltstone lenses.	Alternance of suspension and faint current during turbidity flow
Lenticular dolomitic shale	**2-5**	Clay-rich interbedded with peloidal carbonate-rich laminae of ~2mm-thick, flattened dolostone fragments silt size and microspar to spar calcite.	Fall-out of suspended-load material and bio-induced carbonate precipitation
Laminated dolomitic shale		Oriented micro-carbonate intraclasts, clay material, and pyrite	Biologic-induced carbonate precipitation, seldomly influenced by an oscillatory flow.
Graded marlstone		Mm- to cm-planar beds or cross-laminated strata, grading from siliciclastic- to carbonate-rich mudstone.	Suspended-load alternate with episodic oscillatory flows.
Laminated to massive marlstone		Oriented peloids and clays or structureless homogenous fabric	Fall-out of suspended-load material and bio-induced carbonate precipitation

Carbonates rocks			
dolowackestone with ostracods		Micropeloidal (~10 µm) matrix with intraclasts and rare ostracods and bryozoan fóssil fragments	High energy flow reworking the bottom of the basin
Organic-rich dolomudstone		Submillimeter to insipient peloidal lamination. Grumose texture, with oriented clay floccules, AOM*, and pyrite.	Biologic-induced carbonate precipitation in a hypersaline, calm, and restricted setting with terrigenous inflow. High energy flow.
Finely-laminated dolomudstone		Slightly crenulated dolomitic laminae. Siltstone films, pyrite, and pseudomorphs of gypsum highlight the lamination.	
Laminated to massive peloidal dolomudstone		Massive to cross-laminated or slightly laminated composed of peloids and silt-sized (~50µm) intraclasts with preferential orientation with irregular vug porosity.	
Lithoclastic dolopackstone		Massive peloidal dolomitic intraclasts (~2 mm) and chert nodules (~0,6mm).	Episodes of high energy flow reworking the basin floor
Shell-rich dolograinstone		Bivalve shells molds concentrations cemented by calcite equigranular microspars (~20µm)	
Laminate fenestral dolostone		Dark laminae with silt grains alternating with light and porous dolomite laminae. The light laminae have gypsum pseudomorphs.	Biological-induced lamination linked to microbial activity in calm and saline waters.
Mudstone with gypsum pseudomorphous		Continuous but thin centimetric beds. It has massive structure, grumose texture with graded and oriented gypsum pseudomorphous, replaced by calcite.	

* AOM: amorphous organic matter

Table 2. Facies and microfacies of each paleoenvironment of the mixed siliciclastic-carbonate Irati Sea.

Facies/Microfacies	**Paleoenvironment**
	Offshore
Finely-laminated kerogen shale	
Massive to laminated siltstone	
Graded kerogen shale	
Dark-grey mudstone	
Graded marlstone	
Massive marlstone	
Graded sandy shale	
Laminated silt-shale	
Lenticular dolomitic *shale*	
Laminated dolomitic *shale*	
Organic-rich dolomudstone	
Siltstone/mudrock rhythmite	
Finely-laminated kerogen shale	Outer-mid ramp
dolowackestone with ostracods	
Laminated silt-shale	
Graded sandy shale	
Graded marlstone	
Mudstone with gypsum pseudomorphous	
Shell-rich dolograinstone	
Lenticular dolomitic shale	
Lithoclastic dolopackstone	
Laminate fenestral dolostone	
Finely-laminated dolomudstone	
Laminated to massive peloidal dolomudstone	

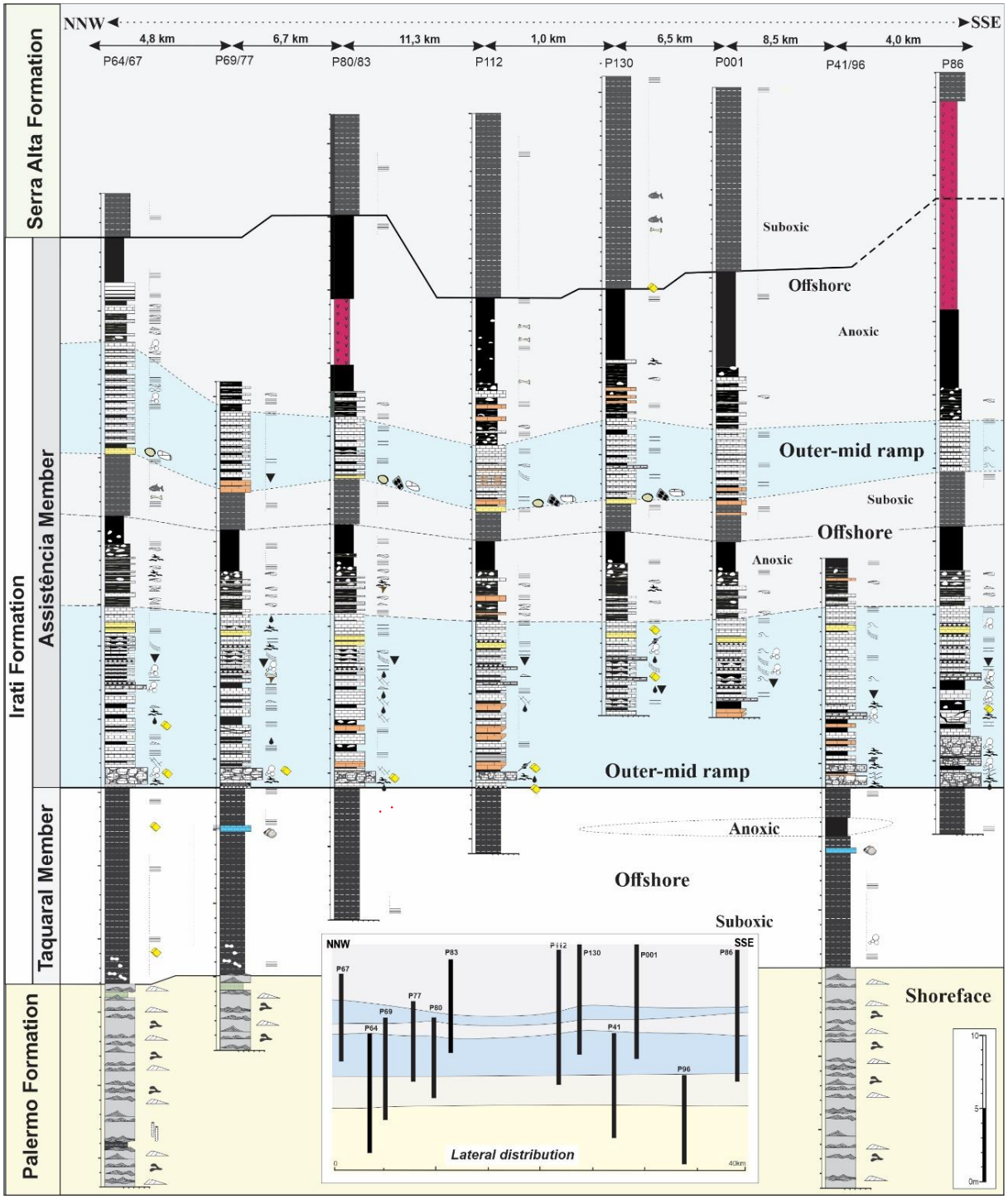

Fig. 3. Lithostratigraphic logs of the studied succession with the correlation of described drill cores facies. Legend of lithology and sedimentary structure in Fig. 4 and drill cores location in Fig. 1.

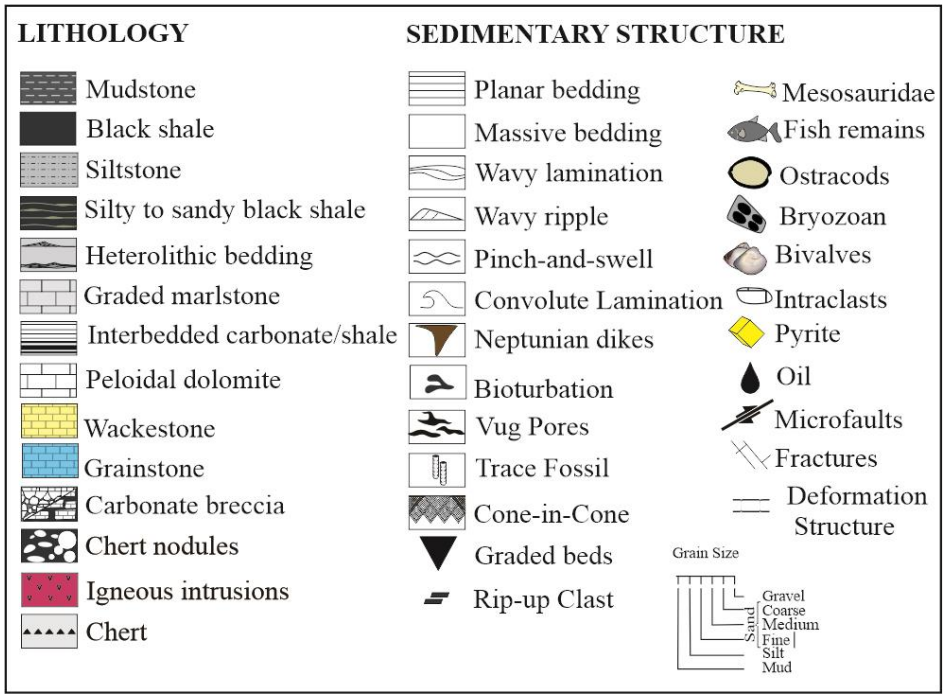

Fig. 4. Legend of the features described in the logs in Fig. 3. Corrigir pores

5.5. FACIES ASSOCIATIONS

5.5.1. Offshore Facies

The proximal offshore facies have a retrogradational stacking pattern of grey fine sandstone to siltstone lenses interbedded with organic-rich thin layers. It is composed of siltstone/mudrock rhythmite, graded sandy, and laminated silt-shale (Fig. 5C and 6A to F) interbedded with 20- to 50-centimeter thickness of laminated dolomitic shale, organic-rich dolomudstone, or less frequent, lenticular dolomitic shale, massive, and graded marlstone. The most distal stratal succession composes deposits of expressive lateral continuity (> 500 km) and regular thickness, characterized by the siliciclastic facies and microfacies of dark-grey mudstone, massive to laminated siltstone, finely-laminated and graded kerogen shale. Finely-laminated shale is the richest in organic matter (up to 23 wt%) and total sulfur (~8 wt%) with rare fossils of mesosaurid reptiles. On the other hand, the dark-grey mudstone facies are relatively organic-poor (TOC less than 2 wt%). Despite the regularity of the thickness, at a large scale, it shows lateral variation, thicker at the south border of the basin and disappearing to the north, where predominate carbonate facies. The siliciclastic layers at the mesoscale have a dark and massive structure appearance. Although in thin sections, are possible to differentiate the

microstructure patterns composing well-defined submillimeter laminations. Usually, the lamination is macroscopically visible only at outcrop due to the action of weathering processes.

The retrogradational stacking patterns have graded sandy- and silty shale varying to laminated silt-shale. Discontinuous sandy- and silty-rich forming lenses produce pinch-and-swell patterns. The lenses are rich in carbonate silt-size fragments and phosphatic fish debris. Fining-upward grading layers compose micro-cycles (~1.0 to 4.0 mm) of fine sand, silt, clay, and organic matter commonly with a shaped base. Graded layers occurrence is observed with the planar and undulated lamination. The lamination (graded and ungraded pattern) is marked by lateral truncation. Graded sandy shale microfacies have a well-marked grain-size transition even in the fine sand to silt lenses. Finely-laminated shale has lateral convergence and low-angle with basal downlap evidenced by organic matter and oriented granular pyrite. Within the thicker lamination intercalation of organic-rich and organic-poor laminae can be observed. Proximal offshore deposits facies are rich in organic matter (5 to 10 wt.%) with a gradual transition to the richest offshore facies. The silty to sandy lenses and lamination is composed mainly of quartz, feldspars, peloidal carbonate, and muscovite grains. Oriented AOM and silt-sized pyrite are commonly associated with siltstone lamination. Rare bright green and blue glauconite grains also occur. The lamination is cemented by dolomite and less calcite. The contact with the dolostone layers can be shaped or gradational (forming the marls layers). Bioturbation is rare, locally observed across the section. Organic matter predation features and trace fossils (Fig. 6E and F) are occasionally observed.

Finely-laminated shale microfacies have a well-developed parallel orientated fabric that is eventually interrupted by the bifurcation of siltstone lenses (Fig. 5D). When associated with organic and claystone laminae it forms a wavy lamination pattern. The nanometric organic and clay laminae in those microfacies can be varying to thicker millimeter lamination with grading fabric formed by silt/clay/organic matter. Seldomly predation features of the organic-rich laminae are present (Fig. 5E). The microfacies are rich in oriented AOM and phosphatic micro-fragments, possible fish remains. The lamination is marked by prominent lenses of oriented millimeter crystal of pyrite with the siltstone lamination (Fig. 6J). in the outer ramp to offshore shale facies, the fossil content is frequent. Throughout the vertical section, *Palaeonisciformes* and *Chondrichthyes* were observed only in the dark-grey mudstone (Fig. 7A to C). Ostracodes and mesosaurid reptile fossil fragments (Fig. 7F to I) are the only ones observed in both lithologies. Also, oriented chert nodules within and deforming the silt lamination are common (Fig. 7E). At outcrop, preserved specimens of *Mesosaurids* are found, plus centimeter euhedral pyrite.

Dark-grey mudstone facies has very fainting lamination in the base and fine planar lamination or undulated lamination in the top, characterizing a variation from clayey to finely-laminated microfabric. This pattern also shows gradual variation from dark to light-grey and light-greenish grey colors. The clayey shale fabric has small dark burrows that gradually disappear to the top where predominate laminated shale. The typical clayey shale layers have similar textural aspects to the finely-laminated kerogen shale. Although the colors and TOC are here a useful criterion to differentiate both. Dark-grey mudstone facies is dominated by clay mineral (95%) and silt-sized quartz grains, rare feldspars are present. Dolomite peloidal grains also occur forming millimeter lamination interbedded with fine siliciclastic laminae in an undulate pattern. Eventually, thin, and discontinuous layers of massive to laminated siltstone occur interbedded with the dark-grey mudstone close to the top. Cladodont teeth, fish remains, and *Mesosaurus* bones fragments are the common ichthyofossils presents in these facies (Fig. 7).

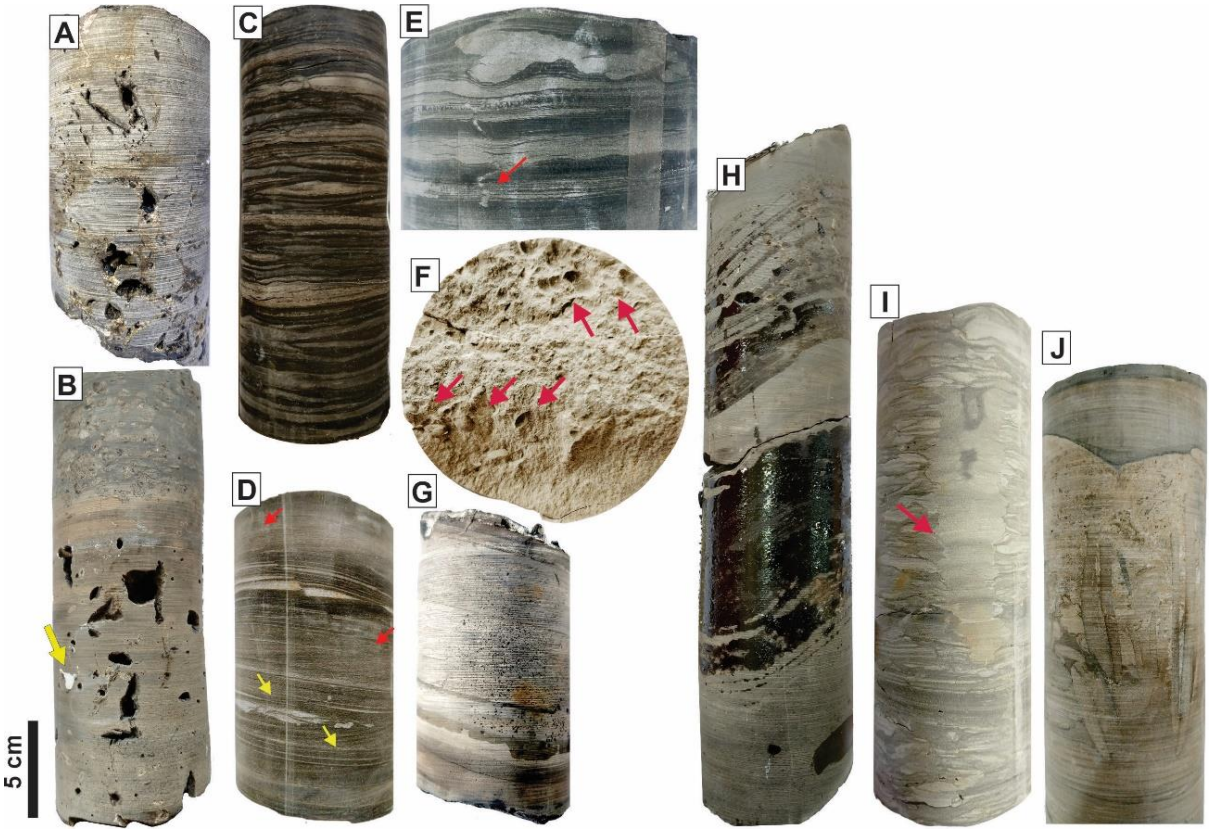

Fig. 5. Core samples showing (A) monomict carbonate breccia rich in vugs and infilled by brown carbonate matrix. B) finely-laminated dolomudstone rich in vugs with rare infilling by calcite (yellow arrow) overlain by silica-rich black shale. Note the brown nodular chert. C) typical siltstone/mudrock rhythmite offshore facies. D) finely-laminated shale with low-angle lamination (yellow arrow) and normal microfaults (red arrows). Note the occurrence of fine sand lenses with scoured bases. E) Graded silty shale showing the organic matter predation and vertically flattened trace fossil (red arrow). F) planar section of the shell-rich dolograinstone. G) Laminate fenestral carbonate with rounded pores following the low-angle lamination. H) deformation low-angle lamination forming pseudo-cross-stratification in the fine dolostone facies evidenced by the oil at the base of Assistência Member. I) the heterolithic bedding with *Teichichnus* (red arrow) of the upper Palermo Formation. J) Edgewise breccia showing the tabular clast with rounded edges of the clasts vertically oriented. The lower ends are penetrating the semi-consolidated carbonate substrate and top with abrupt end overlain by shale layers.

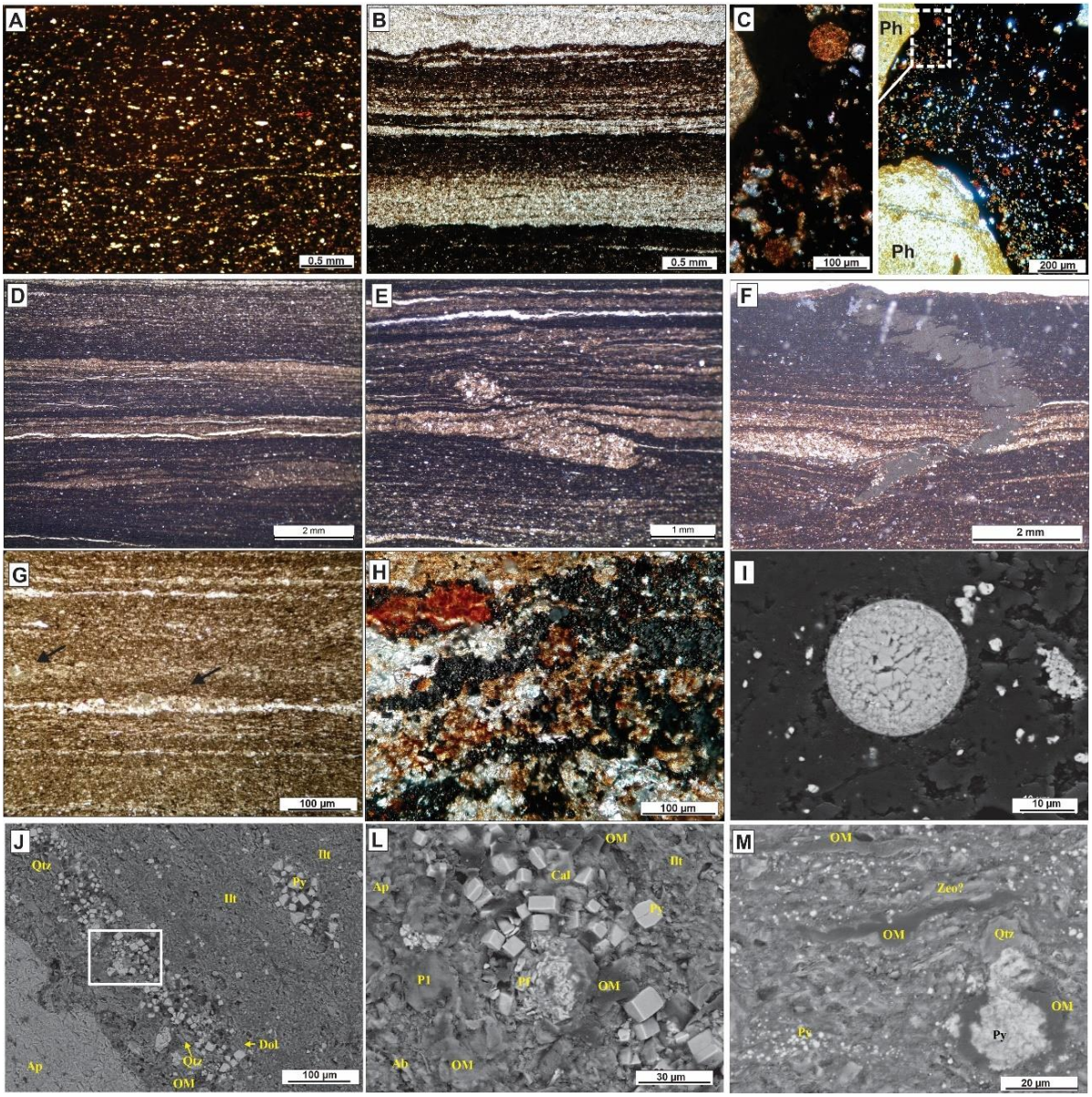

Fig. 6. Photomicrographs of features from the fine-sedimentary rocks of offshore and outer ramp facies. A) Finely-laminated kerogen shale rich in disseminated amorphous organic matter (AOM). B) Kerogen shale with well-defined upward gradation. The bright silt at the base became successively finer upwards where clay and organic matter concentrate. C) Plan view of *Tasmanite* cysts or spores. The preserved spherical shape is due to de early cementation by pyrite in finely-laminated shale. D) Siltstone interbedded with shale laminae with the first composed of siliciclastic and dolostone grains. E) detail of predation of the kerogen lamination and (F) pyritized trace fossil. G) Organic-poor silty shale with the lamination composed of peloidal carbonate grains pointed by the arrows. H) I), J), L) and M) show the variety of pervasive pyritization that dominate the shales of Irati Formation H) massive pyrite cement in silt layers with detail of enveloping AOM. SEM image of (I) pyrite framboids, (J) primary euhedral pyrite surrounding a phosphatic bone. L) details of (J) showing pyrite framboids enveloped by organic material. M) elongated organic matter and pyrite framboids. Also, the oriented bright little points are granular pyrite.

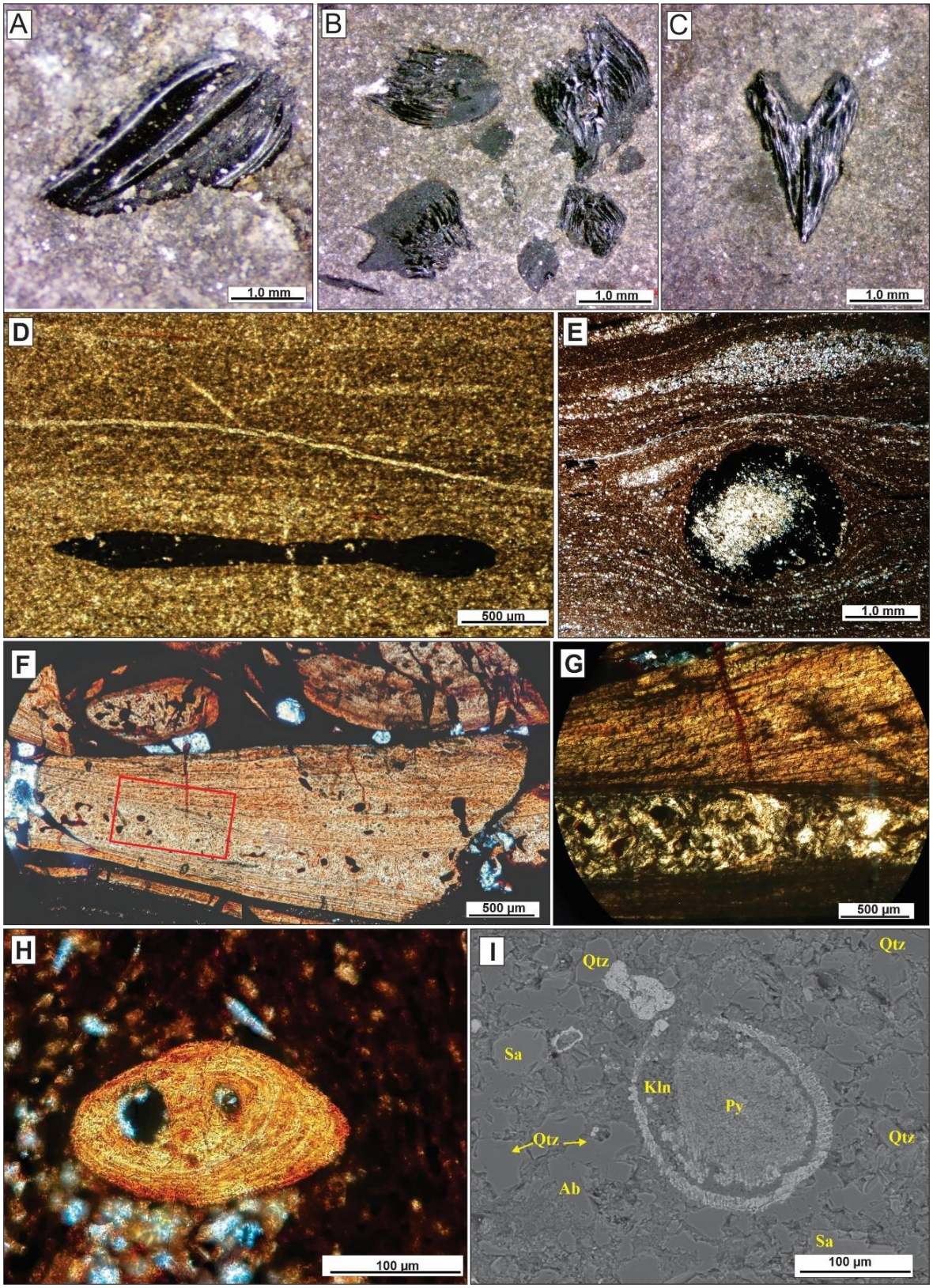

Fig. 7. Detail of the rare fossil content of the Irati Formation Palaeonisciformes with (A) isolated well-preserved *Chondrichthyes* fish scale and (B) forming cumulates. In (C) possible cladodont tooth. (D) large pyritized algal fossil fragment. (E) Silty shale with a chert nodule with a pyritized edge, whose growth deforms the lamination at the base and top. (F) phosphatic bone fragment (mesosaurids?) with detail (red box) of the internal preserved structure in (G) under cross-polarized light. (H) Well-preserved ostracod fossil within silt laminae of bituminous facies and (I) pyritized ostracod within silt laminae. Qtz: quartz, Py: pyrite, Ab: albite, Sa: sanidine, Klm: kaolinite.

Interpretation:

The complex microstructure and microfabric relationship observed within the proximal offshore facies suggest its formation by combined processes under the predominance of anoxic bottom water. Siltstone layers interbedded with organic-rich laminae in a wavy pattern with a predominance of graded layers (fine sand, silt, clay, and organic matter) with sharp basal surface indicate cyclic deposition of fine-grained turbidities (Stow and Shanmugam, 1980; Wignall, 1994; Ulmer-Scholle *et al*. 2014). Likewise, alternation of siltstone and clay/organic matter lamination. The small and smooth channels cutting the underlying shale bedding filled with fine graded sand to silt particles are probable due to turbidity current activity.

The thin-bedded variations with load-casted due to the sinking of siltstone laminae over the unconsolidated mud can generate wavy bedding patterns (Allen, 1982). it can be enhanced by differential compaction of organic matter around silt and carbonate aggregates (Wignall, 1994). Also, the discontinuity of the fine sandstone to siltstone lenses within the mud produces lenticular bedding patterns, suggesting that despite the occurrence of bedload transport, the terrigenous input of grain size greater than 62.5 μm was insufficient to form continuous laminations (Reineck & Singh, 1973).

Scarce but present burrow features with the organic-rich layers exhibiting an anomalous concentration of rounded sand-size grains at the edge of the borrow, grading to fine silt-sized to the center, suggest predation of the organic matter. The bioturbation of kerogen laminae induced local thickness of the silt lenses, forming isolate concentration. Likewise, the rare moments of good oxygenation at the water/sediment interfaces that could be related to turbidities activities and nutrient-rich ground favor the eventual colonization by benthic and endobenthic organisms. Nevertheless, the dominance of organic-rich shales with and gradual transition from the ramp to offshore show a close relationship between the anoxic environmental conditions that prevails in both. In restricted basins, it is common for the outer ramp deposits to be formed by cyclic organic-rich laminae (Droste, 1990) or highly bioturbed which can be confused with lagoon facies (Burchette & Wright, 1992). Dolostone beds interbedded with the black shale facies point to a momentum of low to an absence of siliciclastic input (starvation model). The terrigenous-poor (<3%) dolomudstone with grumose texture, massive or finely-laminated, and laminated peloidal dolomudstone. The laminated dolostone has lines of oriented siliciclastic and pyrite silt grains evidencing the lamination. The very low angle of the ramp also allows bottom current easily carry-out mid-ramp deposits due to the fast shift of the shoreline from transgressive to regressive patterns.

The fine siliciclastic rocks with massive structures to finely-laminated and the lack of current-induced sedimentary structures indicate deposition from suspension in a calm, subaqueous environment below the wave base. Thin cyclic graded layers at the distal portion of the platform, from which the gradation is well-defined particle-by-particle are usually the result of detached turbid layers due to weakly turbidite currents flowing along the top of the pycnocline (Wignall, 1994). The gradual transition of the ramp and offshore facies dominated by graded beds, plus the homoclinal configuration and very low angle of the ramp, suggest that the fine graded layer share a similar process. In ramp dominated by storms that could be related to distal storm deposits, as previously described elsewhere (e.g. Reineck & Singh, 1972; Schieber, 1989). Nevertheless, the here described deposits do not show evidence of storm events.

Finely-laminated shale from which lamination is apparently parallel but in close petrographic examination show low-angle downlap and lateral convergence across the section are a result of bedload transport of the flocculated mud and silt grains by bottom current (Schieber *et al*., 2007; Schieber & Southard, 2009; Ulmer-Scholle *et al*., 2014).

The predominance of prevalent bituminous shale across the ramp (>500 km) indicates deposition below the aerobic/anaerobic interface in a stagnant and flat environment bottom. The presence of pyrite as framboidal, forming lenses within the silt lamination (Fig. 6H to M) and pyritized fossils (Fig. 7D and I) indicate primary origin similar to described by Berner (1984) and Raiswell and Berner (1985), high enough to be reprecipitated as euhedral cubic cement during diageneses. Plus, the absence of bioturbation and high TOC values suggest well-established anoxic bottom water (Thickpenny, 1984). Organic rich lamination rhythmically interbedded with silt and clay imply strong seasonal climate control on the organic matter production, possibly related to algal bloom. Martins *et al*. (2020) observed a high concentration of C_{17} long-chain alkylnaphthalenes related to algal blooms events as a result of freshwater inflows. The grey to black claystone facies less rich in organic carbon (~1 wt%) and the local presence of bioturbation, close to the contact to bituminous shale facies with gradual change of color and pyrite content indicates a rapid rise of oxygenation alternating with anoxia events before oxygenating condition fully dominates the environment.

5.5.2. Outer-mid ramp facies

Continuous metric layers, essentially composed of peloidal dolomite or micritic matrix, form massive to laminated dolomitic layers that occur interbedded with millimeter to meter-

scale layers of black shale. The succession has mudstone with gypsum pseudomorphous, fenestral laminate dolostone with *vug* porosity, finely-laminated dolomudstone, overlaid by lenticular dolomitic shale, grading to laminated shale or graded marlstone. Light grey to beige peloidal dolostone and the thin black shale layer intercalation is interrupted by cyclic graded marlstone. Shell-rich dolograinstone, lithoclastic dolopackstone, and wackestone with ostracods have local occurrence.

Laminate fenestral dolostone (Fig. 8A to C) has a well-defined, essentially dolomicrite lamination, with oriented spaces silt-grain and laminoid-fenestral fabrics and rounded (40-100μm) to elongated pores (~2.4 mm) partially cemented by calcite, pyrite, or chalcedony. The oil infilling pores make the low-angle lamination visible at core samples (Fig. 5G). The variable degree of deformation even forms pseudo-cross-stratifications (Fig. 5H). The essentially dolomitic laminations are rich in gypsum pseudomorphs replaced by calcite. The progressive upward increase of pseudomorphs forms the mudstone with gypsum pseudomorphous facies (Fig. 9D to E). They are thin centimeter layers with a grumose texture and dolomicritic matrix. Commonly associated occurs finely-laminated dolomudstone (Fig. 8D to G) and organic-rich dolomudstone. The last one is common in the distal layers rich in silt-sized siliciclastic grains and phosphatic fish bones fragments (Fig. 9A to B). Millimeter euhedral pyrites are common in these facies forming oriented lenses conformable to the bedding. The massive dolostone beds have an oriented fabric composed of peloids or intraclasts and amorphous organic matter (AOM). Pyrite and clay minerals are also present.

The peloidal dolomudstone microfacies with homogeneous fabric can present preferential orientation of the peloids and are cemented by calcite and chalcedony. These microfacies vary vertically to packstone composed of peloidal intraclasts. Massive peloidal framework also can have a lenticular fabric composed of reworked dolostone fragments (Fig. 9G). Dolowackestone with ostracods microfacies (Fig. 9F) are rich in silt-size carbonate clasts and also present bryozoan fragments. They are observed in longitudinal thin section and has a lattice-like appearance with thick laminated zooecial walls and internal pore filled with microcrystalline calcite cement, resembling fenestrate bryozoans.

The carbonate-shale couplet occurs with shaped contact and pure endmembers (Fig. 10G, H, I) or forming mixing intervals of (i) laminated shale, composed of oriented micro-carbonate intraclasts and clay material; (ii) graded marlstone, characterized by about 2 mm-thick of fining upward lamination or forming centimeter beds (Fig. 10B). In thin sections the first one shows variation from massive dolomicritic to clayey shale in which oriented and flattened peloidal carbonate fragments are rounded by thin dark clay films, forming the

lenticular texture (Fig. 9G). At the base of the succession the carbonate material of the lenticular fabric is represented by structureless peloidal mud; (iii) Lenticular dolomitic shale is characterized by films of clay and organic matter surrounding the amalgamate silt- to fine sand-size fragments of carbonate form the lenticular fabric. Oriented grains of quartz and feldspars are also present. The microfacies can occur with clay-rich alternating carbonate-rich lamination well-marked by pyrite-rich silt lines. Within the thin shale interbedded the carbonates, rare glauconite grains are present.

The uppermost heterolithic bedding forms centimeter-to-meter beds of black shales and dolostone with wavy top and planar bedding. Low-angle bidirectional cross-stratification with reactivation surface and internal well-defined truncated lamination are observed in cores, resembling a close view of wave ripple structures. Soft-sedimentary deformation (e.g, convolute lamination, ptygmatically folded dykes) and load structures are commonly associated with those intervals. The package has abrupt or gradational contact with thicker carbonate layers characterizing stacked asymmetrical shallowing upward cycles.

Isolate thin bed (few centimeters) of dolograinstone (Dg) with bivalve shell molds concentrations occur at the distal portion within a thick package of the offshore grey mudstone. The shells are millimeter-sized that in core samples does not present preferential orientation with packstone fabric in massive pseudospars dolomite. The molds are of complete shells or disarticulated valves and also, fragmented molds. The carapace shell itself is not preserved (Fig. 5F).

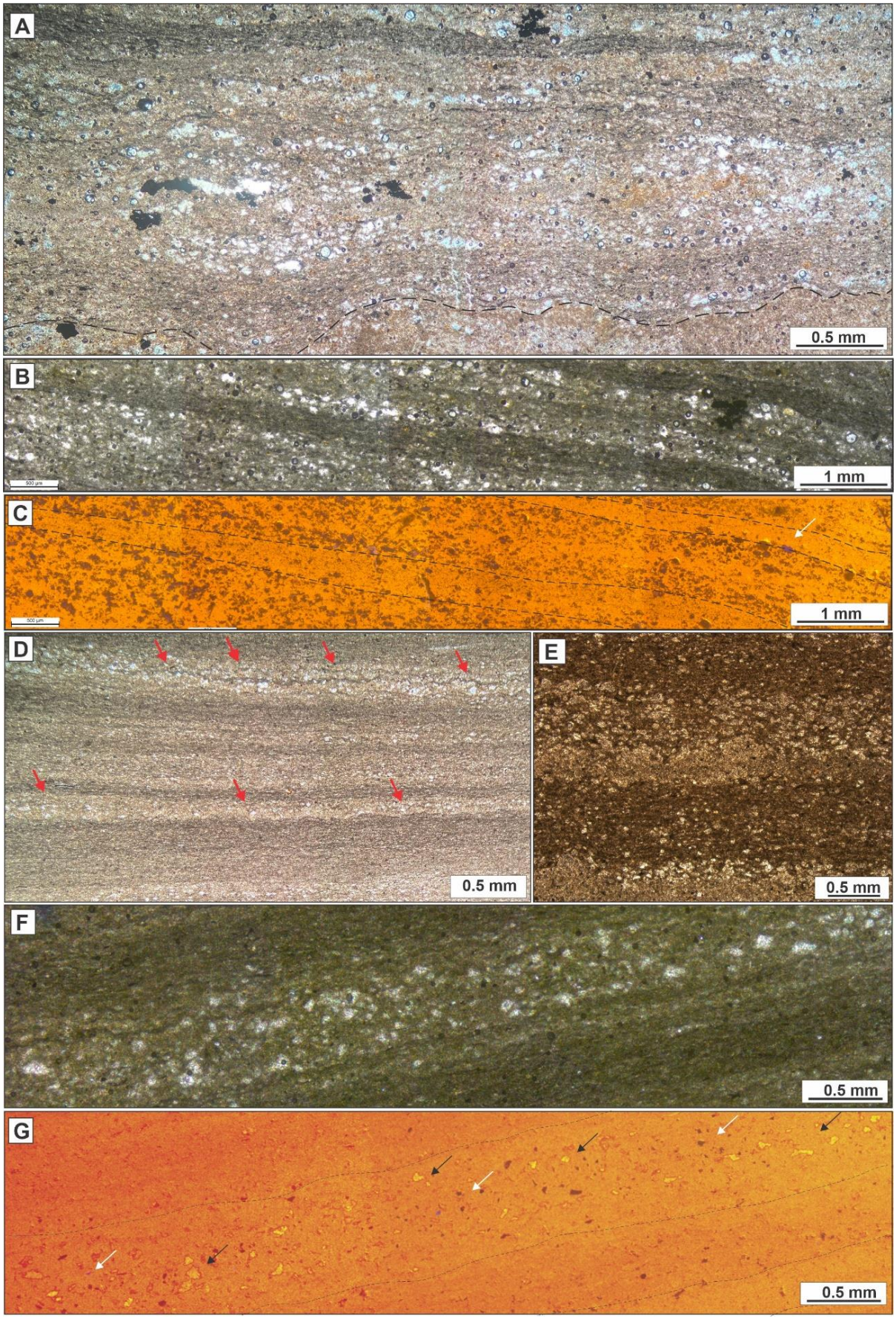

Fig. 8. Photomicrographs of the microbial dolomudstone microfacies. A) Lateral variation of the laminate fenestral carbonate facies showing oriented fenestrae pore and deformed wavy-like lamination.

The dark points are pyrite and the bright elongate points are fenestrae. B) detail of the low-angle lamination in the laminate fenestral carbonate facies and C) under cathodoluminescence showing the oriented pore fabric. D) Finely-laminated dolomudstone with slightly crenulated lamination interbedded lamination with gypsum pseudomorphs. E) local variation of (D) show thicker lamination of dark and bright (with gypsum pseudomorphs-rich) dolostone. F) Similar to (B) these facies have psedoestratification with oriented pores fabric. The low-angle lamination showing the oriented pseudomorphs replaced by calcite, and (G) under cathodoluminescence showing the two generation of calcite cement (black arrow) and the presence of oriented and very small micrometer siliciclastic grains (white arrows).

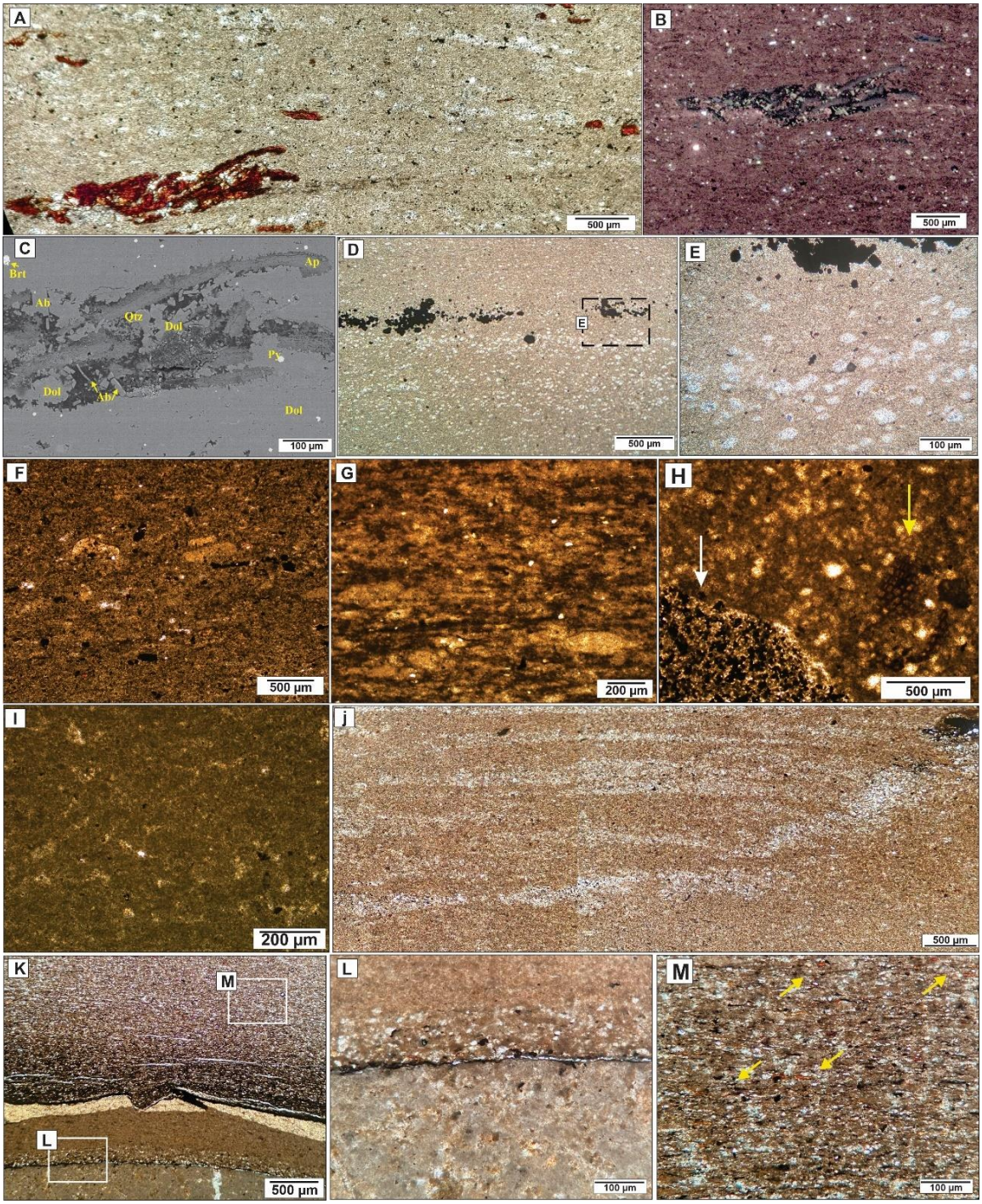

Fig. 9. Photomicrographs of the dolostone and mixed facies. A) Organic-rich dolomudstone with irregular lamination marked by oriented phosphatic and silt grains. B) a closer view of (A) under

cathodoluminescence showing the bright preferential oriented siliciclastic grains. C) SEM image of a detailed perspective of a phosphatic fragment with preserved internal structure. Ap: apatite, Ab: albite, Brt: barite, Dol: dolomite, Py: pyrite, Qtz: quartz. D) Mudstone with gypsum pseudomorphous with pyrite lenses and homogeneous fabric. E) Closer view of the gypsum pseudomorphs infilled by calcite and the idiotypic pyrite. F) peloidal dolowackestone with a rare concentration of reworked ostracodes G) A closer view of the flattened lenses of the lenticular shale. H) Fragment of diatoms in a breccia clast of evaporitic carbonate facies. Detail of the pyrite-rich peloidal matrix infilling (arrow). I) Plane-polarized light of the peloidal fabric. J) Laminated dolomudstone with levels of bioturbation disrupting the lamination. K) The peloidal dolomudstone and graded marlstone facies limit are marked by a thin and tabular lens of chert. L) the local lamination of the peloidal dolomudstone can be evidenced by dissolution seams. M) Graded marlstone showing the preferential orientation of the phosphatic fragments, pyrite, and micropeloids.

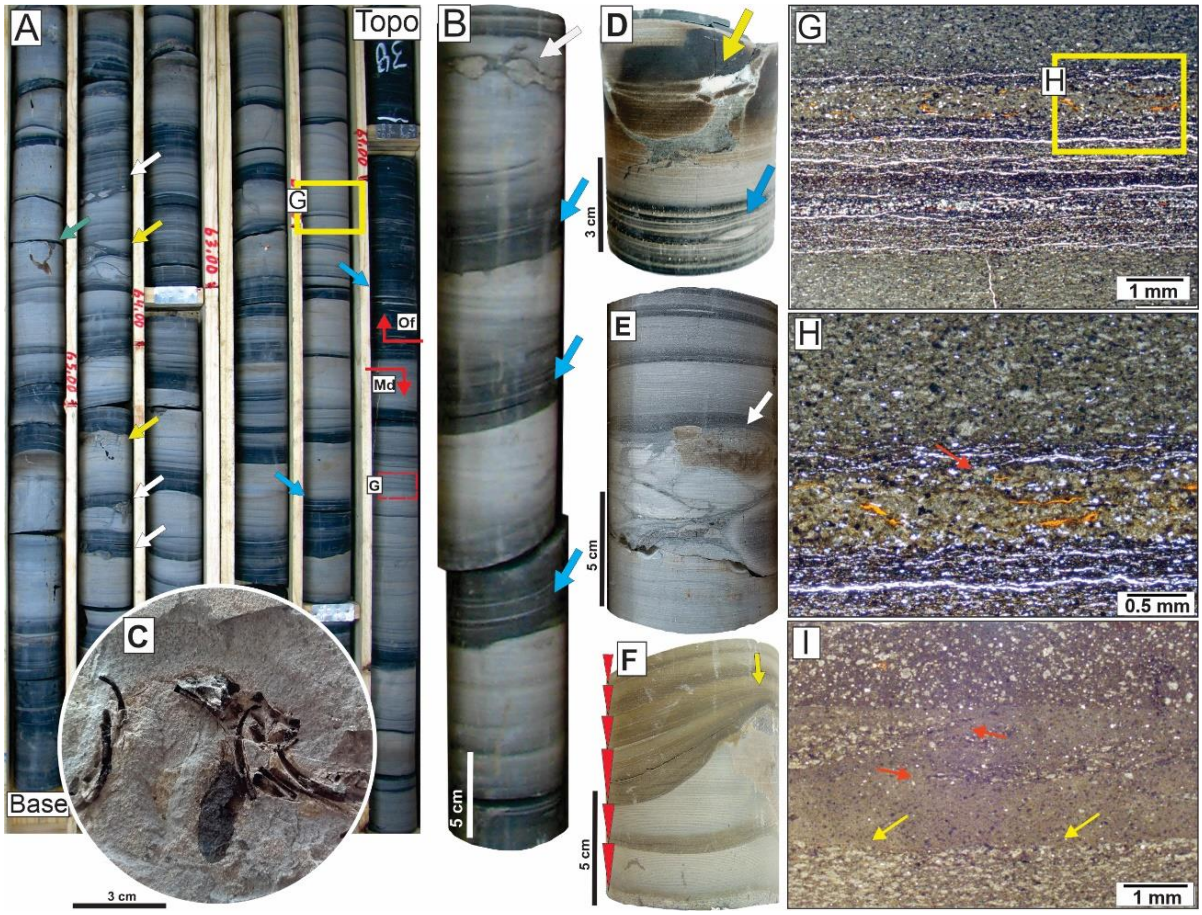

Fig. 10. Photographs of the well-bedded dolostone-shale. A) core log showing fining upward beds with an upward increase of the carbonate/shale ratio. White arrows are nodular cherts. Note the levels of soft-sediment deformation in the dolostone beds top (yellow arrows); thin lenses of fine sandstone within shales bed (blue arrows); and enhanced fracture by dissolution (green arrow). B) cyclic graded beds with even parallel and cross-lamination. The blue arrows pointing bright fine sand laminae at the base of the cycles. C) detail of phosphatic bones of mesosaurid reptiles within peloidal dolomudstone. D) thin reworked carbonate layer with chalcedony cement (yellow arrow). The Blue arrow points to a small ripple. E) milimeter well-bedded dolostone-shale overlying thin layers of conglomerates with reworked chert clast (white arrow). F) Graded marlstone with injection dyke infilled by nodular chert, carbonate matrix, and chalcedony cement. Photomicrographs of the thin heterolithic carbonate layers. G) lamina-set of well-bedded dolostone -shale with oriented fish bone fragments, detailing in (H). Note the lithology cyclic repetition preserved in millimeter-scale with both well-preserved lithologies. Detrital

glauconite (yellow arrows). The cyclic carbonate fabric can vary from peloidal to (I) lenticular formed by flattened reworked sand- to silt-size carbonate fragments. Note levels of reworked lenticular fabric.

Interpretation:

The rhythmical intercalation of organic-rich shale facies (TOC up to 8%) with massive to even laminated dolostone without any evidence of subaerial exposure suggests deposition below the fair-weather wave base. The fine-scale carbonate lamination slightly crenulated is possible cryptalgal limestones analogous to algal laminae in modern shallow carbonate environments (Shinn. 1983; Aigner, 1985) and previously described by Araujo (2001). They are formed by biologically induced seasonal precipitation of carbonates (Mann, 1995; Braissant *et al*., 2007; Zhu & Dittrich 2016; Ortega-Villamagua *et al*., 2020). Pseudomorphic replacement of sulfate minerals (e.g. gypsum, anhydrite) by calcite associated with finely-laminated dolostone and occurrence of early length-slow chalcedony cement also indicate a shallow and hypersaline environment (Folk & Pittman, 1971; Demicco & Hardie, 1995; Flügel, 2004). The gradual increase to form laminated mudstone with gypsum pseudomorphous facies indicated increasing in the hypersaline conditions, possibly related to shallowing-up. Moreover, the presence of primary pyrite, forming lenses in the shale and carbonate facies also indicates anoxic conditions.

The stressful conditions record in the first meters of the Assistência Member is attested by the absence of bioturbation and any other fossil record indicating faunal colonization. Even the phosphatic fish-bones fragments common within other facies were not observed. The prevailing inhospitable environment that remained in the Irati Sea avoided the complete establishment of benthic communities. Evidence of bioturbations on the platform even in the more proximal facies was rare. Characteristic facies of high energy typical of shallow waters (wave, tide), was not observed (e.g. Araújo, 2001; Hachiro, 1996; Lavina *et al*., 1991; Xavier *et al*., 2018). The lack of effective wave and tidal action is due to the Irati Sea being a wide, restricted, and shallow platform that creates a protected environment. Facies analysis and modeling suggest that epeiric seas were mostly microtidal, or even virtually non-tidal (Pratt, 2010).

Fine-grained peloidal carbonate rocks are generally regarded as typical of shallow, low-energy, restricted marine environments (Flüge, 2004). Packstone microfacies with silt-sized intraclasts and millimeter peloidal intraclasts were locally observed, suggesting little wave action capable of reworking the substrate. The absence of prominent erosion features suggests low-wave energy. The dominance of peloidal mud is compatible with the dissipative

morphology reinforced by the smooth gradient (0.0004° to 0.0015° according to Araujo, 2001) in which the damping of wave action favors the formation of typical facies of protected environment (Wright, 1984). In shallow and hypersaline marine carbonate, the sediments are often dolomitic due to the particular water chemistry and hydrology that may develop in the environment (Pratt, 2010). Algal-laminated sediments will form in the uppermost shallow settings (Shinn, 1983). About ninety-three percent of the package are dominated by rhythmical intercalation of the dolostone and shale facies, forming shallowing upward patterns and thinning-up bedding in an aggradational pattern.

The distal dolograinstone with shell molds concentration occurrence within the thick shale package suggests high energy to transport the shell from the oxygenated photic shallow sea to the distal anoxic bottom water, during episodic events of shallow seafloor reworking and long-distance transportation across the ramp.

5.6. GEOCHEMISTRY

5.6.1. Organic Geochemistry

Five hundred samples from ten drill cores of central east the basin show a close relationship of the kerogen type with the facies association present here (Fig. 11). Plus, the gradual facies transition is also reflected in organic geochemistry profiles. Fig. 12 shows the gradual increase of organic matter content and source rock potential. Likewise, the abrupt shift record by organic parameters in the offshore finely-laminated kerogen shale to dark-grey mudstone facies is due to a whole change in the anoxic bottom water condition. The outer-mid ramp shales also have a gradual increase toward the outer ramp portion.

The distal organic-rich offshore facies are the richest oil shale deposits. The Assistência Member comprises two thin and richest economic intervals of the Brazilian intracontinental basins. The first one record between 2.16 to 25.7 wt% of COT and the uppermost about 1.80 to 19.25 wt% with average source rocks potential respectively of 102.32 and 63.90 mg HC/g Rock. Hydrogen Index has average values of 698.68 mg HC/g TOC. A vertical and lateral variation of the organic matter quality and content presents the higher values for the central basin. The same pattern can be observed from the other organic-rich facies. The facies have *oil-prone* kerogen type I and II with a high contribution of type IV on the eastern border. The shale and marlstone facies of the well-bedded dolostone-shale facies predominate the typically marine kerogen type II. The organo-geochemistry composition of the dark-grey mudstone facies is relatively constant low (< 2 %) across the study section, reaching 3 % and source

potential of 4.22 mg HC/g Rock, which is relatively low when compared to the offshore organic-rich facies. the kerogen type is III and IV.

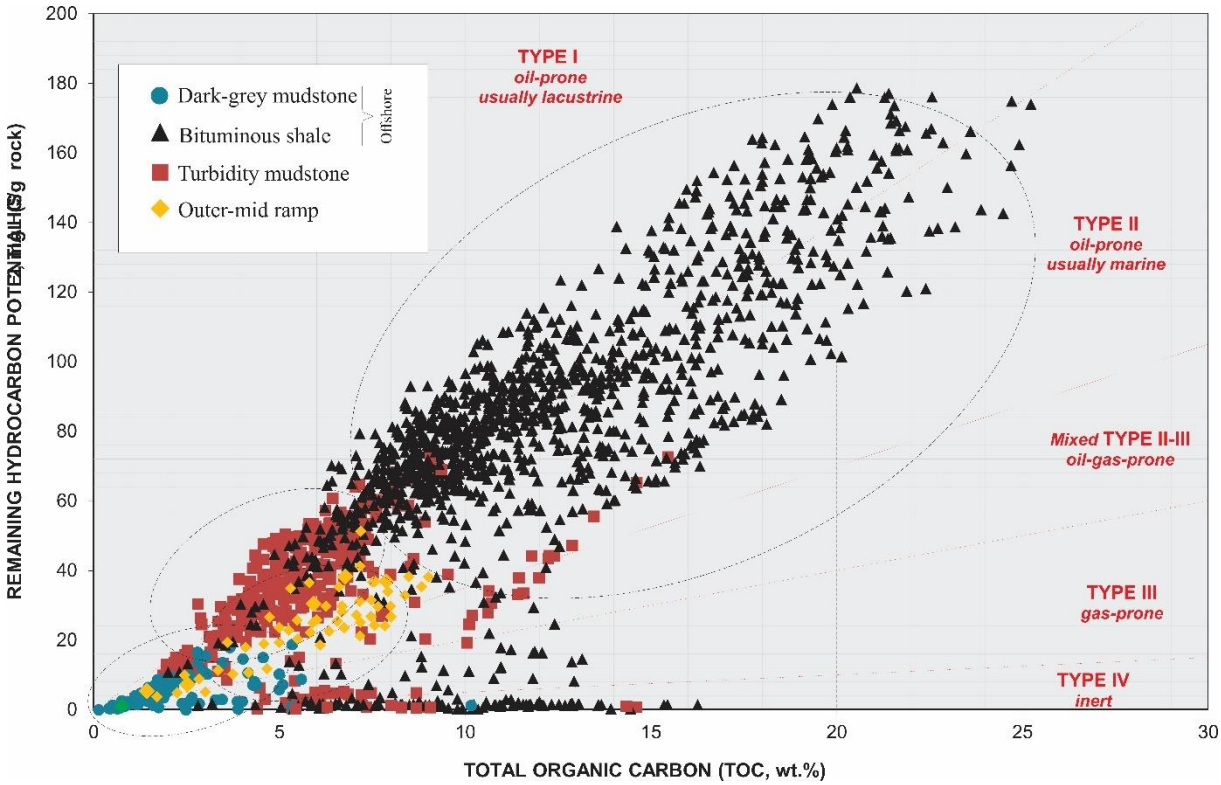

Fig. 11. Kerogen quality diagram with the kerogen type for each organic-rich facies. the organic matter shows a trend towards types I and II. All facies show a little oxidized organic matter contribution.

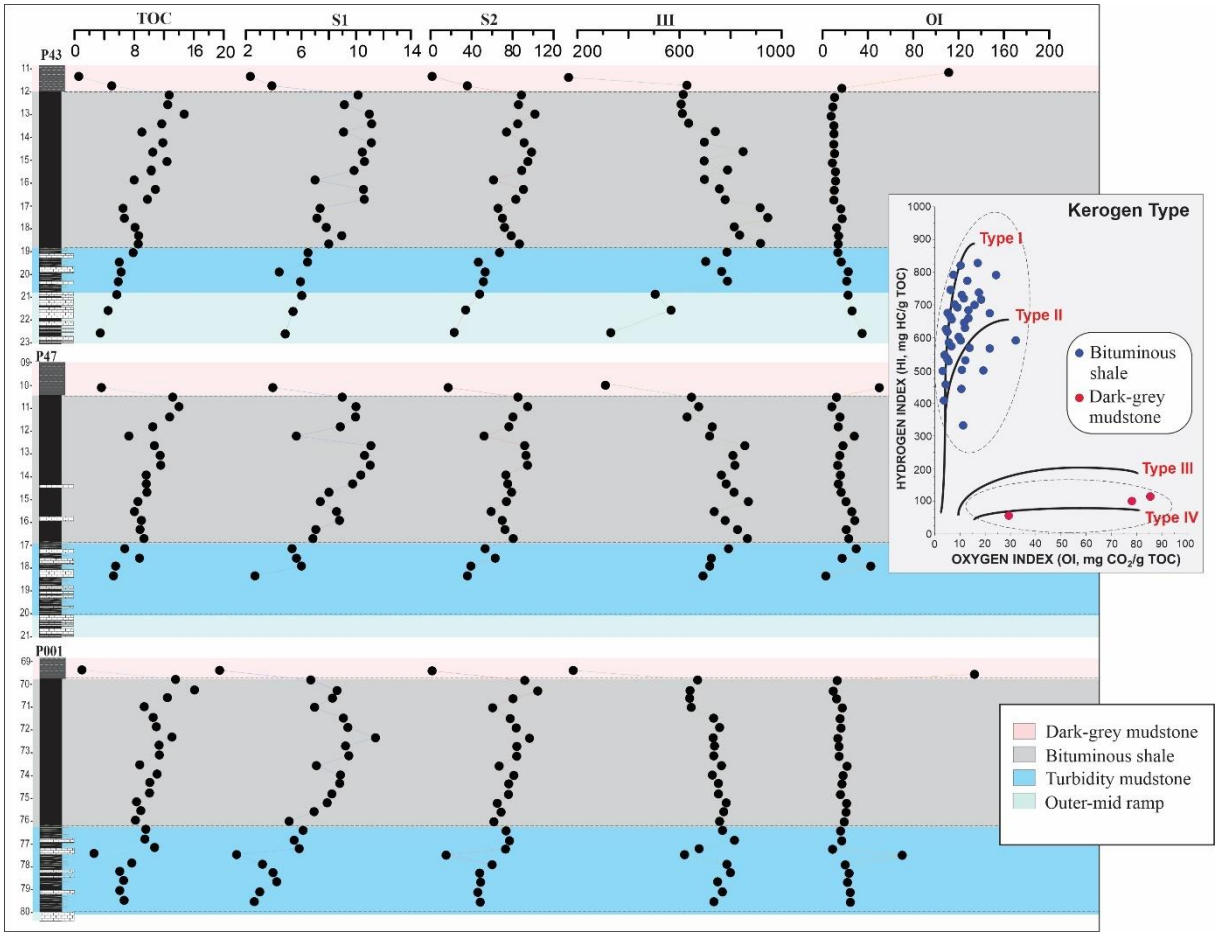

Fig. 12. The gradual lithofacies transition is reflected in the organic carbon content and kerogen. TOC gradually increases towards the offshore facies, with an abrupt reduction to the grey to black shale facies, reflecting the change in oxygenation conditions. The anoxic condition prevailing across the ramp allowed organic-rich facies to form even in the shallower regions. Mm: grey to black shale; Sb: bituminous shale; Sh: sandy black shale; Ch: Well bedded carbonate-shale.

5.6.2. Mineral composition

Multivariate statistical analysis was performed using forty-three representative samples of the mixed deposits. Hierarchical cluster analysis (HCA) and Principal components analysis (PCA) can identify patterns in the multivariate analyzed elements and graphically produce groups with similar geochemical composition. Using both combined was possible to group the mixed siliciclastic-carbonate mineralogical data in eight major clusters. The HCA dendrogram and the PCA three-dimensional chart in Fig. 13 also present the representative composition of each cluster. The PCA principal component 1 (PC1) explains 73.25% of the total data variation. The three components justify 95.5% of the multivariate mineral composition.

MG1 represents the siliciclastic-rich marls of the ramp mainly composed of quartz (51.3%), dolomite (34.7%), albite (8.8%), muscovite (4.0%), and pyrite (1.2%). The dolomite mineral phase forms the oriented micropeloidal fabric and muscovite plates within. Pyrite is disseminating nanocrystals hard to observe in thin sections. **MG2** is the representative group of the carbonate breccia. The dominant mineral phases are dolomite (82.9%), quartz (13.1%), calcite (1.6%), kaolinite (1.3%) and albite (1.1%). The siliciclastic minerals composing the infilling phase have a very similar composition in all analyzed breccia levels. The SiO_2 is represented by quartz (~7%) and chalcedony (~6.1%), based on thin-section point counts. Despite not appearing as major composition, pyrite forms local rework cumulates or cementing fractures. **MG3** represents the finely-laminated dolomudstone with slightly crenulated lamination interbedded lamination with gypsum pseudomorphs that occur underlain the carbonate breccia facies. It has dolomite (67.4%), calcite (24.3%), quartz (6.7%), and analcime (1.5%). **MG4** has a different composition and is the only level of the section with no dolomite. It is dominated by magnesium calcite (81.3%), quartz (16.10%), and albite (2.6%). This level is composed of cone-in-cone structures. In thin section locally concentrated an insoluble fraction of muscovite occurs.

The **MG5** grouped the dominant shale microfacies composition. Although, the complex compositional variations across the succession are identified in the matrix correlation. Based on HCA the composition was here arranged in MG5 subgroups (A to E). MG5A represents the mineral composition of the dark-grey mudstone and massive to laminated siltstone facies present in the Serra Alta Formation (sample 01), Assistência Member (samples 09, 11, 14, 20,) and Taquaral Member (samples 38, 40). Points worth taking are the presence of gypsum (1.1%) in the Taquaral shale, closely associated with the Shell-rich dolograinstone level. Also, Serra Alta shales has hematite even in a few centimeters from the Assistência Member. MG5B makes an interesting analysis grouping the outer ramp turbidity facies with the shoreface deposits of the Palermo Formation (sample 41). MG5C is formed by the widespread distal organic-rich shales. it is composed of quartz (64.1%), kaolinite (17.3%), pyrite (8.2%) albite (6.2%), muscovite (3.2%), and microcline (0.6%). The uppermost organic-rich interval has a greater proportion of kaolinite, increasing toward Serra Alta Formation. The lowermost has an average of 6%. MG5D grouped the proximal organic-rich shale facies interlayers with the dolostone of outer-mid ramp, contrasting with MG5C due to the occurrence of jarosite (8.6%), gypsum (1.2%), and no detectable kaolinite. The **MG6** grouped the siliciclastic-rich marls microfacies facies that have gypsum minerals (~3.6%). **MG7** is the dolomite-rich marlstone present in the mid-ramp facies. **MG8** represents the considered here pure dolostone layers (93.4%) that occur

interbedded with shales even in centimeters intervals. The dolomite phases are composed of peloidal grains. The minor calcite (0.3%) occurs as cement.

Pyrite is a constant mineral phase across the section and EDS corroborates that the main plagioclase phase is albite. SEM/EDS shows that the siltstone laminae with the shales have detrital zircon and shale laminations are mainly composed of muscovite, biotite, chamosite, zeolite. The major clay mineral forming the matrix is illite. In the laminated dolostone were identified barite and glauconite. Booklet kaolinite is frequently observed infilling V-shape fractures and within the breccias, even breccias layers of the mid-ramp facies. Also, halite was observed within those facies.

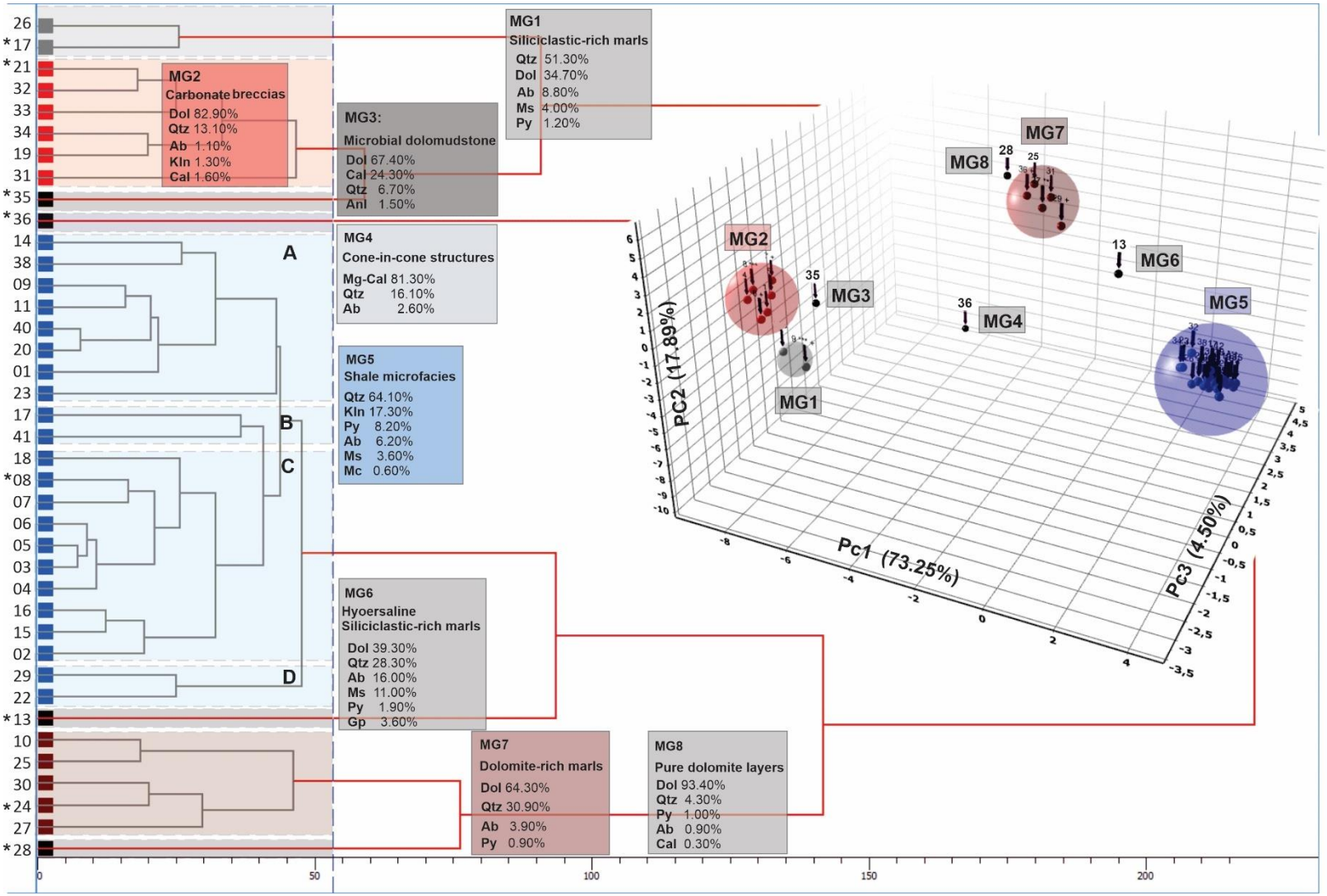

Fig. 13. Hierarchical cluster analysis (right) dendrogram and 3D principal component analysis graphic with the eight main groups representative of the mixed lithology of the study succession. Note the 3D PCA graphically spatializes the shale (MG5), pure dolomite (MG8), carbonate breccias (MG2) siliciclastic-rich, and dolomite-rich marls (MG1 and MG7), marls with gypsum (MG6), microbial dolomite (MG3), and diagenetic cone-in-cone structures (MG2).

5.7. DISCUSSION

5.7.1. Organic-rich shales in shallow marine environments

Organic carbon-rich facies formations require particular conditions in the depositional environment. The primary controls are summarized in three factors: (I) primary organic matter production; (II) anoxic bottom water (bacterial decomposition), and (III) sedimentary rates (Pedersen & Calvert, 1990; Lee, 1992; Arthur & Sageman, 1994; Wignall, 1994; Tyson, 1995; Sageman *et al*., 2003; Jin *et al*., 2020). High sedimentation rates are crucial for the preservation of organic-rich sediment chiefly in a depositional setting with a high level of free oxygen (Bralower & Thierstein, 1984; Calvert, 1987; Betts & Holland, 1991; Rabouille & Gaillard, 1991). Nevertheless, most ancient organic-rich deposits in epeiric ramp appear to have accumulated under very low bulk sedimentation rates (Sageman *et al*., 2003). In the Irati Sea predominates an eolic siliciclastic source. The outer ramp dolostone facies have very little to no siliciclastic silt grains. In the mostly finely-dolostone facies, the siliciclastic grains are visible only under cathodoluminescence or SEM. The terrigenous facies are diagnostic of the distal environment. The falling grains over the outer-mid ramp are dominantly swept to the deep portion of the ramp.

High organic matter preservation rates in the Irati Sea are largely due to high primary production creating *organic overloading*. The aerobic followed by anaerobic degradation of organic matter was possibly one of the causes of the anoxic environment. Pedersen and Calvert (1990) present evidence that primary production controls the accumulation of organic matter in sediments over the anoxic bottom-water. The occurrence of thin and widespread shale beds due to a low accommodation space in a shallow platform difficult to invoke a broad anoxic bottom-water system due to a water-column stratification as the first-order control of the Irati Sea organic rich-facies.

Lee (1992) states that anoxic conditions predominate in locations where organic matter sedimentation rates are highest, leading to the major amount of organic carbon preservation, typically coastal marine environment (Berner, 1982). In herein case, a widespread shallow homoclinal ramp. The low diversity of macro- and meiofauna in the Irati Sea plays an important role in carbon preservation. High biodiversity predominates in well-oxygenated environments, few species are low-oxygen tolerant (Levin *et al*., 1992). The shallow depth may also be contributed for enhance the preservation by reducing the usual organic matter degradation during the settling flux. The organic matter falling exposes the organic particles to oxidation

(Wignall, 1994). Moreover, the already low siliciclastic input associated with sea-level rise led to sediment starvation and organic matter concentration in those distal organic-rich facies, which deposition is associated with transgressive events. Plus, enclosed basins are natural nutrient sinks, due to the inhibition of vertical advection by density interfaces (Tyson, 1987).

Stable tectonic setting, restricted basin connection, and constant deposition are broadly accepted for the Irati Sea. Considering the similar decantation velocity settling for clay and organic matter particles (Wignall, 1994), organic-rich lamination at the top of distal turbidity microcycles, as well as forming intercalation with fine sandstone to siltstone laminae indicates seasonal algal blooms or microbial colonization. The combined factors: (i) shallow and extensive setting; (ii) Stable tectonic conditions; (iii) restricted basin connection to the open ocean, and; (iv) flat bottom and very low-angle slope favor the damping or dissipation of energy, therefore establishment of calm and protected depositional environment. Such conditions allowed fine sediment deposition (carbonatic and siliciclastic mud) across the basin. The prevalence of anoxia and hypersaline conditions also allowed black shales preservation in the proximal areas.

Similar shallow sedimentation is described by Droste (1990) for the Hanifa Formation (Arabian Peninsula), whose high TOC values (up to 6%) are attributed to high organic productivity in a hypersaline environment without subaerial exposure, which would eventually obliterate the organic-rich facies. Anoxic conditions and organic-rich facies are currently recorded in a shallow coastal environment of the coast of Abu Dhabi with type I-II kerogen type, TOC values (0.5 to 2.7%), and hydrogen index (510 and 675 mg HC/g TOC), formed by microbial mat accumulation (Kenig *et al*., 1990).

Kerogen type II, typical of marine settings, dominates in the offshore facies. On the other hand, the high contribution of kerogen type I records in the bituminous and sandy shale facies across the north, west, and south part of the border suggest a periodical establishment of typical lacustrine conditions related to freshwater input during humid seasons. Kerogen type III and IV mainly in the mid- to the outer ramp are possibly related to preserved (type III) and oxidized (type IV) terrestrial organic matter input during the freshwater inflows.

5.7.2. Thin, fine mud laminae across the ramp

Millimeter to sub-millimeter scale even-parallel lamination is a ubiquitous sedimentary structure in black shale (Wignall, 1994). Regardless of the apparent monotony of sedimentary structures in fine siliciclastic rocks, a microscopic analysis may reveal a complexity of

lamination types due to other sedimentary processes besides suspended-load (Fig. 14). They are mainly resulting from individual processes or combining suspend, bedload, or gravitational flow. Plus, black shale can be unlaminated with oriented grains in a homogeneous fabric as well as variable cross-lamination types.

Fine-scale sedimentary structures may be preserved under sedimentation rates higher than benthonic fauna burrowing or exceptional anoxic bottom-water. The first requires sedimentation rates on the order of several meters per million years (Wignall, 1994), which is not the case of the thin Permian deposits study here. Likewise, the fine-scale cross-laminations indicate that the stagnant water is not absolutely but instead deposited under the influence of a very low-velocity bottom flowing current below anoxic stratification (O'Brien, 1996). The increase of the bottom flow current velocity may disrupt the long-lasting anoxic condition and even form ripple marks (O'Brien, 1996). Still, the fine structures preservation demand sedimentation retorn under anoxic free-benthonic burrowing. The excellent preservation of the fine sedimentary structures from the outer-mid ramp to offshore facies is due to the laterally and temporally dominance of anoxic bottom water.

The Irati black shale shows a wide range of microfabrics (see table 01) implying more than one simple process in its formation. Outer ramp facies are dominated by thicker grading beds and interbedded peloidal with clayey shale lamination. The distal cyclic fine-grained laminae with upward gradation (sand/silt/clay/organic matter) and interbedded siltstone and shale can be explained as storm or turbidite event beds (Reineck & Singh, 1972; Pederson, 1985; Schieber, 1989; Wignall, 1994; Ulmer-Scholle *et al*., 2014). The first could be produced by storm-surge ebb currents and storm-generated suspension clouds of the organic-rich sediment. However, there are no diagnostic evidence of storm activity. The alternation of quiescence and these energetic processes (turbidity and bottom current) created organic-rich shale layers (anoxic condition) interbedding with silty to sandy laminae with wide-ranging fabric (energetic and dysoxic condition). The thin finely-laminated shale with lateral convergence and low-angle downlap of the silt laminae and laminae gently inclined towards common surfaces (Fig. 14A) are a result of bedload transport of silt grain size and flocculated muds by currents (Schieber *et al*., 2007; Schieber & Southard, 2009; Ulmer-Scholle *et al*., 2014). Siliciclastic grains (quartz and feldspars) less than 30 μm are often present in the clay laminae. The grains bigger than 65 μm concentrates in the silty to sandy laminae as predicted by Yawar and Schieber (2017). The deposits formed by fell-out of silt grains were reworked by bottom current to form isolated siltstone laminae (Fig. 14D) and cross lamination in mid- to the outer ramp (Pederson, 1985). The graded bedding composed of very fine-grained sand, silt,

clay, and organic matter in outer ramp facies indicates a well-sorting deposition from well-sorting from low-density turbidity flows.

Graded sandy- to silty shale fabric within planar to wavy bedding is a very common feature of the Irati shale facies. The upward gradation of fine sand (when available) or silt grain size (quartz, feldspars, pyrite, carbonate fragment) to clay-rich layer with a concentration of organic matter in the top. The layers can be interbedded with a couplet of normal silt-rich and clay/organic matter-rich lamination, forming even parallel to wavy-laminated silty shale. Those microfacies are identified within cyclic grading beds interpreted as the low-density turbidity flows (Wignall, 1994). Lenticular dolomitic shale was identified the ramp. The flattened carbonate lenses (~200 μm) are evidenced by surrounding clay and organic matter films due to diagenesis compaction. The carbonate lenses are formed as rip-up clasts by wave reworking the soft and water-rich (~80%) seafloor mud (Schieber *et al*., 2010; Ulmer-Scholle *et al*., 2014). The gradational lenticular fabric formations with fabric varying from clay-rich flattened carbonate particles to peloidal carbonate can be interpreted as current rip-ups of the soft seafloor peloidal muds that were redeposited, piled up and compacted during burial. Fig. 15 summarizes the main microstructures observed for the mixed deposits.

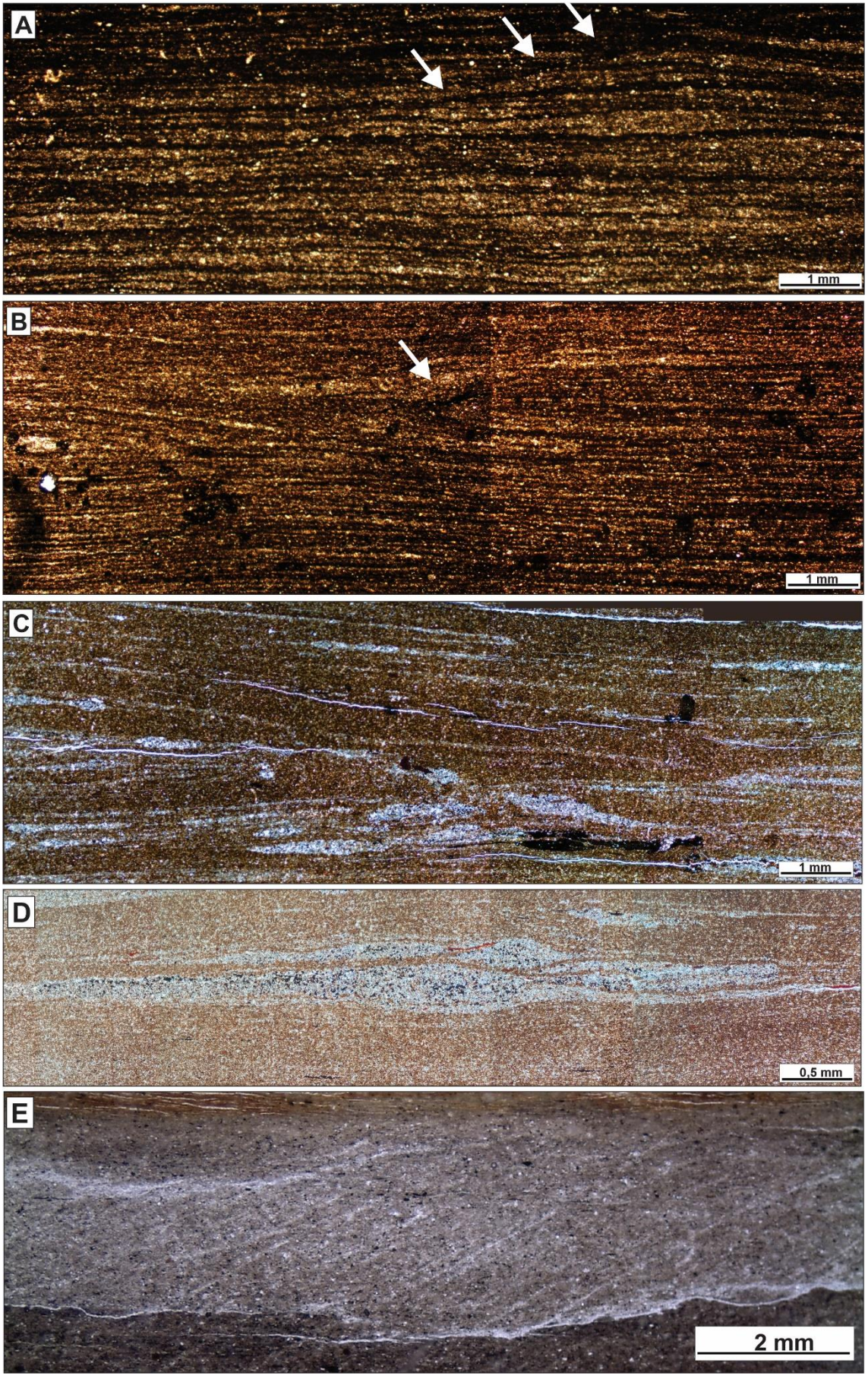
A
1 mm
B
1 mm
C
1 mm
D
0,5 mm
E
2 mm

Fig. 14. Photomicrographs of finely-laminated shale. Despite the substantially lowered primary dip angles by the diagenetic compaction of water-rich shales (A) the thin oriented dark organic matter evidence the variation in thickness, diverge, and converge across the section. Lamination marked by organic matter and pyrite with diffused bedding in (B) and by bright siltstone laminae in (C) shows lateral convergence and low-angle downlap relationships. Moderately bioturbated layers show a concentration of pyrite. D) The lateral thickening of the laminae into small silt concentration related to bedload transport. E) millimeter cross-laminations evidenced by siliciclastic and pyrite silt grains.

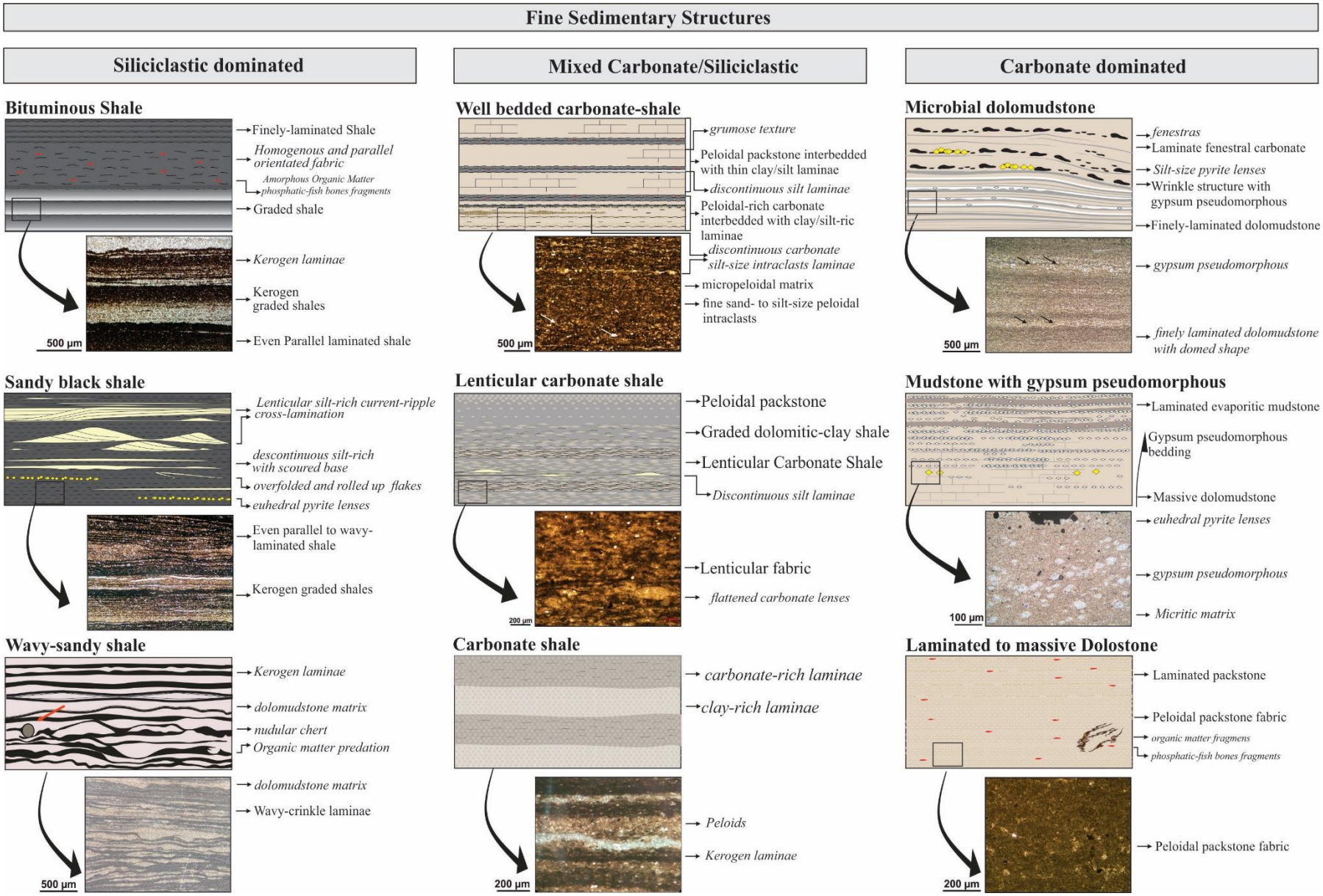

Fig. 15. Summary of the mixed siliciclastic/carbonate microfacies identified of the Lower Permian Paraná Basin. Variation from siliciclastic- to carbonate-dominant are common on the low-angle ramp.

5.7.3. Peloidal dolomite and diagenetic overprinting

The carbonatic microfacies present throughout the Irati succession are dominantly dolomitic. It occurs mainly as mudstone, wackestones, and packstones, seldomly as grainstone. The carbonate deposits occur as peloidal, lenticular, or micritic matrix with a grumose texture in laminated or massive heterolithic microfacies. Peloids are also present in the dolomitic and mixed matrix of breccias and injection dikes. In breccias, idiotopic spar crystals of dolomite filling porosity were also observed. Dolomicrite fragments were also found in the silt lenses of the laminated dolomitic shale. In the study area, the occurrence of calcite is restricted to diagenetic textures.

Peloidal fabric is a common feature of carbonate environments, mainly warm and shallow marine platforms. Laminated micritic carbonates are formed by the fall-out of suspended particles in a low-energy environment, protected from the action of waves and terrestrial input (Scholle & Ulmer-Scholle, 2003). Peloids are generated by aggregates of carbonate micrite whose origin can be microbial, decantation post-nucleation (primary precipitation), and abrasion of carbonate intraclasts forming pellets less than 62µ (Flügel, 2004). The high degree of preservation, roundness, and modal homogeneity suggests that the peloidal matrix observed in the Irati Formation is formed by nucleation with little or no transport. Precipitated peloids are an induced chemical or biochemical in situ nucleation, commonly triggered by biological activity (Tucker, 1991; Flügel, 2004). The macropeloids are interpreted as a product of bottom weak oscillatory flow that promotes the aggregation of micropeloids.

Well-preserved primary sedimentary features are crucial for a correct interpretation of the origin of this rhythmic lithological intercalation. Hence, diagenetic overprinting may play an important role in cyclic carbonate-siliciclastic patterns (e.g. Einsele, 1982; Schwarzacher & Fisher, 1982; Westphal *et al*., 2008). However apparently, it is not the herein case. The good preservation and regularity of textural patterns in the rhythmic intercalations, with the dolomitic layers dominating micritic across the succession, observed for more than 1,000 km in length, makes it unlikely to be a product of post-depositional processes instead of primary compositional control. Microspars dolomite with homogeneous fabric is restricted to the only layer observed for Taquaral Member. These are interpreted here as the results of the eodiagenetic alteration of Mg-rich limestone (Flügel, 2004; Font *et al*., 2006) favored by the hypersaline conditions.

The facies analysis showed that the dolomite layers across the platform, as well as the organic-rich shales, are rich in primary pyrite. Oriented granular pyrite, even forming continuous laminations is observed in thin section, suggests primary origin, and attests to anoxic conditions. The anoxic conditions of the unit are confirmed by the high values of COT, HI, high degree of preservation of AOM, and absence of benthic fauna in all facies of the unit. The formation of primary dolomite in the Irati Formation could be related to the sulfate-reducing bacteria activity, probably as a result of phases of widespread marine anoxia of the Irati sea. The absence of displacive/replacive textures, well-preserved lamination, and peloidal fabric corroborate the primary precipitation for peloidal dolomite present in the Irati Formation. Moreover, the hypersaline condition increased the concentration of Ca^{+2}, Mg^{+2}, and CO_3^{2-}.

Laboratory tests demonstrated that the consumption of the sulfate present in the seawater, an inhibitor to dolomite formation (Baker & Kastner, 1981; Vasconcelos *et al*., 1995), proportionally increase the rate of dolomite precipitation (Vasconcelos *et al*., 1995; Vasconcelos & McKenzie, 1997; Warthmann *et al*., 2000). Sulfate-reducing bacteria induce anoxic low-temperature dolomite formation (Van Lith *et al*., 2003). The metabolic activity of sulfate-reducing bacteria under anoxic conditions may overcome the kinetic barrier to dolomite formation by increasing the pH and carbonate alkalinity (Castanier *et al*., 1999; Wright, 1999; Warthmann *et al*., 2000; Van Lith *et al*., 2003). Diaromatic carotenoids such as isorenieratene found in photosynthetic sulfur bacteria are described for the Irati shale (e.g. Martins *et al*., 2020). Pseudomorphs and nodules of evaporitic crystals associated with dolomudstones found in the north and south of the unit corroborate the crystal's primary origin in shallow waters (Demicco & Hardie, 1995). The hypersaline conditions due to the high evaporation rate during the timing formation of the carbonate layers favor the precipitation of the dolomite. The high Mg/Ca ratios induced the removal of Ca and precipitation of dolomite (Flügel, 2004). The subhedral microcrystals are a product of rapid precipitation at temperatures of 35 ° C and 40 ° C (Warren, 2006).

5.7.4. Depositional control

Mixed carbonatic-siliciclastic systems are characterized by a considerable lateral facies variation with a broad interbedding zone of both lithologies, normally with the ending points composed of thicker packages free from the influence of each other (eg., Mount, 1985; Flood & Orme, 1988; Aquer & Stell; 1990; Zeller *et al*., 2015; Chiarella *et al*., 2017; Kvale *et al*., 2020). They are the result of the interaction of extrabacinal (e.g. fluvial input) and intrabacinal

(e.g. carbonate factory) processes. Less common in the geological record is the expressive contemporaneous accumulation of both lithologies in space and time. Chiarella *et al*. (2017) classified these two mixed lithological phases in (i) strata mixing and (ii) compositional mixing, respectively. The Lower Permian mixed deposits of Paraná Basin include both definitions. The unusual rhythmic intercalation of dolostone and shale can be observed in macro-, meso- and even microscale (lamina set). The lithological heterogeneity is the product of a complex relationship of allocyclic and altocyclic factors. The distribution of these deposits on a wide platform (> 10^6 km^2) strongly implies allocyclic control. The relatively shallow and planar morphological configuration of the ramp, enclosed in a context of relative tectonic stability, is strongly susceptible to wide oscillations of the relative sea level. Burchette and Wright (1992) state that even during minor falls, shallow-ramp facies can shift basinward like a "forced regression". The wide and flat configuration of the platform added to the reduced accommodation space favors the sedimentary bypass instead of promoting erosive surface formation.

The siliciclastic and carbonate intercalation across the platform with the rhythmic intercalation with both pure endmembers (<10% of their antithetic components) suggest: i) short-term climate fluctuations from arid conditions (favorable to biogenic carbonate production) to humid (terrestrial input), inducing ii) short-term sea-level changes, which promotes the overlapping of carbonates (during shallower waters) over the shales (distal facies), and iii) turbidity current producing distal rhythmites. Deposits interpreted as produced by turbidity currents (e.g. cyclic grading beds with or without cross lamination, silt-sized laminations composed of peloidal dolomite fragments in the dolomitic shale) show active participation of turbidity currents in the redistribution of sediment on the offshore.

Inpu t of fine terrigenous sediment: fine siliciclastic sedimentation results in the widespread grey to black shale facies across the platform. Silt grains and fine sand also compose millimeter laminations in carbonate and siliciclastic mudstone. The lateral and vertical persistence of those grains within the carbonates beds or forming marl indicates a constant flow of terrestrial material during freshwater input. Silt to fine sand grains is predominantly composed of quartz with varied roundness degrees from angular (more common) to rounded grains. K-feldspars and plagioclases are less than 8% and muscovites produce oriented blades in the siltstone lenses. Canile *et al*. (2016) show that the Permian siliciclastic sedimentation in the basin was supplied not only by the Choiyoi igneous province but also comes from Argentina (North Patagonia Massif), suggesting that the sedimentation, in addition to being transported by eolian currents, came from long distances via continental subaqueous transportation. However, the low

presence (<2%) and even the absence of terrestrial grains in the basal outer-mid ramp facies imply periods of restricted continental contribution via water flow. Therefore, predominating wind transport, forming thicker layers to the south.

Carbonate factory: The facies analysis shows that carbonate production occurred in the wide and shallow region of the ramp. The carbonates finely-laminated and micro- to macropeloidal texture suggest the dominance of biogenic production. The prevalence of micritic facies with "pure" composition (free or with very low terrigenous content <2%) attests to moments of biogenic carbonate factory with very low or absent input of terrestrial sedimentation (Irwin, 1965).

Gypsum pseudomorphs levels and extensive deposition of dolomites associated with evaporitic conditions are related to arid seasons. Periods of freshwater input are indicated by the presence of *Botryococcus* and highly concentrated C_{17} long-chain alkylnaphthalenes within the shales pointing to algal blooms (Martins *et al*., 2020). Fluctuations in carbonate-dominated to siliciclastic-dominated intervals, even in microscale, are strongly indicative of climate control with variations from arid to humid conditions (Tänavsuu-Milkeviciene *et al*., 2009). Similar deposits are described for Capodarso Formation in the Enna-Caltanissetta Basin (Massari & Chiocci, 2006) and in successions in the Guadix Basin (Garcìa-Garcìa *et al*., 2009). In both examples, the mixed intercalation occurs at the mesoscale (bed set). In Capodarso Formation the carbonate beds occur interbedded with siliciclastic mudstones and in the Guadix Basin, the intercalation is between marl and sandstone. The sedimentary control of repetition in the Capodarso Formation is attributed to glacio-eustatic and climatic variations (Massari & Chiocci, 2006; Massari & D'Alessandro, 2010). Garcìa-Garcìa *et al*. (2009) attribute the rhythmic interbedding in the Guadix Basin to alternating dry and humid climatic episodes. However, Puga-Bernabeu *et al*. (2010) interpreted it as a result of relative sea-level change. Tänavsuu-Milkeviciene *et al*. (2009) describe the mixed carbonate – siliciclastic deposition of Narva succession in the Baltic Basin (Middle Devonian). They are deposits formed on a shallow marine platform, dominated by tides. These authors attributed the mixed intercalation to climate changes from arid to humid phases.

5.8. SEQUENCE STRATIGRAPHY FRAMEWORK

The Lower Permian mixed deposits of Paraná Basin can be divided into four distinct depositional sequences (Fig. 16). The stratigraphic surfaces are well-marked by facies stacking patterns. Likewise, the surfaces are traceable by gamma-ray, biomolecular marker, and stable

isotope profile (see Bastos *et al*., 2021). The maximum transgressive surfaces (MTS) are defined by preeminent inversion of the retrogradational to progradational stacking pattern, recorded by TOC and Rock-Evel HI profile. Araújo (2001) also noticed a directly proportional link with diagenetic uranium enrichment due to the organic matter, making it possible to correlate the stratigraphic surfaces in the gamma-ray, TOC, and facies profiles.

The sequences discussed here overlain the 2nd order Carboniferous-Eotriassic transgressive-regressive sequence of Milani (1997), which comprises the largest sedimentary package in the Paraná Basin, with a total thickness in the order of 2.500 m (Milani *et al*. 2007). The emplacement of this 2nd order thick sedimentary package followed the greater expansion and subsidence of the Paleozoic syneclysis with considerable tectonic and climatic changes (Almeida 1980). Nevertheless, the mixed succession was developed during low accommodation with the sedimentation in a homoclinal ramp.

In the same way that prevails absence of high energy deposits, low system tracts are also not recorded in the homoclinal ramp. Thereby, the maximum regressive surface (MRS) overlaps the sequence boundary (SB). Moreover, the lack of expressive evidence of subaerial exposure in the limits of the sequences indicates a type 2 sequence boundary following (Vail *et al*., 1984) that is directed overlaid by offshore deposits. The transgressive (TST) and highstand systems tracts (HST) are composed of retrogradational, aggradational, and progradational stacking patterns controlled by climate and sea-level changes (accommodation space).

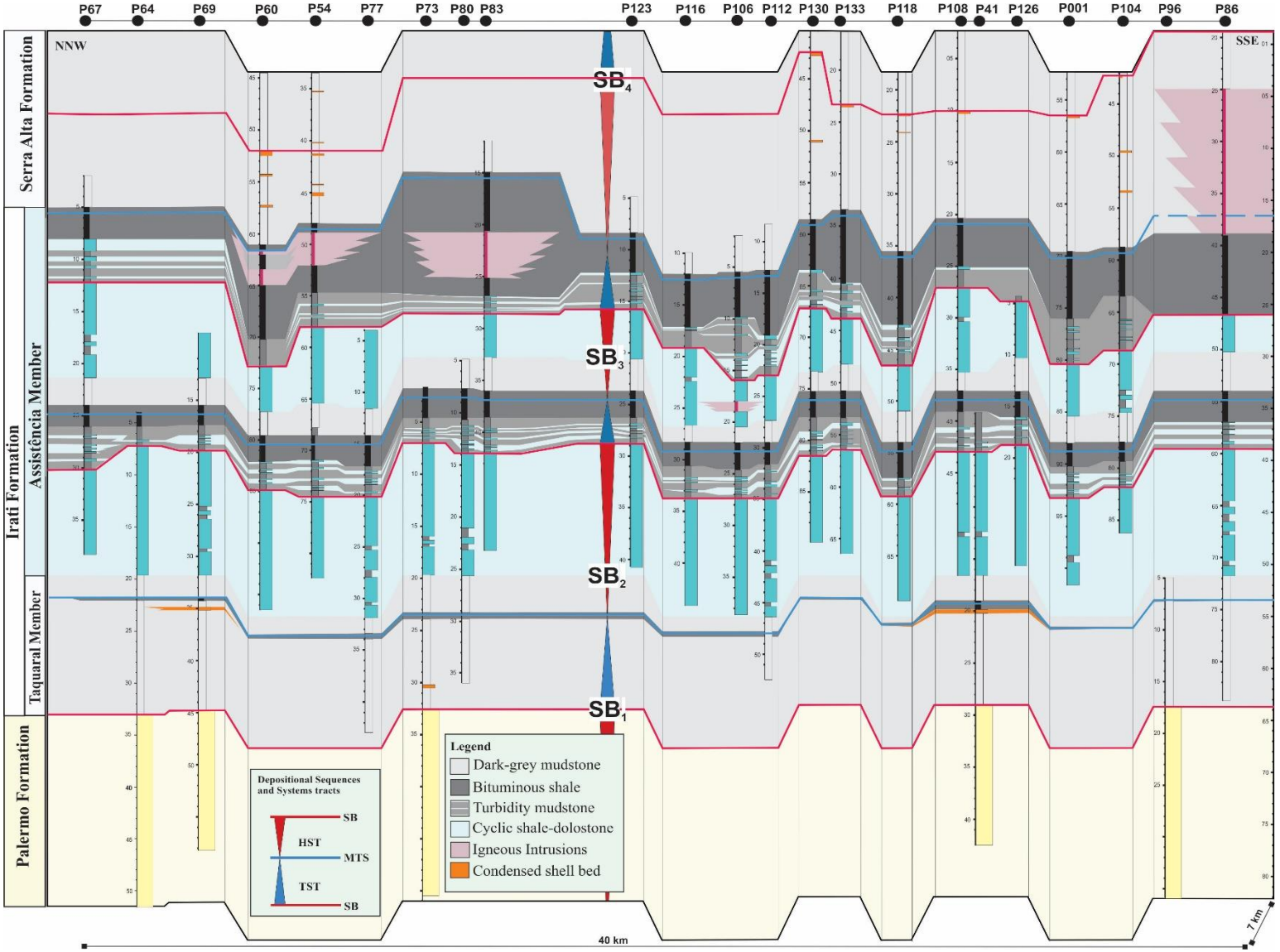

Fig. 16. Schematic cross-section of the mixed siliciclastic-carbonate deposits based on detailed sedimentological descriptions. The stratigraphic section shows the four depositional sequences and the lateral variation of the sequence boundaries.

5.8.1. Depositional Sequences

S1

The progradation pattern that follows the maximum transgressive surface of the Carboniferous-Eotriassic sequence form the third-order sequence that extends to the Palermo Formation and Taquaral Member limit. Araújo (2001) identified the basal limit through the inversion of a stacking pattern from shallowing to deepening upward in the northern portion of the basin. The sequence consists essentially of shoreface to offshore fine siliciclastic.

Towards the top of the Palermo Formation, there is a progressive decrease of bioturbations and sand lenses to finely-laminated shales. The faciological stacking pattern change is also recorded by the increase in the TOC content. The sequence boundary 1 (SB1) is recorded between the aggradational pattern (heterolithic deposits) of the upper portion of the Palermo Formation to the deepening-upward pattern of the Taquaral Member, characterized by grey to black shales at the base (Araujo, 2001; Xavier *et al*., 2018). SB1 marks a shift from shallow and oxidizing conditions to offshore under dysoxic conditions. In the northeastern portion of the basin, the occurrence of a transgressive lag rich in fish and tetrapod fragments is described, marking the base of Taquaral Member (Castro *et al*. 1993; Chahud, 2007). In the middle portion of the basin, rounded clasts with centimeter size were observed at the base of the Taquaral Member.

S2

The relatively homogeneous pattern of the finely-laminated shales of the TST is interrupted by a massive centimetric level of shell-rich dolograinstone forming a condensed shell bed of bivalve with fine sandstone lenses. Also described in the northern portion by Matos *et al*. (2017). These distal deposits are a result of sediment starvation and condensation, swept from proximal areas by shelf currents or major storm waves (Zecchin & Catuneanu, 2013). It is overlaid by thin black shale layers (~1.0 m) that represent the MTS of the S2. Due to the fine lithology and dominating dark color of the Taquaral Member shale, MTS is evidenced only in the organic geochemistry profile in which occurs a conspicuous peak (TOC reaches ~3%).

The homogeneity of the dark grey to black shale layers of the Taquaral Member makes it difficult to observe a faciological pattern in the studied area. Nevertheless, slight variations from clay-rich to silt-rich shales suggest coarsening-up patterns. At the north portion of the basin. Rohn (2007) observed variations from black shale to coarse siltstone, defining four coarsening-up trends that could represent high-frequency cycles. The last and thicker high-

frequency shallowing-up cycle over the MTS has in the top carbonate breccia levels (base of the Assistência Member). It records an increase in salinity identified by lipid biomarkers (e.g. Bastos *et al*., 2021). The following outer ramp mixed carbonate-shale facies also indicates high salinity concentration and anoxic condition due to the restriction of the basin. They are composed of finely-laminated to graded organic-rich black shale interbedded with mudstone with gypsum pseudomorphous, finely-laminated peloidal dolomudstone, graded marlstone, and laminate fenestral carbonate with gypsum pseudomorphs forming an aggradational patten. The following progradational pattern is well-defined by coarsening upward the dolostone facies. Sequences S2 and S3 are well-marked by rhythmic intercalation of shale and dolostone forming predominantly coarsening-up patterns of the carbonate facies. The patterns are characterized by couplet (carbonate/shale) or triplet (carbonate/shale/marl).

SB2 marks a considerable shift from the typical progradational fine siliciclastic-carbonate faciological pattern of the outer-mid ramp to the occurrences of offshore turbidite deposits.

S3

The retrogradational pattern of S3 sequence is composed of superimposed cyclic turbidity facies overlaid by thin dolostone beds and a thicker package of organic-rich shale. The last one records the MTS. The surface is well defined in the organic-rich shale facies by geochemical data that show a prominent peak of organic production. The basal aggradational pattern of HST is has a tabular occurrence of grey to black shale analogous to the S2 offshore shales. There are variations in the oxidation conditions of the medium, probably a record of the Phantalassa ocean incursion on the Irati platform. This statement is supported by the occurrence of open sea fish remains and shark teeth (Fig. 11A to C). The change to progradational is marked by the occurrence of a centimeter tabular bed of a peloidal wackestone/packstone with reworked ostracodes and intraclasts followed by peloidal dolomudstone. The reworked bioclasts and intraclasts imply the return of shallow conditions and energy increase enough to rework the semi lithified substratum. Furthermore, the absence of exposure features indicates prevalent subtidal conditions. S3 is the thinnest sequence of the succession with only 16 meters, indicating the highest subsidence ratio. The homoclinal and shallow platform conditions are indicated by the continuous and tabular cyclic carbonate and shale pattern of the sequences S2 and S3 progradational trends. The sequence boundary SB3 is similar to SB2. However, the organic-rich shale facies occur forming a thicker interval, as well as the shale of the HST (in the base of the Serra Alta Formation).

S4

The retrogradational to aggradational pattern of S4 is similar to the S3 sequence but with thicker packages. The black shale layers interbedded with the thin dolostone have an upward increase in the organic carbon becoming 20 % of TOC toward the MTS. The return of the anoxic and hypersaline conditions with high organic matter preservation again indicates restriction of the oceanic connection. The tabular configuration and the absence of crossbedding of the rhythmic deposits mark the outer ramp. The successive faciological pattern indicates an increase of accommodation with the subsequent disappearance of the carbonate factory. This fact is indicated by the dominance of siliciclastic facies (Serra Alta Formation) and the absence of carbonate layers.

Despite the similarities in the faciological pattern with the last two sequences, S4 has thicker TST and HST deposits. After the shallowing up of the basin whose maximum is recorded by SB2, there was a progressive deepening reaching its maximum in the Serra Alta Formation, dominated by offshore facies. The pattern observed in the TST to HST transition from S3 is also observed for S4. The organic-rich shale (Irati Formation) contact with the dark-grey shale (Serra Alta Formation) facies is easily identifiable in wells due to the conspicuous color difference. As well as the abrupt change in the geochemical profiles due to the abrupt drop in the organic matter preservation. The reduced amount of organic matter preserved in the HST is again attributed to the establishment of an oceanic connection with a fossil record similar to the S3 HST. Plus, the conformable contact (Irati and Serra Alta formation) and perceptive passage of the black to dark-grey color of the facies. No evidence of reworking process (e.g. conglomerates, breccia) was observed, making its interpretation as a sequence boundary difficult, as previously advocated (e.g. Lavina *et al*., 1991; Holz *et al*., 2010).

The occurrence of fine concentrations of fish remains right after the base of the Serra Alta Formation led some authors to interpret it as transgressive lag attributing to a sequence boundary, as third-order limit (e.g. Holz *et al*., 2010). However, the bone remains were observed in this work only in one well and in two levels similar to the HST of the S3 sequence. Thus, following the pattern of the other sequences presented here and considering the deepening process of the basin, the SB4 is here placed at the top of the last centimetric level of carbonate that occurs about 13 m after the base of the Serra Alta Formation, characterized by a progradational pattern.

5.9. DEPOSITIONAL MODEL

The siliciclastic-carbonate mixed succession studied here is compatible with a homoclinal ramp model in an epicontinental sea (Burchette & Wright, 1992; Flügel, 2004). Despite the enclosed basin condition predominates marine settings. Barite minerals are observed within the laminated dolostone facies of the upper outer- mid ramp, also millimeter glauconites are common in the grey shale and within the dolostone beds. Both mineral formation takes place in similar low-sedimentation-rate marine settings (Bishop, 1988; Averyt & Paytan, 2003; Hesse & Schacht, 2011; Griffith & Paytan, 2012). Typical marine fossils such as cladodon teeth and *chondrichthyes*, previously found only for the base of Irati Formation (Taquaral Member), but here was found for the Assistência Member (upper). Furthermore, the high relative abundance of steranes (27aaaR/29aaaR), n-alkanes, isoprenoids and very low hopanes/steranes ratios, plus chroman ratios (< 0.6) are indicative of elevated contributions of the primarily marine red algae (Reis et al., 2018; Martins et al., 2020).

The wide distribution in the basin (> 10^6 km^2) and lateral continuity with a large area of interbedding typical distal and proximal facies attest to the very low gradient of an unrimmed and shallow marine platform. The Choiyoi magmatic arc emerging as a marginal structure to the foreland basin was an important element restricting the communication with the Panthalassa Ocean (Milani, 2004). Probably associated there was a progressive uplift of the southern edge of the basin, favoring a drastic reduction of the ramp slope and shallowing-up of the Irati sea, consequently reducing the accommodation space.

The effective restriction from the Panthalassa Ocean is evidenced by the low fossiliferous and palynological assemblage's characteristics of open-marine environments. Moreover, the dominant facies pattern and anoxic conditions on a very shallow platform. The last record of Permian acritarchs in the basin occurs at Irati Formation, concentrated in the basal portion of the unit (Araújo, 200; Neregato *et al*., 2008). However, the first evidence of paleogeographic adjustment in the Paraná Basin was found in the Rio Bonito Formation (Sakmariano). Canile *et al*. (2016) describe the shifts in the sediment source areas and the beginning of the Choiyoi arch contribution as a sediment source. Also, based on U-Pb, Lu-Hf, and O isotope data from detrital zircons those authors identified a considerable change in the patterns of the sedimentary source in the transition from the Palermo to Irati Formation. This condition was attributed to an intense process of denudation and flattening of the adjacent lands, leading to an increase in the sediment contribution (Irati, Serra Alta, and Teresina formations) from Argentina source rocks. The fine siliciclastic sediment, composed of angular quartz,

feldspar, and muscovites grains are widely distributed in the basin, suggesting a predominance of wind currents transport.

During the deposition of the basal, undisturbed, and poorly fossiliferous shale of the Taquaral Member, the platform already had a shallow and flat configuration. They constitute deposits with wide-ranging distribution (> 600km) and conformable contact with the underlying marine siliciclastic deposits of the Palermo Formation. The transition from bioturbated and oxidizing facies (Formation Palermo) to dark shale with preserved fabric (Taquaral Member) and these to cyclic siliciclastic and carbonates beds (Assistência Member), culminating in the formation of bituminous shale facies, indicates (i) long-term sea-level change (ii) seasonal climatic variation (wet vs. dry); (iii) changes in the chemical composition of the water with brine restriction; (iv) generation of anoxic conditions and progressive shallowing up of the basin. The basin restriction and shallowing up process under the effect of cyclic climatic changes favored the development of the mixed layers.

The very low slope creates a wide-ranging zone in the ramp for the fair-weather wave base. The occurrence of halite and length-slow chalcedony within dolostone beds suggests hypersaline condition even for the outer ramp. Likewise, lipid biomarker diagnostic of hypersaline condition (e.g. Nascimento et al., 2021) found with the bituminous offshore shale indicates that during dry seasons these conditions dominate the entirely Irate Sea. The marine platform with stratified water column and anoxic-bottom water favored organic matter preservation just below the water/sediment interface, producing the bituminous shale facies with COT values above 5% even in the beds cyclic alternating with the carbonate across the ramp.

The *Bothryococcus* occurrences recorded throughout the succession (Reis *et al*., 2018) concentrated in the oxidizing phases (Araújo, 2001) indicate the wet moments of freshwater influx that promoted salinity reduction and establishment of typical lake conditions at the photic zone. This environmental situation created a window of high planktonic organic production that was responsible for the elevated TOC values, with the high contribution of kerogen type I. The increasing water column during humid periods (high rainfall rate and continental inflow) generated accommodation and reduced the brine conditions required for the primary dolomite precipitation. Terrestrial input generated thicker shale beds and thin seaward dolostone-shale rhythmic sequences. Dry periods favor carbonate precipitation forming shallowing upward cycles.

The presence of mesosauridius fossils throughout the entire studied stratigraphic section, as well as described for San Miguel Formation (Chaco-Paraná Basin), Whitehill

Formation (Karoo Basin), and Huab Formation Huab Basin (Oelofsen & Araujo, 1983; Filippi *et al*., 2001; Werner, 2006; Xavier *et al*., 2018) indicates that the Whitehill-Irati sea was its natural habitat.

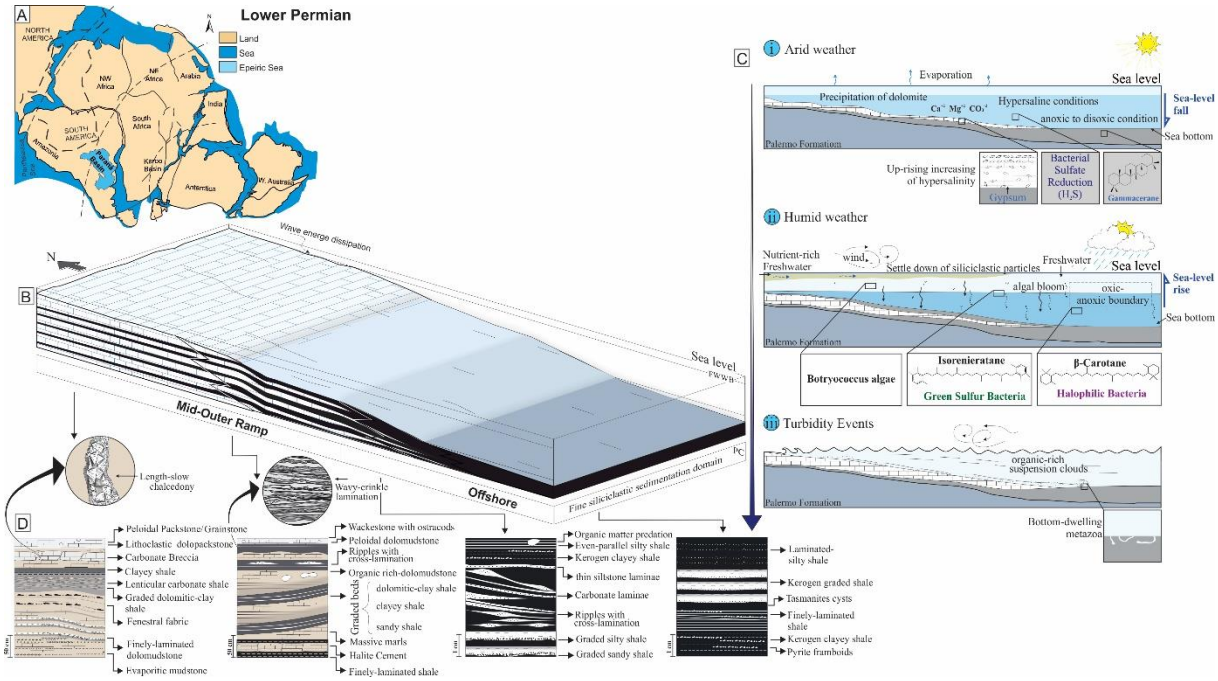

Fig. 17. Depositional model of the cyclic mixed siliciclastic-carbonate deposits of the Cisuralian Epicontinental Sea of the Paraná Basin. The cyclic sedimentation of the (A) shallow Irati Sea during the Lower Permian was characterized by (B) fine siliciclastic input, mainly eolic, during the wet season and carbonate-dominated production during the arid season. (C) The well-defined rhythmically intercalation was favored by the dominant low energy reworking process that remained throughout the ramp. i) Under arid climate predominates evaporation, hypersaline condition, and relative sea-level fall. ii) The nutrient-rich cyclic freshwater input induced high planktonic organic matter production and organic-rich shales formation. iii) The quiescence was sporadically interrupted by triggered turbidity currents that resuspend previously fell-out nutrient and plus, created short intervals of oxygenation in the anoxic environment. The shallow condition enhance carbonate production basinwards due to the low-angle slopes. (D) Main facies and microfacies pattern of the environmental subdivisions of the mixed homoclinal ramp.

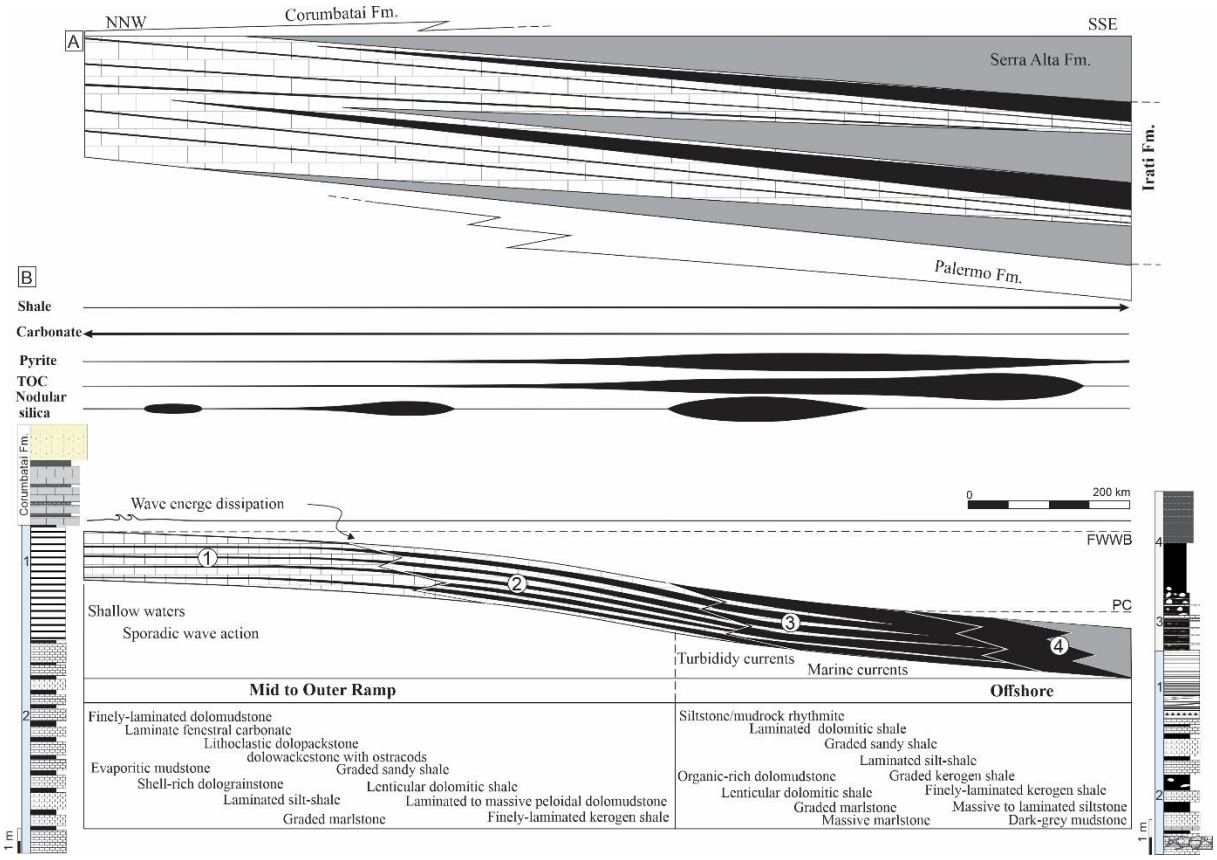

Fig. 18. Spatial distribution of the mixed siliciclastic-carbonate deposits of the Lower Permian, Paraná Basin. A) Lateral variation of the mixed deposits across the basin grading up to carbonate-free siliciclastic mudstone of Serra Alta Formation. The southernmost portion of the basin predominate offshore facies that become thinner toward the northernmost border, dominated by carbonate facies. B) temporal distribution of facies and microfacies grouped in retrogradational stacking pattern.

5.10. CONCLUSIONS

Detailing small-scale variation observed in fine-grained sedimentary facies show quite useful in the reconstruction of the paleoenvironment of fine sediment succession. The mixed lithological succession has a wide mixing spectrum that varies from siliciclastic- to carbonate-pure endmembers, where carbonate deposition coexists with siliciclastic in micro-, meso- and macro-scale with extensive lateral distributions. The Serra Alta Formation records a high rate of accommodation space and deepening of the basin. This process reduced the carbonate factory, typical of shallow conditions until it was totally overcome by siliciclastic inflow. The analysis of the rhythmic succession allowed the following conclusions:

i. Mixed sedimentation recorded on a very shallow platform during a greenhouse period is highly susceptible to the cyclic oscillation of sea-level related alternations between wet periods and dry periods.

ii. The low siliciclastic input on the platform, predominantly wind blow, was enhanced during wet periods by terrigenous inflow. The high carbonate production during dry periods diluted the siliciclastic input sedimentary bypass predominated. the resulting dolostones beds incorporate generally less than 3% of siliciclastics grains.

iii. The fine sedimentary mixed deposits can be grouped into twenty-one facies/microfacies records of a shallow sea. They are arranged in thickening upward patterns grouped into four depositional sequences.

iv. The lack of effective wave action enabled the platform to be mud-dominated.

v. The basal breccias of the Assistência Member occur with wide lateral distribution observed from north to south of the basin over the mudrocks of the Taquaral Member. Likewise, the rhythmic siliciclastic-carbonate layers overlying the breccias occur unaltered and undeformed. The carbonate level of the Taquaral Member also does not show any change. Thus, during burial compaction, the Taquaral Member shale acted as a geochemical barrier for fluid percolation, inducing the brecciation of the immediately overlying carbonates. The processes of post-depositional transformations at the base of Assistência Member were limited to a thin interval but basinwide.

vi. The anoxic and hypersaline conditions prevented effective colonization by macrobenthic fauna of the substrate by the benthic fauna. Therefore, carbonate production was restricted to biochemical and planktonic fauna induction in the photic zone and direct precipitation in the shallow ramp. Hypersaline conditions favor dolomite formation, as well as dolomitization under eogenetic conditions.

ACKNOWLEDGEMENTS

We thanks the National Council for Scientific and Technological Development (CNPq) for the Ph.D. scholarship of the first author (CNPq - 140630/2019-8) in the Programa de Pós-Graduação em Geologia e Geoquímica (PPGG) of the Federal University of Pará (UFPA). We are grateful to IRATI PETRÓLEO E ENERGIA LTDA for donate the drilling core. Thanks also extended to the Pró-Reitoria de Pesquisa e Pós-Graduação (PROPESP/UFPA) for linguistic revision support.

REFERENCES

Afonso, J.C., Cardoso, J.N. and **Schmal, M**. (1994) Hydrocarbon distribution in the Irati shale oil. *Fuel*, **73**, 363-366.

Aigner, T. (1985). An ancient storm depositional system: Dynamic stratigraphy of intracratonic carbonates, upper muschelkalk (middle Triassic), south-german basin. In: *Storm Depositional Systems: Dynamic Stratigraphy in Modern and Ancient Shallow-Marine Sequences* (Ed Aigner, T.), pp. 51-158. Springer, Berlin, Heidelberg.

Alferes, C.L., Rodrigues, R. and **Pereira E.** (2011) Geoquímica orgânica aplicada à Formação Irati, na área de São Mateus do Sul (PR), Brasil. *Geochimica Brasiliensis*, **25,** 47-54.

Allen, J.R.L. (1982) *Sedimentary structures, their character and physical basis*. *Developments in Sedimentology*, Elsevier, Amsterdam, 292 pp.

Almeida, F.F.M. (1980) Tectônica da Bacia do Paraná no Brasil. *Relatório da PAULPETRO n° 14091*, São Paulo, 187 pp.

Amaral S.E. (1971) Geologia e Petrologia da Formação Irati (Perminano) no estado de São Paulo. *PhD Thesis*, Universidade de São Paulo, São Paulo, 81 pp.

Anjos, C.W.D. and **Guimarães, E.D.** (2008) Metamorfismo de contato nas rochas da Formação Irati (Permiano), norte da Bacia do Paraná. *Rev. Bras. de Geociências*, **38**, 629-641

Araújo, L.M. (2001) Análise da expressão estratigráfica dos parâmetros de geoquímica orgânica e inorgânica nas sequências Irati. *PhD Thesis*, Universidade Federal do Rio Grande do Sul. 342 pp.

Arthur, M.A. and **Sageman, B.B.** (1994). Marine black shales: depositional mechanisms and environments of ancient deposits. *Annual Review of Earth and Planetary Sciences*, **22**, 499-551.

Averyt, K.B. and Paytan, A. (2003) Empirical partition coefficients for Sr and Ca in marine barite: implications for reconstructing seawater Sr and Ca concentrations. Geochem. Geophys. Geosyst., 4, 1043.

Baker, P.A. and **Kastner, M.** (1981). Constraints on the formation of sedimentary dolomite. *Science* **213**, 214–216.

Barnaby, R.J. and **Ward, W.B.** (2007). Outcrop analog for mixed siliciclastic–carbonate ramp reservoirs-stratigraphic hierarchy, facies architecture, and geologic heterogeneity: Greyburg Formation, Permian Basin, USA. *Journal of Sedimentary Research*, **77**, 34-58.

Bastos, L.P.H., Rodrigues, R., Pereira, E., Bergamaschi, S., Alferes, C.L.F., Augland, L.E., Domeier M., Svensen, H.H. (2021). The birth and demise of the vast epicontinental Permian Irati-Whitehill sea: Evidence from organic geochemistry, geochronology, and paleogeography. *Palaeogeogr. Palaeoclimatol. Palaeoecol*. **562**, 110103**.**

Bennett, R. H., O'Brien, N. R., and **Hulbert, M. H.** (1991) Determinants of clay and shale microfabric signatures: processes and mechanisms. In: *Microstructure of Fine-Grained Sediments* (pp. 5-32). Springer, New York, NY.

Berner. A. (1982). Burial of organic carbon and pyrite in the modem ocean: Its geochemical and environmental significance. *Amer. J. Sci.* **282**, 45l-475.

Berner, R.A. (1984). Sedimentary pyrite formation: an update. *Geochimica et cosmochimica Acta*, **48**, 605-615.

Betts, J.N. and **Holland, H.D.** (1991). The oxygen content of the ocean bottom waters, the burial efficiency of organic carbon, and the regulation of atmospheric oxygen. *Palaeogeogy, Palaeoclimatol., Palaeoecol.*, **97**, 5 –18.

Bishop, J.K.B. (1988) The barite-opal-organic carbon association in oceanic particulate matter. Nature, **311**, 341–343.

Borer, J.M. and **Harris, P.M.** (1991). Depositional facies and model for mixed siliciclastics and carbonates of the Yates Formation, Permian Basin. In: *Mixed Carbonate–Siliciclastic Sequences* (Eds. Lomando, A.J., and Harris, P.M.), SEPM, Core Workshop 15, pp. 1–133.

Braga, J.C., De Neira, A.D., Lasseur, E., Mediato, J., Aguirre, J., Abad, M., HernaizHuerta, P.P., Monthel, J., Perez-Valera, F. and **Lopera, E.** (2012) Pliocene-lower Pleistocene shallow-water mixed siliciclastics and carbonates (yanigua and los haitises formations) in eastern hispaniola (Dominican Republic). *Sediment. Geol.*, **15**, 182-194

Braissant, O., Decho, A. W., Dupraz, C., Glunk, C., Przekop, K. M. and **Visscher, P. T.** (2007) Exopolymeric substances of sulfate-reducing bacteria: interactions with calcium at alkaline pH and implication for the formation of carbonate minerals. *Geobiology*, **5**, 401-411.

Bralower, T.J. and **Thierstein, H.R.** (1984) Organic carbon and metal accumulation rates in Holocene and mid-Cretaceous sediments: paleoceanographic significance. In: *Marine Petroleum Source Rocks* (Eds. Brooks, J. and Fleet, A.J.). Geological Society, pp. 345– 369. London Special Publication

Branch, T., Ritter, O., Weckmann, U., Sachsenhofer, R.F. and **Schilling, F.** (2007) The Whitehill Formation–a high conductivity marker horizon in the Karoo Basin. *South African Journal of Geology*, **110**, 465-476.

Brandano, M., Tomassetti, L., Bosellini, F. and Mazzucchi, A. (2010). Depositional model and paleodepth reconstruction of a coral-rich, mixed siliciclastic-carbonate system: he Burdigalian of Capo Testa (northern Sardinia, Italy). *Facies* **56**, 433-444

Burchette, T.P. and **Wright, V.P.** (1992) Carbonate ramp depositional systems. *Sedimentary geology*, **79**, 3-57.

Calvert, S.E. (1987) Oceanographic control on the accumulation of organic matter in arine sediments. In: *Marine petroleum source rocks* (eds. J. Brooks and A.J. Fleet), pp. 137-52. Geological Society Special Publication, 26

Canile, F.M., Babinski, M. and **Rocha-Campos, A.C.** (2016) Evolution of the Carboniferous-Early Cretaceous units of Paraná Basin from provenance studies based on U-Pb, Hf and O isotopes from detrital zircons. *Gondwana Research,* **40**, 142-169.

Castanier S., Métayer-Levrel G.L. and **Perthuisot J.P.** (1999) Ca-carbonates precipitation and limestone genesis – the microbiogeologist point of view. *Sedimentary Geology* **126**, 9–23.

Castro, J.C., Maciel, U., Alves, C.F.C. and **Grecchi, R.C. (**1993) O Grupo Guatá na margem nordeste da Bacia do Paraná: uma revisão. *In*: I Simpósio sobre a cronoestratigrafa da Bacia do Paraná, Rio Claro**.** *Boletim de Geociências*, p. 55-56.

Chahud A. (2007) Paleontologia de Vertebrados da Transição entre os grupos Tubarão e Passa Dois no Centro-Leste do Estado de São Paulo. MS Dissertation, Programa de Pós-graduação em Geologia Sedimentar. IGc-USP. São Paulo. 172p

Chiarella, D. and **Longhitano, S.G.** (2012). Distinguishing depositional environments in shallow-water mixed bio-siliciclastic deposits on the base of the degree of heterolithic segregation (Gelasian, Southern Italy). *J. Sediment. Res*. **82**, 962-990.

Chiarella, D., Longhitano, S. G. and **Tropeano, M.** (2017). Types of mixing and heterogeneities in siliciclastic-carbonate sediments. *Marine and Petroleum Geology*, **88**, 617-627.

Conti, B., Gristo, P., Torres, M., Castiglioni, J., Portugau, P., Demarco, M. M., and **Cuña, A.** (2019) Characterization of Permian Mangrullo Formation (Uruguay) Oil Shale as a Source Rock and its Correlation with Irati (Brazil) and Whitehill (South Africa) Formations. *Geologica Acta,* **1**, 349-361.

Correa da Silva Z.C. and Cornford C. (1985) The kerogen type, depositional environment and maturity, of the Irati Shale, Upper Permian of Paraná Basin, Southern *Brazil. Org. Geochem.*, **8,** 399-411.

Daemon, R. F. (1996) Ensaio sobre a distribuição e zoneamento dos esporomorfos do Paleozóico Superior da Bacia do Paraná. *Boletim Técnico da PETROBRAS*, **9** p. 211-218.

De Figueiredo, A.M.F., Gabaglia, G.P.R. (1986) Sistema classificatório aplicado às bacias sedimentares brasileiras. *Revista Brasileira de Geociências*, **16,** 350·369.

De Medeiros, R. S. P., Nogueira, A. C. R., da Silva Junior, J. B. C. and **Sial, A. N.** (2019) Carbonate-clastic sedimentation in the Parnaiba Basin, northern Brazil: Record of carboniferous epeiric sea in the Western Gondwana. *Journal of South American Earth Sciences*, **91**, 188-202.

Demicco, R.V. and **Hardie, L.A.** (1995) Sedimentary structures and early diagenetic features of shallow marine carbonate deposits. *Atlas Series No. 1. Tulsa: SEPM (Society for Sedimentary Geology),* 265 pp.

Dickson, J.A.D. (1966) Carbonate identification and genesis as revealed by staining. *J. Sediment. Petrol.* **36**, 491–505.

Droste, H. (1990) Depositional cycles and source rock development in an epeiric intra-platform basin: the Hanifa Formation of the Arabian peninsula. *Sedimentary Geology*, **69**, 281-296.

Einsele, G. (1982) Limestone-marl cycles (periodites): diagnosis, significance, causes—a review. *Cyclic and event stratification*, 8-53p.

Filippi, V.A., Presser, J.L.B. and **Kochalka, J.** (2001). Sedimentos de relleno del rift de Asunción junto al área entre Sapucai – Ybytymí – La Colmena – Chauria, se equivaldrían con la Formación San Miguel (Pérmica)? o la Formación Misiones (Mesozoica)?. In: *II Simposio Paraguayo de Geologia & III Simposio Paraguayo de Aguas Subterráneas y Perforación de Pozos*. AGP, SPAS, SEAM. Assuncion.

Flood, P.G. and **Orme, G.R.** (1988) Mixed siliciclastic/carbonate sediments of the northern Great Barrier reef province, Australia. *In Developments in Sedimentology*, Elsevier. **42**, 175-205.

Flugel, E. (2004) *Microfacies of Carbonate Rocks, Analysis, Interpretation and Application*. Springer, Berlin, 924 pp.

Folk, R. L. and **Pittman, J. S.** (1971) Length-slow chalcedony; a new testament for vanished evaporites. *Journal of Sedimentary Research*, **41**, 1045-1058.

Font, E., Nédélec, A., Trindade, R.I.F., Macouin, M. and **Charrière, A.** (2006) Chemostratigraphy of the Neoproterozoic Mirassol d'Oeste cap dolostones (Mato Grosso, Brazil): an alternative model for Marinoan cap dolostone formation. *Earth and Planetary Science Letters*, **250**, 89-103.

Franco, N., Kalkreuth, W. and **Peralba, M.D.C.R.** (2010) Geochemical characterization of solid residues, bitumen and expelled oil based on steam pyrolysis experiments from Irati oil shale, Brazil: A preliminary study. *Fuel*, **89**, 1863-1871.

Garcia-Garcia, F., Soria, J.M., Viseras, C. and **Fernandez, J.** (2009) High-frequency rhythmicity in a mixed siliciclastic–carbonate shelf (Late Miocene, Guadix Basin, Spain): a model of interplay between climatic oscillations, subsidence, and sediment dispersal. *Journal of Sedimentary Research*, **79**, 302-315.

Gramigna, P., Bassi, D. and **Russo, F. (**2012). An Upper Miocene siliciclastic-carbonate ramp: depositional architecture, facies distribution, and diagenetic history (Capo Vaticano area, southern Italy). *Facies* **58**, 191-215.

Hachiro, J. (1996) O subgrupo Irati (Neopermiano) da Bacia do Paraná. *PhD Thesis*, Universiade de São Paulo. 248 pp.

Hachiro, J. and **Coimbra A.M.** (1992). Bone beds e shell beds como feições diagnósticas de tempestitos da formação irati no estado de são paulo. In: *37° Congresso Brasileiro de Geologia*, SBG/SP, São Paulo anais... 511-512.

Hender, K.L.B. and **Dix, G.R.** (2008). Facies development of a Late Ordovician mixed carbonate-siliciclastic ramp proximal to the developing Taconic orogen: Lourdes Formation, Newfoundland, Canada. *Facies* **54**, 121-149.

Hofmann, Richard. (2016) The end-Permian mass extinction. In: Mángano, M. G., and Buatois, L. A. (Eds.). The Trace-Fossil Record of Major Evolutionary Events. *Springer*, Dordrecht, p. 325-349.

Holz M., França A.B., Souza P.A., Iannuzzi R. and **Rohn R.** (2010.) A stratigraphic chart of the Late Carboniferous/Permian succession of the eastern border of the Paraná Basin, Brazil, South America. *Journal of South American Earth Sciences*, **29**, 381-399.

Irwin, M. L. (1965) General theory of epeiric clear water sedimentation. *AAPG Bulletin*, **49**, 445-459.

Jin, C., Liao, Z. and **Tang, Y.** (2020) Sea-level changes control organic matter accumulation in the Longmaxi shales of southeastern Chongqing, China. *Marine and Petroleum Geology*, **119**, 104478.

Kenig, F., Huc, A. Y., Purser, B. H. and **Oudin, J. L.** (1990) Sedimentation, distribution and diagenesis of organic matter in a recent carbonate environment, Abu Dhabi, UAE. *Organic Geochemistry*, **16**, 735-747.

Kiehl, J.T. and **Shields C.A.** (2005) Climate simulation of the latest Permian: Implications for mass extinction. *Geology*, **33,** 757–760.

Kvale, E.P., Bowie, C.M., Flenthrope, C., Mace, C., Parrish, J.M., Price, B., Anderson S. and **DiMichele, W.A.** (2020) Facies variability within a mixed carbonate–siliciclastic sea-floor fan (upper Wolfcamp Formation, Permian, Delaware Basin, New Mexico). *AAPG Bulletin*, **104**, 525-563.

Lages L.C. (2004) A formação Irati (grupo passa dois, permiano, bacia do Paraná) no furo de sondagem FP-01-PR (Sapopema, PR). *MS Dissertation*, Universidade Estadual Paulista, Rio Claro, 117p.

Lankarani, M., Amini, A. and **Mosadegh, H.** (2009) Facies Analysis and Depositional Environment of the Permian Siliciclastic-Carbonate Transition, Central Alborz, Iran. *Journal of Damghan University of Basic Sciences*, **2**, 25-36.

Laporte, L. F. (1978) Recognition of a transgressive carbonate sequence within an epeiric sea: Helderberg Group (lower Devonian) of New York State. Depositional Processes in Ancient Carbonates: *Society of Economic Paleontologist and Mineralogist, reprint series*, **7**, 54-75.

Lavina, E., Barberena, D. A. and **Azevedo, S. A.** (1991) Tempestades de inverno e altas taxas de mortalidade de répteis mesossauros. Um exemplo a partir do afloramento Passo São Borja, RS. *Pesquisas em Geociências*, **18**, 64-70.

Lee, C., (1992). Controls on organic carbon preservation: the use of stratified water bodies to compare intrinsic rates of decomposition in oxic and anoxic systems. *Geochim. Cosmochim. Acta,* **56**, 3323– 3335

Levin, L.A., Huggett, C. L. and **Wishner, K.F.** (1991) Control of deep-sea benthic community structure by oxygen and organic-matter gradients in the eastern Pacific Ocean. *Journal of Marine Research*, **49**, 763-800.

Limarino, C.O. and **Spalletti, L.A.** (2006) Paleogeography of the upper Paleozoic basins of southern South America: An overview. *Journal of South American Earth Sciences*, **22**, 134-155.

Longhitano, S.G., Sabato, L., Tropeano, M. and **Gallicchio, S.** (2010). A mixed bioclasticesiliciclastic flood-tidal delta in a microtidal setting: depositional architectures and hierarchical internal organization (Pliocene, southern apennine, Italy). *J. Sediment. Res*. **80**, 36e53

Mann, S. (1995) Biomineralization and biomimetic materials chemistry. *J Mater Chem,* **5**, 935-946.

Maraschin, A.J. and **Ramos, A.S.** (2015) Breve abordagem histórica sobre o potencial energético dos folhelhos da formação Irati (Bacia do Paraná) no Estado do Rio Grande do Sul. *Boletim Geográfico do Rio Grande do Sul*, **25**, 174-183.

Martins, L. L., Schulz, H. M., Ribeiro, H. J. P. S., do Nascimento, C. A., de Souza, E. S., and Da Cruz, G. F. (2020). Organic gepchemical of freshwater dynamics contolling salinity stratification in organic-rich sgales in the Lower Permian Irati Formation (Paraná Basin, Brazzil. *Organic Geochemistry*, 140, 103958.

Massari F. and **Chiocci F.** (2006) Biocalcarenite and mixed cool-water prograding bodies of the Mediterranean Pliocene and Pleistocene: architecture, depositional setting and forcing factors. In: Cool-water carbonates: depositional systems and palaeoenvironmental controls (Eds. Pedley H.M. and Carannante G.). *Geol. Soc. Lond. Spec. Publ.* **255**, 95–120.

Massari, F. and **D'Alessandro, A.** (2010) Icehouse, cool-water carbonate ramps: the case of the Upper Pliocene Capodarso Fm (Sicily): role of trace fossils in the reconstruction of growth stages of prograding wedges. *Facies,* **56**, 47.

Matos, S. A., Warren, L. V., Varejão, F. G., Assine, M. L. and **Simoes, M. G.** (2017) Permian endemic bivalves of the "Irati anoxic event", Paraná Basin, Brazil: Taphonomical, paleogeographical and evolutionary implications. *Palaeogeography, Palaeoclimatology, Palaeoecology*, **469**, 18-33.

Mazzullo, S.I. and **Reid,** AM. (1989) Lower Permian platform and basin depositional systems, northern Midland Basin, Texas. In: *Controls on Carbonate Platform and Basin Development* (Eds. Crevello, P.D., Wilson, J.L., Sarg, IF. and Read, J.F.). SEPM Spec. Publ. **44**, 305-320.

Meyer, K.M., Kump, L.R. and **Ridgwell, A.** (2008) Biogeochemical controls on photic-zone euxinia during the end-Permian mass extinction. *Geology*, **36,** 747-750.

Milani, E.J. (1997) Evolução tectono-estratigráfica da Bacia do Paraná e seu relacionamento com a geodinâmica fanerozóica do Gondwana sul-ocidental. *PhD Thesis,* Universidade Federal do Rio Grande do Sul, Porto Alegre.

Milani, E.J. (2004). Comentários sobre a origem e a evolução tectônica da Bacia do Paraná. In: *Geologia do continente sul-americano: evolução da obra de Fernando Flávio Marques de Almeida* (Eds. Mantesso Neto V., Bartorelli A., Carneiro C.D.R., Brito Neves B.B.). São Paulo, Beca, pp. 265-279.

Milani, E.J. and **Ramos V.A.** (1998). Orogenias paleozóicas no domínio sul-ocidental do Gondwana e os ciclos de subsidência da Bacia do Paraná. *Revista Brasileira de Geociências*, **28,** 473-484.

Milani E.J., França A.B. and **Medeiros R.A.** (2007). Rochas geradoras e rochas-reservatório da Bacia do Paraná, faixa oriental de afloramentos, Estado do Paraná. *Boletim de Geociências da PETROBRÁS,* **15,** 135-162.

Milani, E.J., Melo, J.H.G., Souza, P.A, Fernandes, L.A. and **França A.B** (2007) Bacia do Paraná. *B. Geoci. Petrobras*, Rio de Janeiro, **15**, 265-287.

Mount, J.F., 1985. Mixed siliciclastic and carbonate sediments: a proposed firstorder textural and compositional classification. *Sedimentology* **32**: 435-442.

Myrow, P.M., Taylor, J.F., Runkel, A.C. and **Ripperdan, R.L.** (2012) Mixed siliciclastic–carbonate upward-deepening cycles of the Upper Cambrian inner detrital belt of Laurentia. *Journal of Sedimentary Research*, **82**, 216-231.

Neregato, R., Souza, P. A. D. and **Rohn, R.** (2008) Registros palinológicos inéditos nas formações Teresina e Rio do Rasto (Permiano, Grupo Passa Dois, Bacia do Paraná): implicações biocronoestratigráficas e paleoambientais. *Pesquisas em Geociências*,**35,** 9-21.

Ng, C., Vega, C. S. and **Maranhão, M. D. S. A. S.** (2019) Mixed carbonate-siliciclastic microfacies from Permian deposits of Western Gondwana: evidence of gradual marine to continental transition or episodes of marine transgression?. *Sedimentary Geology*, **390**, 62-82.

O'Brien, N.R. (1996) Shale lamination and sedimentary processes. *Geological Society, London,* Special Publications, **116**, 23-36.

Oelofsen, B. and **Araújo, D.C.** (1983) Paleoecological implications of the distribution of mesosaurid reptiles in the Permian Irati Sea (Paraná Basin), South America: *Rev. bras.* 1-6.

Ortega-Villamagua, E., Gudiño-Gomezjurado, M. and **Palma-Cando, A.** (2020) Microbiologically induced carbonate precipitation in the restoration and conservation of cultural heritage materials. *Molecules*, **25**, 5499.

Pedersen, G.K. (1985) Thin, fine grained storm layers in muddy shelf sequences: an example from the lower Jurassic in the Stenhille 1 Well, Denmark. *Journal of the Geological Society*, **142**, 357-373.

Potter, P. E., Maynard, J. B., and **Pryor, W. A.** (2012) Sedimentology of shale: study guide and reference source. *Springer Science & Business Media*. 327 p.

Pratt, B.R. (2010) Peritidal Carbonates. In: *Facies Model 4* (Eds. James N.P. and Dalrymple R.W.), Geological Association of Canada, pp. 401-420

Puga-Bernabéu, Á. N. G. E. L., Martin, J. M., Braga, J. C. and **Sánchez-Almazo, I. M.** (2010) Downslope-migrating sandwaves and platform-margin clinoforms in a current-dominated, distally steepened temperate-carbonate ramp (Guadix Basin, Southern Spain). *Sedimentology*, **57**, 293-311.

Quintas M.C.L., Mantovani M.S.M. and **Zalán P.V.** (1999) Contribuição ao estudo da evolução mecânica da Bacia do Paraná. *Revista Brasileira de Geociências*, **29**, 217-226.

Rabouille, C. and **Gaillard, J.F.** (1991) Towards the EDGE: Early diagenetic global explanation. A model depicting the early diagenesis of organic matter, O, NO, Mn, and 0 4. *Geochimica et Cosmochimica Acta*, **55**, 2511-2525

Raiswell, R. and **Berner, R.A.** (1985) Pyrite formation in euxinic and semi-euxinic sediments. American Journal of Science, **285,** 710-724.

Reading, H.G. (1996) *Sedimentary environments: processes, facies and stratigraphy*. 3rd Edition. Blackwell Science, New Jersey, 688 p.

Reineck, H.-E. and **Singh, I.B.** (1972) Genesis oflaminated sand and graded rhythmites in storm-sand layers of shelf mud. *Sedimentology* **18**, 123-128

Reineck, H.E. and **Singh, I.B.** (1973) Depositional environments. In: Depositional Sedimentary Environments. Springer, Berlin, Heidelberg. pp. 4-6.

Reis D.E.S., Rodrigues R., Moldowan J.M., Jones C.M., Brito M., Cavalcante D.C. and **Portela H.A.** (2018) Biomarkers stratigraphy of Irati Formation (Lower Permian) in the southern portion of Paraná Basin (Brazil). *Marine and Petroleum Geology*, **95,** 110-138.

Rohn R. (2007) The Passa Dois group (Paraná Basin, Permian): investigations in progress. In: **Ianuzzi, R., Boardman, D.R.** (Eds.), I Workshop - Problems in Western Gondwana Geology, South America - Africa Correlations: *Du Toit Revisited. Petrobrás*, Gramado, pp. 151–157.

Sageman, B. B., Murphy, A. E., Werne, J. P., Ver Straeten, C. A., Hollander, D. J. and **Lyons, T. W.** (2003) A tale of shales: the relative roles of production, decomposition, and dilution in the accumulation of organic-rich strata, Middle–Upper Devonian, Appalachian basin. *Chemical Geology*, **195**, 229-273.

Santos R.V., Dantas E.L., Olveira C.G., Alvarenga C.J.S., Anjos C.W.D., Guimarâes E.M. and **Oliveira F.B.** (2009) Geochemical and thermal effects of a basic sill on black shales and

limestones of the Permian Irati Formation. *Journal of South American Earth Sciences*, **28,** 14-24.

Santos, R. V., Souza, P. A., de Alvarenga, C. J. S., Dantas, E. L., Pimentel, M. M., de Oliveira, C. G. and **de Araújo, L. M.** (2006) Shrimp U–Pb zircon dating and palynology of bentonitic layers from the Permian Irati Formation, Paraná Basin, Brazil. *Gondwana research*, **9**, 456-463.

Schieber, J. (1989) Facies and origin of shales from the Mid-Proterozoic Newland formation, Belt basin, Montana, U.S.A. *Sedimentology* **36**, 203–219.

Schieber, J. (2011) Reverse engineering mother nature: shale sedimentology from an experimental perspective: *Sedimentary Geology*, **238**, 1–22.

Schieber, J. and **Southard, J.B.** (2009) Bedload transport of mud by floccule ripples – direct observation of ripple migration processes and their implications. *Geology* **37**, 483–486.

Schieber, J., Southard, J.B. and **Schimmelmann, A.** (2010) Lenticular shale fabrics resulting from intermittent erosion of muddy sediments - comparing observations from flume experiments to the rock record. *Journal of Sedimentary Research* **80**, 119–128

Schieber, J., Sur, S. and **Banerjee, S.** (2007) Benthic microbial mats in black shale units fromthe Vindhyan Supergroup, Middle Proterozoic of India: the challenges of recognizing the genuine article. In: *Atlas of Microbial Mat Features Preserved within the Clastic Rock Record* (Eds. Schieber, J., *et al*.). Elsevier, Amsterdam, pp. 189–197.

Scholle, P.A. and **Ulmer-Scholle, D.S.** (2003) A color guide to the petrography of carbonate rocks: grains, textures, porosity, diagenesis, *AAPG Memoir 77*, pp. 470.

Schwarzacher, W., and **Fischer, A.G.,** (1982) Limestone — shale bedding and perturbations in the earth's orbit. *In*: Einsele, G., Seilacher, A. (Eds.), Cyclic and Event Stratification. Springer-Verlag, Berlin, pp. 72–95.

Shinn, E. A. (1983) Tidal flat environment. Carbonate depositional environments: *AAPG Memoir*, **33**, 172-210.

Soares, M. B. (2003) A taphonomic model for the Mesosauridae assemblage of the Irati Formation (Paraná Basin, Brazil). *Geologica Acta: an international earth science journal*, **1**, 349-361.

Soares P.C., Soares A.P. and **Bettú D.F.** (2014) Formação da sequência triássico-jurássica na Bacia do Paraná. *Boletim de Geociências da Petrobrás*, **22,** 135-160.

Stanley S. M. (2009) *Earth System History*, third edition. New York, W. H. Freeman and Company, pp. 580.

Stow, D. V., and **Piper, D. W.** (1984) Fine-grained sediments: deep-water processes and facies: Proceedings and discussion of the International workshop, held Halifax, Canada, in August 1982. *Special Publication-Geological Society of London*, **15,** p. 633.

Stow, D. A., and **Shanmugam, G.** (1980). Sequence of structures in fine-grained turbidites: comparison of recent deep-sea and ancient flysch sediments. *Sedimentary Geology*, **25**(1-2): 23-42.

Tänavsuu-Milkeviciene, K.A.T.I., Plink-Björklund, P.I.R.E.T., Kirsimäe, K. and **Ainsaar, L.** (2009) Coeval versus reciprocal mixed carbonate–siliciclastic deposition, Middle Devonian Baltic Basin, Eastern Europe: implications from the regional tectonic development. *Sedimentology*, **56**, 1250-1274.

Thickpenny, A. (1984) The sedimentology of the Swedish alum shales. *Geological Society*, London, Special Publications, **15**, 511-525.

Tucker, M.E. 1991. Sequence stratigraphy of carbonate-evaporite basins: models and application to the Upper Permian (Zechstein) of northeast England and adjoining North Sea. *Journal of the Geological Society*, **148,**1019-1036.

Tucker, M.E. and **Wright, V.P.** (1990) *Carbonate Sedimentology*. Blackwell Scientific Publications, Oxford, 468 pp.

Tyson, R.V. (1987) The genesis and palynofacies characteristics of marine petroleum source rocks. In: *Marine Petroleum Source Rocks* (Eds. Brooks J. and Fleet A.J.), Geological Society Special Publication, **26**, 47-67

Tyson R.V. 1995. *Sedimentary Organic Matter: Organic Facies e Palynofacies Analysis*. London, Chapman & Hall, pp.615

Ulmer-Scholle, D. S., Scholle, P. A., Schieber, J. and **Raine, R. J.** (2014). *Diagenesis: Carbonate Cements and Authigenic Precipitates*. AAPG Memoir 109, pp. 540.

Van Lith, Y., Warthmann, R., Vasconcelos, C. and **McKenzie, J.A.** (2003) Sulphate-reducing bacteria induce low-temperature Ca-dolomite and high Mg-calcite formation. *Geobiology* **1**, 71–79.

Vasconcelos, C. and **McKenzie, J.A.** (1997) Microbial mediation of modern dolomite precipitation and diagenesis under anoxic conditions (Lagoa Vermelha, Rio de Janeiro, Brazil). *J. Sed. Res*. **67**, 378–390.

Vasconcelos, C., McKenzie, J. A., Bernasconi, S., Grujic, D. and **Tiens, A. J.** (1995) Microbial mediation as a possible mechanism for natural dolomite formation at low temperatures. *Nature*, **377**, 220-222.

Walker, R.G. (1992) Facies, facies models and modern stratigraphic concepts. *In*: Walker, R. & James, N. (Eds.) Facies Models – Response to sea Level Change. Ontario, Geological Association of Canadá. 265-275p.

Walker R.G. and James N.P. (1992) *Facies Models Response to sea level change*. Ontario, Geological Association of Canada, pp. 409.

Warthmann R, van Lith Y, Vasconcelos C, McKenzie JA, Karpoff AM (2000) Bacterially induced dolomite precipitation in anoxic culture experiments. *Geology* **28**, 1091–1094.

Werner, M. (2006) The stratigraphy, sedimentology, and age of the Late Palaeozoic Mesosaurus Inland Sea, SW-Gondwana: new implications from studies on sediments and altered pyroclastic layers of the Dwyka and Ecca Group (lower Karoo Supergroup) in southern Namibia. *PhD thesis*, Universität Würzburg, pp. 428.

Westphal, H., Munnecke, A., Böhm, F. and **Bornholdt, S.** (2008) Limestone–marl alternations in epeiric sea settings–witnesses of environmental changes or diagnesis?. *Special Paper–Geological Association of Canada*, **389**, 406.

Wignall, P.B. (1994). *Black shales*. Oxford: Clarendon Press. Pp.136.

Wright, V. P. (1984) Peritidal carbonate facies models: a review. *Geological Journal*, **19**, 309-325.

Wright, V. P. (1992) A revised classification of limestones. *Sedimentary geology*, **76**(3-4), 177-185.

Wright D. (1999) The role of sulfate-reducing bacteria and cyanobacteria in dolomite formation in distal ephemeral lakes of the Coorong region South Australia. *Sedimentary Geology*, **126**, 147–157

Xavier P.L.A., Silva A.F., Soares M.B., Horn B.L.D. and **Schultz C.L.** 2018. Sequence stratigraphy control on fossil occurrence and concentration in the epeiric mixed carbonate-siliciclastic ramp of the Early Permian Irati. *Journal of South American Earth Sciences*, **88**, 157-178.

Yawar, Z. and **Schieber, J.** (2017) On the origin of silt laminae in laminated shales. *Sedimentary Geology*, 360, 22-34.

Zalán, P. V., Wolff, S., Astolfi, M. A. M., Vieira, I. S., Conceição, J. C. J., Appi, V. T., Santos Neto, E. V., Cerqueira, J. R. and **Marques, A.** (1990) The Paraná Basin, Brazil. In: *Interior cratonic basins* (Eds. Leighton, M. W., Kolata, D. R., Oltz, D. F., Eidel, J. J.). Tulsa: American Association of Petroleum Geologists. AAPG. Memoir, 51. pp. 681-708.

Zecchin, M. and **Caffau, M.** (2011) Key features of mixed carbonate-siliciclastic shallow marine systems: the case of the Capo Colonna terrace (southern Italy). *Ital. J. Geosci. Boll. Soc. Geol. It.* **130**, 370-379.

Zecchin, M. and **Catuneanu, O.** (2013) High-resolution sequence stratigraphy of clastic shelves I: units and bounding surfaces. *Marine and Petroleum Geology*, **39**, 1-25.

Zeller, M., Verwer, K., Eberli, G. P., Massaferro, J. L., Schwarz, E. and **Spalletti, L.** (2015) Depositional controls on mixed carbonate–siliciclastic cycles and sequences on gently inclined shelf profiles. *Sedimentology*, **62**, 2009-2037.

Zhu, T. and **Dittrich, M.** (2016) Carbonate precipitation through microbial activities in natural environment, and their potential in biotechnology: a review. *Frontiers in bioengineering and biotechnology*, **4**, 4.

CAPÍTULO VI

6. High-Frequency cyclicity and organic matter distribution in Shallow Mixed Carbonate-Siliciclastic Ramp: a case of Irati Formation, Paraná Basin, Brazil

Ailton da Silva Brito[1], Afonso César Rodrigues Nogueira[1], Lorena Tuane Gomes de Almeida[2], Sidney Gonçalo de Lima[2]

[1]*Programa de Pós-Graduação em Geologia e Geoquímica, Instituto de Geociências, Universidade Federal do Pará, Rua Augusto Corrêa s/no, 66075-110, Belém, PA, Brazil, R. Augusto Corrêa 01, Belém 66075-110, Brazil*

[2]*Programa de Pós-Graduação em Química, Universidade Federal do Piauí, Campus Ministro Petrônio Portela, 64049-550, Teresina-PI, Brazil*

ABSTRACT

Mixed deposition in the shallow sea is high sensitivity to climate variation and sea-level change, becoming the primary controls of high-frequency cycles in the stratigraphic record. The widespread Cisuralian mixed carbonate-siliciclastic succession of Paraná Basin is composed of rhythmically organic-rich shale interbedded with dolostone beds. They are organized in superimposed asymmetrical facies stacking patterns developed in a broad epeiric sea that extended over 10^6 km^2 of the Permian Gondwana land. Detailed sedimentological and stratal stacking analysis allowed the hierarchical organization to be identified in small-scale, medium-scale, and large-scale stacking patterns. The high-frequency depositional cycles compose four 3rd-order sequences. They comprise grey to black shale, marls, and peloidal to micritic dolostone. Due to shallow water settings, the minimal available accommodation space is responsible for the reduced cycles thickness and the overall mixed succession. The rhythmic deposits host highly productive hydrocarbon source-rock. Two widespread thicker intervals of bituminous shale developed during 3rd-order sequence transgression events are highly organic-rich oil-shale (27 wt%). In high-frequency stacking patterns, the succession formed by dolostone interbedded with bituminous laminae is also rich in organic carbon (2 to 8 wt%). The alternation of high carbonate and organic matter production was controlled by wet-dry seasons. Dry phases were prone to carbonate precipitation due to shallower and hypersaline conditions. Freshwater discharge in the shallow and hypersaline environment during wet stages induces water column stratification. This condition is indicated by the occurrence of kerogen type III and IV, high gammacerane index, variable Pr/Ph ratios, and C_{35} homo hopane indices. Also, the nutrient-rich in terrigenous favor algal blooms, enhancing the anoxia in bottom water responsible for the organic-rich shale facies indicated by kerogen type I and II, high hydrogen index, high C_{27}/C_{29} sterane rations, and combined with higher values of β-carotane. Based on the hierarchical organization of the studied succession and previously U-Pb SHRIMP zircon ages from volcanic-ash layers was possible to correlate with the global sea-level curve. An age of 8.0 Ma was determined for the Irati Sea, likewise an average of 2.7 Ma for the 3rd-order sequences. Furthermore, 26.6 ka, 135.5 ka, and 400 ka were calculated for the high-frequency

patterns compatible with the precession and eccentricity of short (± 100 ka) and significant periodicity (± 400 ka) of Earth orbit. The high-frequency cycles of organic-rich shales and carbonate deposited during thousands of years under long-term sea-level changes and correlated along the basin suggest a wet-dry climatic control driven by the Earth's orbital perturbation in the Milankovitch frequency band.

Keywords: Epicontinental sea, Organic-rich shale, Lipid biomarkers, Milankovitch cycles, Sea-level change.

6.1. INTRODUCTION

Mixed carbonate-siliciclastic sediments can occur from shallow to deep marine water. They are dominantly typical pelagic and hemipelagic basinal features (Burchell et al., 1990; Virgone et al., 1994; Eldrett et al., 2015). They are also a common feature in deep lakes, as exemplified by the Green River Formation. The generation of primary rhythmical stacking patterns are due to autocyclic (e.g., terrigenous input, carbonate factor, currents) and allocyclic factors (e.g., eustatic sea-level fluctuations, subsidence, climate) generally induced by orbital forcing (Schwarzacher, 1975; Burchell et al., 1990; Goldhammer et al., 1990; Virgone et al., 1994). Cyclicity in the stratigraphical record is a more robust indicator of cyclicity in time (Schwarzacher, 1975; Goldhammer et al., 1990). Cycles are a common element of marine platform successions throughout the geologic record, from Precambrian to Recent, which the stratigraphic record can be analyzed. The intracratonic basins are stable regions favoring the deposition control mainly by high-frequency sea-level changes (e.g., Droste, 1990; Crevello, 1991) and climate variation (e.g., Tresch and Strasser, 2011; Wallace and Elrick, 2014). The high-frequency shallowing-upward cycles become the building blocks of larger-scale, lower-frequency (third-order) depositional sequences (Goldhammer et al., 1993; Crevello, 1991; Kerans and Tinker, 1997; Bosence, 2000). The internal architecture of carbonate platform sequences commonly contains a record of superimposed orders of cyclicity (Grotzinger 1989; Goldhammer et al. 1990; 1991). A similar situation can be assumed for mixed deposits of shallow marine settings.

The hierarchic bundling of high-frequency cycles commonly has 10^5-10^6 years into stratigraphic packages. Nevertheless, sequence stratigraphic units are defined by stratal stacking patterns and specific bounding surfaces, not by inferred controls, age, time-span, or physical scales (Goldhammer et al., 1991; Catuneanu, 2019b). The application of sequence stratigraphic in intracratonic basins must consider their intrinsic characteristic. The scales, origins, and the composition of systems tract within sequences are a product of each basin,

reflecting the local conditions of accommodation and sedimentation (Catuneanu, 2019b). In intracratonic basin predominate ramp morphology with a low ratio of subsidence. The establishment of epicontinental seas creates reduced water depth and accommodation space, developing thin but extensive successions with horizontal sequence boundaries (Della Fávera, 2001), with typical tabular geometry. The shallow conditions make the storms, and turbidity currents are crucial in sediment redistribution. Likewise, sedimentation became strongly controlled by sea-level fluctuation ratios. Transgressive and highstand systems tracts commonly form depositional sequences in the intracratonic basins. Lowstand and forced regression systems are hardly recognized. In addition, lowstand deposits are missing or reworked in the subsequent transgressive events (Strasser et al. 1999). The authors state that the transgressive surface thus directly overlies the sequence boundary, and maximum flooding surface is not always developed. Still, the relatively deepest or most open-marine facies with reduced sedimentation rate indicate an interval of maximum flooding.

The Lower Permian (Cisuralian) mixed deposits of the Paraná Basin (Fig. 1) are the Brazilian intracontinental basins' primary oil shale source rocks. The bituminous shale is thin but widespread layers interbedding carbonate facies. The main intervals reaching 27 %wt of total organic carbon (TOC) occur at the uppermost portion of the second 3º order transgressive cycles. The carbonate and shale alternations of Irati formation produce thin bundles, however, widely distributed across the basin. The record shows more than 1,000,000 km of extension. Currently, there are many examples in the literature of mixed siliciclastic-carbonate systems. Nevertheless, detailed analyses of cyclicity are rare in this hybrid system with oil shales deposits. The purpose of this work is to determine the general features of these ubiquitous dolomudstone-black shale rhythmites previously interpreted as shallow to relatively deep-water deposits of a Lower Permian epicontinental sea. Meter-scale stacking pattern cycles analyzed combined with architectural geometry study provide a more robust paleogeographic model for the Irati shallow sea. Besides, the geochemical data presented here allow a better understanding of high organic matter production during the cyclic depositional controls.

6.2. GEOLOGY SETTING

The sedimentary succession in the Brazilian Phanerozoic basins is dominated by siliciclastic sediment. Mixed or carbonate-dominant deposits are rare (e.g., Itaituba Formation, Amazonas Basin). The mixed siliciclastic-carbonate succession of the Lower Permian Paraná Basin represents a particularity in this scenario. The wide deposition of carbonate interbedded

with shale occur in the context of the Pangea Supercontinent closure. The rhythmical intercalation produces a thin succession but is widespread in the Paraná Basin, from the southmost to the central portion of Brazil (Fig. 01). Those deposits extend to other South American countries of Argentina, Paraguay, and Uruguay. Also, they are correlated to Whitehill Formation in South Africa (Milani et al., 1998; Holz et al., 2010). The succession is part of the regressive deposits of the transgressive-regressive sequence that perdured from Upper-Carboniferous to Lower-Triassic (Milani, 1997).

The Upper-Carboniferous to Lower-Triassic Supersequence has in the base deposits related to the end of the Carboniferous glaciation (Caputo & Crowell, 1985) and at the top record of the desertification process of the end-Permian. This supersequence, also called Gondwana I (Fig. 01), encompasses the most significant sediment volume of the Paraná Basin, with a total thickness of 2,500 m (Milani et al., 2007). The development of this thick sedimentary package followed the more significant expansion and subsidence of the Paleozoic syneclisis with considerable tectonic and climatic changes (Almeida 1980). Overlying the peri-glaciers deposits of Itararé Group, under post-glacial transgressive conditions, occurred the deposition of coastal sediments of Rio Bonito Formation, composed of sandstone (deltaic), shale (marine), and coal (lagunar) deposits (Milani, 1997). The bioturbed fine shoreface deposits of the Palermo Formation record the Maximum Transgressive Surface (Milani et al., 1998). The following regression is recorded by Irati, Serra Alta, and Teresinha formations.

The Lower Permian mixed deposits of Paraná Basin are composed of four third-order sequences of transgressive-highstand succession separated by unconformities (Fig. 02). The Palermo Formation is composed of about 300m of marine deposits that record the maximum transgressive surface of the Gondwana I Supersequence (Milani et al., 2007). The uppermost heterolithic mudstone and sandstone deposits are overlaid by the Irati Formation divided into the Taquaral (down) and the Assistência Member (upper). The first is composed of grey to black shale with only one level of carbonate where the shell beds concentration occurs. The second member recorded the dominant high-frequency cyclicity composed of well-defined intercalation of carbonate and shale. The sediment deposits of the Serra Alta Formation are similar to Taquaral Member with thin intercalation of carbonate close to the base, however with a significant increase of the shale package thickness (60 a 90 m-thick) and occurrence of sandstone layers at the top. The limit between Irati and Serra Alta Formation is well-marked by the transition of organic-rich facies of Irati Fm. (black) to organic-poor (grey) shale of Serra Alta Fm. Also, the limit is evidenced in the geochemical profile (e.g., TOC, HI, $\delta^{13}C$). Toward the top, a thickening upward of sandstone interbedded with bioturbated mudrock layers forming

wavy-linsen-flaser bedding. Wavy cross-stratified sandstone in the uppermost portion of this succession defines the Teresinha Formation with 300 to 400 m-thick (Meglhioratti, 2006). The sandstone, siltstone, and shale of Rio do Rastro Formation finalized the Gondwana I sequence, representing the end of marine incursions initiating the continentalization of the Paraná Basin preceding the Permian arid conditions (Milani et al. 1998). The development of the *Choiyoi* magmatic arc from the Cisuralian (~286 Ma) to the early Triassic (~247 Ma) (Sato et al., 2015) was a crucial element for restricting the Paraná Basin connection with the Panthalassa Ocean (Milani, 2004).

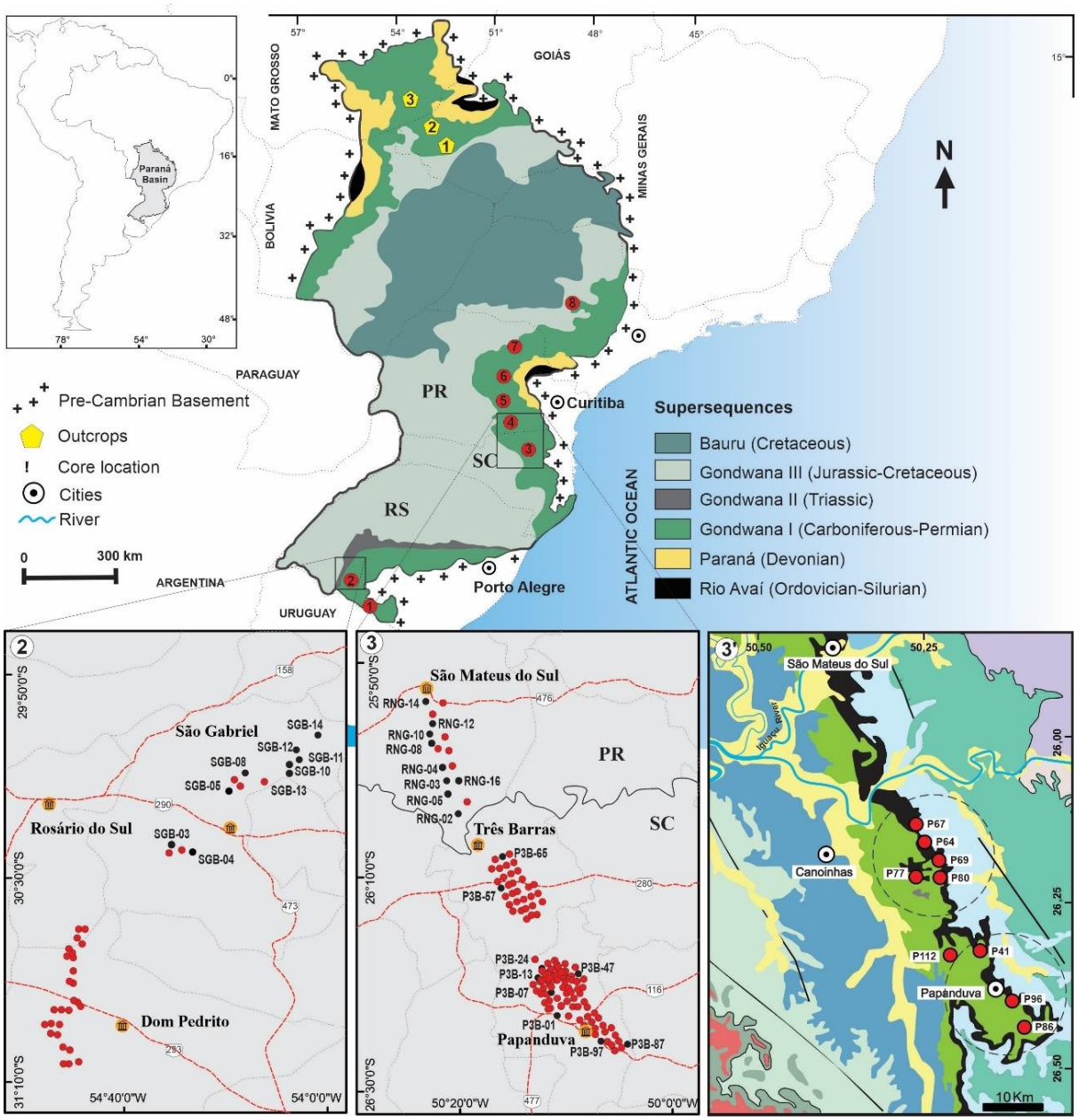

Fig. 1. Geology of the Paraná Basin. Above the distribution map of the second-order sequences of Paraná Basin with the location of the studied drill cores and outcrops. Below, the location of the drill cores in the southmost (B) and middle portion (C) of the basin, and (C') the location of the cores used to compose the representative profile shown in Fig. 03. The geochemical data is from the cores of the three southmost states: Paraná (PR), Santa Catarina (SC), and Rio Grande do sul (RS) states.

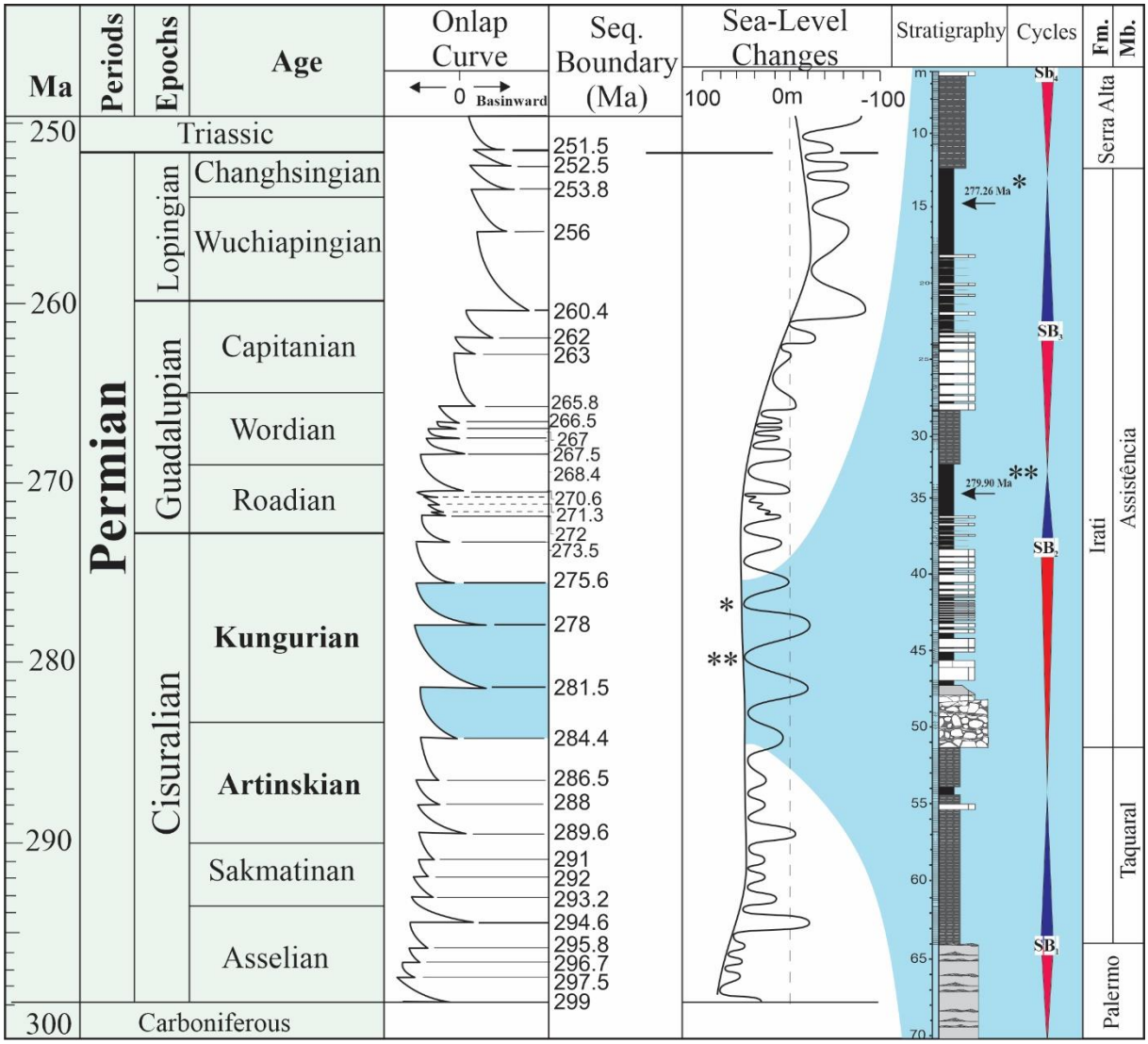

Fig. 2. Permian sea-level changes and the sequence boundary of the third-order cycles of the Cisuralian mixed siliciclastic-carbonate deposits of Paraná Basin. The time scale and sea-level curve are after Haq & Schutter (2008) and Gradstein et al (2012). The mixed -deposits cycles were recognized using the stratal stacking pattern, fisher plot, and high-resolution $\delta^{13}C$ curve correlated with the global sea-level curve. U-Pb zircon ages from volcanic-ash layers from *Bastos et al. (2021) and **Rocha-Campos et al. (2019).

6.3. METHODS

6.3.1 Sedimentology and Cyclicity

The 60 m-thick siliciclastic-carbonate succession of the Lower Permian Paraná Basin is essentially cyclic shales and dolostones forming tabular strata deposits, simplifying identification and correlation. Detailed logs were made of ten drill cores throughout 40 km^2. Different stacking patterns were identified from the depositional stacking pattern following Schwarzacher (2000) and Strasser et al. (2006). The characterization of cyclic patterns was improved by faciological analyses, thickening and thinning upward, retrogradational,

aggradational, and progradational trends, and defining key surfaces such as flooding surfaces. Facies descriptions supported by thin-section petrographic analyzes facilitated the definitions of the stacking patterns types. The high-frequency depositional cycles are equivalent to parasequences (Van Wagoner et al. 1988; Goldhammer et al., 1993; Holland, 1997; Catuneanu, 2019a). Decimeter- to meter-scale, asymmetrical patterns are defined as the 3rd, 4th, and 5th order (Fig. 03) high-frequency sequences (Catuneanu et al., 2011). Fisher Plots were used to illustrate cycles thickness variation (Sadler et al. 1993; Husinec et al. 2008), defining key surfaces, 'missing beats' (e.g., Balog et al. 1997), and subsurface correlation criteria.

6.3.2 Bulk organic matter analyses

The organic geochemistry data are from 102 drill cores distributed across the middle to southmost of Paraná Basin. The Weatherford Laboratories analyzed three thousand samples for total organic carbon and Rock-Eval pyrolysis to identify the generative potential, organic matter types, quality, quantity, and thermal maturity of the shale and marls. Selective samples were collected for biomarker analyses to characterize the organic matter preserved in the different types of mixed siliciclastic-carbonate cycles observed in succession.

6.3.3 Biomarker analyses

Three times, the powdered samples were extracted with 50 mL of dichloromethane/methanol (88:12 v/v) in ultrasonic baths. Approximately 500 mg of powdered copper metal was added to obtained extract for sulfur removal using ultrasound for 30 min under heating at 60 °C. The extracts were filtered and solvent-evaporated on a rotary evaporator. The extracts were fractionated by chromatographic column using silica as stationary phase and eluent system was *n*-hexane, hexane/ethyl acetate 12% (v/v), ethyl acetate/methanol 5% (v/v).

The GC-MS analysis of the saturated fractions was performed on a Shimadzu GCMS-QP2010 SE chromatograph equipped with AOC-5000 auto-injector, according to the following analysis conditions: injector temperature of 290 °C, splitless mode, initial oven temperature of 60 °C (1 min), then a heating ramp of 4 °C min^{-1} to 315 °C remaining for 15 min. For chromatography of components, a DB-5MS UI column, 30 m × 0.25 mm, 0.25 μm internal film thickness, helium as the carrier gas with a constant flow of 1.0 mL min^{-1}. The temperature of the interface and the ion source were 320 °C and 230 °C, respectively. The mass analyzer used was of the quadrupole type operating by electronic impact (70 eV) and fragments detected in

the range of 57 to 600 Da. The identification of the biomarkers was carried out by comparing the elution orders, retention times, and mass spectra with literature data.

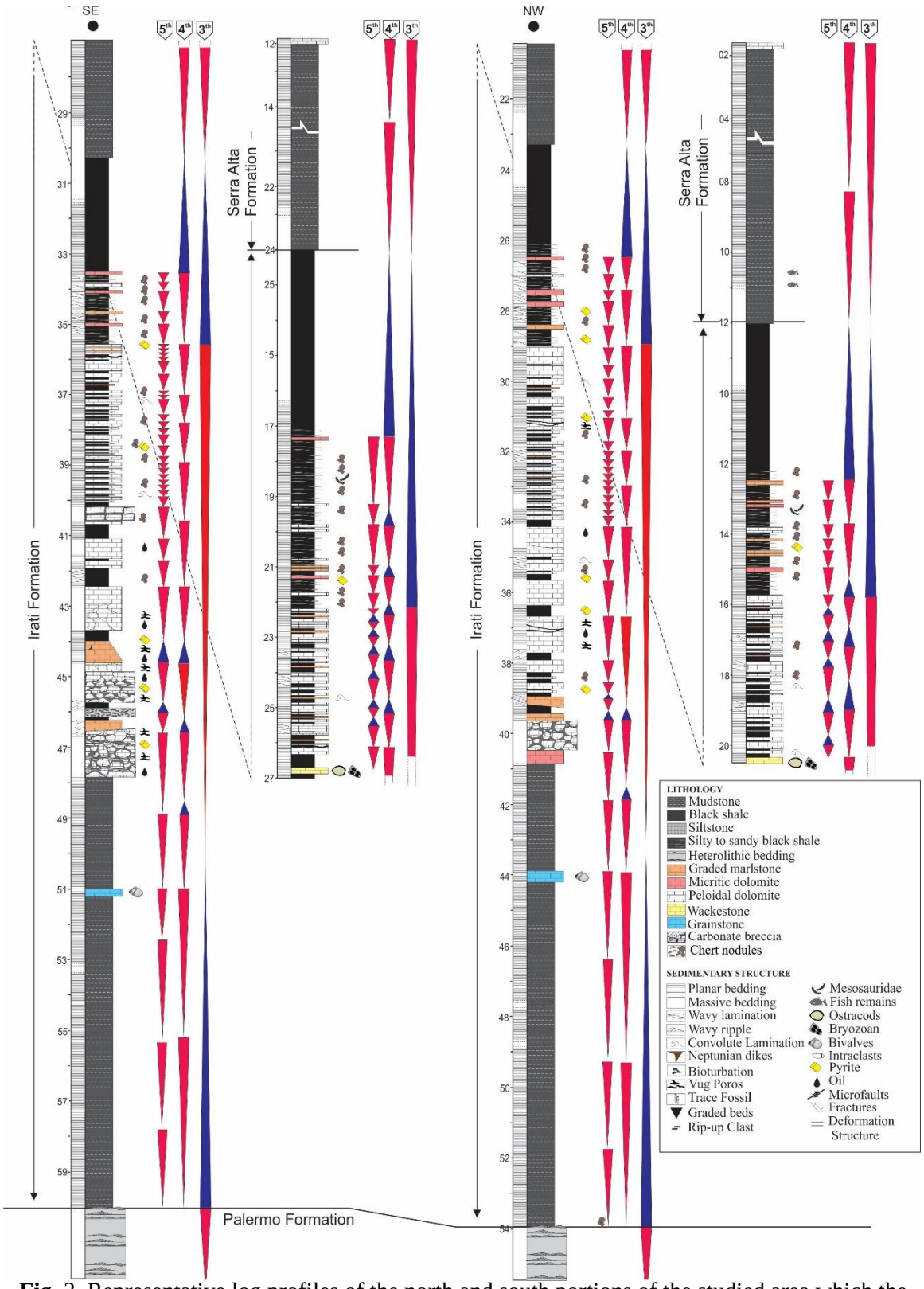

Fig. 3. Representative log profiles of the north and south portions of the studied area which the location is indicated in Fig. 01. The succession presents two high-frequency cycles order that composes three 3rd -order sequences.

6.4. STACKING PATTERN AND HIGH-FREQUENCY CYCLES

Detailed sedimentological and stratigraphic analyses of the succession reveal a suite of eight main mixed clastic-carbonate stacking patterns types (Fig. 04). It presents dominant asymmetric facies stacks composed of superimposed decimeter- to meter-scale oscillation patterns. The succession is assembled mainly of rhythmical intercalation of shale, marls, and dolostone. The cyclicity is observed across the ramp, where typical offshore black shale shows a continuous distribution and overlying the shallow carbonate deposits. The poor fossil diversity (e.g., Mesosaurus remains) hinders its application in the stacking patterns characterization, which is usually used in similar research and paleoenvironmental interpretation.

The cyclicity observed in the mixed deposits of Paraná Basin is formed by about 300 bundles (dolomite-shale or dolomite-marls-shale) separated by sharp surface or graded marls intervals. It presents thinning-up or thickening-up trends. The bundles can be organized in small-scale, shallowing upward patterns that can be described in four scale hierarchical stacking patterns: small-scale (5th-order), medium-scale (4th-order), and large-scale (3rd-order). The cycles are limited by flooding surface. The rhythmical stacking patterns of clastic and carbonates are dominant in the Assistência Member, disappearing at the first meters of Serra Alta Formation. In the studied succession was identified 59 small-scale stacking patterns with an average of 1.0 meters, 28 progradational and 31 retrogradational. They are mixed shale-dolostone asymmetrical cycles of the mid-outer ramp to offshore (Figs. 04 and 05).

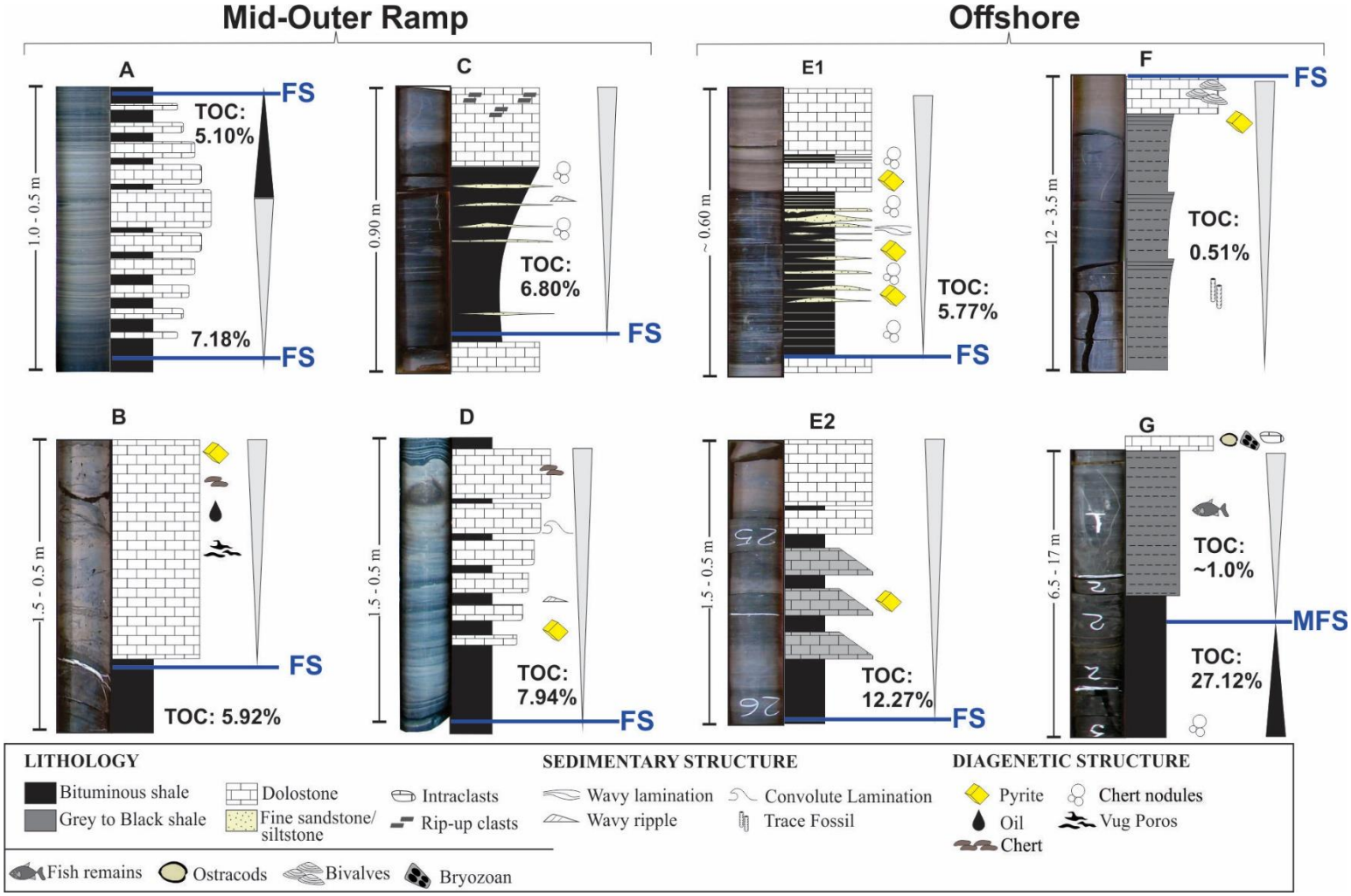

Fig. 4. High-frequency stacking pattern types that compose the Lower Permian mixed siliciclastic-carbonate succession of Paraná Basin. Note that all cycles present TOC higher than 1%. The grey shale of cycles F and G predominate TOC < 1. However, F and G can reach 2.6% and 1.7%, respectively, predominating in G ~1.0%. the bituminous shale of G has the highest TOC values.

Fig. 5. Core photographs of the second 3rd-order sequence of the mixed deposits (S2). The sequence is overlying the breccia facies in the base of Assistência Member. Note the high-frequency cycles with shallowing-up patterns and the predominance of deepening upward trend of the sequence.

6.4.1 Small-scale depositional cycles

Stratigraphic sections show cyclic repetitions on all scales, from millimeters to hundreds of meters, representing time intervals from seconds to millions of years, known as cycles (Schwarzacher, 2000). Goldhammer et al. (1993) define depositional cycles as the thinnest recognizable allocyclic or autocyclic depositional units with progradational and/or aggradational patterns. There is no evidence of subaerial exposure meaning that cycles never reach the intertidal setting. Those types of sequences are named subtidal cycles by Osleger (1991). The constant inflow of siliciclastic sediment alternating with carbonate production can be considered an "opportunity window" facilitating the recognition of the cycles.

Due to the vast organic geochemical database available for Irati Formation, mainly focusing on the two oil-shale intervals, many of the biomarkers identified herein for each cycle type in the middle portion of the basin were previously reported for the central-north or south border. The data includes biomolecular marks indicative of freshwater input, hypersaline, and anoxic conditions (Alferes et al., 2011; Reis et al., 2018; Martins et al., 2020a; Bastos et al., 2021; Nascimento et al., 2021). The previous information combined with news data (table 01)

enhanced the spatial and temporal understanding of the depositional conditions of the Irati Sea. Furthermore, insights into the cyclic variation of high-organic preservation and carbonate production.

Table 1. TOC content, pyrolysis analysis, and biomarker parameters of biological source, paleoenvironment condition, and thermal maturity of the organic matter extracted from rocks of Irati Formation.

Parameters	Cycle B	Cycles C	Cycle D	Cycle E		Cycle F	Cycle G			
				E1	E2		Organic-poor shale	Organic-rich shale		
	P3B69-30	P3B69-26	P3B69-22	P3B130-66	P3B130-78	P3B69-32	P3B130-74	SGB12-68	P3B92-59	RN-005-54
TOC [a]	5.92	6.80	7.18	8.73	6.12	0.60	0.76	13.15	19.92	18.24
S2 [b]	30.93	38.61	43.92	50.74	36.38	0.37	1.41	93.73	169.29	118.60
HI [c]	522	568	612	581	594.44	62	186.26	712.89	624.23	650.22
OI [d]	18	19	20	12	15.69	0	198.15	4.64	9.99	0.33
TAR [e]	0.32	0.45	0.32	0.31	0.23	0.92	0.66	0.15	0.56	0.56
CP1 [f]	1.05	0.61	0.80	0.58	0.91	0.81	1.02	1.18	0.80	0.86
OEP [g]	1.34	0.84	0.70	0.51	0.54	0.78	0.99	1.08	2.94	0.91
Pr/Ph [h]	0.92	0.45	0.77	0.90	1.24	1.09	0.68	1.19	0.60	1.29
Pr/nC_{17} [i]	3.92	2.53	5.05	4.20	3.87	0.94	1.01	1.69	5.71	2.68
Ph/nC_{18} [j]	7.28	12.70	7.10	8.43	7.03	1.65	1.42	3.48	23.63	4.78
Ts/ (Ts + Tm) [k]	0.26	0.42	0.31	0.26	0.26	0.33	0.26	0.15	0.19	0.21
C_{31} 22S/ (22S+22R) homohopane [l]	0.51	0.56	0.57	0.53	0.55	0.57	0.51	0.53	0.20	0.56
C_{35} 22S/ (22S+22R) homohopane [m]	0.40	0.51	0.55	0.41	0.46	0.52	0.38	0.81	1.0	0.56
C_{27} 20S/ (20S+20R) sterane [n]	0.31	0.40	0.38	0.29	0.32	0.44	0.33	0.29	0.21	0.36
C_{34}/C_{35} hopane [o]	2.43	1.07	1.94	2.72	3.73	0.38	1.13	0.57	1.70	2.25
C_{27}/C_{29} sterane [p]	0.80	0.27	0.98	0.89	0.76	0.37	0.45	0.78	0.55	0.75
hopane/sterane [q]	3.04	4.13	1.65	2.75	2.22	1.43	1.80	6.13	3.57	4.54
C_{30} βα/ (αβ+βα) [r]	0.14	0.14	0.13	0.11	0.12	0.16	0.16	0.19	0.38	0.15
iβCarotane [s]	29.46	27.39	19.63	17.95	30.79	-	-	2.40	5.65	10.80
*i*G [t]	138.29	147.96	120.47	128.48	90.56	-	-	53.10	55.96	41.48

a TOC: total organic carbon (%)
b S2: mg HC/g rock
c HI: mg HC/g TOC
d OI: mg CO_2/g COT
e TAR: $(nC_{27} + nC_{29} + nC_{31})/(nC_{15} + nC_{17} + nC_{19})$, Bourbonniere and Meyers (1996);
f CPI: ½ × $[(C_{25} + C_{27} + C_{29} + C_{31} + C_{33})/(C_{24} + C_{26} + C_{28} + C_{30} + C_{32}) + (C_{25} + C_{27} + C_{29} + C_{31} + C_{33})/(C_{26} + C_{28} + C_{30} + C_{32} + C_{34})]$ in TIC;
g OEP: $(C_{25} + 6C_{27} + C_{29})/(4C_{26} + 4C_{28})$ in TIC;
h From peak height of Pr/(Pr+Ph) in TIC;
i Pr/n-C_{17} in TIC;
j Ph/n-C_{18} in TIC;
k Peak areas of C_{27} 18α(H)-22,29,30-trisnorneohopane (Ts)/[(C_{27} 18α(H)-22,29,30-trisnorneohopane + C_{27} 17α(H)-22,29,30-trisnorhopane)] in RIC *m/z* 191;
l,m Peak areas of 17 α(H), 21 β(H), 22S/17 α(H), 21 β(H), 22S + 17 α(H), 21 β(H), 22R, in RIC *m/z* 191;
n C_{27} 20S/(20S + 20R): C_{27} 5α(H),14α(H),17α(H) 20S/C_{27} 5α(H),14α(H),17α(H) 20(S + R) in RIC *m/z* 217;
o Peak areas of C_{34} –17α(H),21β(H)-Pentakishomohopane/C_{35} –17α(H),21β(H)-Homohopane;
p Peak areas of 20R 5α, 14α, 17α(H)-cholestanes/20R 5α, 14α, 17α(H)-ethylcholestanes in RIC *m/z* 217;
q (C_{30} 17α, 21β-hopane in RIC *m/z* 191)/(C_{27} 20R e 20S 5α, 14α, 17α(H)-cholestanes in RIC *m/z* 217); low < 4, medium 4-7, high>7, Mello et al. 1988;
r Peak area in m/z 125 chromatogram over C_{30} 17α,21β-hopane peak area in m/z 191 chromatogram of aliphatic fraction;
s Peak area in m/z 125 chromatogram over C30 17α,21β-hopane peak area in m/z 191 chromatogram of aliphatic fraction, Mello et al., 1995;
t Gammacerane peak area over C_{30} 17α,21β-hopane peak area in m/z 191 chromatogram of aliphatic fraction, Mello et al., 1995.

6.4.1.1. Symmetrical depositional trend

Couplets (shale and dolomitic layers) or triplets (shale/marls/carbonate) rhythmites with progressive thickening upward of carbonate beds and thinning of shale layers form an inverse pattern: progressive thickening-up of shale beds and thinning of carbonate beds, forming meter-scale symmetrical trends (type A cycle). When the marls occur, a transitional gradation from shale to carbonate is observed. cycle A (Fig. 04) has lesser nodular chert and deformation structures than ramp stacking patterns. Predominate planar lamination and stratification in the siliciclastic- and carbonate-rich beds.

The organic matter is composed of opaque phytoclasts and partially oxidized bisaccate pollen grains (Reis et al., 2018), generating dominantly kerogen type III. However, the shale has low hopane/sterane, Pr/Ph ratio, and the highest values for C_{27} cholestane, attesting green algae contribution (Moldowan et al., 1985; Volkman, 2003; Kodner et al., 2008).

6.4.1.2. Asymmetrical stacking patterns

At the base of Assistência Member, an aggradational trend formed by shallowing-upward asymmetrical stacking patterns compose the outer ramp deposits. They comprise millimeter- to centimeter-scale black shale layers sometimes grading to marls. The upper layer is thicker brecciated dolostone beds (type B cycle). The brecciation of dolostone is interpreted as formed during burial diagenesis. The main facies are mudstone with evaporite crystal, finely-laminated dolomudstone, intraclastic packstones, massive dolomicrite, and peloidal packstones (for more details, see Cap. V of this thesis). The thickening upward of carbonate beds indicates high carbonate production accumulated during catch-up phases linked to the relative sea-level rise.

The occurrence of evaporite minerals and stromatolite (Callefo et al., 2018) in the type B cycle indicate deposition in the most hypersaline and shallow conditions. These conditions are confirmed by the presence of higher β-carotane, and high gammacerane index. Also presents low Pr/Ph, hopane/sterane ratios and regular isoprenoids (Fig. 06). Kerogen type II/III to III, low values of HI, and partially oxidized amorphous organic matter and opaque phytoclasts (Reis et al., 2018). The authors also calculate low values of the ratio C27 cholestane/C29 ethylcholestanes, which indicates the presence of green algae. Samples near the flooding surface can reach 5.92 % of TOC (Table 01) and kerogen type II. Primitive green algae (e.g., prasinophytes) is the first to recover after extinction event and thrive in the absence of grazing feeders is previously pointed by Bastos et al. (2021).

The type C Cycle has a coarsening upward trend formed by black shale with amalgamed and discontinuous silty to sandy ripples laminae overlain by peloidal dolostone with rip-up carbonates clasts. They are less frequent in succession. The dolostone layers can be massive or with a nodular fabric. Nodular carbonate and silex are commonly associated with the sandy laminae within the shale layers. The black shale occurs over a sharped and deformed carbonate surface, marked by vertical dissolution, followed by dolomicrite and peloidal dolostone. The carbonate microfacies often presents solution-enlarged pores, nodular silex with length-slow chalcedony, reworked and micrite-coated intraclasts.

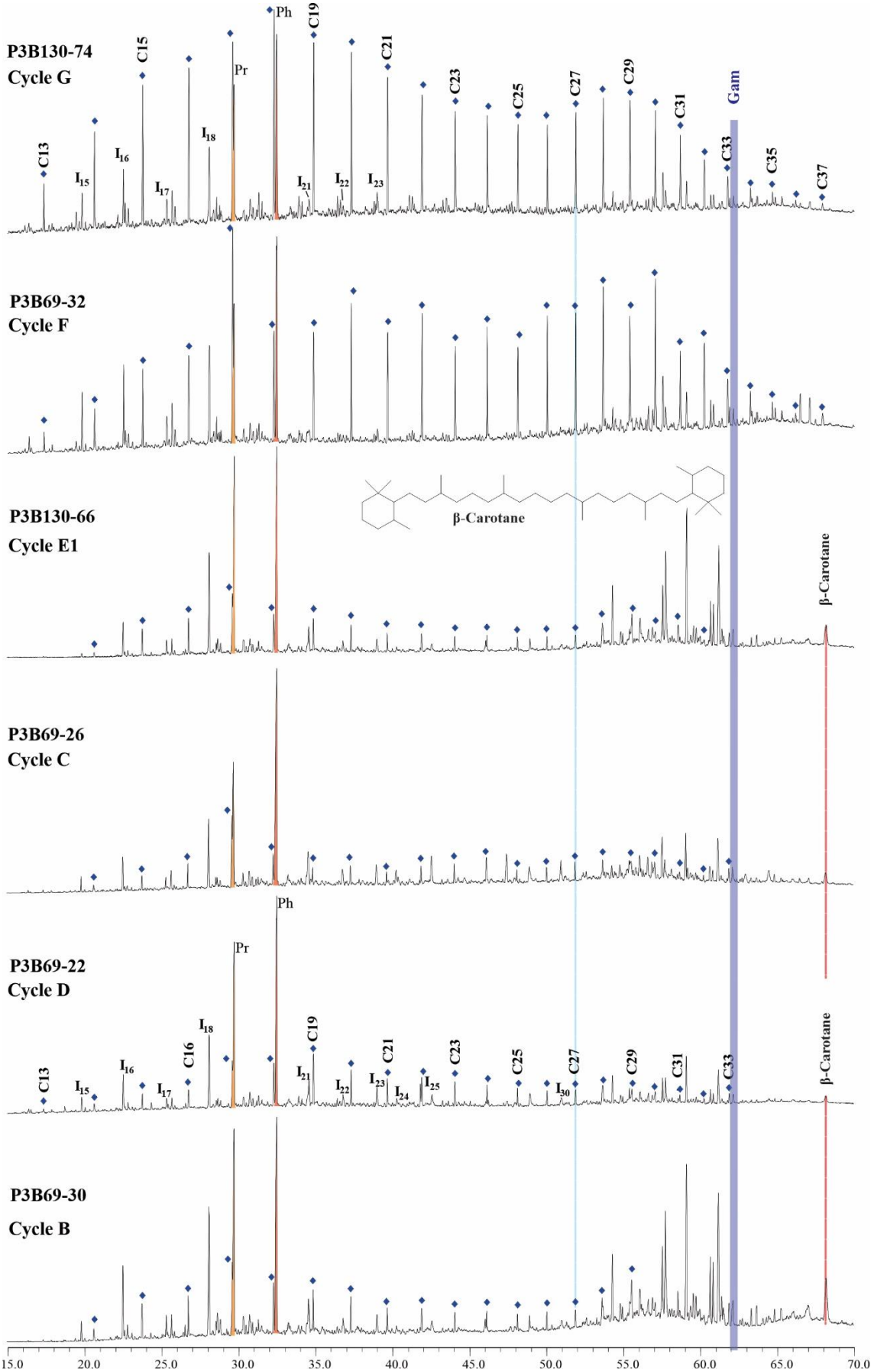

Fig. 6. The representative TIC of the stacking patterns showed in Fig. 3. P3B130-74 (organic-poor shale) and P3B130-32 (cycle F) samples showed a high relative abundance of *n*-alkanes and absence of

gammacerane and β-carotane. The subsequent cycles (A to E) predominates the high abundance of isoprenoids and gammacerane and the β-carotane is present.

Those asymmetrical cycles have high hopane/sterane, low TAR, CPI the lowest values of C_{27}/C_{29} sterane, and Pr/Ph ratio. Moreover, higher gammacerane and high values of β-carotane. The cycles record recurrent shallowing-up, causing restriction and hypersaline stressful conditions. β-carotane from cyanobacteria and algae are common in anoxic, saline lake settings and rare in marine environments (Peters et al., 2005). However, β-carotane can be found in shale from highly restricted marine environments where halophilic bacterias can flourish (e.g., Irwin and Meyer, 1990; Fu Jiamo et al., 1990). Although, the shallow conditing associated with the high organic matter production act as the primary control to create anoxic bottom water, preserving high organic carbon (6.80 %).

Cycles D are the dominant stacking pattern of the ramp deposits. They have thickening upward of carbonate beds and thinning upward of shale beds with preservation of the purity degree of the carbonate (< 10% of siliciclastic). Meter-, centimeter- to millimeter-scale intercalations formed by carbonate interbedded with shale have generally sharp or gradual contact. The black shale passes to the dolostone beds, which mixed peloid and clay/silt particles, grading from siliciclastic-rich to carbonate-rich layers. The asymmetrical stacking of these facies is interpreted as a shallowing-up tendency. The sharp contact between the shallowest (carbonate) and deeper facies (shale) is indicative of the retrogradation or flooding surface directly covering the sequence boundary, as described by Strasser et al. (1999). Also, the limit can present carbonate breccias with fitted clasts, fragmented nodular chert layers. The brecciation can reach up to 50% of the package and present length-slow chalcedony besides the chert beds. Well-preserved cross-stratification to fine lamination is marked by siltstone lamination. However, it is dominated by planar lamination. The silicified carbonate marks this contact and can mean an early diagenetic phase. D cycles predominate at the middle to the uppermost outer-mid ramp association. They have an average organic carbon of 7.0 % low terrigenous contribution (CP1= 0.61 and OEP= 0.84) and high gammacerane and *β*-carotane.

6.4.1.3. Turbidity cycles

Thinning upward patterns of sandy black shale overlain by thin beds of laminated peloidal or micritic dolostone comprised the cyclic turbidity deposits (cycle type E1). There is a variation from wavy-like silty to sandy shale within the shale beds with a graded couplet or triplet beds and finely laminate siltstone and shales. The dolostone is finely micropeloidal, and

macropeloidal massive fabric occurs with a preferential orientation of clastic particles. Pyrite- and nodular chert-rich forming level of upward nodular enrichment, comprising a clast-support framework at the top. Those diagenetic features cause a whole modification in the original laminated fabric. Mesosaurus bones fossil is also present. The distal facies is characterized by stratal stacking patterns type E2, comprising finely laminated shale beds with homogeneous fabric and predominance of graded marls stead of pure shale. However, the top is marked by carbonate beds (< 33% of siliciclastic material).

The turbidity events interrupted the stratified water mass, resulting in bioturbation and oxidation of the organic matter. The turbidity cycles form the second richest intervals of the succession. TOC reaches 13.0 % and HI (< 581 mgHC/gTOC). The deposits record high Ph/nC$_{18}$, β-carotane, and gammacerane ratios.

6.4.1.4. Distal asymmetrical cycles

The distal offshore deposits have two types of asymmetrical trends. Cycle type F (Fig. 04) is composed of grey to black shale (~ 1% of TOC), finely laminated to homogeneous fabric with carbonate nodules and fish fossil fragments, comprising the Taquaral Member deposits. Despite the relative homogeneity of the shale, the type F cycle is characterized by a slightly coarsening upward variation in the fine clastic fraction, from clay, coarse silt until fine-grained sand grains, locally bioturbed. (Lages, 2014). Upsection occurs (i) dolograinstone with a concentration of bivalve shells; (ii) the brecciated carbonate beds are the limit of the superimposed cycle. Matos et al. (2017) also describe levels of a fine sand layer with bivalves and crustaceans associated with the dolograinstone.

The organic matter is characterized by low proportion to the absence of gammacerane, regular isoprenoids, and β-carotane, associated with normal salinity and suboxic conditions. Predominate kerogen type III, odd-carbon n-alkanes in the high molecular weight (n-C$_{27}$ and n-C$_{29}$), high C$_{29}$ sterane, and hopene/sterane ratio indicating terrestrial organic material contribution (Tissot and Welte, 1984; Volkman, 1986). However, occurrences of kerogen type II and a high proportion of C$_{27}$ sterane are suggestive of dominant marine red algae and zooplankton (Schwark and Empt, 2006; Peters et al., 2005; Kodner et al., 2008). Reis et al. (2018) found opaque phytoclasts, oxidized amorphous organic matter, and acritarchs possibly related to intervals of a dominant aerobic environment in the proximal marine realm (Tyson, 1987). This evidence points to an open marine condition without water-column stratification during the deposition of Taquaral Member.

The offshore cycle type G is present in the Assisstência Member to Serra Alta Formation. It is composed of bituminous shale (organic-rich), overlain by gray shale (organic-poor), producing a progradational pattern. The cycles have the thicker and most economically important oil-shale intervals. The basal bituminous shale records a peak of 27.12% of TOC and the highest HI value (1000 mg HC/g TOC). Predominates kerogen types I and II. Reis et al. (2018) describe amorphous organic matter for those intervals. It is characterized by low TAR, high Ph/nC$_{18}$, Pr/nC$_{17}$, gammacerane index, and variable β-carotane, indicating salinity and reducing condition with periodic freshwater inflow. The upper layers of black to grey organic-poor shale (< 2%) have an organic matter composition similar to the shale of cycles A. This deposit has opaque phytoclasts, high molecular weight n-alkanes, low Pr/Ph ratio, and HI (< 100 mg HC/g TOC), reaching 186.26 mg HC/g TOC. Similar to cycle F, β-carotane and gammacerane index is not detected. The organic-poor shale indicates intervals of an open connection to the ocean before the coming back of restriction conditions. Plus, both have bimodal distributions of the n-alkanes C$_{15}$ to C$_{23}$ and C$_{24}$ to C$_{35,}$ suggesting a mix of marine and terrestrial organic matter (Fig. 06). Reis et al. (2018) describe an upward increase of gammacerane in the upper portion of the organic-poor shale (cycle 43), corroborating the shallowing-up and return of the hypersaline condition of the cycle.

6.4.2. Medium- (4th-order) and large-scale cycles (3rd-order)

The 59 small-scale depositional cycles compose twenty 4th-order stacking patterns (Fig. 03 and 07). These mixed high-frequency and symmetrical stacking patterns are the building blocks of the larger-scale, lower-frequency (third-order) depositional sequences of the Irati sea. The uppermost heterolithic sandstone and mudstone of Palermo Formation with an aggradational pattern compose the HST of the succession's first 3rd-order cycle (S1). The cyclic coarsening upward patterns of the fine clastic facies of Taquaral Member with a retrogradational trend compose the TST of the second 3rd-order depositional cycle, named S2 sequence of the lower Permian mixed succession. The MTS is recorded in the thin organic-rich shale layers overlying the condensed shell beds of the upper portion of the Taquaral Member. The basal aggradational to progradational patterns of the Assistência Member compose the HST. The following two shallowing upward 3rd-order cycles (S3 and S4) have thicker intervals of bitumen-rich shale mark the maximum transgressive surface (MTS), overlaid by gray shale deposits (organic-poor), corresponding to the base of the highstand systems tract (HST).

The bituminous shale layers have the highest TOC values of the mixed deposits. The superimposed small-scale depositional cycles show a dominance of progradational trends highlighted by the fisher plot (Fig. 07). Despite being a shallow sea, the succession has no evidence of subaerial exposure characterizing type 2 sequence boundary following (Vail et al., 1984). The conformity surface is identified by the occurrence of transgressive offshore deposits overlying the most proximal facies of the ramp.

The S2 cycle record the main shallowing-upward phase comprising 37 superimposed asymmetrical high-frequency cycles (Fig. 07). S3 and S4 cycles with 14 and 8 small-scale depositional cycles, respectively. The cycle was developed during lass agitated and deeper waters. Both have aggradational trends composing a deepening-upward phase that result in the 90 m-thicker offshore shale deposits of the Serra Alta Formation.

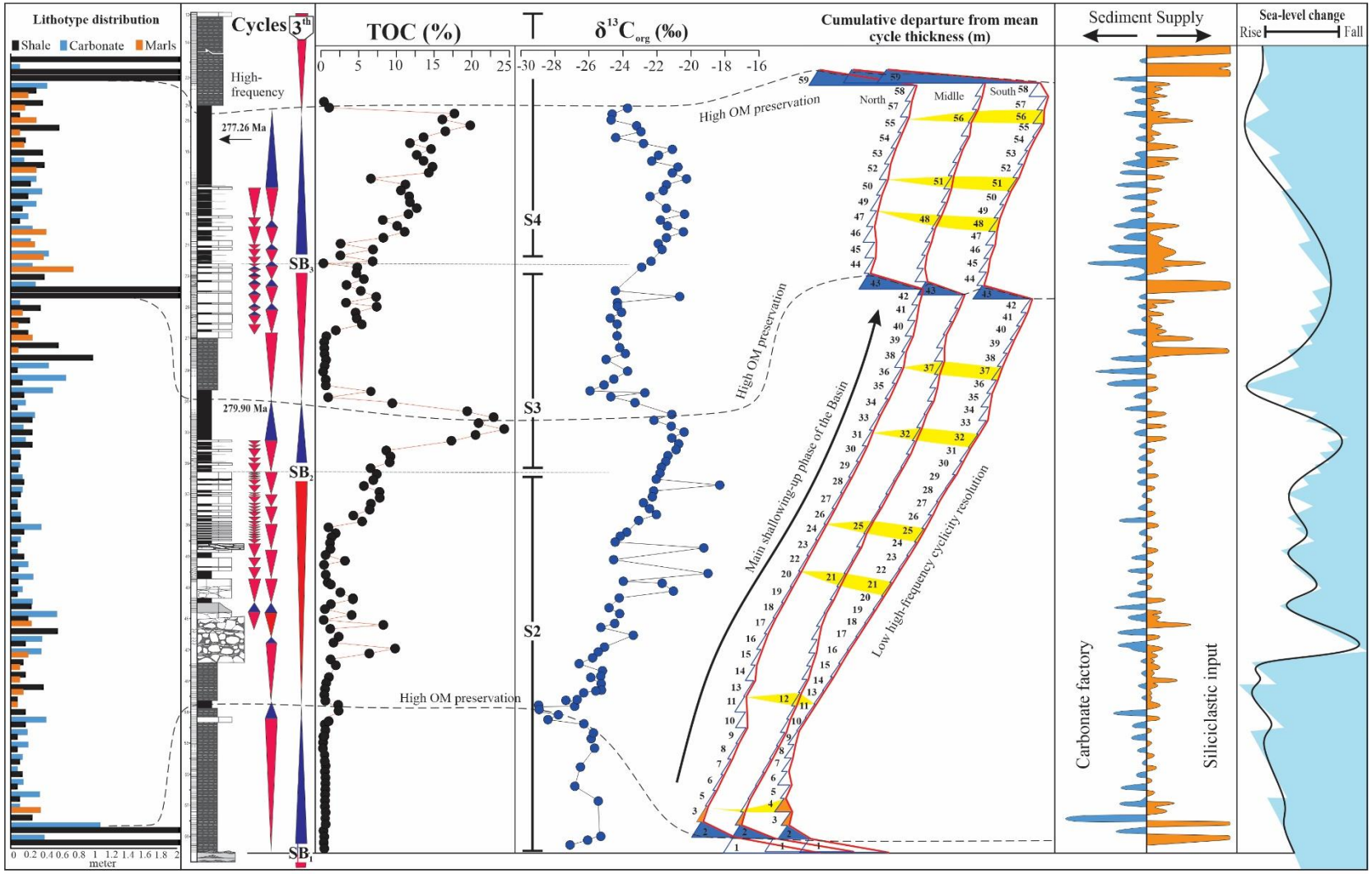

Fig. 7. Correlation of the accumulated cycle thickness of Fischer plot of the three main points of the study area. Total organic matter and δ $^{13}C_{org}$ (Bastos et al., 2021) has a positive correlation with the 3rd-order sequences. Yellow highlights 'missing beats' of the record, predominating for the north shallower portion. It has only 50 preserved cycles. The middle and more distal plot have more preserved cycles (59). Note that the S2 sequence has very low accommodation space and progradational pattern. S1 predominate aggradational stacks. The high-frequency terrigenous mud signal show peaks correlated to the MTS and higher organic matter production.

6.5. ORGANIC-RICH FACIES DISTRIBUTION

The two thicker bituminous shales related to TST of the S3 and S4 sequence of Assistência Member form the most rich-organic matter levels of the Paraná Basin (Fig. 8). Those intervals are described here as Oil-Shale S3 and S4. Oil-Shale S3 has the highest organic carbon (27,12%) and generating potential (192 mgHC/g Rock) values. Both oil shale intervals have the highest source potential in the southernmost Brazilian states. When compared between them, there is a convergence of the quantity and quality to the middle portion of the basin (location 4 – see Fig. 01). Considering the three thousand samples analyzed from those three locations (southernmost: 2, middle: 3, and northernmost: 4) on the basin, the most significant peak values for TOC were 19.40% (location 4), 27.12% (3), and 22.23% (2). Across the basin, there is predominate kerogen type I and II (oil-prone) with increased contribution of type I toward the middle portion (location 4 - Fig. 9). Tmax has an average of 416°C (2), 430°C (3), and 425°C (4). Regardless of the lateral variation of maturation degree identified by biomarker parameters (CPI, OEP, Pr/*n*-C_{17}, Ph/*n*-C_{18}, C_{30} βα/(αβ+βα) for Irati shales, the organic matter is immature except for the levels cross-cut by the Mesozoic magmatism, as previously reported elsewhere (e.g., Santos et al., 2009; Martins et al., 2020b). The igneous intrusion was responsible for the generated oil present in the carbonate breccia and fractures.

The geochemical data (TOC, S1, S2 e HI) of Oil-Shale S3 present a peculiar configuration in all analyzed profiles. A progressive rise from the contact with the interbedded carbonate-shale to the middle portions of the bituminous shale followed by a continuing decrease to the uppermost part (Fig. 10). Taking an analogy with the geophysics log representation, the oil-Shale S3 chemical profiles (Fig. 10) have a dominant symmetrical shape with lateral variation to funnel shape, recording well-defined and traceable peaks across the basin. The dominant symmetrical configuration reveals an increased production and/or preservation of organic matter, which reaches 27% wt% of organic carbon followed by the decay of the preeminent environment condition. The favorable conditions related to the transgressive phases and the extensive lateral continuity of the symmetrical shape allowed the MTS to identify (Fig. 10). Despite the shallow conditions, the water column stratification and persistence of anoxic-bottom water promote high preservation of the organic matter during long-term transgressions.

The progressive rising of the water column is directly linked to creating accommodation without necessarily developing bottom upwelling. MTS represents the maximum ideal conditions for generating and preserving organic matter. During transgression occur a renew of

the nutrient supply and in broad, shallow epicontinental sea algal bloom can produce a large amount of organic material. The consecutive sea-level fall promotes an inversion of those ideal conditions. Biomarker parameters of samples from the S3 MTS present a slightly lateral variation of the organic matter source. The middle portion record the lowest values for TAR e C_{34}/C_{35} Hopane ratio and highest values for Hopane/Sterane, suggesting a low continental organic matter input and increased contribution of prokaryotic organisms (bacteria) in the kerogen formation. Plus, the lowest values of Ts/Tm e Ph/*n*-C_{18} indicate that the organic matter of this location was less affected by thermal maturation.

Oil-Shale S4 is very similar to S3. It is also composed of bituminous shale and has the second-highest potential for oil generation. There is a progressive increase of organic matter content toward the top (Fig. 10). Nevertheless, differing from the S3, the progressive increase goes until the uppermost portion of the bituminous facies with a sharp decrease in the first centimeter of the Serra Alta dark-grey shale, forming a serrated funnel shape. In the southernmost part of the basin (location 2), the geochemical parameters have an abrupt shift from the values of the interbedded shale (lower) of the turbidity facies to the bituminous shale (higher), becoming vertically constant until the top (Fig. 10), forming a cylindric shape. The geochemical logs are very useful in identifying and correlating the facies due to the predominance of fine and dark material (carbonate and shale) of the succession. Negative shifts promoting a breakup of the predominant shape configuration above described are due to diabase sill beds. However, they are generally amygdaloidal, acting as a reservoir for the generated oil that produces low TOC and S3 Rock-Eval pyrolyze values. The southmost portion has TOC (8,8%), S3 (62 mgHC/g Rock), and HI (712 mg HC/g TOC).

The Middle portion (3) presents maximum values of TOC (21,7%), S3 (132 mg HC/g Rock), and HI (1000 mg HC/g TOC) at the top of the bituminous shale facies. Toward the north (4), the geochemical log shows high oscillation of the values; nevertheless, the log shapes are similar in the middle portion profiles, with a predominant increase to the top to the northeast. In the southmost region occur a decrease of the values to the top, with a high contribution of the oxidized organic matter indicated by high values of OI. (107 mg CO_2/g TOC). Similar to S3, the middle portion records the highest values of TOC and Potential for hydrocarbon. Anjos et al. (2006) used pollen/spores ratio from the black shale to demonstrate that there is no significant variation in the paleo flora in the source area from north to south. The kerogen is type II with a high contribution of type I and fewer proportions of type III in the southernmost region.

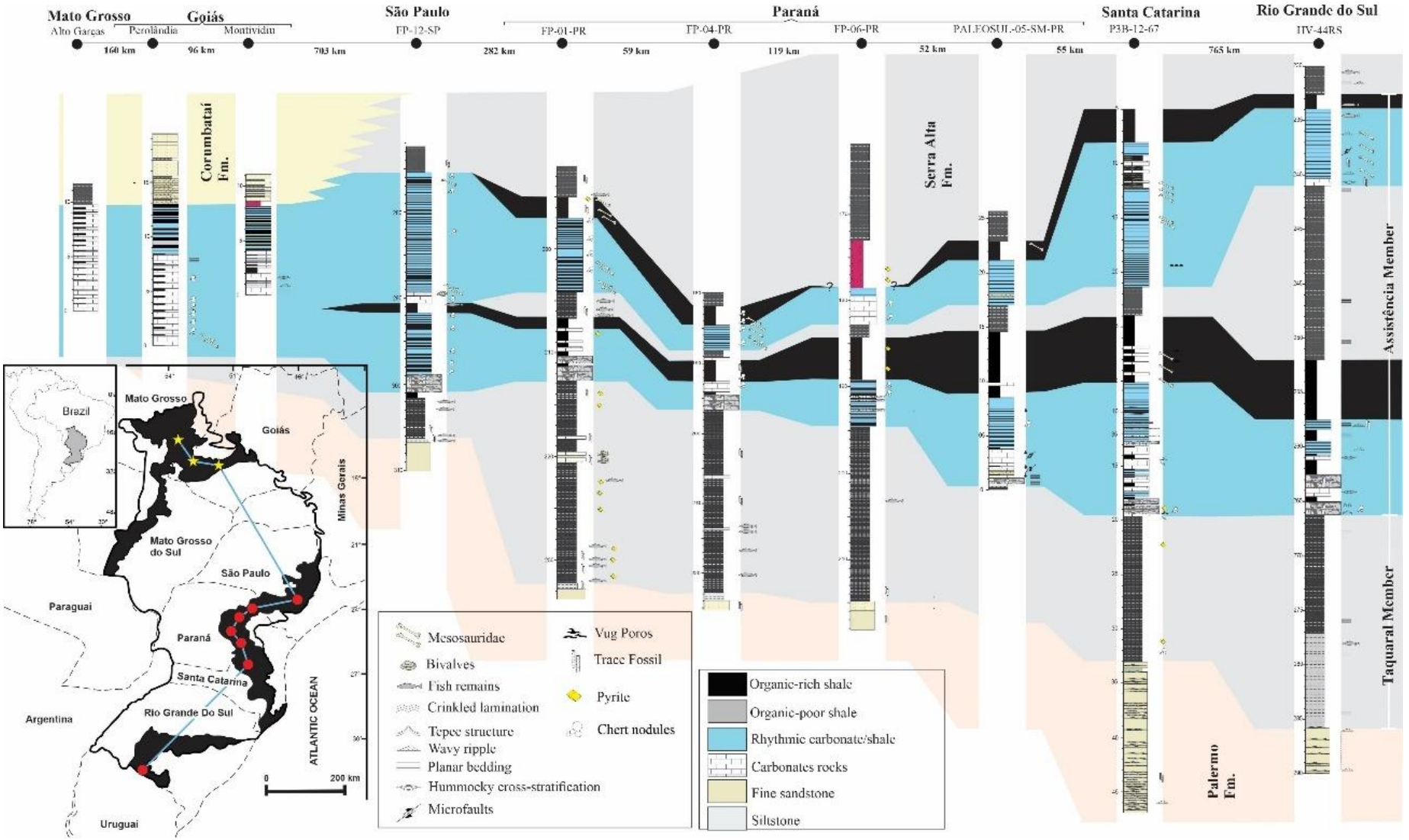

Fig. 8. Sequence correlation diagram along the regional south-to-north cross-section. The diagram shows the distribution of the two richest oil-shale intervals across the basin. The section was built using new and old data from Lages (2004); Anjos (2008); Soares (2014); Xavier et al. (2018) and Oishi et al. (2019).

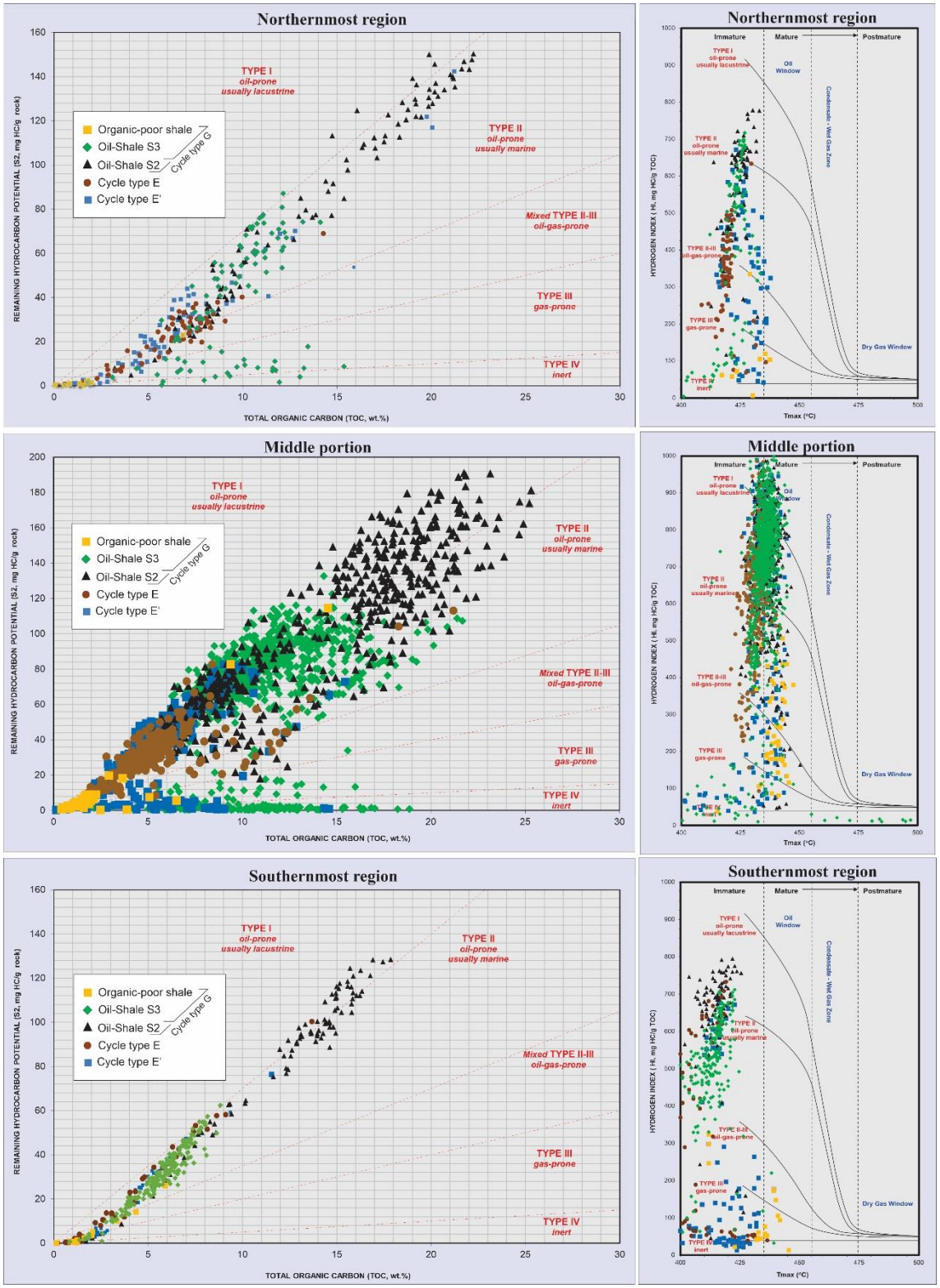

Fig. 9. Van Krevelen type diagram showing the distribution of the samples in the three studied sectors of the Paraná Basin. The three diferent locations predominate kerogen types I and II for the oil-shale deposits. Nevertheless, type III and IV contributed considerable contributions in the northernmost and middle portions. Likewise, immature organic matter prevails, but in the middle portion intervals along the succession, the oil window reaches.

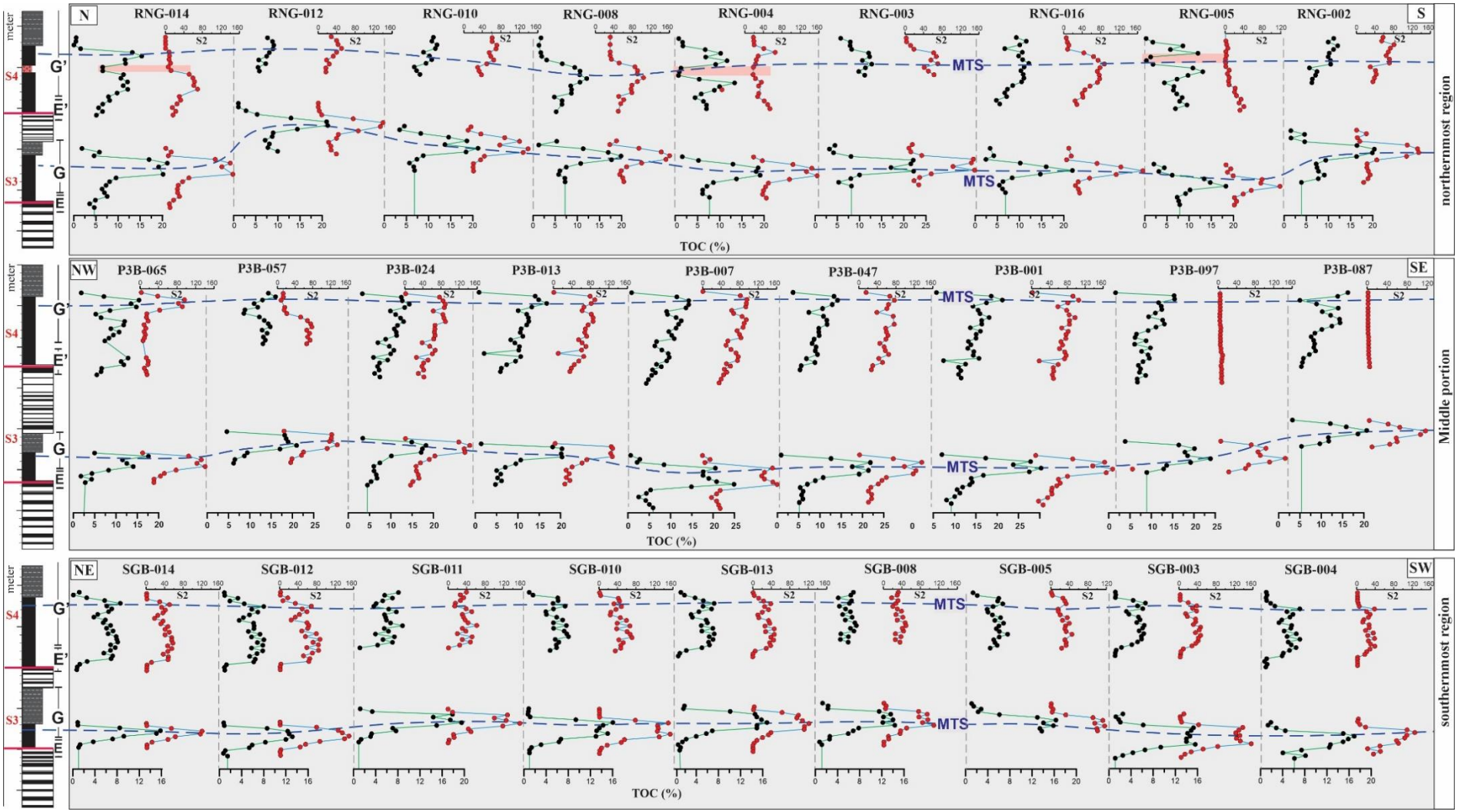

Fig. 10. Geochemical profiles (TOC and S2 Rock-Eval pyrolyze) compose a north to South section (A-A') for the northernmost region, northwest to the southwest for middle portion (B-B'), and northeast to the southeast section for southernmost region of the basin (C-C'. see Fig. 01). Based on the stratigraphic and geochemical profiles is possible to trace the MTS across the section because it records the maximum organic matter production. In the Irati Formation, the quantity of preserved organic matter has a positive correlation with the generating potential for hydrocarbons. Red boxes in the first section indicate an igneous intrusion.

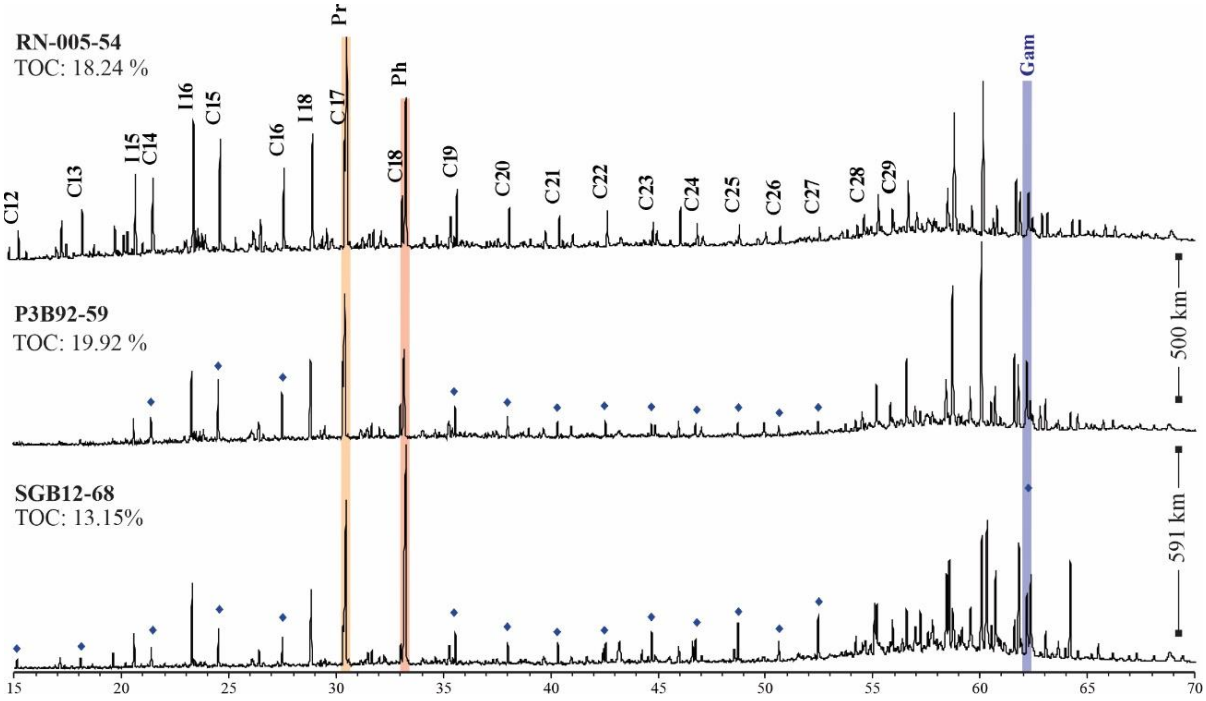

Fig. 11. Total ion chromatograms (TIC) of the oil-shale S2 in the central-east, middle, and southmost portion of the basin. Despite the thousand kilometers of lateral variation of the deposits, it has very little variation of the organic matter composition.

6.6. DISCUSSION

6.6.1. Resolution of the mixed siliciclastic-carbonate sequences

Sequence stratigraphic can be described from different scales of observation in which lower-order sequence is composed of higher-order superimposed stacking pattern (see Schwarzacher, 2000, and Catuneanu, 2019b). Each hierarchical sequence of a sedimentary succession can be understood as the result of accommodation/sediment supply (A/S) created in different magnitudes and durations (Fragoso et al., 2021). High rates of long-term accommodation with constant or even high sediment input favor a well-preserved record of high-frequency signals. On the other hand, if there are low A/S ratios, a decrease in the high-frequency sequence resolution will occur due to a lack of increased long-term accommodation space. The Resolution of the stratigraphic record varies according to the potential for accommodation space to be created (Fragoso et al., 2021). Despite the broad range of the Irati ramp that records cyclic alternation of shale and carbonate from the north to the south border of the Paraná Basin (10^6 km). It was formed during very low creation of accommodation producing high-frequency stacking patterns dominated by cycles smaller than one meter. It is possible to identify cyclicity hierarchies in the stratigraphic record up to the sedimentary facies and microfacies level. The identification will be a function of sedimentary capacity to record

such temporal variation. The mixed deposits of Irati succession have been shown high sensitivity to the depositional processes. The cyclic alternation of shale and dolostone allowed the identification of several superimposed stacking patterns arranged as 3rd- to the 7th-order cycle hierarchies shown in Fig. 12.

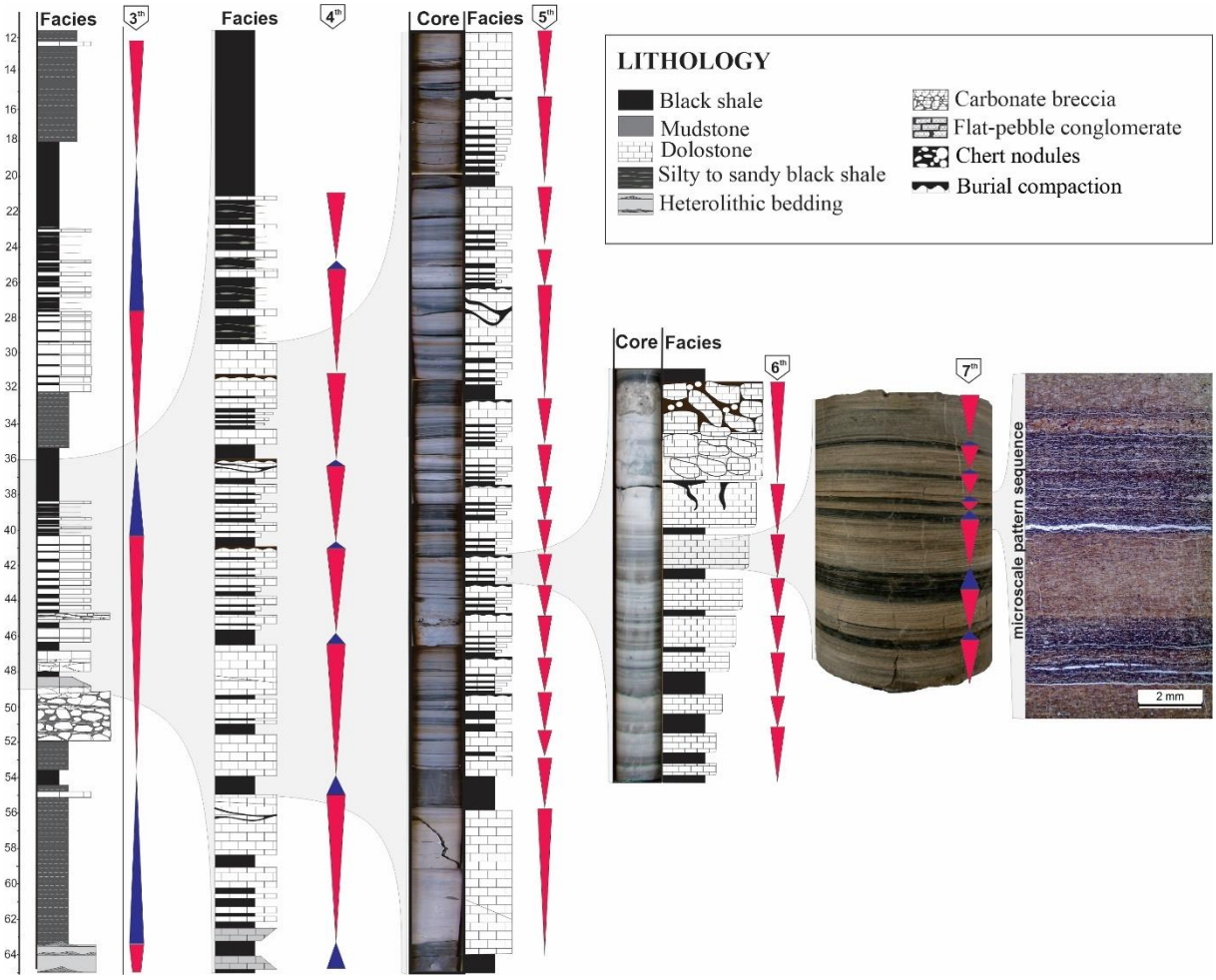

Fig. 12. Hierarchical stacking patterns of the mixed deposits of Irati to Serra Alta formations. The cyclicity can be organized in the 3rd- to the 7th-order. They are characterized by the rhythmic intercalation of fine siliciclastic and dolostone beds, forming thickening and thinning trends. Note the carbonate and shale cyclicity is recognizable even in the thin-section scale, composing the 7th-order with preservation of the carbonate and shale lamination.

6.6.2. Allocyclic and Autocyclic driving cycle-stacking patterns

Autocyclic controls driving cycle-stacking patterns are related to the depositional processes and inherent environmental mechanisms (e.g., internal sediment redistribution, seiches in a lake, carbonate factory) that can be quasi-periodic or episodic (Ginsburg, 1971; Pratt and James, 1986; Fragoso et al., 2021). Allocyclic processes (e.g., regional subsidence,

sea-level changes, climate) are the external forces that modify and control the environmental dynamics (e.g., climatic, eustatic, tectonic dynamics). They may synchronously affect the entire basin, allowing regional stacking patterns analyses and correlation (Catuneanu, 2006; Catuneanu et al., 2011; Fragoso et al., 2021). As approached by Burchell et al. (1990), the terrigenous input and so carbonate factory could be controlled by three main factors: i) tectonic setting; ii) eustatic fluctuations, and iii) climate changes. The subsidence favors accommodation space generation and can increase the fluvial channel's equilibrium profile angle that supplies the basin, enhancing the sediment input ratio. Also, uplift can induce total obstruction of the fluvial and basin connection. The low continental sediment record in the most proximal carbonate facies of Irati and the shallow conditions with lateral correlation for more than one thousand kilometers suggests a stable tectonic setting as previously stated by Zálan et al. (1990) and Milani (2004). The quiescence phase existing during the Irati Sea is indicative of the minor influence of tectonic over the cyclic variation of the accommodation space/sediment input.

Rhythmical repetitions of carbonate-marls or carbonate-shale represent a fluctuation between two phases of sedimentation supply. The constant ratio of the thickness of both lithologies forms a particular type of bundle (Schwarzacher, 1947). The pervasive and regular intervals with a significant lateral distribution of the bundle comprising higher-order cycles are difficult to explain without an alternating periodic processes. Deposition of deep-water setting mixed carbonate-siliciclastic sediments may poorly record fluctuations in relative sea level because of a decreased sensitivity to sea-level changes (Holland, 1997). However, a mixed succession of epicontinental seas, an example of Irati has shown high susceptibility to the sea-level fluctuations due to horizontal morphology of the ramp and shallow conditions. The cycles' small thickness could directly respond to the reduced accommodation space prevailing in the ramp as previously advocated by Araújo (2001). The third-order cycles are well-marked by total organic carbon and $\delta\ ^{13}C_{org}$ in which the MTS has a positive correlation with the maximum organic matter production (Fig. 07). Sea-level fluctuation, possibly related to fluctuating zones of fair-weather and storm-wave reworking, appears to be likely the primary mechanism controlling the development of thin successions of subtidal carbonate cycles, as stated by Osleger (1991). Nonetheless, the development of a wide-ranging rhythmically intercalation of carbonate and siliciclastic rocks across the Paraná Basin diminishes a possible autocyclic influence. In the same way, it is difficult to evoke sea-level change triggering the cycle-stacking patterns, demanding another allocyclic mechanism as the pristine control (Grotzinger 1986; Osleger 1991; Goldhammer et al., 1993; Eldrett et al., 2015).

The cyclic intercalation of dolomite and black shale with dominant tabular bedding is the more conspicuous characteristic of the Irati sedimentation. The intercalation is recognized in micro-, meso- and macroscale cyclicity, allowing for the identification of decimeter to meter-scale hierarchical stacks, organized in elementary cycles (bundle), fifth-, fourth-, and third-order cycles. In the petrographic section, millimeter intercalation forms a well-defined planar lamination in the rocks (Fig. 12). Plus, in micro to mesoscale are possible to observe compositional mixing that the form decimeter beds with lateral correlation with other cores. The marls are interpreted as the result of sindepositional mixing, formed of peloidal grains and siliciclastic particles, essentially quartz. The compositional mixed is possible the result of high organic production (biochemical carbonate) associated with low, but continuous input of fine terrigenous grains. The sediment supply was not enough to compromise the carbonate factory (e.g., Chiarella, 2011; Longhitano et al., 2012; Chiarella et al., 2016). Limestone-marls rhythms commonly reflect deposition below the storm-wave base (Einsele, 1982a). The occurrence of turbidity currents was an active process responsible for the redistribution of the sediment.

The wide distribution of the succession, in which the deposits are recorded from north to south of the Paraná Basin (10^6 km^2), is possible a basin-wide response to cyclic climate changes. The occurrence of pure carbonate interbedded with siliciclastic clay shale suggests a wholly change in the environmental conditions in a relatively short time span. Furthermore, the occurrence of pure fine terrigenous rocks at the base of each cycles and pure carbonate (less than 3% of siliciclastic material) at the top implicates that carbonate was the primary supply variant, controlled by an external factor. The highly productive carbonate platform was constantly affected by terrigenous inflows. A similar model is described by Burchell et al. (1990) for the Uppermost Triassic Alpine Rhaetic (cyclic shale/carbonates) deposits of Northern Italy. The authors hypothesized that a high-frequency terrigenous mud signal is superimposed over a carbonate mud supply that gradually increases in intensity from zero at the base. The cyclic variation produces marls-limestones couplets on a decametric scale. Fluctuations in carbonate-dominated to siliciclastic-dominated intervals, mainly in microscale, further, cyclic intercalation in micro to mesoscale strongly indicate climate as the primary control (Tänavsuu-Milkeviciene et al., 2009). The carbonate-shale bundles may record climatic oscillations related to alternating periods of arid and humid conditions affecting the source areas which cause fluctuations in sediment supply. In addition, the hierarchical organization of the stacking patterns (small-scale, medium-scale, and large-scale depositional sequences) is strong evidence of relative sea-level fluctuation played an important role in their formation, induced by the Earth orbit perturbation related to the Milankovitch periodicity (Borer & Harris, 1991;

Pasquier and Strasser, 1997; Pittet and Strasser, 1998a; Strasser and Hillgärtner, 1999). The systematic thickness variations of the cycles reflect variations in the accommodation space as a response to longer-term environmental change.

6.6.3. Orbital forcing climate control.

The concept of time-rhythmic control of cyclic deposition is well acknowledged worldwide. For Schwarzacher (1975) and Goldhammer et al. (1990), the regular pattern observed in the record cannot be a random process but a result of cyclic time events controlling the sedimentation ratio/or accommodation space. Orbitally induced climatic modulations may have played an essential role in controlling ancient cyclic deposition (Burchel et al., 1990). Schwarzacher (2000) stated that cycles containing a constant number of beds could be understood as responding to a composite periodic signal. Assuming that the cyclic variation represents the same time interval, the individual thickness of dolomites beds increases upwards due to the growth of the carbonate factory (Burchell et al., 1990). Another point worth to be taken is that in basins with very low sediment supply, bioturbation can mix up the sediment of both interbedded carbonate and siliciclastic layers obliterating the original cyclicity (Einsele, 1982b). However, the mixed deposits study here presents a well-preserved cyclic succession of carbonate and shale with a rare occurrence of bioturbation due to the prevalence of anoxic bottom water in the Irati Sea.

U-Pb zircon ages from volcanic-ash layers of the mixed siliciclastic-carbonate deposits indicate a 278.4 ± 2.2 Ma from U-Pb SHRIMP (Santos et al., 2006). Rocha-Campos et al. (2019) found ages ranging from 279.9 ± 4.8 to 280.0 ± 3.0 Ma from bentonite layer in the middle part of the thick bituminous shale interval that contains the MTS of the S3 3rd-order sequence of Irati Formation. A more precise age (277.26 ± 0.62 Ma) from the volcanic ash of the second thick bituminous shale interval of the S4 sequence is present by Bastos et al. (2021). All data came from SHRIMP U-Pb zircon collected from ash fall deposits in drill cores carried out in São Mateus do Sul, Paraná State.

The stratal stacking patterns orders can be laterally correlated over kilometers in drill cores. Considering the above-described ages was possible to correlate the 3rd-order cycles of the mixed deposits with the global sea-level curve (Haq & Schutter, 2008). Thus the Irate Sea had a duration of 8.0 Ma, and each 3rd-order cycle had about 2.7 Ma. The stacking patterns of the identified elementary cycles (300) and the previous age estimated for the duration of the succession indicate that each bundle has *ca* 26.6 ka. (8.0×10^6 yr./300 cycles = 26 600 yr./cycle). The 5th-order cycles (59) calculation indicates 135.50 ka and 4th-order cycles (20) 400 ka. The

high-frequency cyclicity strongly resembles the Milankovitch signal known respectively as precession and eccentricity of short (± 100 ka) and long (± 400 ka) periodicity of earth orbit. The average 100 ka eccentricity cycle compared with the average precession cycle gives a ratio of 1:5 which is the average ratio commonly observed in the successions (Schwarzacher, 2000; Strasser et al. 2006). In addition, a rough estimate from the calculated age of the MTS of the S3 sequence to the MTS of the S4 gives similar results.

Total solar radiation maxima resulting from Milankovitch periodicities enhanced the atmospheric-ocean thermal gradient, the possible primary control responsible for the dolostone beds. The dry periods are characterized by (i) lower fluvial terrigenous input; (ii) more energetic environments (e.g., more significant and more frequent storms); (iii) high chemical and biochemical carbonate production; (iv) de-stratification of the water column and enhanced oxygenation; v) high salinity and reduced carbonate dissolution. Radiation minima favor a lesser energetic sedimentary process and consequent stratified water development and persistence. It results in water column stagnation, restriction, and notably reduced biogenic carbonate production leading to the deposition and preservation of organic-rich facies (Eldrett et al., 2015). The formation of distinct horizons containing sapropelites in the well-developed cyclic deposits in the lower Pleistocene and Pliocene of Calabria and Sicily is assumed by Schwarzacher (2000) to be due to an increased sea surface productivity related to strong precession minima. Plus, the hypersaline and anoxic conditions were an essential factor in recording the total solar radiation signals. The anoxic-bottom water conditions induced by the high organic matter production are enhanced, resulting in organic-rich shale prevailing across the basin. The detailed analyses of the core do not reveal definitive evidence of subaerial exposure marking each shallowing upward cycle. There is a dominant occurrence of subtidal cycles facies. Sadler (1981) and Osleger (1991) states that to maintain deposition within the subtidal zone without shallowing to peritidal depths, the sedimentation rates active over the duration of a typical shallowing-upward cycle (20-200 ka) must approach accumulation rates (perhaps 0.01-0.2 m/ka) characteristic of longer periods.

The diagenetic influence over the cyclicity is an important consideration that must be made. The well-preserved studied succession shows minimum overprinting by diagenetic features, favoring the identification of primary structure and texture, becoming unequivocal the interpretation of the sedimentary processes.

6.6.4. Cyclicity and high organic matter production

A peculiar characteristic of the Irati Formation is the occurrence of organic-rich shale intercalated with carbonates beds, generating thickening upward trends in different stacking pattern scales (Fig. 02 and 07). Climate season was responsible for developing alternative dominated-dry and dominated-wet seasons in the Irati Sea, acting as the first-order sedimentation control. Therefore, is difficult to evoke a permanent steady-state water-column stratification, anoxic and hypersaline condition for the entire succession.

During dry season predominates carbonate deposition with low input of siliciclastic sediment indicated by the very low presence of terrigenous grains in the carbonates facies. In addition, gypsum pseudomorphs and length-slow chalcedony are associated with micritic to peloidal dolostone beds. Despite the dominance of carbonate production during total solar radiation maxima, the gradual transition from wet to dry seasons is recorded by the upward increase of carbonate deposition. Also, lipid biomarkers analyses have shown high hypersaline conditions indicated by the high gammacerane index and presence of C_{32} lanostane and C_{32}–C_{35} benzohopanes associated with the marls and even shale layers (Nascimento et al., 2021).

High freshwater input in the hypersaline environment induced the stratification of the water column, defining the beginning of wet seasons. Freshwater inflow rich in terrigenous organic matter is indicated by lexane indexes, TPP/Dia27, C_{29}/C_{27} Sterane, and C_{28}/C_{26} TAS ratios, also the occurrence of cadalene, simonellite, β-carotane and, sempervirane (Martis et al., 2020; Nascimento et al., 2021). The renewal of terrigenous nutrients in the platform induces algal bloom in the photic zone. The microbial blooms are suggested by the prominent high TOC and hydrogen index observed in the bituminous shale facies interbedded with carbonate layers (reaching 1000 mg HC/g TOC). Also elevated hopane/sterane ratio, and concentration of C_{17} long-chain alkylnaphthalenes. Seasonal high freshwater discharge with the enclosed Irati Sea created a fresh, brackish environment favorable for *Botryococcus* algae to flourish. *Botryococcusi* was identified across the succession by Correa da Silva and Cornford (1985) and Reis et al. (2018).

Despite the shallow condition, high organic matter production, and induced water column stratification were the primary factors responsible for high organic matter preservation, generating the bitumen-rich shale facies interbedded with carbonate rocks. The occurrence of pyrite as framboids, millimeter to centimeter euhedral cubic shapes, and disseminates nanometric crystals forming lenses in the shale lamination is indicative of the anoxic-bottom water. Low Pr/Ph ratios, higher C_{27}/C_{29} sterane ratios, and C_{35} homohopane indices were also

considered as evidence of reducing and hypersaline conditions (Martins et al., 2020a). Bastos et al. (2021) observed a gradual increase of Pr/Ph ratios while regular isoprenoid concentrations decreased in the shale overlying the breccias. The input of freshwater rich in terrestrial material reduced the salinity and fast induced water-column stratification. The hypersaline and reducing bottom condition favor preservation of organic matter, forming bituminous shale across the basin.

The organic-richer shale was accumulated in the offshore zone during long periods of low sediment influx between turbidity events. Reis et al., (2018) identified *Botryococcus* algae and oxidized organic matter correlated with the offshore turbidity cycles for the southern border. Turbidity currents resuspended the organic-rich sediment and oxygenated the environment. Also, the environmental condition will be favoring bioturbation. Organic matter predation can be observed in the turbidity shale facies. Bioturbation can easily mix the rhythmic beds under very low sediment rate (Einsele, 1982b). Nevertheless, the predominance of anoxic conditions prevents complete benthonic fauna colonization of the substrate.

The thin and widely distributed organic-rich shale beds of the two uppermost third-order cycles of Assistência Member represent the maximum transgression due to a gradual eustatic rise combined with constant subsidence. The lack of high fluvial sediment input, indicated by the more proximal facies, causes sediment starvation and organic matter concentration in the distal basin setting, as previously stated by Sageman et al. (2003). They represent the maximum algal bloom and widespread anoxic-bottom water conditions in the basin. The geochemical profile configuration with a gradual increase of the total organic carbon and source potential shown in Fig. 10 indicates a gradual increase of the preservation potential, which is (as described above) related to the freshwater input and algal bloom. Martins et al. (2020a) and Nascimento et al. (2021), studying these intervals, observed an increase of Chroman ratio (CR; 5,7,8-triMe-MTTC/total MTTCs) and decrease of Gam/C_{30}H and βC/C_{30}H ratios toward the top. This data suggests a progressive decline in salinity and stratification of the water column due to freshwater inflow, corroborating the seasonal climate variation.

The black to grey organic-poor siltstone and incipiently laminated shale that occurs overlying the organic-rich bituminous shale of the cycle type G suggests a shift in the environmental condition. There was an increase of free oxygen and a decrease in organic matter production due to the rise of sea-level and Panthalassa Ocean connection during the HST aggradational phase.

6.7. CONCLUSIONS

Mixed siliciclastic-carbonate sedimentation in the shallow epicontinental sea of Irati has been shown high sensitivity to climate changes, providing a sensitive gauge for recording orbitally controlled high-frequency sea-level fluctuations in the Lower Permin of the Paraná Basin and correlating it with the global sea-level curve. The hierarchical organization of the superimposed high-frequency Cyclicity stacking patterns resulted from cyclic sea-level oscillation induced by orbital forcing climate changes related to Milankovitch cycles. The minor base-level variations of the Irati Sea were not enough to expose the substratum and produce subaerial exposure surfaces. Though, it created shallow conditions favorable to high carbonate production across the basin. The following upper raising base levels were induced by freshwater inflow during solar radiation minima. Continental input in the hypersaline environment renews the organic nutrient allowing algal-bloom in the photic zone and induced water-column stratification which caused anoxic bottom water and high organic carbon preservation. The terrigenous material that came with it, plus the elevation of the base level and the anoxic condition, cease the carbonate factory. The extreme conditions (e.g., high salinity, anoxic bottom water) was crucial for inhibiting the benthic fauna colonization and well-preserved record. The thicker shales deposits of the Serra Alta Formation overlying the S3 sequence indicate a considerable increase in accommodation and the end of the shallow Irati Sea.

ACKNOWLEDGMENTS

We thank the National Council for Scientific and Technological Development (CNPq) for funding this research through grants a Postgraduate Scholarship (CNPq - 140630/2019-8) on the Programa de Pós-Graduação em Geologia e Geoquímica (PPGG) of the Federal University of Pará (UFPA). We are grateful to IRATI PETRÓLEO E ENERGIA LTDA for donate the drilling core.

REFERENCES

Alferes, C.L.F., Rodrigues, R., Pereira, E., 2011. Geoquímica orgânica aplicada à Formação Irati, na área de São Mateus do Sul (PR). Brasil. Geochim. Bras. 25, 47–54.

Almeida, F.F.M., 1980. Tectônica da Bacia do Paraná no Brasil. Relatório da PAULPETRO n° 14091, São Paulo, pp. 187.

Anjos, C.W.D., Guimarães, E.M., Souza, P.A., 2006. Mineralogia e palinologia de níveis de folhelhos negros da Formação Irati (Permiano) nas porções norte e sul da Bacia do Paraná, In: XLIII Congresso Brasileiro de Geologia, *Coletânea*... Salvador, Brasil, p. 646-649.

Araújo, L.M., 2001. Análise da expressão estratigráfica dos parâmetros de geoquímica orgânica e inorgânica nas sequências Irati. PhD *Thesis*, Universidade Federal do Rio Grande do Sul. pp. 342.

Balog, A., Haas, J., Read, J.F., Coruh, C., 1997. Shallow marine record of orbitally forced cyclicity in a Late Triassic carbonate platform, Hungary. Journal of Sedimentary Research, 67 (4), 661-675.

Bastos, L.P.H., Rodrigues, R., Pereira, E., Bergamaschi, S., Alferes, C.L.F., Augland, L.E., Domeier M., Svensen, H.H., 2021. The birth and demise of the vast epicontinental Permian Irati-Whitehill sea: Evidence from organic geochemistry, geochronology, and paleogeography. Palaeogeogr. Palaeoclimatol. Palaeoecol. 562, 110103.

Borer, J.M., Harris, P.M., 1991. Depositional facies and model for mixed siliciclastics and carbonates of the Yates Formation, Permian Basin.

Bosence, D.W.J., Wood, J.L., Rose, E.P.F., Qing, H., 2000. Low-and high-frequency sea-level changes control peritidal carbonate cycles, facies and dolomitization in the Rock of Gibraltar (Early Jurassic, Iberian Peninsula). J. Geol. Society, 157 (1), 61-74.

Bourbonniere R.A., Meyers P.A., 1996. Sedimentary geolipid records of historical changes in the watersheds and productivities of Lakes Ontario and Erie. Limnology and Oceanography, 41(2), 352-359.

Burchell, M.T., Stefani, M., Masetti, D., 1990. Cyclic sedimentation in the Southern Alpine Rhaetic: the importance of climate and eustasy in controlling platform-basin interactions. Sedimentology, 37, 795-815.

Callefo, F., Arduin, D. H., Ricardi-Branco, F., Galante, D., Rodrigues, F., Branco, F. C. 2018. The giant stromatolite field at Santa Rosa de Viterbo, Brazil (Paraná Basin)–A new paleoenvironmental overview and the consequences of the Irati Sea closure in the Permian. Journal of South American Earth Sciences, 84, 299-314.

Caputo, M.V., Crowell, J.C., 1985. Migration of glacial centers across Gondwana during Paleozoic Era. Geological Society of America Bulletin, 96 (8), 1020-1036.

Catuneanu, O., 2006. Principles of sequence stratigraphy. Elsevier, p. 387.

Catuneanu, O., 2019a. Model-independent sequence stratigraphy. Earth-Science Reviews, 188, 312-388.

Catuneanu, O., 2019b. Scale in sequence stratigraphy. Marine and Petroleum Geology, 106, 128-159.

Catuneanu, O., Galloway, W.E., Kendall, C.G.S.C., Miall, A.D., Posamentier, H.W., Strasser, A., Tucker, M.E., 2011. Sequence stratigraphy: methodology and nomenclature. Newsletters on stratigraphy, 44 (3), 173-245.

Chiarella, D., 2011. Sedimentology of Pliocene-pleistocene Mixed (Lithoclastic bioclastic) Deposits in Southern Italy (Lucanian Apennine and Calabrian Arc): Depositional Processes and Palaeogeographic Frameworks. Ph.D Thesis. University of Basilicata.

Chiarella, D., Moretti, M., Longhitano, S.G., Muto, F., 2016. Deformed cross-stratified deposits in the Early Pleistocene tidally-dominated Catanzaro strait-fill succession, Calabrian Arc (Southern Italy): triggering mechanisms and environmental significance. Sediment. Geol. 344, 277-289.

Crevello, P. D., 1991. High-frequency carbonate cycles and stacking patterns: interplay of orbital forcing and subsidence on Lower Jurassic rift platforms, High Atlas, Morocco. Sedimentary Modeling: Computer Simulations and Methods for Improved Parameter Definition: Kansas Geological Survey, Bulletin, 233, 207-230.

Correa da Silva Z.C., Cornford C., 1985. The kerogen type, depositional environment and maturity, of the Irati Shale, Upper Permian of Paraná Basin, Southern Brazil. Org. Geochem., 8, 399-411.

Della Fávera, J.C., Della Fávera, J.C., 2001. Fundamentos de estratigrafia. Ed. Uerj.

Droste, H., 1990. Depositional cycles and source rock development in an epeiric intra-platform basin: the Hanifa Formation of the Arabian Peninsula. Sediment. Geol., 69 (3-4), 281-296.

Einsele, G., 1982a. General remarks about the nature, occurrence, and recognition of cyclic sequences (periodites). In: Einsele, G, Seilacher A., (Eds.) Cyclic and event stratification Springer, Berlin, Heidelberg, pp. 3-7.

Einsele, G. (1982b). Limestone-marl cycles (periodites): diagnosis, significance, causes—a review. In: Einsele, G, Seilacher A., (Eds.) Cyclic and event stratification (. Springer, Berlin, Heidelberg, pp. 8-53.

Eldrett, J.S., Ma, C., Bergman, S.C., Ozkan, A., Minisini, D., Lutz, B., Kelly, A.E., 2015. Origin of limestone–marlstone cycles: astronomic forcing of organic-rich sedimentary rocks from the Cenomanian to early Coniacian of the Cretaceous Western Interior Seaway, USA. Earth and Planetary Science Letters, 423, 98-113.

Fragoso, D.G.C., Gabaglia, G.P.R., Magalhães, A.J.C., Scherer, C.M.D.S., 2021. Cyclicity and hierarchy in sequence stratigraphy: an integrated approach. Braz. J. Geol., 51 (2), 1-32.

Fu, Jiamo., Sheng, G., Xu, J., Eglinton, G., Gowar, A.P., Rongfen j., Shanfa, S., Pingan, P., 1990. Application of biological markers in the assessment of paleoenvironments of Chinese non-marine sediments. Organic Geochemistry, 16, 769–79

Ginsburg, R.N., 1971. Landward movement of carbonate mud – new model for regression cycles in carbonates (abs.): American Association of Petroleum Geologists Bulletin, 55, 340.

Goldhammer, R.K., Dunn, P.A., Hardie, L.A., 1990. Depositional cycles, composite sea-level changes, cycle stacking patterns, and the hierarchy of stratigraphic forcing: examples from Alpine Triassic platform carbonates. Geological Society of America Bulletin, 102 (5), 535-562.

Goldhammer, R.K., Lehmann, P.J., Dunn, P.A., 1993. The origin of high-frequency platform carbonate cycles and third-order sequences (Lower Ordovician El Paso Gp, West Texas); constraints from outcrop data and stratigraphic modeling. J. Sediment. Research, 63 (3), 318-359.

Goldhammer, R.K., Oswald, E.J., Dunn, P.A., Franseen, E.K., Watney, W.L., 1991. Hierarchy of stratigraphic forcing: Example from Middle Pennsylvanian shelf carbonates of the Paradox Basin. Sedimentary Modeling: Computer Simulations and Methods for Improved Parameter Definition: Kansas Geological Survey, Bulletin, 233, 361-413.

Grotzinger, J. P. 1986. Cyclicity and paleoenvironmental dynamics, Rocknest platform, northwest Canada. Geological Society of America Bulletin, 97(10), 1208-1231.

Grotzinger, J.P., 1989. Facies and evolution of Precambrian carbonate depositional systems: emergence of the modern platform archetype.

Haq, B. U., & Schutter, S. R. 2008. A chronology of Paleozoic sea-level changes. Science, 322(5898), 64-68.

Holland, S.M., Miller, A.I., Dattilo, B.F., Meyer, D.L., Diekmeyer, S.L., 1997. Cycle anatomy and variability in the storm-dominated type Cincinnatian (Upper Ordovician): Coming to grips with cycle delineation and genesis. The J. of Geol., 105, 135-152.

Holz, M., França, A.B., Souza, P.A., Iannuzzi, R., Rohn, R., 2010. A stratigraphic chart of the Late Carboniferous/Permian succession of the eastern border of the Paraná Basin, Brazil, South America. J. S. Am. Earth Sci. 29, 381–399.

Irwin, H., Meyer, T., 1990. Lacustrine organic facies. A biomarker study using multivariate statistical analysis. Organic Geochemistry, 16, 176–210.

Kerans, C., Tinker, S. W., 1997. Sequence stratigraphy and characterization of carbonate reservoirs Tulsa: SEPM, 40, 130.

Kodner, R.B., Pearson, A., Summons, R.E., Knoll, A.H., 2008. Sterols in red and green algae: quantification, phylogeny, and relevance for the interpretation of geologic steranes. Geobiology 6, 411–420.

Lages L.C., 2004. A formação Irati (grupo passa dois, permiano, bacia do Paraná) no furo de sondagem FP-01-PR (Sapopema, PR). MS Dissertation, Universidade Estadual Paulista, Rio Claro, 117p.

Longhitano, S.G., Chiarella, D., Di Stefano, A., Messina, C., Sabato, L., Tropeano, M., 2012. Tidal signatures in Neogene to Quaternary mixed deposits of southern Italy straits and bays. Sediment. Geol., 279, 74-96.

Martins, L.L., Schulz, H.M., Ribeiro, H.J.P.S., Do Nascimento, C.A., De Souza, E.S., Da Cruz, G.F., 2020a. Organic geochemical signals of freshwater dynamics controlling salinity

stratification in organic-rich shales in the Lower Permian Irati Formation (Paraná Basin, Brazil). Org. Geochem., 140, 103958.

Martins, C.M., Cerqueira, J.R., Ribeiro, H.J.P., Garcia, K.S., Da Silva, N.N., Queiroz, A.F. S., 2020b. Evaluation of thermal effects of intrusive rocks on the kerogen present in the black shales of Irati Formation (Permian), Paraná Basin, Brazil. J. South Am. Earth Sci 100, 102559.

Matos, S.A., Warren, L.V., Varejão, F.G., Assine, M.L. Simoes, M.G., 2017. Permian endemic bivalves of the "Irati anoxic event", Paraná Basin, Brazil: Taphonomical, paleogeographical and evolutionary implications. Palaeogeogr. Palaeoclimatol. Palaeoecol., 469, 18-33.

Meglhioratti, T., 2006. Estratigrafia de seqüências das formações Serra Alta, Teresina e Rio do Rasto (Permiano, Bacia do Paraná) na porção nordeste do Paraná e centro-sul de São Paulo. Master *thesis*. Universidade Estadual Paulista, Rio Claro (SP), 147p.

Mello, M.R., Gaglianone, P.C., Brassell, S.C., Maxwell, J.R., 1988. Geochemical and biological marker assessment of depositional environments using Brazilian offshore oils. Mar. Petrol. Geol. 5, 205–223.

Mello, M.R., Telnaes, N., Maxwell, J.R., 1995. The hydrocarbon source potential in the Brazilian marginal basins: a geochemical and paleoenvironmental assessment. In: Huc, A.-.Y. (Ed.), Paleogeography, Paleoclimate, and Source Rocks. American Association of Petroleum Geologists, Tulsa, OK, 233–272.

Milani, E.J., 1997. Evolução Tectono-Estratigráfica da Bacia do Paraná e o seu relacionamento com a geodinâmica fanerozoica do Gondwana Sul-Ocidental. Tese de doutorado em Geociências, Instituto de Geociências, Universidade Federal do Rio Grande do Sul, Porto Alegre, pp. 255.

Milani, E.J., 2004. Comentários sobre a origem e a evolução tectônica da Bacia do Paraná. In: Mantessoneto, V., Bartorelli, A., Carneiro, C.D.R., Brito-Neves, B.B. (Eds.), Geologia do Continente Sul-Americano: Evolução da Obra de Fernando Flávio Marques de Almeida. São Paulo, pp. 265–279.

Milani, E.J., Faccini, U.F., Scherer, C.M.S., Araújo, L.M., Cupertino, J.A., 1998. Sequences and stratigraphic hierarchy of the Paraná Basin (Ordovician to Cretaceous), southern Brazil. Bol. IG-USP 29, 125–173.

Milani, E.J., França, A.B., Medeiros, R.A., 2007. Rochas geradoras e rochas-reservatório da Bacia do Paraná, faixa oriental de afloramentos, Estado do Paraná. Roteiros Geológicos (in memoriam). Bol. Geociencias Petrobras 15, 135–162.

Moldowan, J.M., Seifert, W.K., Gallegos, E.J., 1985. Relationship between petroleum composition and depositional environment of petroleum source-rocks. Am. Assoc. Petrol. Geol. Bull. 69, 1255–1268.

Nascimento, C.A., De Souza, E.S., Martins, L.L., Ribeiro, H.J.P.S., Santos, V.H., Rodrigues, R., 2021. Changes in depositional paleoenvironment of black shales in the Permian Irati Formation (Paraná Basin, Brazil): Geochemical evidence and aromatic biomarkers. Mar. Petrol. Geol., 126, 104917.

Osleger, D., 1991. Subtidal carbonate cycles: Implications for allocyclic vs. autocyclic controls. Geology, 19 (9), 917-920.

Pasquier, J. B., Strasser, A., 1997. Platform-to-basin correlation by high-resolution sequence stratigraphy and cyclostratigraphy (Berriasian, Switzerland and France). Sedimentology, 44 (6), 1071-1092.

Peters, K. E., Peters, K. E., Walters, C. C., Moldowan, J. M. 2005. The biomarker guide (Vol. 2). Cambridge university press.

Peters, K.E., Walters, C.C., Moldowan, J.M., 2005. The Biomarker Guide Biomarkers and Isotopes in the Environment and Human History, second ed. University Press, Cambridge V.2.

Pittet, B., Strasser, A., 1998. Long-distance correlations by sequence stratigraphy and cyclostratigraphy: examples and implications (Oxfordian from the Swiss Jura, Spain, and Normandy). Geologische Rundschau, 86 (4), 852-874.

Pratt, B.R., James, N.P., 1986. The St George Group (Lower Ordovician) of western Newfoundland: tidal flat island model for carbonate sedimentation in shallow epeiric seas. Sedimentology, 33 (3), 313-343.

Reis, D.E., Rodrigues, R., Moldowan, J.M., Jones, C.M., Brito, M., da Costa Cavalcante, D., Portela, H.A., 2018. Biomarkers stratigraphy of Irati Formation (lower Permian) in the southern portion of Paraná Basin (Brazil). Mar. Petrol. Geol., 95, 110–138.

Rocha-Campos, A. C., Basei, M. A. S., Nutman, A. P., Santos, P. R., Passarelli, C. R., Canile, F. M., ... & Veroslavsky, G. (2019). U-Pb zircon dating of ash fall deposits from the paleozoic Paraná basin of Brazil and Uruguay: a reevaluation of the stratigraphic correlations. The Journal of Geology, 127(2), 167-182.

Sadler, P. M., 1981. Sediment accumulation rates and the completeness of stratigraphic sections. The Journal of Geology, 89 (5), 569-584.

Sadler, P. M., Osleger, D. A., Montanez, I. P. 1993. On the labeling, length, and objective basis of Fischer plots. Journal of Sedimentary Research, 63(3), 360-368.

Sageman, B.B., Murphy, A.E., Werne, J.P., Ver Straeten, C.A., Hollander, D.J., Lyons, T.W., 2003. A tale of shales: the relative roles of production, decomposition, and dilution in the accumulation of organic-rich strata, Middle–Upper Devonian, Appalachian basin. Chemical Geology, 195 (1-4), 229-273.

Santos R.V., Dantas E.L., Olveira C.G., Alvarenga C.J.S., Anjos C.W.D., Guimarâes E.M. Oliveira F.B. 2009. Geochemical and thermal effects of a basic sill on black shales and limestones of the Permian Irati Formation. J. S. Am. Earth Sci., 28, 14-24

Santos, R.V., Souza, P.A., de Alvarenga, C.J.S., Dantas, E.L., Pimentel, M.M., de Oliveira, C.G., de Araújo, L.M., 2006. Shrimp U-Pb zircon dating and palynology of bentonitic layers from the Permian Irati Formation, Parana´ Basin, Brazil. Gondwana Res. 9, 456–463.

Sato, A.M.; Llambías, E.J.; Basei, M.A.S.; Castro, C.E. 2015. Three stages in the Late Paleozoic to Triassic magmatism of southwestern Gondwana, and the relationships with the volcanogenic events in coeval basins. Journal of South American Earth Sciences 63: 48-69.

Schwark, L., Empt, P., 2006. Sterane biomarkers as indicators of Palaeozoic algal evolution and extinction events. Palaeogeogr. Palaeoclimatol. Palaeoecol., 240 (1-2), 225-236.

Schwarzacher, W., 1947. Uber die sedimentare Rhytmik des Dachsteinkalkes von Lofer. Verhandlungen der Geologischen Bundesanstalt, 175–188

Schwarzacher, W., 1975. Sedimentation Models and Quantitative Stratigraphy. Elsevier, Amsterdam, pp. 382.

Schwarzacher, W., 2000. Repetitions and cycles in stratigraphy. Earth-Science Reviews, 50 (1-2), 51-75.

Strasser, A., Hilgen, F.J., Heckel, P.H., 2006. Cyclostratigraphy-concepts, definitions, and applications. Newsletters on Stratigraphy, 42 (2), 75-114.

Strasser, A., H. Hillgärtner 1998: High-frequency sea-level fluctuations recorded on a shallow carbonate platform (Berriasian and Lower Valanginian of Mount Salève, French Jura). – Eclogae Geol. Helv. 91: 375–390, Basel.

Strasser, A., Pittet, B., Hillgärtner, H., Pasquier, J. B., 1999. Depositional sequences in shallow carbonate-dominated sedimentary systems: concepts for a high-resolution analysis. Sedim. Geol., 128 (3-4), 201-221.

Tänavsuu-Milkeviciene, K. A. T. I., Plink-Björklund, P. I. R. E. T., Kirsimäe, K., & Ainsaar, L. 2009. Coeval versus reciprocal mixed carbonate–siliciclastic deposition, Middle Devonian Baltic Basin, Eastern Europe: implications from the regional tectonic development. Sedimentology, 56(5), 1250-1274.

Tissot, B.P., Welte, D.H., 1984. Petroleum Formation and Occurrence. Second revised and enlarged edition. Springer Verlag, Berlin, Heidelberg, New York, Tokyo, pp. 699.

Tresch, J., Strasser, A., 2011. Allogenic and autogenic processes combined in the formation of shallow-water carbonate sequences (Middle Berriasian, Swiss and French Jura Mountains). Swiss Journal of Geosciences, 104 (2), 299-322.

Tyson, R.V., 1987. The genesis and palynofacies characteristics of marine petroleum source rocks. In: Brooks, J., Fleet, A.J. (Eds.), Marine Petroleum Source Rocks Geological Society. Special Publication No. 26, pp. 47–67.

Van Wagoner, J.C., Posamentier, H.W., Mitchum, R.M.J., Vail, P.R., Sarg, J.F., Loutit, T.S., Hardenbol, J., 1988. An overview of the fundamentals of sequence stratigraphy and key definitions.

Virgone, A., Masse, J.P., Babinot, J.F., 1994. Palaeoenvironmental significance of shallow water carbonate-marls rhythms: The Upper Berriasian of the Marseille region (Southeast France). Géologie Méditerranéenne, 21 (3), 185-187.

Volkman, J. K., 1986. A review of sterol markers for marine and terrigenous organic matter. Org. Geochem., 9 (2), 83-99.

Volkman, J.K., 2003. Sterols in microorganisms. Appl. Microbiol. Biotechnol. 60, 495–506.

Wallace, Z. A., Elrick, M., 2014. Early Mississippian orbital-scale glacio-eustasy detected from high-resolution oxygen isotopes of marine apatite (Conodonts). J. Sedim. Research, 84 (10), 816-824.

Zalán, P.V., Wolff, S., Astolfi, M.A.M., Vieira, I.S., Conceição, J.C.J., Appi, V.T., Santos Neto, E.V., Cerqueira, J.R. Marques, A., 1990. The Paraná Basin, Brazil. In: Interior cratonic basins (Eds. Leighton, M. W., Kolata, D. R., Oltz, D. F., Eidel, J. J.). Tulsa: American Association of Petroleum Geologists. AAPG. Memoir, 51. pp. 681-708.

CAPÍTULO VII

7. Organic-Rich Shale Profile of the Permian Irati Formation, Paraná Basin: Statistical and Paleoenvironment Implications of High Organic Matter Production within a Shallow and Cyclic Carbonate-Shale Sequence

Lorena Tuane Gomes de Almeida[a], Ailton da Silva Brito[b], Giovani Matte Cioccari[c]; Ana Maria Pimentel Mizusaki[d], Alexandre Araújo de Souza[a]; Sidney Gonçalo de Lima[a*]

[a]*Programa de Pós-Graduação em Química, Universidade Federal do Piauí, Campus Ministro Petrônio Portela, 64049-550, Teresina-PI, Brazil*

[b]*Programa de Pós-Graduação em Geologia e Geoquímica, Universidade Federal do Pará, 66075-110, Belém – PA, Brazil*

[c]*Instituto de Geociências, Universidade Federal do Rio Grande do Sul - Campus do Vale, 91501-970 Porto Alegre - RS, Brazil*

[d]*Centro de Engenharia, Universidade Federal de Pelotas, 96010-440, Pelotas - RS, Brazil.*

**Corresponding author. Tel.: +55 86 99989-2160.*

E-mail address: sidney@ufpi.edu.br

ABSTRACT

rati Formation (Paraná Basin) is a carbonate and organic-rich shale sequence intruded by Jurassic-Cretaceous basic rocks, featuring Brazil's most important oil shale deposits with different maturity levels. For the first time, the distribution of oil shale biomarkers from the Irati Formation (northern area) was analyzed by GC-MS and GC-MS/MS in order to determinate the thermal evolution, organic matter origin and the depositional paleoenvironment. The overall organic-rich shales cyclic interbedded with limestones and dolostone at the northernmost border has high similarity with the central and southernmost areas related a major control able to induce the cyclic sedimentation in a broad (106 km2) and restricted environment. There are slight differences in bulk parameters and molecular composition along the stratigraphic column. Nonetheless, significant differences when compared to previous studies for the south and southeast area. The TOC and Rock-Eval pyrolysis data showed fair hydrocarbon generation potential for the northernmost border. Biomarker parameters and hydrocarbon distributions indicate hypersalinity marine depositional paleoenvironment with stratified and anoxic water column for the mixed deposits. Contrasting

with the southern region here predominates biphytane, low abundance of gammacerane and the β-carotane is absent. Pr/n-C17, Ph/n-C18, HI and OI values suggest type II/III kerogen from marine organic matter with freshwater input, also corroborated by the presence of macrocyclic alkanes and 1-methyl macrocyclic alkanes usually associated with the lacustrine alga B. braunii. Among the steranes, those of stereochemistry ααα 20R predominate over ααα 20S and for pentacyclic terpanes the presence of βTm that indicate the shales are less thermally evolved. Nevertheless, the igneous intrusions fast induced the organic matter maturation generation oil that is widespread within the carbonate beds.

Keywords: Irati Formation, Black shales, Biomarkers, Multivariate statistical analysis.

7.1. INTRODUCTION

The marine organic-rich black shale of the Lower Permian Irati Formation has a wide distribution overall Paraná Basin, reaching 1,000 km^2, being one of the geological formations most studied among the Brazilian sedimentary formations mainly for its unique fossiliferous occurrences. Barbosa and Gomes (1958) were the first to define the Irati deposits in inferior Taquaral Member composed of dark grey siliciclastic mudstones and siltstones with low organic carbon contents, and superior Assistência Member, which consists of bituminous black shale rich in immature organic matter.

Since the beginning of the 20th century, there has been an economic interest in the Irati Formation due to the higher total organic carbon contents (TOC) and the potential oil shale as a result of the presence of organic rich-shales and tar sands (mainly south and southeast borders), leding to a significant increase in the number of publications regarding aspects on the characterization of the quantity, quality and thermal evolution of the organic matter of these portions (Almeida et al., 2020; Martins et al., 2020a; Martins et al., 2020b; Rocha et al., 2020; Teixeira et al., 2020; Holanda et al., 2019; Ng et al., 2019; Holanda et al., 2018; Osorio et al., 2018; Reis et al., 2018; Xavier et al., 2018; Matos et al., 2017; Ribas, et al. 2017; Goldberg and Humayun 2016; Alferes et al., 2011; Franco et al, 2010; Santos et al., 2006; Afonso et al., 1994; Afonso et al., 1991; Correa da Silva and Cornford 1985). Little is known about organic matter behavior in the rest of the Paraná Basin. In the northern border of the Irati Formation, the carbonate/siliciclastic ratio is higher, which probably influences the preserved organic matter**.**

Previous studies of Irati shales in the southern portion show a high proportion of isoparaffins over *n*-alkanes, high concentration of pristane and phytane isoprenoids, low

abundance of terpanes, and steranes, and variable gammacerane index. The biomarkers associated with the origin indicate that the oil comes from transitional organic matter deposited in an anoxic evaporitic marine environment (Souza et al., 2008; Franco et al., 2010; Alferes et al., 2011; Reis et al., 2018). The occurrence of a considerable amount of igneous intrusion within the mixed deposits in the north border of the basin, well-exposed in quarries, stimulated many works about its influence over the source rock of the Irati Formation.

Anjos and Guimarães (2008) noted that the thermal effect of the intrusive modified the preexisting mineralogy of the shale, forming talc and calcite, through dolomite reaction with quartz in anchimetamorphism zone. Souza et al. (2008) carried out the geochemical study in sections of Irati Formation affected by igneous intrusion revealed adequate quality and quantity of organic matter for petroleum generation in the northern region. The Spore Color Index (ICE) ranged from 4 to 10; the highest values were related to the proximity of the intrusive rock that thermally affected 6.85 m of the analyzed section. The range that shows maturation compatible with the wet/dry gas generation window is 1.8 m, while the range compatible with the oil generation window has a thickness of 5.5 m.

More recently, Cioccari (2018) analyzed samples of the Irati Formation concerning organic, inorganic, and petrographic parameters to evaluate the thermal influence of the sill in the embedding rock and determine the generated contact aureole. The result showed an increase in thermal maturation about the proximity of the diabase. The stages of thermal maturation demonstrated that the supermature zone varied from the point of contact with the sill to approximately 7.4 m and the oil generation window from 7.4 to 1.2 m.

The interest in characterizing the organic matter in this unit is due to its high potential for oil generation, the unique presence of varying levels of maturation due to intrusive rocks that acted as catalysts for hydrocarbon generation. Despite many studies on the Irati Formation in Brazil's southern and southeastern regions, there is still a significant gap regarding the geological processes on the northern frontier, especially regarding molecular parameters (biomarker data). The northmost border predominates the shallowest conditions and thicker carbonates beds; nevertheless, the shales also present a potential for hydrocarbon generation. In this sense, we present a detailed analysis of biomarkers using GC-MS and GC-MS/MS techniques associated with total organic carbon content (TOC) and Rock-Eval for the thin black shales cyclic interbedded with carbonate layers of the Irati Formation in the north border of Paraná Basin, Brazil.

7.2. GEOLOGICAL SETTING

The intracratonic Paraná Basin is located in the central-eastern part of the South American continent, covering about 1,700,000 km² with a sedimentary strata thickness of 7000 meters (Milani et al., 2007; Holz et al., 2010). The Irati deposits are placed on the beginning regressive phase of the second-order transgressive-regressive cycle of the Carboniferous-Triassic sequence (Milani, 1997). Santos et al. (2006) found a Lower Permian age of 278 ± 2.2 Ma, (Cisuralian) for Irati Formation using zircons of benthic layers within the Irati Formation.

The siliciclastic-carbonate succession is interpreted as having been deposited in a marine paleoenvironment, characterized by shallow and relatively still waters, with restricted communication with the open sea, with high water column stratification (Lavina, 1986; Araújo, 2001). Eventually, the sea became more turbulent, recorded in hummocky-type sedimentary structures, typical of these events (Xavier, 2014). The initial paleoenvironmental conditions allowed the deposition of organic shales that now are reflected in economic interest, since these rocks, found in the southern portion of the basin, have TOC values up to 25% and whose organic matter is predominantly algal and rich lipid composition, with a tendency to generate oil (Milani et al., 2006).

The Irati Formation has an overall thickness between 40 and 70 meters, mainly constituted of pyrobituminous shales, black shales, gray dolomites alternating with dark shales, sometimes nodular, more or less dolomitized limestones, siltstones, shales and fine sandstones, gray, fine-grained to coarse-grained sandstone conglomerates (Maraschin and Ramos, 2015). The dark gray mudstones and siltstones of the lower Taquaral Member were deposited under low dysoxic to suboxic conditions below the storm wave base. The uppermost Assistência Member record anoxic column water and salinity-stratified, which allowed the formation of bituminous shales interbedded with carbonate (Reis et al., 2018; Xavier et al., 2018).

Also, Irati Formation is studied mainly due to its fossiliferous content, composed predominantly of aquatic reptiles and floras, correlated with the Whitehill Formation in southern Africa, indicating that during the Permian period, both continents were united in the same mass of continental land, denominated Supercontinent Gondwana as postulated by Alfred L. Wegener in 1912 (Barberena and Timm, 2001; Guerra-Sommer and Cazzulo-Klepzig, 2001; Maraschin and Ramos, 2015).

7.3. METHODS

7.3.1. Sampling

The organic-rich shales were sampled at the SUCAL quarry, an excellent exposure of the Irati Formation located in the northern part of the Paraná Basin, distant 4 km of the Perolândia city (Goias, Brazil, Figure 1). The selected samples, as showed in the stratigraphic profile, was submitted to for TOC and Rock-Eval analysis, and biomarker data. Before geochemical analyses, all samples have been thoroughly cleaned, dried at 70 °C, and crushed to a powder.

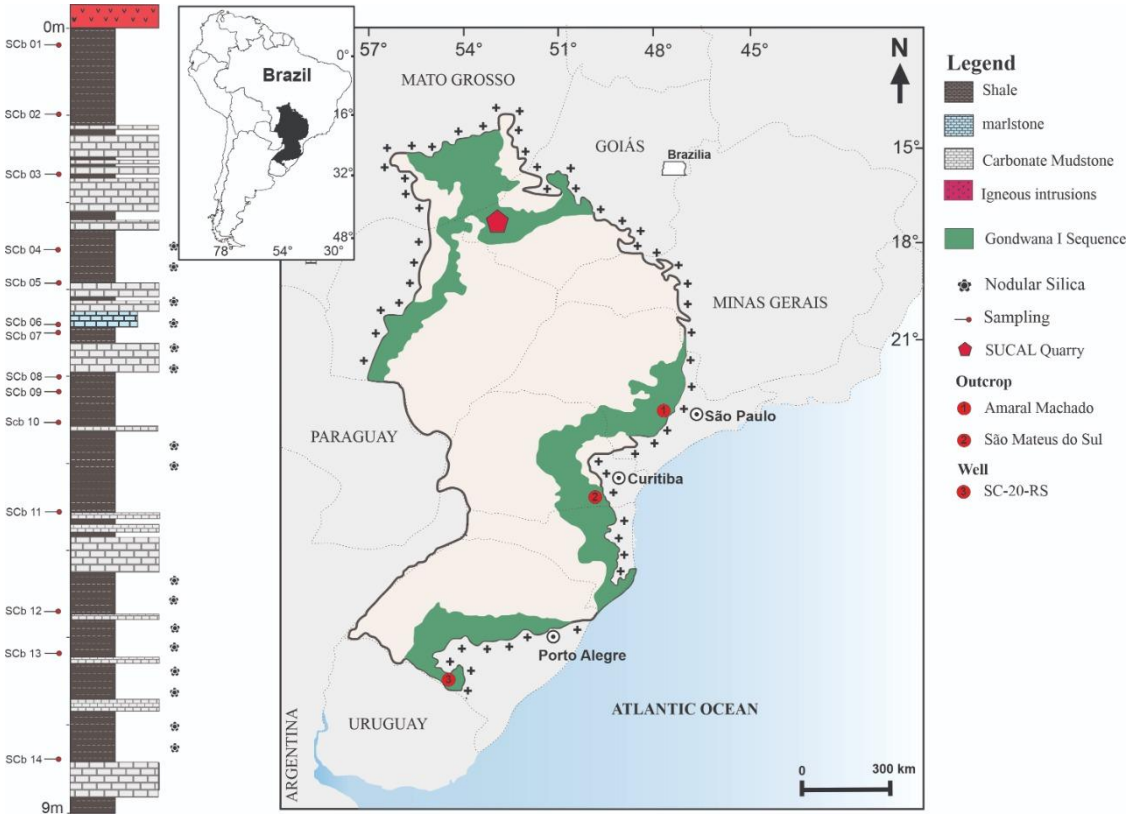

Figure 1. Geological map showing the Paraná basin area, the locality of samples studied herein are indicated by red pentagon (northern area, Goias state). The numbered points represent those Irati Formation areas previously studied: (1) Amaral Machado (São Paulo state, northeastern border); (2) São Mateus do Sul (Paraná state, central east area); (3) SC-20-RS (Rio Grande do Sul, southern area).

7.3.2. Total Organic Carbon and Rock-Eval Analysis

A representative homogenized fraction (250 mg) of which powdered samples were pre-treated with hydrochloric acid (1:1) to remove any possible inorganic carbon present in the samples. Then, the samples were combusted in a LECO SC-444 instrument for Total Organic Carbon (TOC) contents (wt%). Pyrolysis analysis was also conducted on the crushed samples using Rock-Eval 6 equipment (VINCI Technologies). The pyrolysis of organic matter was performed on 80 mg of sample rock, then heated to 600 °C with a heating rate of 25 ºC/min in a helium atmosphere. At 300 °C, the free hydrocarbons (S1) were volatilized and detected by a flame ionization detector (FID), the additional hydrocarbons (S2) present in the rock are cracked at the temperature range of 300-600 ºC.

7.3.3. Extraction and Fractioning of Organic Matter

The samples were ground and subjected to three successive extractions with 50 mL of dichloromethane/methanol (88:12 v/v). The extraction procedure was carried out in an ultrasonic bath, approximately 500 mg of powdered copper metal was added to obtained extract for sulfur removal using ultrasound for 30 min under heating at 60 °C. The extracts were filtered, and the solvent evaporated on a rotary evaporator. The extracts were fractionated by chromatographic column using silica/$AgNO_3$ 10 % as stationary phase and eluent system was *n*-hexane (100%), hexane/ethyl acetate 20% (v/v), ethyl acetate/methanol 5% (v/v) (Moura et al., 2015).

7.3.4. Urea Adduct

The samples SCb-04, SCb-07, and SCb-11 were submitted to urea treatment, and the aliphatic fractions were separated into linear and branched-cyclic sub-fractions according to the methodology proposed by Marotta *et al*., 2014. Briefly, 1 mL of a saturated solution of urea in methanol (0.3 g mL^{-1}) was added to the aliphatic fraction dissolved in *n*-hexane/acetone (2:1 v/v), the urea crystals were solubilized in a 50 °C water bath and then cooled at room temperature to rest for the urea recrystallization, after that, the solution was placed in a freezer at 0 °C for 12 h. The solvent was evaporated under nitrogen flow until the crystals were dried.

The branched-cyclic fraction was obtained by washing the crystals with *n*-hexane 2 mL (five times). The *n*-alkanes were recovered by solubilizing the urea crystals in distilled water; liquid-liquid extraction was performed repeatedly with 2 mL of *n*-hexane.

7.3.5. GC-MS Analysis

The GC-MS analysis of the saturated fractions was performed on a Shimadzu GCMS-QP2010 SE chromatograph equipped with AOC-5000 auto-injector, according to the following analysis conditions: injector temperature of 290 °C, split ratio of 1:10, initial oven temperature of 60 °C (1 min), then a heating ramp of 6 °C min^{-1} to 280 °C remaining for 5 min. A second heating ramp of 1 °C min^{-1} to 315 °C remaining for 15 min. For chromatography of components, a Rtx-5MS column, 30 m × 0.25 mm, 0.10 μm internal film thickness with diphenyl 5% and diphenyldimethylpolysiloxane 95% as stationary phase, helium as the carrier gas with a constant flow of 1.0 mL min^{-1}. The temperature of the interface and the ion source were 300 °C and 260 °C, respectively.

The mass analyzer used was of the quadrupole type operating by electronic impact (70 eV) and fragments detected in the range of 47 to 650 Da. The identification of the biomarkers was carried out by comparing the elution orders, retention times, and mass spectra with literature data.

7.3.6. GC-MS/MS Analysis

GC-MS/MS analysis was performed on ThermoScientific, TRACE GC Ultra gas chromatography, coupled to a TSQ Quantum XLS mass spectrometer, Triple Quadrupole. The chromatographic separation was performed on a 30 m x 0.25 mm capillary column with a 0.10 μm inner film thickness coated with dimethylpolysiloxane 100% (EquityTM-1, PerkinElmer) according to the following analysis conditions: initial oven temperature of 60 °C for 4 min, with a heating ramp of 6 °C min^{-1} to 280 °C remaining for 5 min and then a second heating ramp of 1 °C min^{-1} to 310 °C remaining for 10 min. The split/splitless PVT injector was used in split mode with a ratio of 1:10 at a temperature of 290 °C (phase injector at the same temperature). Helium (99.9999%) was used as a carrier gas with a constant flow of 1.0 mL min^{-1}. The triple quadrupole was operated in full scan mode with a mass range of 50 to 600 Da. The transfer line temperature was 300 °C, and the source temperature was 230 °C in electron impact mode with ionization energy of 70 eV.

After the optimization of the analysis conditions, the precursor and product ions were selected. The sample was reanalyzed to determine the most appropriate collision energy for the proposed fragmentations set, with optimized conditions: energy collision of 70 eV, collision gas pressure (argon) was maintained at 1 mTorr, scan cycle time 1 s. The identification of

biomarkers was performed by comparing the order of elution, retention times, and mass spectra in the scanning mode with data from the literature.

7.3.7. Statistical Analysis

Analytical data are assigned to the Origin Pro 2018 (30-day trial) program to carry out the principal component analysis (PCA) and hierarchical cluster analysis (HCA) to identify the different types of kerogen and the variation of the biomarker parameters throughout the stratigraphic profile.

7.4. RESULTS AND DISCUSSION

7.4.1. Quality and Quantity of Organic Matter

The total organic carbon (TOC) varies from 0.59% to 3.18% (Figure 2; Supplementary Data - Table 1). The high oscillation on the TOC directly reflects the sedimentary process and fluctuation record in the heterolytic carbonate-siliciclastic bedding present in analyzed deposits. The largest amount of organic matter is recorded in three moments during the sediment deposition (TOC about 3.00% for SCb-04, SCb-07, and SCb-12 samples), indicating organic matter enrichment that has been preserved under favorable conditions during the sediment deposition. Deposition of the sediments. The higher peak occurs in a very thin black shale layer between thicker carbonate beds (SCb-07 sample) which also coincides with the greater amount of S1 (free hydrocarbons), S2 (source rock potential) and HI (hydrogen index). Also, the OI (oxygen index) is lower, reflecting the best paleoenvironment condition for preserving organic matter appropriated for hydrocarbon generation, possible related to the flooding surface of the succession.

The paleoenvironment condition of the northern part of this huge Irati Sea is very different from the south portion, where there was the more significant deposition of organic matter; TOC shows values up to 26% for the shales related to the chemostratigraphic unit D (Alferes et al., 2011; Reis et al., 2018; Xavier et al., 2018).

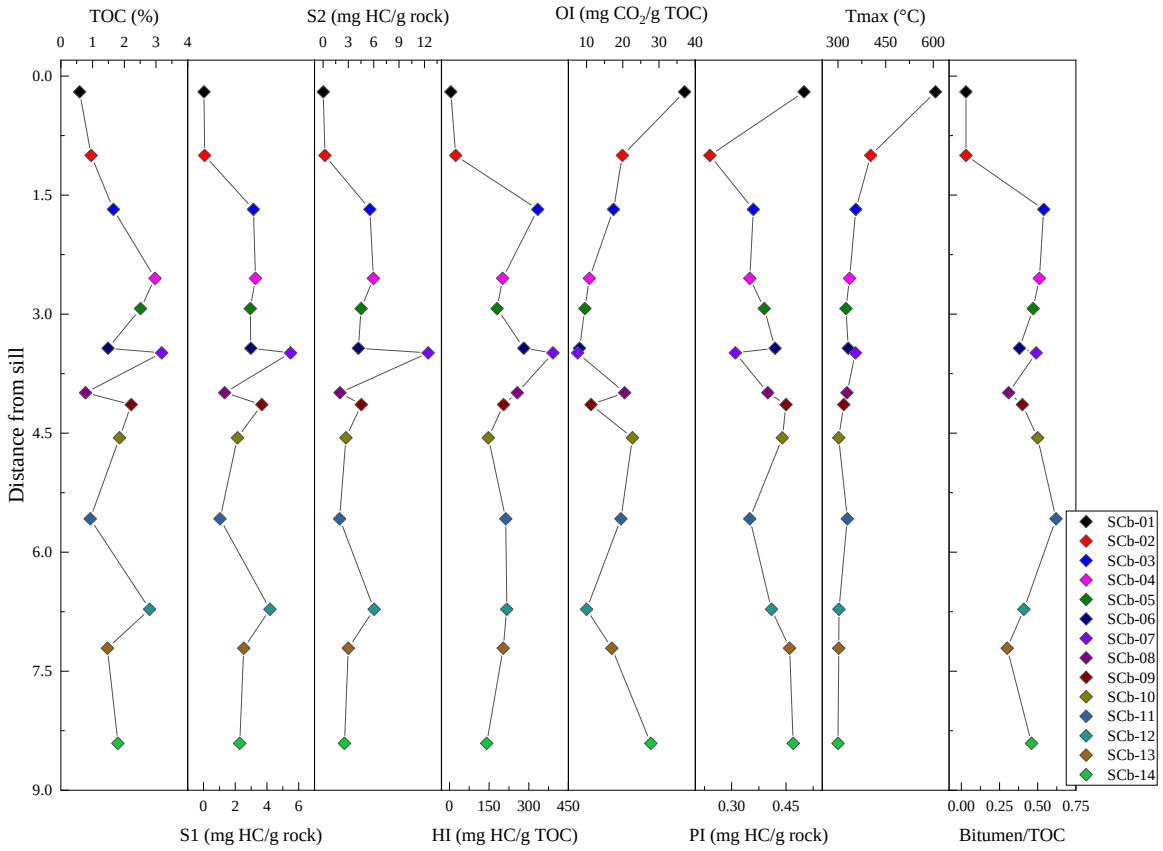

Figure 2. Profiles showing the variation of TOC and Rock-Eval pyrolysis data of the samples investigated in this study.

7.4.2. Organic matter type and Source rock

The samples showed pyrolysis S1 and S2 yields in the range of 0.03-5.49 and 0.03-12.45 mg HC/g rock, respectively. HI values ranged between 141-392 mg HC/g TOC, except SCb-01 and SCb-02 that showed low values (5 and 23 mg HC/g TOC, respectively). The relationship between S2 versus TOC (Figure 3A) shows that the north portion of Irati Formation is considered poor to fair oil source rocks (this conclusion is confirmed by the plot of TOC versus HI, Figure 3B), just the SCb-07 sample are good source rock due to showing the highest S2 value among the samples.

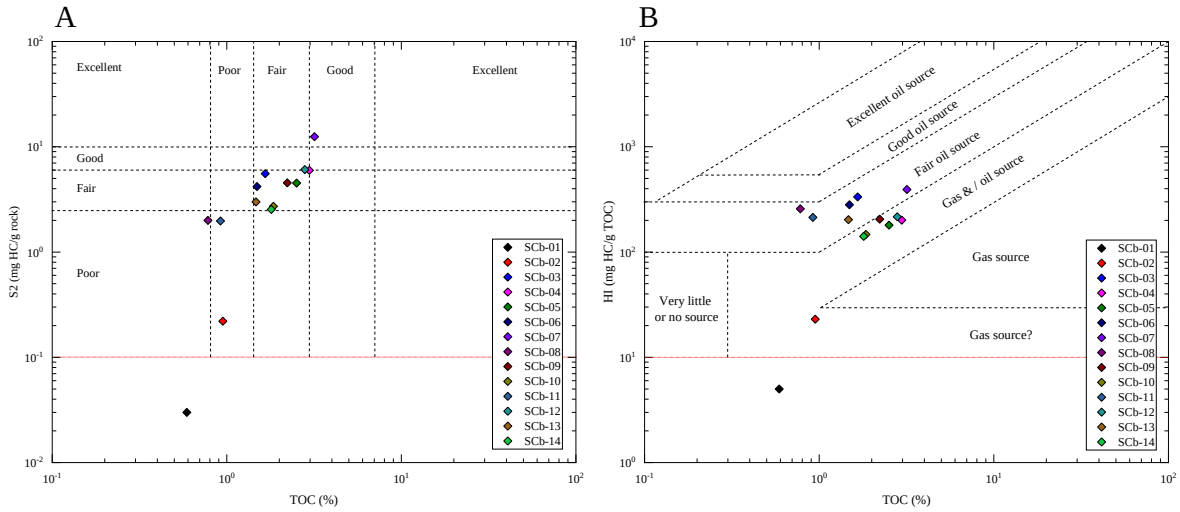

Figure 3. Source potential rating of Irati Formation source rocks based on: **(A)** S2 versus TOC and **(B)** HI versus TOC (by Jackson et al., 1985). The graphs were modified to show the SCb-01 sample.

The plot of S1 versus TOC (Figure 4A) can be used to discriminate between nonindigenous (allochthonous) and indigenous hydrocarbons (autochthonous) (Rabbani and Kamali, 2005; Nady et al., 2015; Mashhadi and Rabbani, 2015). This relation shows that some samples were characterized by allochthonous hydrocarbons, indicating oil generation and primary migration throughout the source rock. Mature oil-prone source rocks with type I-II kerogen commonly show Bitumen/TOC (Figure 2) ratios in the range 0.05-0.25, the Irati Formation samples showed high values for this ratio (0.30 to 0.62, except SCb-01 and SCb-02 samples), according to Peters and Cassa (1993) values higher of 0.25 can indicate contamination or migrated oil. It is confirmed by the plot PI versus Tmax (Figure 4B), PI values are considered too high for immature samples. In this region, the source rock possibly produces and accumulates hydrocarbons with the diabase sill acting as a trap, forming an atypical petroleum system (Magoon and Dow, 1994).

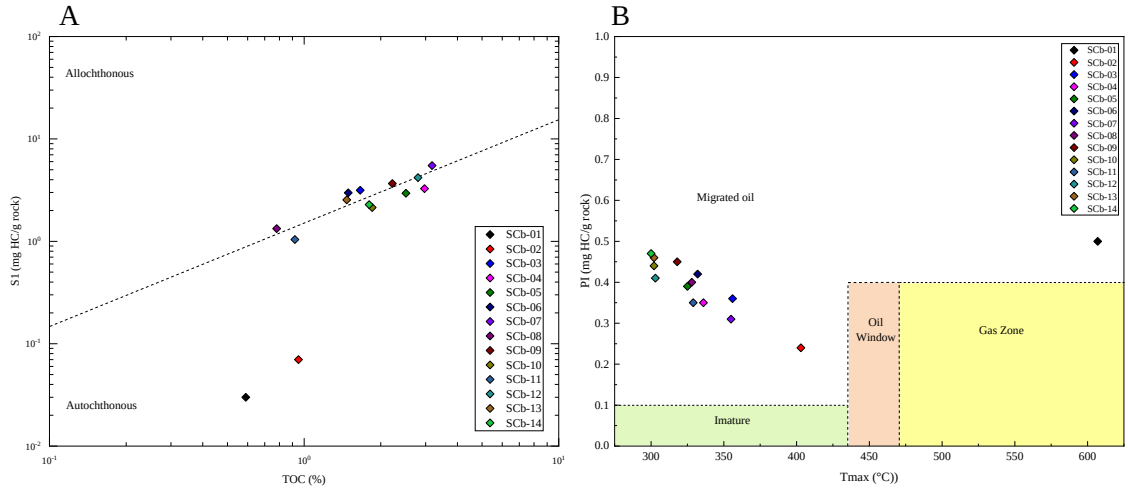

Figure 4. Plot diagram of: **(A)** S1 versus TOC (Hunt, 1996), the inclined line represents S1/TOC = 1,5; **(B)** PI versus Tmax (modified from Nady et al., 2015), this plot diagram is based on Peters and Cassa (1993).

A usual method to identify kerogen type is by diagrams constructed using the HI versus OI plot (Figure 5), according to Van Krevelen (Espitalié et al., 1977). The kerogen type for most samples is type II/III. The SCb-01 and SCb-02 samples are shown as kerogen type III due to their proximity to the igneous intrusion or a high input of oxidized organic matter. Multivariate statistics is a powerful tool for data analysis and evaluation. Multivariate statistical methods and multivariate statistical analysis tools study the behavior of three or more variables simultaneously. The principal components analysis (PCA) and hierarchical cluster analysis (HCA) are essential techniques used in multivariate statistics to transform and visualize complex data sets.

PCA can convert multiple indices into few comprehensive indices that are independent. However, the original information is unaffected (Wang et al., 2016; Mashhadi et al., 2015; Lin et al., 2020), while HCA is a statistical method of partitioning a sample into homogeneous classes to produce a functional classification (Edwards et al., 1999; Nady et al., 2015). In HCA, distances between samples (or variables) in the data set are calculated and compared, typically using a dendrogram, providing a simple view of groups of samples in the data set, where cluster distance is a relative measure of the degree of similarity among samples (Peters and Moldovan, 2005b).

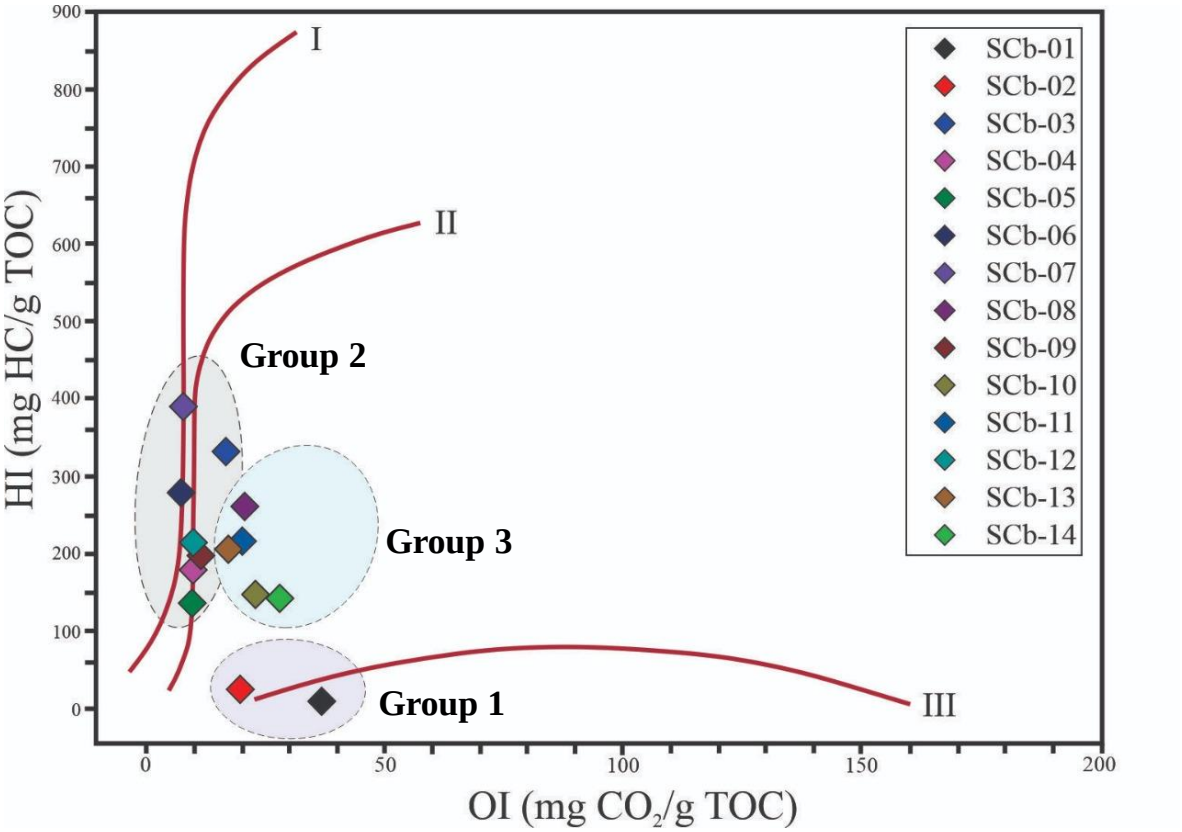

Figure 522. Cross diagrams of and HI versus OI (Van Krevelen diagram) for the Permian source rocks, Parana Basin, Goias-Brazil. The groups' divisions are based on PCA and HCA results.

For PCA and HCA analyses, TOC and Rock-Eval (S1, S2, HI, OI, PI, Tmax) standardized data were used. The PCA (Figure 6A) demonstrates that the first three factors explain 89.3% (PC1 = 63,4%, PC2 = 14.7% and PC3 11,2%) of the variance (see Supplementary Data for Factor Loadings, Figure 1). The Irati Formation samples, when analyzed by PCA and HCA (Figure 6B) showed three groups related to three organic matter types.

Group 1 is formed by SCb-01 and SCb-02 samples that have shown the lowest TOC, HI, S1, and S2 parameters, related to their proximity to the igneous intrusion (0.20 and 1.00 m, respectively). Group 2 are source rocks characterized by TOC from 1.49 to 2.97wt%, S1 and S2 yields in the range of 2.95 to 4.19 and 4.19 to 6.06 mg HC/g rock, respectively, and HI from 180 to 334 mg HC/g TOC indicating good to excellent source rocks with kerogen of type I/II and can generate hydrocarbons. The SCb-07 sample showed the highest TOC, S1, S2, and HI values and was classified as a separate group by PCA and HCA. However, Van Krevelen diagrams allowed this sample to be characterized as kerogen type I/II.

Group 3 are source rocks characterized by TOC from 0.59 to 1.85 wt%, S1 and S2 yields in the range of 0.03-2.54 and 0.03-2.99 mg HC/g rock and HI from 5 to 213 mg HC/g TOC indicating fair to good source rocks with kerogen of type II/III and can generate oil and gas.

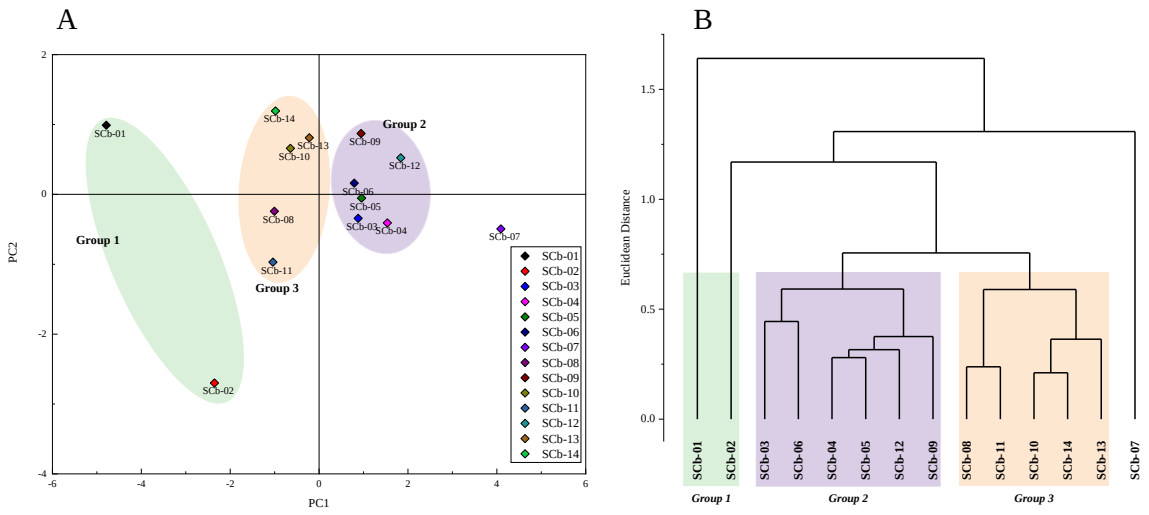

Figure 6. (A) Loadings plot for first and second principal components (PC1 versus PC2). **(B)** Dendrogram of hierarchical cluster analysis calculated using Euclidean distance.

7.4.3. Molecular parameters of thermal evolution

The maximum pyrolysis temperature (Tmax) attained was between 300 and 403 °C (Figure 2, Supplementary Data - Table 1), indicating a low maturation, only sample SCb-01 that is in direct contact with the diabase threshold exhibited a higher value (607 °C) showing high thermal maturation. The organic matter here is predominantly immature, as well as observed in the south and southeast portion (Reis et al., 2018; Afonso et al., 1991; Nascimento et al., 2021); the only mature or senile part of the Irati shales is those affected by igneous intrusion as observed for the SCb-01 sample.

Bitumen yields for the analyzed sample are high and range of 0.24 to 1.55% (Table 1, Supplementary data), SCb-01 and SCb-02 showed the lowest yield, 0.02 and 0.03%, respectively. Using the SARA analysis data, Tissot and Welte (1984) have proposed a ternary diagram to classify crude oils and bituminous extracts. Figure 7 shows that the samples are primarily aromatic-asphaltic with slight differences between them. SCb-01 and SCb-02 exhibit aromatic-intermediate characteristics while SCb-04 and SCb-14 are classified as paraffinic and paraffinic-naphthenic.

CPI (carbon preference index) and EOP (odd-to-even predominance) values range of 0.45-0.77 and 0.60-0.77 (Figure 8, Supplementary Data - Table 2), respectively, showing even

over odd preference for the *n*-alkanes distribution (Figure 9) and indicating organic matter with low thermal evolution. Just the samples closer the diabase threshold, SCb-01, and SCb-02 showed values ~ 1, suggesting high thermal evolution (Bray and Evans, 1961; Scalan and Smith, 1970; Marzi et al., 1993). The SCb-01 and SCb-02 saturated fractions chromatogram showed a large unresolved hump that indicates a complex mixture of hydrocarbons, probably originates from thermally initiated non-selective free radical polymerization induced by the igneous intrusion.

Maturation parameters using hopane and steranes hydrocarbons (Figure 10 and Figure 11), which present better thermodynamic stability and resistance to biodegradation, were calculated (Peters et al., 2005b). Tricyclic terpanes (TT) were observed in most samples, and their chromatograms varied along with the stratigraphic profile, the samples unaffected by igneous intrusion showed TTC_{23}, $TTC_{24,}$ and TTC_{27}. The rocks from the significantly altered zone (SCb-01 and SCb-02) presents C_{19} to C_{27} homologs. Tricyclic terpanes were noted by Grande et al., (1993) in highly mature oils and extracts from saline lacustrine and marine carbonate source rocks, suggesting that the precursor organisms lived in moderate salinity conditions. However, Zumberge (1983) indicates that C_{19} - C_{20} tricyclics may also be produced by the thermal cleavage of the alkyl side chain in sester- and triterpanes. 18α(H)-trisneohopane (Ts) is more resistant to thermal degradation than 17α(H)-trisnorhopane (Tm), so it is expected that the values of the Ts/Tm ratio will increase with increasing maturation. The ratio of these isomers expressed as Ts/Tm and Ts/(Ts+Tm), exhibited similar values from 0.04 to 0.41 and 0.03 to 0.39 (Figure 9, Supplementary Data - Table 2) suggesting immature samples (Seifert and Moldowan, 1978; Moldowan et al., 1986; Moldowan et al., 1994; Peters et al., 2005b), as observed in the Rock-Eval analysis.

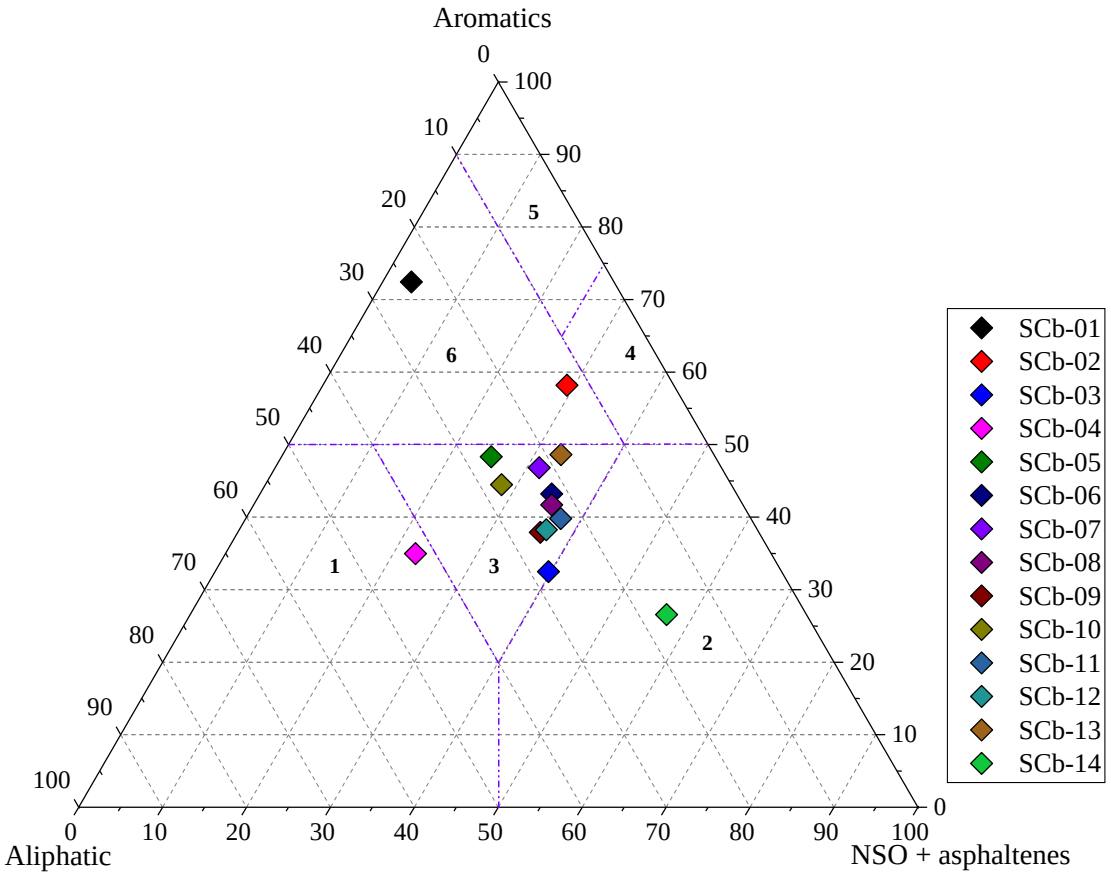

1. Paraffinic	2. Paraffinic-Naphthenic	3. Aromatic-Asphaltic
4. Naphthenic	5. Aromatic-Naphthenic	6. Aromatic-Intermediate

Figure 7. Ternary diagram showing the bulk SARA (saturate, aromatic, resins and asphaltenes) composition of Irati Formation samples.

The C_{27} 17β(H)-22,29,30-trinorhopane (βTm) was identified in all the samples, this compound has already been reported by Reis et al., (2018), it is characteristic of immature source rocks, as thermal maturation increases, the relative concentration of βTm is expected to decrease because it is thermally unstable when compared to Ts and Tm (Hong et al., 1986). Rock extracts from the Irati Formation showed a low relative abundance of Ts and it was observed that it is practically absent at 1.68 to 8.41 m from the diabase intrusion.

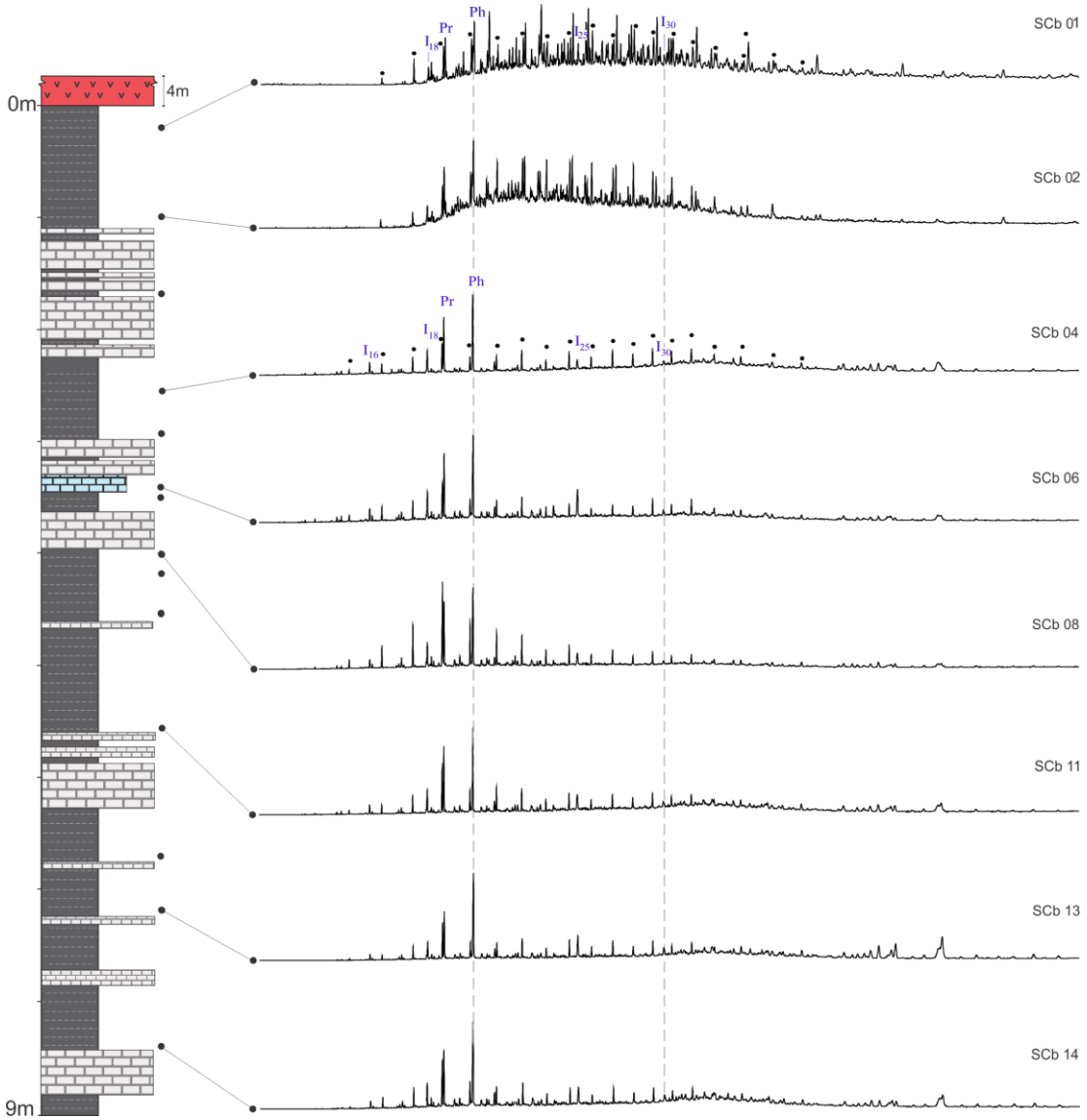

Figure 8. Total Ion Chromatogram (TIC) profile of saturated fractions. Pr = pristane; Ph = phytane; black dots = C_{13} to C_{34} *n*-alkanes.

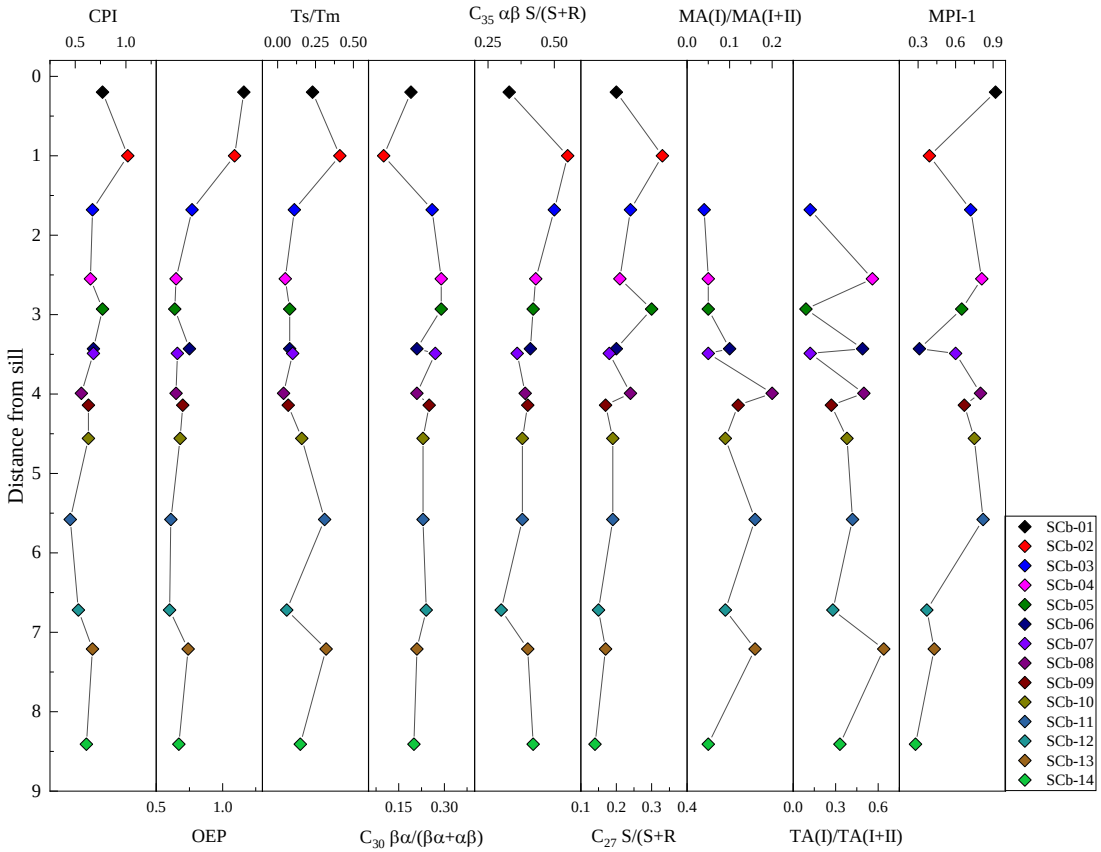

Figure 9. Profiles showing the variation of geochemical maturation parameters calculated based on *n*-alkanes, hopanes, and steranes.

Usually, in immature sediments, the 17β(H),21β(H)-hopanes are the dominant structures, although 17β(H),21α(H)-moretanes and 17α(H),21β(H)-hopanes are still present. The stability of hopanes and moretanes increases according to the sequence ββ <βα <αβ, with αβ being the most stable. The C_{30} βα/(αβ+βα) ratio can reach values from 0.9 to 1 at the beginning of the oil generation window, the values of this ratio for the samples ranged from 0.10-0.29, while the C_{31} αβ 22S/(22S+22R) and C_{35} αβ 22S/(22S+22R) ratios ranged from 0.26-0.55 and 0.30-0.55, respectively (Ensminger et al., 1977; Seirfert and Moldowan, 1980; Peters, 2005b).

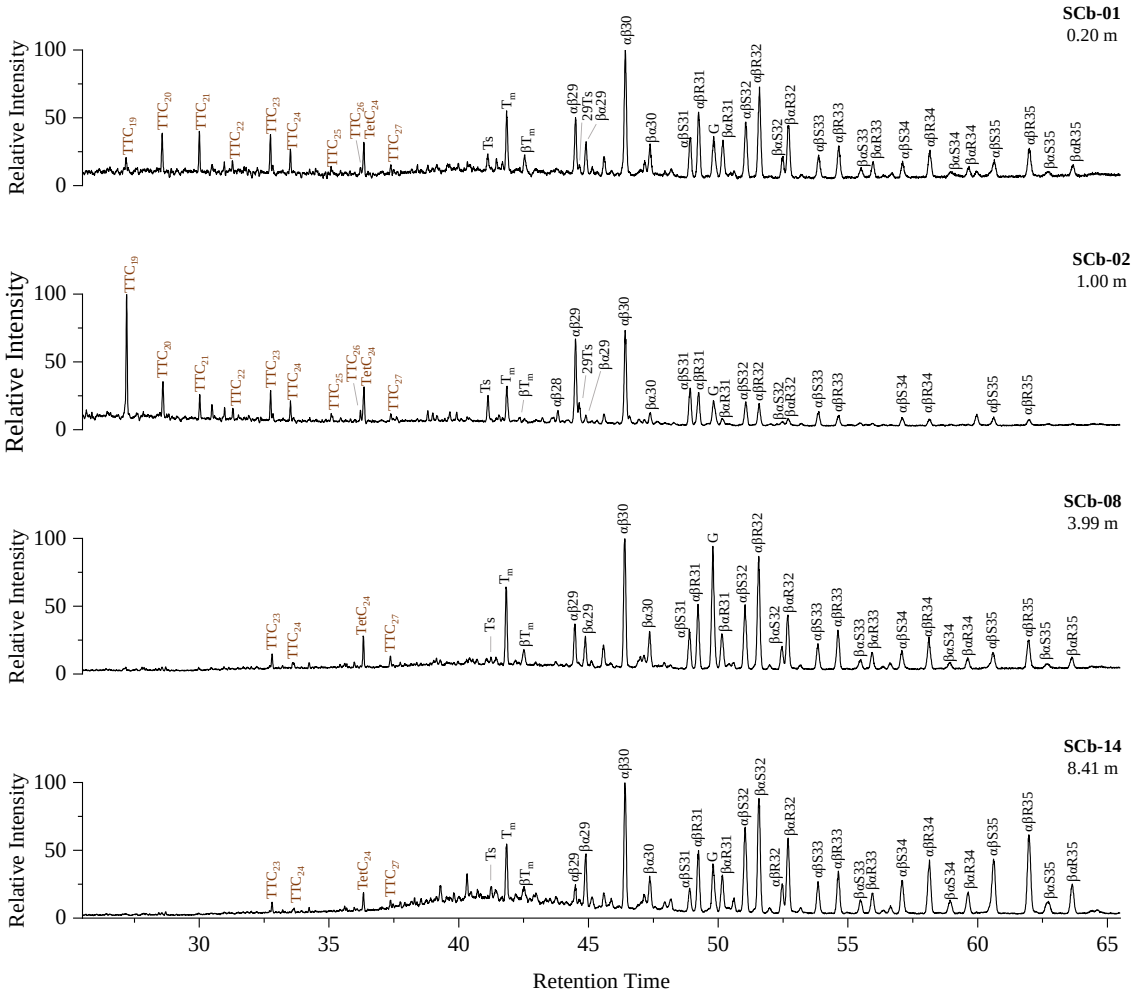

Figure 10. Partial mass chromatograms *m/z* 191 of tricyclics, tetracyclic and pentacyclic terpanes of Irati Formation source rocks.

The parameter for C_{29} steranes was plotted in correlation graphs with the parameters of C_{29} sterane αββ/(αββ + ααα) (Seifert and Moldwan, 1978) and S/(S + R) of C_{31} homohopanes, Figure 12 (Seifert and Moldowan, 1980). The ratio C_{29} αββS/(αββ+ααα) ranged from 0.23 to 0.31 (Supplementary Data - Table 2), indicating immature stage since this ratio didn't reach the maximum value at 75% of conversion (Mackenzie and McKenzie, 1983; Beaumont et al., 1985; Peters and Moldovan, 2005b). The 20S/(20S+20R) ratios for steranes ranged 0.14 to 0.3 for C_{27} and 0.11 to 0.36 for C_{29} also supports this interpretation; since this ratio did not reach the equilibrium window of 0.52–0.55 (Seifert and Moldowan, 1978).

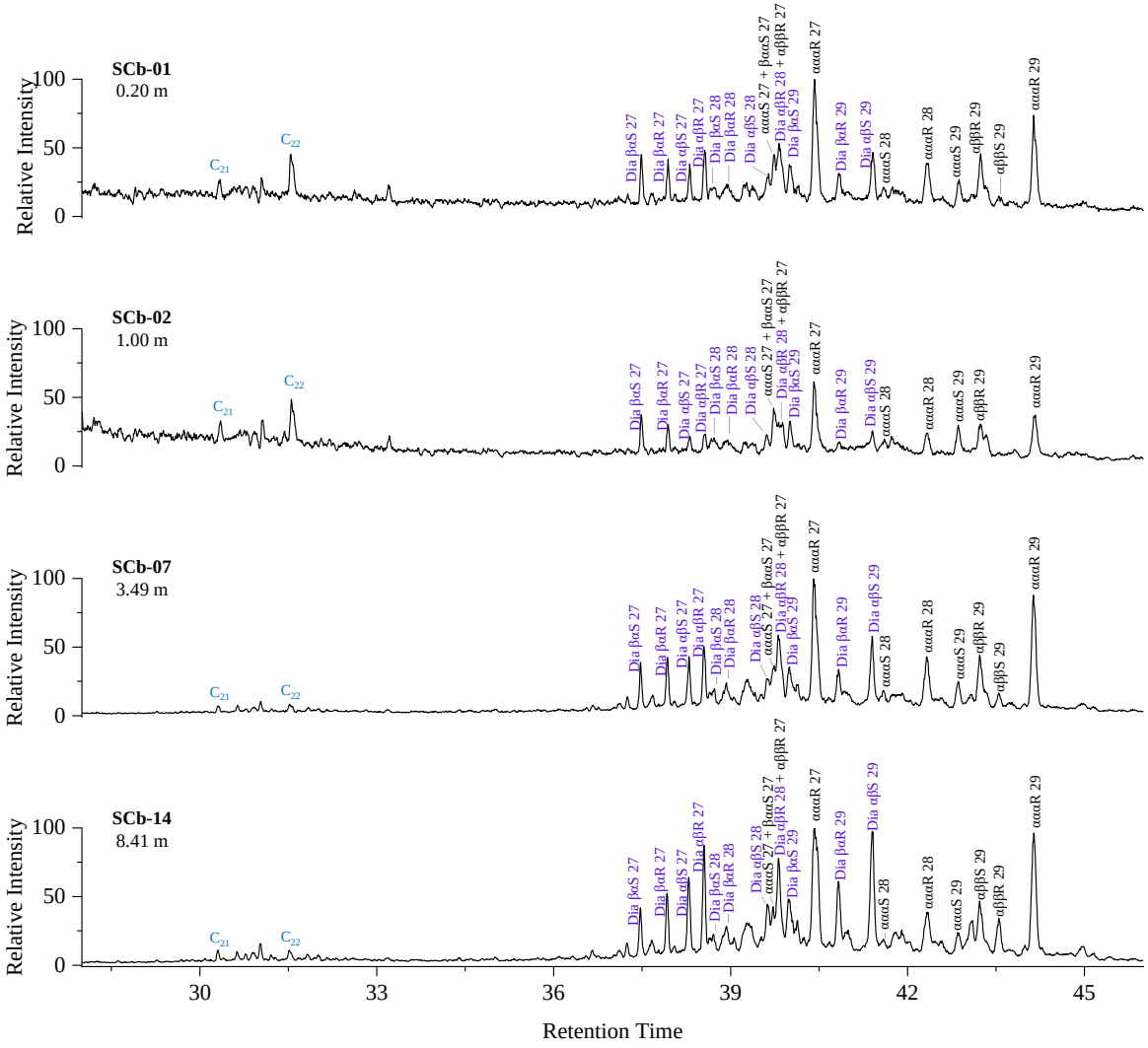

Figure 11. Partial mass chromatograms *m/z* 217 of steranes and diasteranes from C_{27}–C_{29} of Irati Formation source rocks.

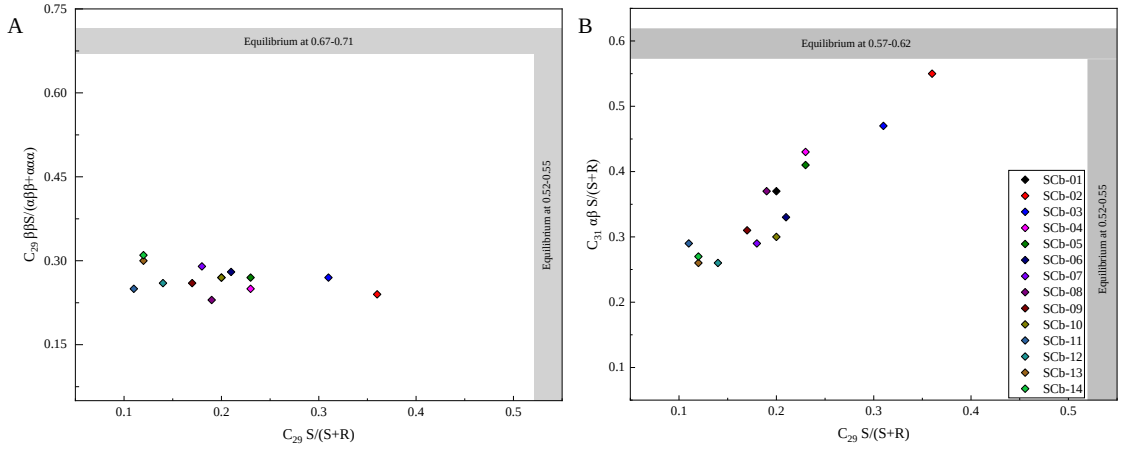

Figure 12. Crossplot of the parameters of C_{29} S/(S+R) steranes versus (A) C_{29} αββ/(αββ + ααα), and (B) C_{31} homohopanes S/(S + R).

In these samples, a diasterene series (Figure 13A) was identified by the *m/z* 257 fragments, hop-17(21)-enes (*m/z* 367) were not identified. The high abundance of diasteranes is usually associated with the low degree of thermal evolution; since they are formed during diagenesis and have also been associated with immature rocks (Brassel et al., 1986). The rearrangement involves the migration of C-10 and C-13 methyl groups to C-5 and C-14 and is favored by acidic conditions, clay catalysis, and/or high temperatures (Peters and Moldovan, 2005b).

The monoaromatic and demethylated triaromatic steranes (MA and TA) distributions (Figure 13A and C) are similar to that reported in the literature by Osorio et al. (2017) for Irati Formation. However, methylated triaromatic steranes (*m/z* 245) appear to be absent or in low intensity in the northern portion Irati Formation. MA (I)/MA (I + II) and TA(I)/TA(I+II) ratios (Supplementary Data - Table 2) presented values of 0.08- 0.20 and 0.09-0.64, respectively, being below the equilibrium value of 1.0. Samples from the contact zone (SCb-01 and SCb-02) showed chromatographic profiles for monoaromatic and demethylated triaromatic steranes extremely altered. For this reason, it was not possible to calculate MA (I)/MA (I + II) and TA(I)/TA(I+II) ratios.

The distribution of the phenanthrene and alkylphenanthrenes (m/z 178+192+206) to the SCb-07 sample is shown in Figure 14. In samples with low thermal evolution, the 1-MP and 9-MP (α -isomers) display a higher abundance, whereas as maturation increases, geological isomers increase (2-MP and 3-MP, β-isomers), due to the greater stability of the β positions to α positions (Peters, 2005b; Peters Heckmann et al., 2011). For the studied samples, the predominance of the more stable isomers (2-MP and 3-MP) in relation the less stable isomers (1-MP and 9-MP), this is reflected too on the geochemical parameters based on methylphenanthrene isomerization, MPI-1, MPI-2, MPI-3 and RMP (Supplementary Data - Table 6), that suggest medium to high maturation, these parameters also exhibited a decreasing order of maturation according to the distance from the diabase threshold.

Some maturity parameters based on steranes and hopanes suggested a tendency of OM, which is rapidly heated (case of igneous intrusion), to show less developed maturity; when compared to OM that reaches the same stage, being exposed to slow heating due to natural burial. Peters and Moldowan (1993) have summarized that almost all of maturity biomarkers parameters will reach when Ro (vitrinite reflectance) increases to 1.4% in the natural burial sequence. However, Zhu et al., (2007) has observed on the organic matter exposed to high heating due to diabase intrusion, 20S/(20S+20R) and αββ/(ααα+αββ) steranes and Ts/(Ts+Tm) ratios had not yet reached their equilibrium values at Ro = 1.5%.

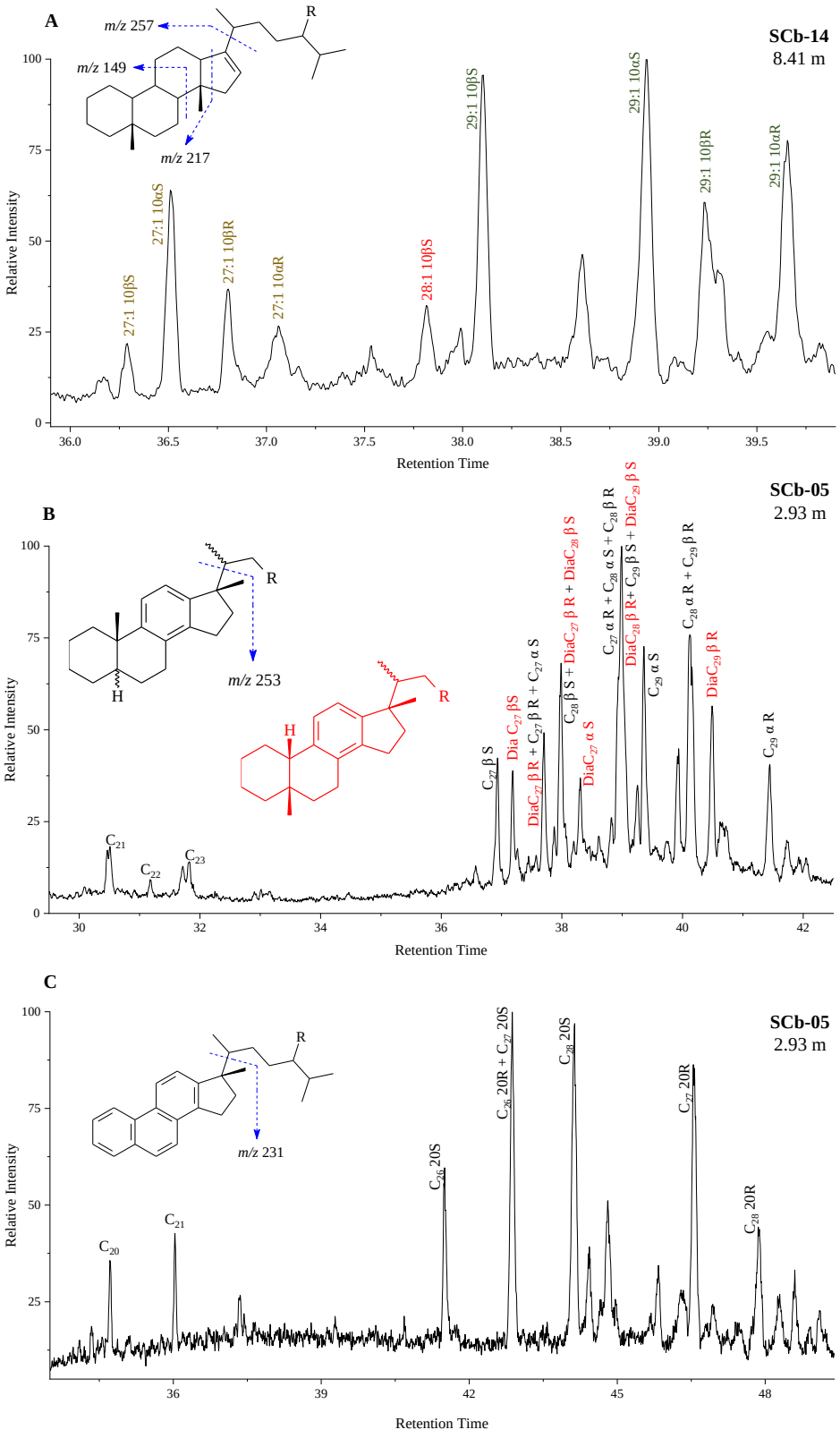

Figure 13. Reconstituted ion chromatogram showing distribution of **(A)** diasterenes (*m/z* 257); **(B)** monoaromatic steranes (*m/z* 253) and; **(C)** demethylated triaromatic steranes (*m/z* 231).

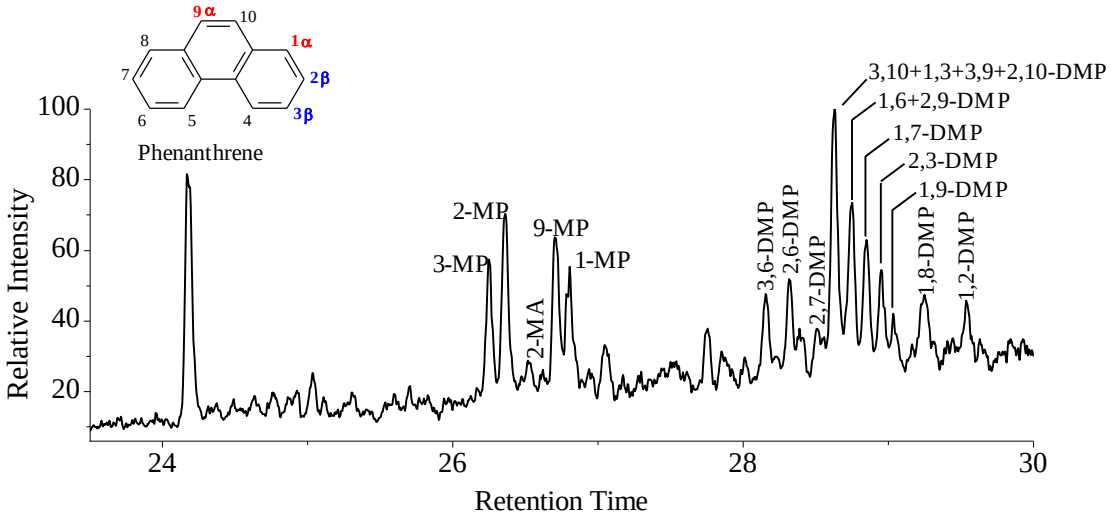

Figure 14. Chromatographic profile showing phenanthrene, methylphenanthrenes, and dimethylphenanthrenes monitored by the *m/z* 178+192+206 ions.

7.4.4. Molecular parameters of organic matter source and depositional environment

The *n*-alkanes series ranged from C_{13}-C_{34}, with a predominance of C_{15}-C_{17}, TAR <1, Figure 15 (Supplementary Data - Table 3), and slightly unimodal distribution for all samples, indicating organic matter of marine origin with land plant input (Bray and Evans, 1961; Scalan and Smith, 1970; Mello et al., 1995).

Two distinct chromatogram types were observed for the stratigraphic profile analyzed (Figure 8), the first one formed by the samples SCb-01 and SCb-02, which are closer to the diabase (0.20 and 1.00 m, respectively), that presents the predominance of isoprenoids and cycloalkanes (*n*-alkylcyclohexanes, methyl-*n*-alkylcyclopentanes, macrocyclic alkanes, and 1-methyl-macrocyclic alkanes), Figure 16. The second interval is formed by the other samples (SCb-03 to SCb-14), which presents a low relative abundance of *n*-alkanes and cycloalkanes and a high relative abundance of isoprenoids.

N-alkylcyclohexanes and related compounds such as alkylphenols have long been recognized as important components of sedimentary hydrocarbon assemblages. Potential precursors are cyclohexyl fatty acids that are known from some thermophilic and non-thermophilic bacteria. However, the limited carbon number distributions of these biological lipids compared to the long-chain lengths of the cyclohexanes in sediments suggest there are fewer exotic sources (Brocks et al., 2014). A wide variety of alkylcyclohexanes has been reported in pyrolysis products of fatty acids, aliphatic polyaldehydes and algaenans (Fowler et al., 1986; Gelin et al., 1994; Rubinstein and Strausz, 1979).

The relative percentage of the three groups of *n*-alkanes, *n*-C_{13-18}; *n*-$C_{19-24,}$ and *n*-C_{25-35}, (Supplementary Data - Table 3) were calculated. These groups correspond to the three main biological sources producing fatty acids. The first group comes from phytoplankton and zooplankton, the second from bacteria, and the third from land plants (Tissot and Welte, 1984; Fabiańska et al., 2013). SCb-01 and SCb-03 to SCb-05 samples have the *n*-alkanes in the range of *n*-C_{25-33} in greater abundance. SCb-02, SCb-07, SCb-09, SCb-10 and SCb-12 showed the highest abundance of *n*-C_{19-24} compounds while SCb-06, SCb-08, SCb-11, SCb-13 and SCb-14 had a higher content of *n*-alkanes in the first group (*n*-C_{13-18}).

The treatment of the samples with urea allowed the identification of isoprenoids $I_{18,}$ I_{21}, I_{25}, I_{30}, I_{39}, and I_{40} (biphytane), Figure 17. The low relative abundance of linear *n*-alkanes and the predominance of isoprenoids and branched alkanes are also characteristic of organic matter from an aquatic origin in environments with high salinity (Alferes et al., 2011). A significant source of biphytane is caldarchaeol, a prominent core lipid in methanogens (Koga et al., 1993) and members of the kingdom Crenarchaeota (Kates, 1993). Crenarchaeotes and some methanogens produce polar lipids with variants of the caldarchaeol core with cyclopentane and, occasionally, cyclohexane rings. Biphytane has long been recognized as a prominent sedimentary hydrocarbon (Moldowan and Seifert, 1979).

Martins *et al*. (2020b) identified β-carotane in Irati Formation samples from the northeastern and central-eastern Paraná Basin (southern Brazil). β-Carotane from halophilic bacteria is abundant in some crude oils from arid, lacustrine source-rock settings (Jiang and Fowler, 1986; Fu et al., 1990), but it is rare and generally low in marine oils (Clark and killops, 1989).

In general, samples from the central-eastern basin were deposited in a deeper marine setting with lower salinity than samples from the northeastern basin, which displays signals of a shallower marine environment with reducing bottom water conditions, the presence of β-carotane was associated with freshwater influxes (Martins et al., 2020b).

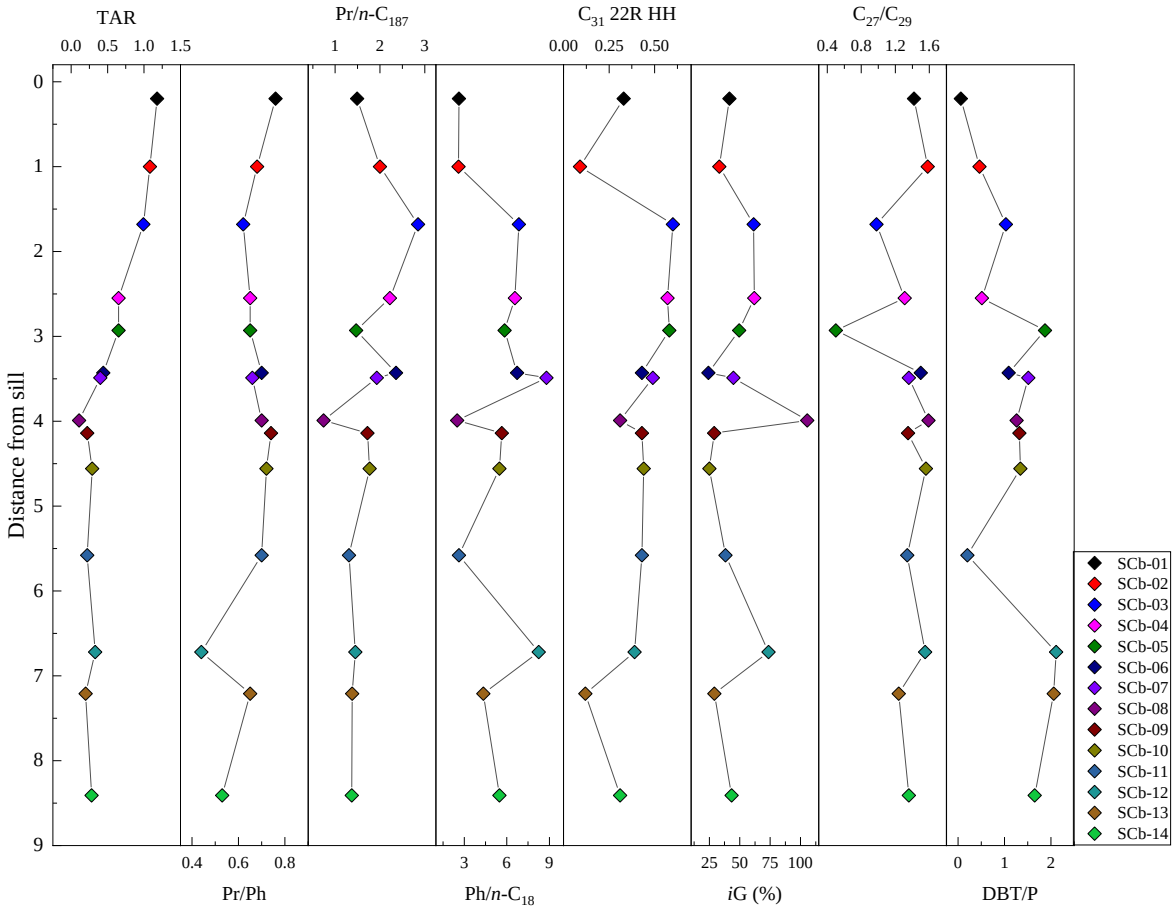

Figure 15. Profiles showing the variation of biomarkers parameter of biological source and depositional environment based on *n*-alkanes, hopanes, steranes, dibenzothiophene (DBT), and phenanthrene.

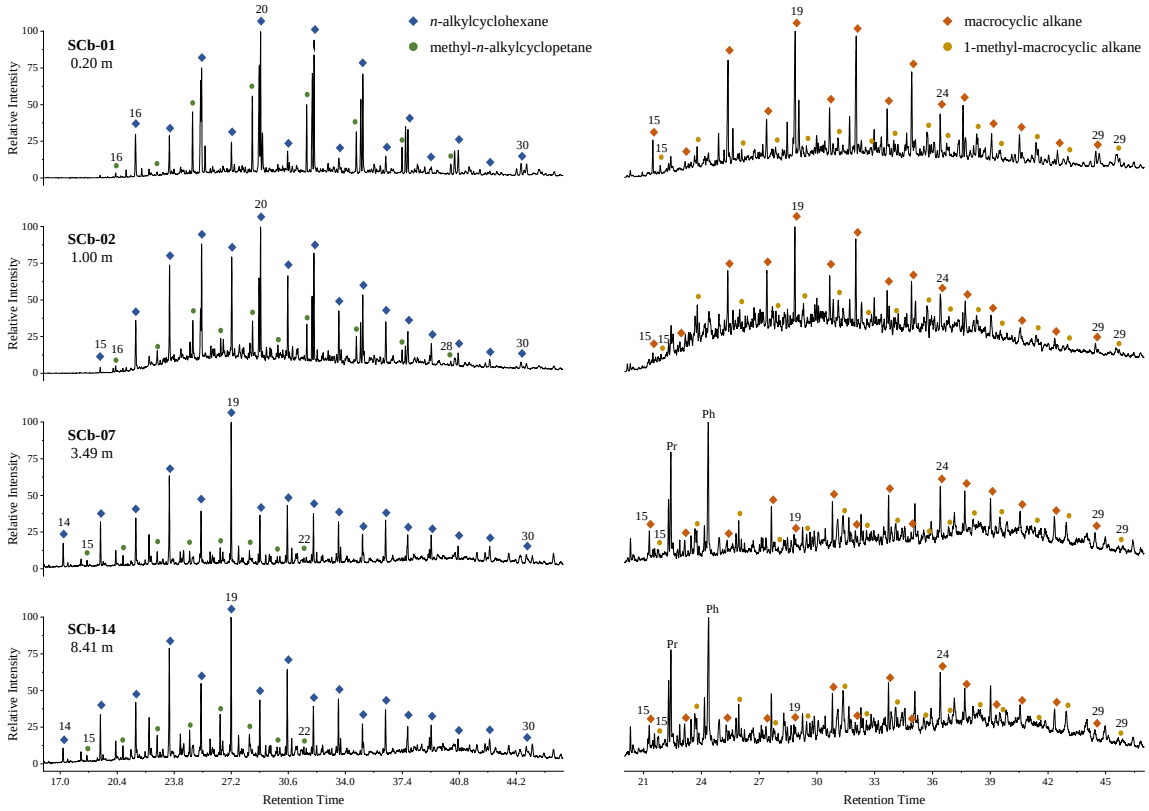

Figure 16. *n*-alkylcyclohexane (*m/z* 83); methyl-*n*-alkylcyclopentane (*m/z* 83); macrocyclic alkane (*m/z* 111) and 1-methyl macrocyclic alkane (*m/z* 111) distributions in the extracts of rocks from Irati Formation.

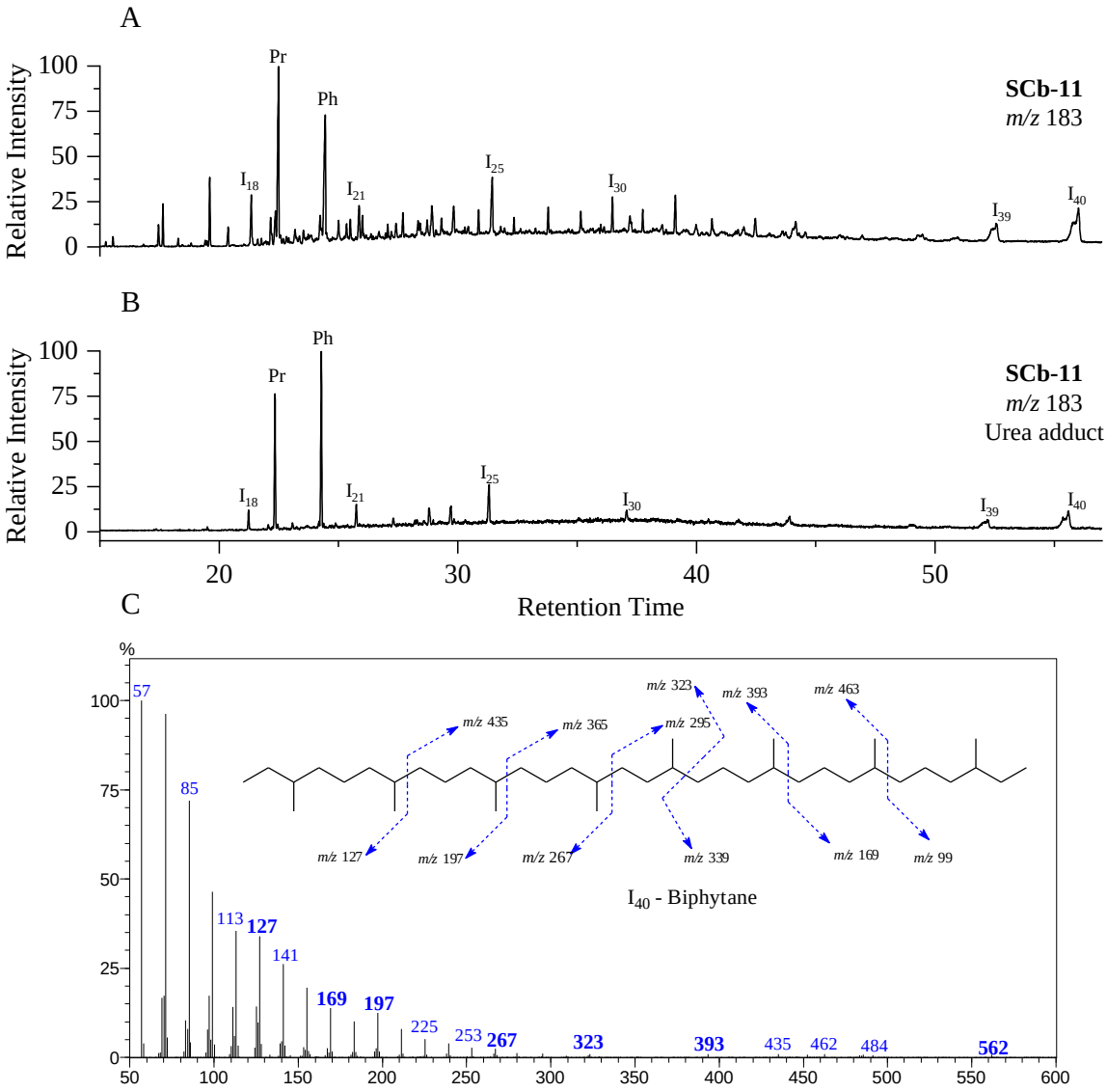

Figure 17. Comparative profiles for the SCb-11 sample (A) before and (B) after treatment with urea; (C) mass spectra of the peak I_{40}.

Pristane (Pr) and phytane (Ph) are the main acyclic isoprenoids detected in the analyzed samples. The Pr/Ph ratio, used as a redox parameter, showed values between 0.44- 0.76 (Figure 15), indicating a reducing depositional environment. These values are generally applied for the evaluation of the oxidation of the depositional environment. Despite its many limitations, since it can be quickly and easily measured, it is considered that the values of these ratios above 1.0 indicate the oxic depositional environment, while values <1.0 indicate anoxic conditions (Didyk et al. 1978; Kelly et al., 2011; Tao et al., 2015).

The relationship between the isoprenoids Pr/*n*-C_{17} and Ph/*n*-C_{18} (Peters et al., 1999) can be used to infer the type of kerogen and redox condition of the depositional environment. According to the correlation graph (Figure 18), the studied samples have marine characteristics

and anoxic depositional environment. Correlation of the DBT/P parameter (dibenzothiophene to phenanthrene ratio) to Pr/Ph ratio (Figure 19A) allows classification of the analyzed rocks into one of the five zones according to the Hughes diagram (Hughes et al., 1995). Most samples are found in zone 1B related to marine carbonate and marls or lacustrine sulfate-rich rocks. This is caused by the low value of Pr/Ph and high DBT/P ratios. The samples that have shown lacustrine sulfate-poor (zone 2) characteristics present very low values for Pr/Ph and DBT/P ratios.

Values greater than 0.25 for parameter $C_{31}22R$ HH/C_{30} Hop may indicate hydrocarbon generation from organic matter deposited marine shale, carbonate, or marl type. Thus, when this parameter is combined with Pr/Ph ratio (Figure 19B), the result corroborates the marine origin for the studied shales.

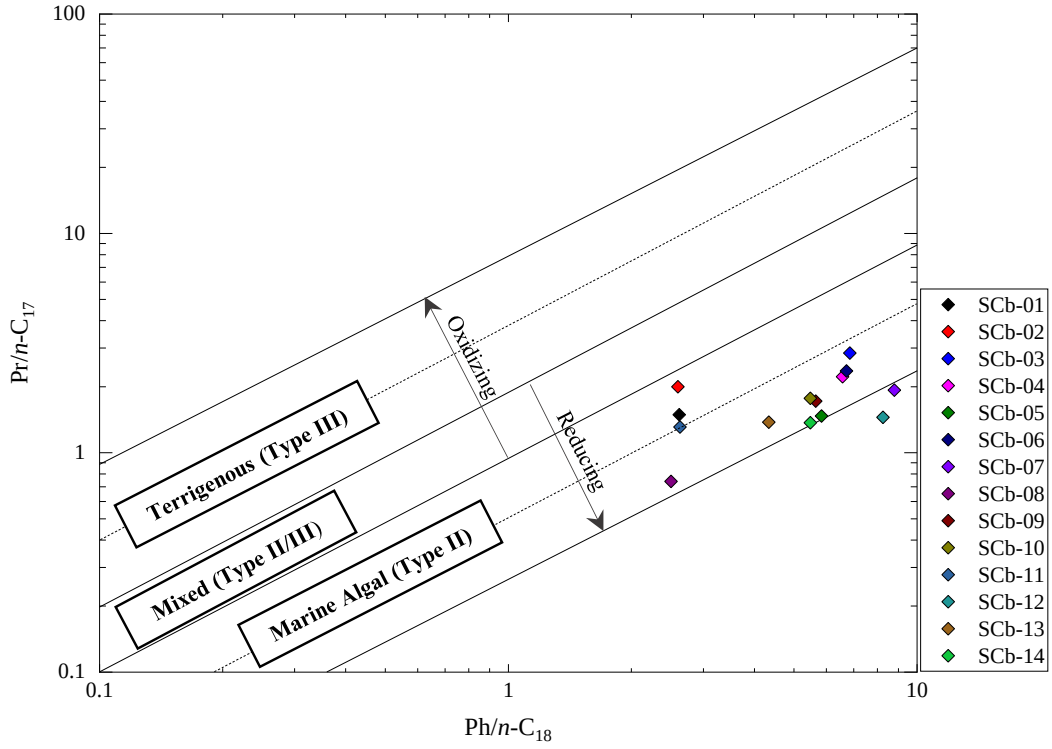

Figure 18. Correlation Pr/ *n*-C_{17} x Ph/*n*-C_{18} showing the source of the organic matter and the depositional environment.

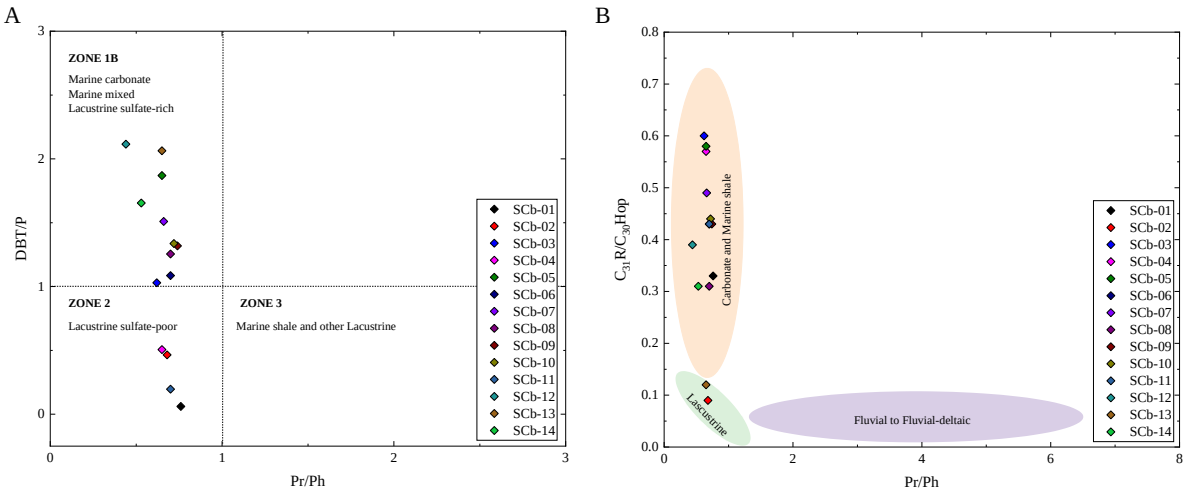

Figure 19. (A) Crossplot of pristane/phytane (Pr/Ph) vs. DBT/P (Hughes et al., 1995); **(B)** $C_{31}R/C_{30}$Hop vs. Pr/Ph suggesting the depositional environment of the source rocks.

Tetracyclic terpanes have already been found in rock samples and oils in several depositional environments; they represent a narrow homologous series in the range C_{24}-C_{27}. Although the origin of the C_{24} tetracyclic terpane is uncertain, it is believed that its origin is due to thermal and microbial degradation of the hopanes (Tao et al., 2015). Only one homolog was observed for the class of tetracyclic terpanes, Tet-C_{24}, since these compounds are more stable than their tricyclic analogs, and their presence may be related to hypersaline evaporitic carbonate depositional environment (Connan et al., 1986).

Gammacerane is a pentacyclic terpane found in large quantities in organic extracts and oils associated with saline environments (Sinninghe-Damsté et al., 1995). However, some evidence indicates that this compound comes from certain protozoa, bacteria, and other organisms (Peters and Moldovan, 2005b). Its origin is still uncertain but can be formed by reducing tetrahymanol (gamacer-3β-ol), a lipid that substitutes steroids in the membrane of certain protozoa. The primary source of tetrahymanol is ciliates protozoa, which occur at the interface between oxic and anoxic zones in stratified water columns (Sinninghe-Damsté et al., 1995). The ratio between gammacerane and C_{30}-17α(H),21β(H)-hopane (*i*G) showed a range from 24.23 to 105.52, indicating a high variation of salinity all over the stratigraphic section reaching the moment of a hypersaline condition during the deposition of the shales.

Sterols, like cholesterol, are essential lipids present in all eukaryotic organisms and are often considered essential components in the cell membrane, where they control permeability and rigidity. Recent sediments contain various functionalized sterols, characterized by the position and number of double bonds, hydroxy groups, alkyl groups, and several other

substituents. Although double bonds and heteroatoms are generally lost during diagenesis, it is still possible in maturing sedimentary rocks to distinguish fossil steroids with different alkyl substituents. The distribution of regular sterols can be used to indicate the contribution of organic matter from algae and higher plants (Brocks and Summons, 2014).

The presence of 5α(H),14α(H),17α(H)-pregnane (21ααα) and 5α(H),14α(H),17α(H)-22-homopregnane (22ααα) was observed. The occurrence of these compounds in sediments and oils has been attributed to the breaking of the lateral chain of larger molecular weight steranes. However, other authors suggest that these compounds have an unknown biological origin and are related to hypersaline environments (Peters and Moldovan, 2005a).

Steranes and diasteranes were present in high concentrations, and their distributions are dominated by C_{27} sterane (cholestane), C_{27}/C_{29} ratio varies 0.50 to 1.59 (Figure 15). The predominance of C_{27} steranes indicates mainly algal/planktonic organic matter, while the predominance of C_{29} steranes is associated with terrestrial plant organic matter. In the analyzed samples, C_{27} and C_{29} steranes relative abundance (%) are predominant over C_{28} sterane when plotted in a ternary diagram reflecting deposition in a coastal marine shelf as present in Figure 20A (Huang and Meinschein, 1979). The cross plot of Pr/*n*-C_{17} and Ph/*n*-C_{18} ratios in Figure 20B also attests to a high continental to transitional setting contribution in bulk organic matter.

The rhythmic intercalation of siliciclastic and carbonate layers of the Irati Formation is interpreted as low energy deposits in a shallow marine environment classified by Araújo (2001) in inner- mid- and outer-ramp. Currently, those deposits are distributed from the southernmost to the middle region of Brazil. The northernmost deposits of the basin record the most proximal facies, dominated by the outer-mid ramp carbonates deposits. Thus, those facies received the higher terrestrial material input.

Grainstones, packstones, and floatstone carbonate texture with ripple lamination, bidirectional and hummocky cross-stratification that occur interbedded with the organic-rich shales beds indicate that the cyclic alternation is marked by periods of high organic matter production and times of high energy and, therefore, oxygenated conditions.

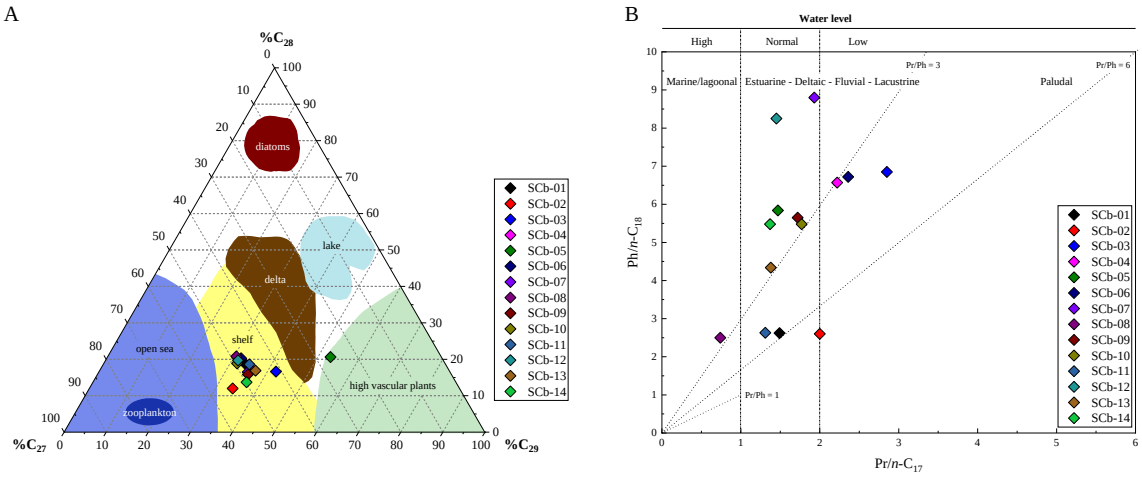

Figure 20. (A) Ternary diagram of steranes indicating primary organic matter/depositional environment (Huang and Meinschein, 1979); **(B)** Diagram of Pr/*n*-C_{17} vs Ph/*n*-C_{18} indicating primary organic matter/depositional environment assessment of the Irati Formation (modified from Scheffler, 2004).

Aromatic steranes are formed during sediment diagenesis due to high temperatures and pressures followed by oxidation and subsequent aromatization of the sterols. Monoaromatic and triaromatic steranes are used as source indicators (eukaryotic species), useful in correlation studies and evaluation of thermal stress, as well as to evaluate maturity in sediments samples (Moldowan and Fago, 1986; Mackenzie et al. (1981; Peters et al., 2005b). The short-chain (C_{22} and C_{23}) and long-chain (C_{27} to C_{29}) monoaromatic steranes were identified through the *m/z* 253 ions. Information on the depositional environment can also be provided by distributing monoaromatic steranes from the ratio between the C_{27}-C_{28}-C_{29} carbons. In the case of the samples under study, the predominance of C_{27} over C_{29} monoaromatic sterane was observed, indicating a little contribution of terrestrial organic matter.

7.4.4.1.PCA and HCA analysis of the biomarkers data of biological source

Hierarchical cluster analysis (HCA) and principal component analysis (PCA) were applied to establish genetic groups for the 14 rock samples studied. Eight source-related biomarker parameters were used for chemometrics: CPI, OEP, TAR, $C_{13\text{-}18}$, $C_{19\text{-}24}$, $C_{15\text{-}33}$, *i*G, and C_{27}/C_{29} sterane ratio. HCA separates the analyzed extract samples into three groups, as shown in Figure 21A. The results of the HCA analysis are further supported by PCA, Figure 21B (see Supplementary Data for factor loadings, Figure 2), which is used to reduce complex geochemical data to a few components, or new variables called eigenvectors that best explain variations in the data (Peters et al., 2016).

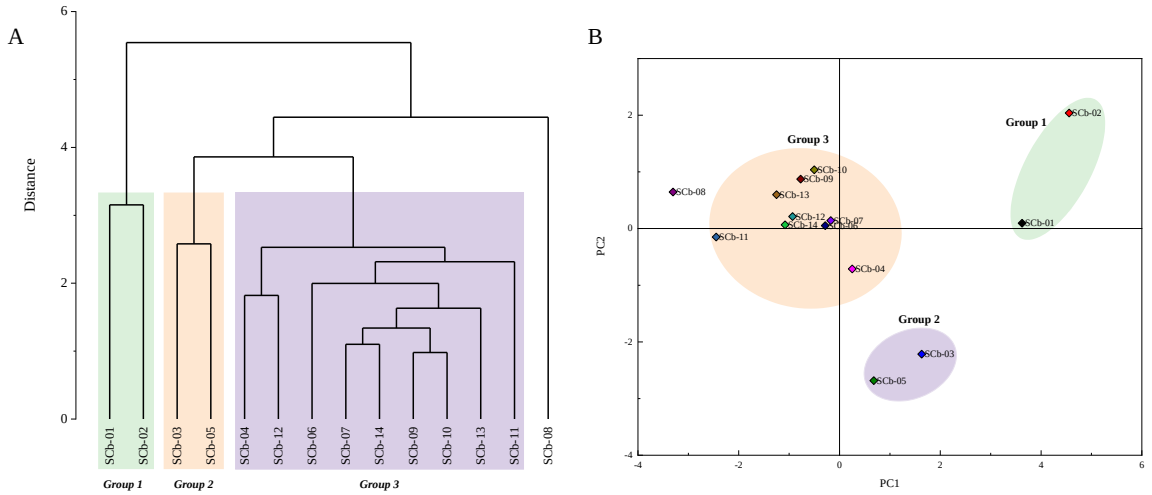

Figure 21. (A) Dendrogram resulting from the hierarchical cluster analysis-HCA. **(B)** Plot of scores from principal component analysis-PCA.

Group-1 consists of samples SCb-01 and SCb-02, which are closer to diabase intrusion and showed OEP and TAR ratios >1, low values *i*G (41.55 and 33.24%), and high relative abundance of two groups of *n*-alkanes, $\%C_{19\text{-}24}$ and $\%C_{25\text{-}33}$, which correspond to two biological sources of fatty acids, bacteria and higher vascular plants (Tissot and Welte, 1984; Fabiańska *et al*., 2013). Group-2 is composed of the SCb-03 and SCb-05 samples, which showed low CPI and OEP ratios (0.65-0.77 and 0.64-0.77), TAR ratio <1, medium values *i*G (49.58-61.95), and high relative abundance of $\%C_{19\text{-}24}$ and $\%C_{25\text{-}33}$ *n*-alkanes (33.6-35.95 and 36.18-45.93) as observed to the Group-1.

The SCb-04 and SCb-06 to SCb-14 samples (except SCb-08) forms Group 3, which exhibited low CPI and OEP ratios (0.45-0.68 and 0.60-0.75) as the previous groups. However, this group showed a higher of $\%C_{13\text{-}18}$ and $\%C_{19\text{-}24}$ *n*-alkanes groups (30.75-45.58 and 30.44-38.76) which correspond to two biological sources of fatty acids, phytoplankton/zooplankton and bacteria, low TAR and *i*G values (0.20-0.44 and 24.23-44.77%), just the SCb-12 showed a high *i*G ratio, 73.75%.

Although the samples used in this study are all from the same unit, the statistical analyses identified three extract groups associated suggesting differences related to the deposition paleoenvironment and biological organic matter source. The Irati Formation is related to a restrict marine condition during the Permian period, represented by bituminous shales and interspersed by limestones deposited (Millani et al., 2007).

Biomarker parameters also indicate significant variations in organic facies in the Irati Formation, reflecting deposition in anoxic conditions. CPI, OEP, and C_{27}/C_{29} sterane ratios showed similar values throughout the stratigraphic profile. However, it is perceptible the change

in the chemical composition of the three main groups of *n*-alkanes as well as the decrease for TAR and *i*G ratios with increasing depth, suggesting a higher contribution of organic matter derived from phytoplankton/zooplankton and bacteria for base samples contrasting with the top of the profile. The SCb-08 sample was characterized as the marine transgression peak in the Paraná Basin with the highest *i*G and $\%C_{13-18}$ *n*-alkane group (105.52 and 53.81%) and lowest TAR ratio, 0.11. The top samples of the stratigraphic profile showed high CPI and OEP ratios, and high relative abundance of C_{19-24} and C_{25-33} *n*-alkanes compared with the base samples.

More significant terrigenous contribution to the top outcrop samples was observed by Nascimento et al. (2021) for the northeastern border and the central east of the Paraná Basin and was associated with a higher freshwater inflow. The Irati Sea was a hypersaline and restricted marine paleoenvironment with episodes of freshwater input, leading to a water column stratification, resulting in a euxinic photic zone and reducing bottom conditions that enhanced preservation of deposited organic matter.

7.5. CONCLUSION

Due to its territorial extension and economic interest, the Irati Formation is one of Brazil's most studied geological formations. However, most of these works are concentrated on analyzing samples from the south and southeast regions of Brazil (or southern and central east areas and the northeastern border of the Paraná Basin). Fourteen organic-rich shales samples of Irati Formation from SUCAL quarry (northern border) were subject to TOC, Rock-Eval, and biomarkers analysis. Despite the excellent extraction yield for most samples, TOC and Rock-Eval data indicated poor to moderate organic matter as source rocks; only sample SCb-07 (IH=392, S2=12.45 mg HC/g rock) showed satisfactory quality for hydrocarbon generation. Bitumen/TOC and the correlation plots S1 versus TOC and PI versus Tmax confirm the presence of migrated hydrocarbons due to the thermal effect resulting from igneous intrusions.

The general distribution of hydrocarbons and/or biomarkers parameters suggested that the samples showed low thermal evolution, anoxic (Pr<Ph) and marine depositional paleoenvironment. The values of Pr/*n*-C_{17}, Ph/*n*-C_{18}, hydrogen index (IH), and oxygen index (IO), suggest type II/III kerogen formed from marine OM with freshwater OM input, corroborated by the presence of macrocyclic alkanes and 1-methyl macrocyclic alkanes usually associated with the lacustrine alga *B. braunii*. Among the steranes, the ααα20R stereochemistry predominates concerning ααα20S. All the extract rock showed a high relative abundance of βTm and the diasterene serie, characteristic of thermally poorly developed samples.

It is well-known in the literature that igneous intrusion can act as heat source and generate an atypical petroleum system, and so affecting the carbon skeleton of the hydrocarbons. As can be observed for the sample SCb-01 and SCb-02, the heat from the intrusion was able to affect even the amount of preserved organic matter and led to a miss interpretation of the source. Van krevelen type diagram shows kerogen type III for the SCb-02 but biomarkers revealed a bacteria origin. Nevertheless, Rock-eval pyrolysis and classical biomarkers has limitation in the record of the overall igneous intruction heat affect. Less than two meters below the igneous intrusion sill the samples have no record of its influence (staying immature). Though, the phenanthrene and alkylphenanthrenes parameters (Supplementary Data - Table 2) showed highly sensitivity to those igneous intrusion heat, been able to record a progressive degree of its influence, becoming an excellent parameter for assessment lateral variaton of maturation.

Based on PCA and HCA analysis of some molecular parameters, changes in OM composition and kerogen type were observed, related to the freshwater inflow episodes that brought a higher amount of terrigenous OM. All the samples analyzed showed more phytane than pristane, a high relative proportion of gammacerane, biphytane and the regular *i*-C_{25} isoprenoid indicating conditions of the high salinity of the depositional environment. The general data on origin (marine), maturation (immature), redox environment (reducing) agree with previous studies regarding classic parameters of saturated biomarkers.

ACKNOWLEDGMENTS

The authors thank FAPEPI, PETROBRAS, and CAPES for financial support, as well as B. Timah for grammatical revision.

REFERENCES

Afonso J.C., Cardoso J.N., Schmal M. 1991. Distribution and origin of organic Sulphur compounds in lrati shale oil. Fuel 71, 409-415.

Afonso J.C., Cardoso J.N., Schmal M. 1994. Hydrocarbon distribution in the Irati shale oil. Fuel 73, 363-366.

Alferes, C.L.F., Rodrigues, R., Pereira, E. 2011. Geoquímica orgânica aplicada à Formação Irati, na área de São Mateus do Sul (PR), Brasil. Geochimica Brasiliensis 27(1), 47-54.

Almeida N.S.; Sawakuchi H.O.; Teixeira C.A.S.; Bertassoli Jr D.J. Furukawa, L.Y. Pelissari M.; Sawakuchi A.O. 2020. Incubation experiments to constrain the production of methane and carbon dioxide in organic-rich shales of the Permian Irati Formation, Paraná Basin. Marine and Petroleum Geology 112, 104039.

Anjos C.W.D., Guimarães E.M. 2008. Metamorfismo de contato nas rochas da Formação Irati (Permiano), norte do Paraná. Revista Brasileira de Geociências 38(4), 629-641.

Araújo L.M., Rodrigues R., Scherer C.M.S. 2001. Sequências deposicionais Irati: arcabouço quimioestratigráfico e inferências paleoambientais. Ciência, Técnica, Petróleo 20, 193-202.

Araújo L.M. Análise da expressão estratigráfica dos parâmetros de geoquímica orgânica nas sequências deposicionais Irati. 342 f. Tese de Doutorado. Universidade Federal do Rio Grande do Sul, Porto Alegre. 2001.

Barberena D., Timm L.L. 2001. Características estruturais dos Mesossauros e suas adaptações ao meio aquático. In: Holz, M.; & De Ros, L. F. Paleontologia do Rio Grande do Sul, Porto Alegre, CIGO/UFRGS. p.194-209.

Barbosa O., Gomes F.A. 1958. Pesquisa de petróleo na bacia do rio Corumbataí, Estado de São Paulo. Divisão de Geologia Mineral – DNPM, Boletim 171, 40.

Beaumont C., Boutlier R., Mackenzie A. S., Rullkotter J. 1985. Isomerization and aromatization of hydrocarbons and the paleothermometry and burial history of Alberta Foreland Basin. American Association of Petroleum Geologists Bulletin 69, 546–66.

Brassel S.C., Eglinton, G., Mo, F.J. 1986. Biological marker compounds as indicator of the depositional history of the Maoming oil shale. Organic Geochemistry 10, 927-941.

Bray E. E., Evans E. D. Distribution of *n*-paraffins as a clue to recognition of source beds. Geochimica et Cosmochimica Acta, 22, 2–15, 1961.

Brocks J.J.E, Summons R.E. 2014. 10.3 - Sedimentary Hydrocarbons, Biomarkers for Early Life A2 - Holland, Heinrich D. Treatise on Geochemistry (Second Edition). K. K. Turekian. Oxford, Elsevier: 61-103.

Cioccari G.M. 2018. Interpretação de Modelagem Térmica na Geração Atípica de Hidrocarbonetos – Um Exemplo na Formação Irati, Bacia do Paraná. Tese de Doutorado. 205 f. Universidade Federal do Rio Grande do Sul, Porto Alegre.

Clark J. P., Philp R. P. 1989. Geochemical characterization of evaporite and carbonate depositional environments and correlation of associated crude oils in the Black Creek Basin, Alberta. Canadian Petroleum Geologists Bulletin 37, 401–16.

Connan J., Bouroullec J., Dessort D., Albrecht P. 1986. The microbial input in carbonate-anhydrite facies of a sabkha palaeoenvironment from Guatemala: a molecular approach. Organic Geochemistry 10, 29–50.

Correa da Silva Z.C., Cornford C. 1985. The kerogen type, depositional environment and maturity, of the Irati Shale, Upper Permian of Paraná Basin, Southern Brazil. Organic Geochemistry 8, 399-411.

De Grande S. M. B., Aquino Neto F. R., Mello M. R. 1993. Extended tricyclic terpanes in sediments and petroleum. Organic Geochemistry 20, 1039–47

Didyk B.M., Simoneit B.R.T. Brassell S.C., Eglinton G. 1978. Organic geochemical indicators of palaeoenvironmental conditions of sedimentation. Nature 272, 216–22.

Edwards D.S., Struckmeyer H.M., Bradshaw M.T., Skinner J.E. 1999. Geochemical characteristics of Australia's Southern margin petroleum systems, APPEA J. 39, 297–321.

Ensminger A., Albrecht P., Ourisson G., Tisso B. 1977. Evolution of polycyclic alkanes under the effect of burial (Early Toarcian shales, Paris Basin). In: Advances in Organic Geochemistry 1975 (R. Campos and J. Goni, eds.), ENADIMSA, Madrid, pp. 45–52.

Espitalié J., La Porte J.L., Madec M., Marquis F., Le Plat P., Paulet J., Bautefeu A. 1977. Methodé rapide de caractérisation des roches mètres, de leur potentiel pétrolier et de leur degré d'évolution. Revue de l'Institut Français du Pétrole 32, 23–43.

Fabiańska M.J.; Ćmiel S.R.; Misz-Kennan M. 2013. Biomarkers and aromatic hydrocarbons in bituminous coals of Upper Silesian Coal Basin: Example from 405 coal seam of the Zaleskie Beds (Poland). International Journal of Coal Geology 107, 96-111.

Fowler M.G, Abolins P, Douglas A.G. 1986. Monocyclic alkanes in Ordovician organic matter. Organic Geochemistry 10, 815–823.

Franco N., Kalkreuth W., Peralba M.C.R. 2010. Geochemical characterization of solid residues, bitumen and expelled oil based on steam pyrolysis experiments from Irati oil shale, Brazil: A preliminary study. Fuel 89, 1863-1871.

Jiamo F., Guoying S., Jiayou X, Eglinton G., Gowar A.P., Rongfen J., Shanfa F., Pingan P. 1990 Application of biological markers in the assessment of paleoenvironments of Chinese non-marine sediments. Organic Geochemistry 16, 769–79.

Gelin F., De Leeuw J.W., Sinninghe Damste´ J.S., Derenne S., Metzger P. 1994. The similarity of chemical structures of soluble aliphatic polyaldehyde and insoluble algaenan in the green microalga *Botryococcus braunii* race A as revealed by analytical pyrolysis. Organic Geochemistry 21, 423–435

Goldberg K., Humayun M. 2016. Geochemical paleoredox indicators in organic-rich shales of the Irati Formation, Permian of the Paraná Basin, southern Brazil. Brazilian Journal of Geology 46(3), 377-393. DOI: 10.1590/ 2317- 4889201620160001.

Guerra-Sommer M., Cazzulo-Klepzig M. 2001. As floras gondwânicas do Paleozóico Superior do Rio Grande do Sul. Paleontologia do Rio Grande do Sul, Editora da UFRGS, 67-84.

Heckmann J.R., Landau L., Gonçalves F.T.T., Pereira R., Azevedo D.A. 2011. Avaliação geoquímica de óleos brasileiros com ênfase nos hidrocarbonetos aromáticos. Química Nova 34(8), 1328-1333.

Holanda W., dos Santos, A.C., Bertolino L.C., Bergamaschi S., Rodrigues R., da Costa D.F., Jones, C.M. 2019. Paleoenvironmental, paleoclimatic and stratigraphic implications of the mineralogical content of the Irati Formation, Paraná Basin, Brazil. Journal of South American Earth Sciences 94, 102243.

Holanda W., Bergamaschi S., Santos A.C., Rodrigues R., Bertolino L. C. 2018. Characterization of the Assistência Member, Irati Formation, Paraná Basin, Brazil: Organic Matter and Mineralogy. Journal of Sedimentary Environments 3 (1), 36-45.

Holz M., França A.B., Souza P.A., Iannuzzi R., Rohn R. 2010. A stratigraphic chart of the Late Carboniferous/Permian succession of the eastern border of the Paraná Basin, Brazil, South America. Journal of South American Earth Sciences 29, 381-399.

Hong, Z.-H., Li, H.-X., Rullkötter, J., Mackenzie, A.S. 1986. Geochemical application of sterane and triterpane biological marker compounds in the Linyi Basin. Organic Geochemistry 10, 433-439.

Huang, W.-Y., Meinschein, W.G., 1979. Sterols as ecological indicators. Geochimica et Cosmochim Acta 43, 739–745

Hughes W.B., Holba A.G., Dzou L.I.P. 1995. The ratios of dibenzothiophene to phenanthrene and pristane to phytane as indicators of depositional environment and lithology of petroleum source rocks. Geochimica et Cosmochimica Acta 59(17), 3581-3598.

Jackson K.S., Hawkins P.J., Bennett A.J.R. 1985. Regional facies and geochemical evaluation of southern Denison Trough. APEA J. 20, 143-158.

Jiang Z., Fowler M.G. 1986. Carotenoid-derived alkanes in oils from northwestern China. Organic Geochemistry 10, 831–9.

Kates M. 1993. Membrane lipids of Archaea. In: Kates M, Kushner DJ, and Matheson AT (eds.) The Biochemistry of Archaea (Archaebacteria), pp. 261–295. Amsterdam: Elsevier.

Kelly A.E., Love G.D., Zumberge J.E., Summons R.E. 2011. Hydrocarbon biomarkers of Neoproterozoic to Lower Cambrian oils from eastern Siberia. Organic Geochemistry 42, 640-654.

Koga Y., Nishihara M., Morii H., Akagawa-Matsushita M. 1993. Ether polar lipids of methanogenic bacteria: Structures, comparative aspects, and biosynthesis. Microbiological Reviews 57, 164–182

Lavina E.L., Lopes R.C. 1986. A transgressão marinha do Permiano Inferior e a evolução paleogeográfica do Supergrupo Tubarão no Estado do Rio Grande do Sul. Paula Coutiana, Porto Alegre, n. 1, 51-103.

Lin X.H., Zhan Z.W., Zou Y.R.; Sun J. N., Ping'an Peng P. 2020. Geochemically Distinct Oil Families in the Gudong Oilfield, Zhanhua Depression, Bohai Bay Basin, China. ACS Omega 5, 26738−26747.

Mackenzie A.S., Maxwell J.R. 1981. Assessment of thermal maturation in sedimentary rocks by molecular measurements. In: Organic Maturation Studies and Fossil Fuel Exploration (J. Brooks, ed.), Academic Press, London, pp. 239–54.

Mackenzie A.S., McKenzie D. 1983. Isomerization and aromatization of hydrocarbons in sedimentar basins formed by extension. Geology Magazine, 120, 417–70.

Magoon L.B., Dow W.G. 1994. The Petroleum System. In: The Petroleum System-From Source to Trap. Tulsa: The American Association of Petroleum Geologists, AAPG Memoir.

Maraschin A.J., Ramos A.S. 2015. Breve Abordagem Histórica sobre o Potencial Energético dos Folhelhos da Formação Irati (Bacia do Paraná) no Estado do Rio Grande do Sul. Boletim Geográfico do Rio Grande do Sul 25, 174-183.

Marotta E., Aquino Neto F.R., Azevedo D.A. 2014. Separação e Determinação Quantitativa dos Alcanos Lineares e dos Cíclicos/Ramificados em Petróleos Brasileiros por Aduto de Ureia e Cromatografia Gasosa: Um Estudo de Caso Revisitado. Quim. Nova 37(10), 1692-1698.

Martins C.M.S., Cerqueira J.R., Ribeiro H.J.P.S., Garcia K.S., da Silva N.N., Queiroz A.F.S. 2020a. Evaluation of thermal effects of intrusive rocks on the kerogen present in the black shales of Irati Formation (Permian), Paraná Basin, Brazil. Journal of South American Earth Sciences 100, 102559.

Martins L.L., Schulz H.M., Ribeiro H.J.P.S., do Nascimento, C.A., Souza E.S., da Cruz, G. F. 2020b. Cadalenes and norcadalenes in organic-rich shales of the Permian Irati Formation (Paraná Basin, Brazil): Tracers for terrestrial input or also indicators of temperature-controlled organic-inorganic interactions? Journal of South American Earth Sciences 100, 102559.

Marzi R., Torkelson B.E., Olson, R.K., 1993. A revised carbon preference index. Org. Geochem. 20, 1303–1306. https://doi.org/10.1016/0146-6380(93)90016-5.

Mashhadi Z. S., Rabbani A.R. 2015. Organic geochemistry of crude oils and Cretaceous source rocks in the Iranian sector of the Persian Gulf: An oil−oil and oil−source rock correlation study. Int. J. Coal Geol. 146, 118−144.

Matos S.A., Warren L.V., Varejão F.G., Assine M.L., Simões M.G. 2017. Permian endemic bivalves of the "Irati anoxic event", Paraná Basin, Brazil: Taphonomical, paleogeographical and evolutionary implications. Palaeogeography, Palaeoclimatology, Palaeoecology 469, 18-33.

Mello M.R., Telnaes N., Maxwell J.R. 1995 The hydrocarbon source potential in the Brazilian marginal basins: a geochemical and paleoenvironmental assessment. In: Paleogeography, Paleoclimate, and Source Rocks (A.-Y. Huc, ed.), American Association of Petroleum Geologists, Tulsa, OK, pp. 233–72.

Milani E.J., França A.B., Medeiros R.A. 2007. Rochas geradoras e rochas-reservatório da Bacia do Paraná, faixa oriental de afloramentos, Estado do Paraná. Boletim de Geociências da PETROBRÁS 15, 135-162.

Milani E.J. 1997. Evolução tectono-estratigráfica da Bacia do Paraná e seu relacionamento com a geodinâmica fanerozóica do Gondwana sul-ocidental. Doctorate Thesis, 2v. Universidade Federal do Rio Grande do Sul (UFRGS), Porto Alegre 255.

Milani E.J., França A.B., Medeiros R.A. 2006. Rochas geradoras e rochas-reservatório da Bacia do Paraná, faixa oriental de afloramentos, Estado do Paraná. Boletim de Geociências da Petrobras 15(1), 135-162.

Moldowan J.M., Seifert W.K. 1979 Head-to-head linked isoprenoid hydrocarbons in petroleum. Science 204, 169–171

Moldowan J.M., Fago F.J. 1986. Structure and significance of a novel rearranged monoaromatic steroid hydrocarbon in petroleum. Geochimica et Cosmochimica Acta, 50, 343–51.

Moldowan J.M., Peters K.E., Carlson R.M.K., Schoell M., Abu-Ali M.A. 1994. Diverse applications of petroleum biomarker maturity parameters. Arabian Journal for Science and Engineering 19, 273–98.

Moldowan J.M., Sundararaman P., Schoell M. 1986. Sensitivity of biomarker properties to depositional environment and/or source input in the Lower Toarcian of S. W. Germany. Organic Geochemistry 10, 915–26.

Moura A.K.S., Santos A.L.S., Citó A.M.G.L. 2015. Otimização de Metodologia para Fracionamento Cromatográfico da Matéria Orgânica de Óleo Cru e Extratos de Rochas. XIII Congresso de Geoquímica dos países de Língua Portuguesa, p. 1.

Nady M.M.E., Ramadan F.S., Hammad M.M., Lotfy N.M. 2015. Evaluation of organic matters, hydrocarbon potential and thermal maturity of source rocks based on geochemical and statistical methods: Case study of source rocks in Ras Gharib oilfield, central Gulf of Suez, Egypt. Egyptian Journal of Petroleum 24, 203–211.

Nascimento C.A., Souza E.S., Martins L.L., Ribeiro H.J.P.S., Santos V.H., Rodrigues R. 2021. Changes in depositional paleoenvironment of black shales in the Permian Irati Formation (Parana´ Basin, Brazil): Geochemical evidence and aromatic biomarkers. Marine and Petroleum Geology 126, 104917.

Ng C., Vega C.S., Maranhão M.D.S.A.S. 2019. Mixed carbonate-siliciclastic microfacies from Permian deposits of Western Gondwana: Evidence of gradual marine to continental transition or episodes of marine transgression? Sedimentary Geology 390, 62-82.

Osorio L.L., Reis D.E.S., Rodrigues R. 2018. Aromatic steroids biomarkers applied to high resolution stratigraphy: Irati Formation, southern of Paraná Basin, Brazil. Journal of Sedimentary Environments 2 (4): 174-182.

Peters K., Cassa M.R. 1993. Applied source rock geochemistry. In: The Petroleum System - From Source to Trap (L. B. Magoon and W. G. Dow, eds.), American Association of Petroleum Geologists, Tulsa, OK, 93-117.

Peters K.E., Fraser T.H., Amris W., Rustanto B. Hermanto E. 1999. Geochemistry of crude oils from eastern Indonesia. American Association of Petroleum Geologists Bulletin 83, 1927–42.

Peters K.E., Walters C.C., Moldowan J.M. 2005a. The Biomarker Guide. Biomarkers and Isotopes in the Environment and Human History. v.1, Ed. 2nd, Cambridge University Press.

Peters K.E., Walters C.C., Moldovan J.M. 2005b. The Biomarker Guide. Biomarkers and Isotopes in the Environment and Human History. v. 2. Ed 2nd. Cambridge University.

Peters K.E., Wright T.L., Ramos L.S., Zumberge J.E. 2016. Chemometric recognition of genetically distinct oil families in the Los Angeles basin, California. Am. Assoc. Petrol. Geol. Bull. 100, 115–135.

Rabbani A.R., Kamali M.R. 2005. Source rock evaluation and petroleum geochemistry, offshore SW Iran. Journal of Petroleum Geology 28(4), 413-428.

Raymond A. C. Murchison D.G. 1992. Effect of igneous activity on molecular-maturation indices in different types of organic matter. Org.Geochem. 18(5), 725-735.

Reis D.E.S., Rodrigues R., Moldowan J.M., Jones C.M., Brito M., Cavalcante D.C., Portela H.A. 2018. Biomarkers stratigraphy of Irati Formation (Lower Permian) in the southern portion of Paraná Basin (Brazil). Marine and Petroleum Geology 95, 110-138.

Ribas L., Neto J.M.R., França A.B., Porto Alegre H.K. 2017. The behavior of Irati oil shale before and after the pyrolysis process. Journal of Petroleum Science and Engineering 152, 156-164. DOI: http://dx.doi.org/10.1016/j.petrol.2017.03.007.

Rocha H.V., Mendes M., Pereira Z., Rodrigues C., Fernandes P., Lopes G., Sant'Anna L.G., Tassinari C.C.G., Lemos de Sousa M. J. 2020. New palynostratigraphic data of the Irati (Assistência Member) and the Corumbataí formations, Paraná Basin, Brazil, and correlation with other south American basins. Journal of South American Earth Sciences Volume 102, 102631.

Rubinstein I., Strausz O.P. 1979. Geochemistry of the thiourea adduct fraction from an Alberta petroleum. Geochimica et Cosmochimica Acta 43, 1387–1392.

Santos R.V., Souza P.A., Alvarenga C.J.S., Dantas E.L., Pimentel M.M., Oliveira C.G., Araújo L.M. 2006. Shrimp U–Pb zircon dating and palynology of bentonitic layers from the Permian Irati Formation, Paraná Basin, Brazil. Gondwana Research 9(4), 456-463.

Scalan R.S., Smith J.E. 1970. An improved measure of the odd-to-even predominance in the normal alkanes of sediment extracts and petroleum. Geochimica et Cosmochimica Acta 34, 611–20,

Scheffler K. 2004. Reconstruction of sedimentary environment and climate condition by multigeochemical investigations of Late Palaeozoic glacial to postglacial sedimentary sequences from SW-Gondwana. Dissertation zur Erlangung des Doktorgrades der Mathematisch-Naturwussenschaftlichen Fakultat der Rheinischen Fredrich-Wilhelms-Universitat, Bonn.

Seifert W.K., Moldowan J.M. 1978. Applications of steranes, terpanes and monoaromatics to the maturation, migration and source of crude oils. Geochimica et Cosmochimica Acta 42, 77–95.

Seifert W.K., Moldowan J.M. 1980. The effect of thermal stress on source-rock quality as measured by hopane stereochemistry. Physics and Chemistry of the Earth 12, 229–37.

Sinninghe Damsté, J.S., Kenig F., Koopmans M.P. 1995. Evidence for gammacerane as an indicator of water column stratification. Geochimica et Cosmochimica Acta 59(9), 1895-1900.

Souza I.V.F., Mendonça Filho J.G., Menezes T.R. 2008. Avaliação do efeito térmico das intrusivas ígneas em um horizonte potencialmente gerador da Bacia do Paraná: Formação Irati. Revista Brasileira de Geociências 32(2), 138-148.

Tao S., Wang C., Du J., Liu L., Chen Z. 2015. Geochemical applications of tricyclic and tetracyclic terpanes biomarkers in crude oils of NW China. Marine and Petroleum Geology 67, 460-467.

Teixeira C.A.S., Bello R.M.S., Almeida N.S., Pestilho A., Brochsztain S., de Queiroz T.B., Andrade L.S., Gregório Júnior D.F., Sawakuchi A.O. 2020. Hydrocarbon generation in the Permian Irati organic-rich shales under the influence of the early cretaceous Paraná Large Igneous Province. Marine and Petroleum Geology117, 104410.

Tissot B.P., Welte D.H. 1984. Petroleum formation and occurrence, 2° ed. Berlim, Springer-Verlag.

Wang Y.-P., Zhang F., Zou Y.-R., Zhan Z.-W., Peng Pa. 2016. Chemometrics reveals oil sources in the Fangzheng Fault Depression, NE China. Org. Geochem. 102, 1-13.

Xavier P.L. 2014. Grandes tempestades na Formação Irati (Permiano inferior) do Rio Grande do Sul: interpretações tafonômicas e Faciológicas. Universidade Federal do Rio Grande do Sul, Porto Alegre.

Xavier P.L.A., Silva A.F., Soares M.B., Horn B.L.D., Schultz C.L. 2018. Sequence stratigraphy control on fossil occurrence and concentration in the epeiric mixed carbonate-siliciclastic ramp of the Early Permian Irati. Journal of South American Earth Sciences 88, 157-178.

Zhu D., Jin Z., Hu W., Song Y., Gao X. 2007. Effect of igneous activity on hydrocarbon source rocks in Jiyang sub-basin, eastern China. Journal of Petroleum Science and Engineering 59, 309–320.

Zumberge J.E. 1983. Tricyclic diterpane distributions in the correlation of Paleozoic crude oils from the Williston Basin. In: *Advances in Organic Geochemistry* 1981 (M. Bjorøy, C. Albrecht, C. Cornford, et al. eds.), John Wiley & Sons, New York, pp. 738–45.

CAPÍTULO VIII

8. DISTRIBUIÇÃO ESPACIAL DOS INTERVALOS *OIL SHALE* PERMIANOS DA BACIA DO PARANÁ

SPATIAL DISTRIBUTION OF THE PERMIAN OIL SHALE INTERVALS OF THE PARANÁ BASIN.

Ailton da Silva Brito

Programa de Pós-Graduação em Geologia e Geoquímica, Universidade Federal do Pará (PPGG-UFPA), Belém-Pá

http://lattes.cnpq.br/9873489431846769

Lorena Tuane Gomes de Almeida

Programa de Pós-Graduação em Química-PPGQ, Centro de Ciências da Natureza–CCN, Universidade Federal do Piauí-UFPI

Teresina – Piauí

http://lattes.cnpq.br/7505926250231164

Sidney Gonçalo de Lima

Programa de Pós-Graduação em Química-PPGQ, Laboratório de Geoquímica Orgânica-LAGO, Centro de Ciências da Natureza–CCN, Universidade Federal do Piauí-UFPI.

Teresina – Piauí

http://lattes.cnpq.br/1655930426274093

Data de submissão: 14/10/2021

Capítulo do livro Fósseis moleculares e aplicações em geoquímica orgânica (2021)

CAPÍTULO 9

DISTRIBUIÇÃO ESPACIAL DOS INTERVALOS *OIL SHALE* PERMIANOS DA BACIA DO PARANÁ

Data de aceite: 01/01/2022
Data de submissão: 14/10/2021

Ailton da Silva Brito
Programa de Pós-Graduação em Geologia e Geoquímica, Universidade Federal do Pará (PPGG-UFPA), Belém-Pá
http://lattes.cnpq.br/9873489431846769

Lorena Tuane Gomes de Almeida
Programa de Pós-Graduação em Química-PPGQ, Centro de Ciências da Natureza–CCN, Universidade Federal do Piauí-UFPI
Teresina – Piauí
http://lattes.cnpq.br/7505926250231164

Sidney Gonçalo de Lima
Programa de Pós-Graduação em Química-PPGQ, Laboratório de Geoquímica Orgânica-LAGO, Centro de Ciências da Natureza–CCN, Universidade Federal do Piauí-UFPI.
Teresina – Piauí
http://lattes.cnpq.br/1655930426274093

RESUMO: A Bacia do Paraná registra no Permiano Inferior dois relativamente pouco espessos intervalos contudo, amplamente distribuídos de *oil shale*. Ambos se estendem do Rio Grande do Sul ao Paraná, tornando-se delgados e ritmicamente intercalado a camadas carbonáticas em direção a São Paulo, Goiás e Mato Grosso. Litoestratigraficamente compõem o Membro Assistência da Formação Irati. Os intervalos possuem teores de carbono orgânico que ultrapassam os 25%. São dominantemente imaturos, com temperatura máxima de pirólise de 430 °C, a exceção dos níveis afetados pelas intrusões de diabásio relacionadas ao magmatismo Cretáceo. Ambos os intervalos apresentam querogênio tipo I e II, qualidade que os torna excelente para a geração de hidrocarboneto, assim como possuem alto potencial gerador indicado pelo parâmetro S2 de pirólise Rock-Eval, chegando a 180 mgHC/g rocha. Lateralmente, ao longo dos três estados do Sul do país, há variações na estratificação da coluna d`água, indicado por gamacerano, e na contribuição de matéria orgânica continental indicado pela presença de *Botryococcus*.
PALAVRAS-CHAVE: Formação Irati, Permiano Inferior, biomarcadores, geoquímica orgânica, rochas geradoras.

SPATIAL DISTRIBUTION OF THE PERMIAN OIL SHALE INTERVALS OF THE PARANÁ BASIN

ABSTRACT: The Paraná Basin records in the Lower Permian two relatively thin, but widely distributed intervals of oil shale. Both extend from Rio Grande do Sul to Paraná state, becoming thin and rhythmically intercalated with carbonate layers towards São Paulo, Goiás, and Mato Grosso states. Lithostratigraphically comprise the Assistance Member of the Irati Formation. The intervals have organic carbon content that exceeds 25%. They are predominantly immature, with a maximum pyrolysis temperature of 430 °C, except for levels affected by diabase intrusions related to Cretaceous magmatism. Both intervals have kerogen type I and II, a quality that makes

them excellent for hydrocarbon generation, as well as having high source rock potential indicated by the Rock-Eval pyrolysis S2 parameter, reaching 180 mgHC/g rock. Laterally, across the three southern states of Brazil, there are variations in the water column stratification, indicated by gammacerane, and in the continental input of organic matter suggested by Botryococcus occurrences.
KEYWORDS: Irati Formation, Lower Permian, biomarkers, organic geochemistry, source rocks.

1 I INTRODUÇÃO

A Formação Irati é uma sucessão mista siliciclástica-carbonática permiana da Bacia do Paraná. Uma unidade amplamente estudada devido a ocorrências de dois intervalos com alto teor de carbono orgânico (ultrapasando 25%) e presença dos fosseis de Mesosauros utilizados na correlação continental por Alfred L. Wegener para identificação do supercontinente Pangeia.

O Potencial econômico dos folhelhos Irati já vem sendo abordado desde os primeiros trabalhos sobre essa formação. Amaral (1967), Pádula (1968) e Mezzalira (1971) mostram que F. P. Oliveira (1889) já havia descrito os "schistos betuminosos" e Auguste Collen (1897) apresentou o primeiro estudo sobre os hidrocarbonetos da formação no estado de São Paulo, já I. C. White (1908) estudou a composição química da fração betuminosa ainda no início do século XX. O alto potencial dessa formação associado a necessidade energética no final do século passado levou a Petrobrás implantar a primeira unidade para exploração do *Oil Shale* da Formação Irati em 1972 no Município de São Mateus do Sul (PR). Desde 1991 a exploração desses folhelhos é executada utilizando uma tecnologia de patente nacional de alto rendimento denominada Petrosix®.

Os folhelhos betuminosos do Membro Assistência da Formação Irati representam um importante depósito de *Oil* and *Gas shale* amplamente distribuídos nos estados da porção sul do Brasil. Novas frentes de pesquisa vêm sendo implantadas por empresas privadas nos estados do Paraná, Santa Cataria e Rio grande do Sul, onde encontram-se os maiores valores de COT. Dessa forma, a grande quantidade de material disponibilizada dessa unidade permite a ampliação do conhecimento acerca da variação lateral do amplo sistema deposicional Irati.

2 I FORMAÇÃO IRATI: UMA DA SUCESSÃO MISTA CARBONÁTICA-SILICICLÁSTICA

A Formação Irati (figura 01) representa um caso especial na sedimentação, dominantemente siliciclástica das bacias intracratônicas brasileiras. Compreende uma sucessão sedimentar mista siliciclástica-carbonática com cerca de 50 metros de espessura, contudo, a unidade é amplamente distribuída na Bacia. Abrange sete estados das regiões

Centro-oeste, Sudeste e Sul do país (Goiás, Mato Grosso, Mato Grosso do Sul, São Paulo, Paraná, Santa Catarina e Rio Grande do Sul), ainda apresenta correlação com a Bacia Chaco-Paraná, no continente Sul-Americano, e na África do Sul com a Formação Whitehill das bacias Huab e Karoo (BRANCH *et al*., 2007; ARAÚJO, 2001). A pequena espessura, associada aos folhelhos negros característicos, com ampla distribuição na Bacia tornou a Formação Irati um estrato de referência bem conhecido para o Permiano (XAVIER *et al*., 2018).

No estado de São Paulo a formação apresenta uma sequência de folhelhos negros intercalados por calcários de 20 a 30 m, aumentando para 40 a 50 m em direção ao centro da bacia, chegando a 70 m no depocentro (AMARAL, 1967). Segundo esse mesmo autor, as camadas mergulham 1º20' NW para o interior da bacia com direção N35ºE. No estado do Paraná as camadas estão dispostas com direção NW e mergulho <1º para SW, constituída por calcários na base e folhelhos negros intercalados por lentes de 5 a 20 cm de calcários perfazendo um empilhamento de 12 a 20 m. No estado de Santa Catarina as camadas apresentam direção N10ºE e mergulho <1º W, a formação inicia com pacote de calcários com 30 m. Putzer (1955) apud Amaral (1967) observou uma variação brusca no estado de Santa Catarina, onde ocorre um adelgaçamento de norte a sul, passando de 70 para 32 metros em menos de 40 km. No Rio Grande do Sul as camadas estão dispostas com direção NW e mergulho para Norte. Xavier *et al*. (2018) descreve perfis da base com a Formação Palermo ao topo, em contato com a Formação Serra Alta com empilhamento de 40 e 60 m, onde identificou doze fácies com predominância de folhelhos com intercalações centimétricas de carbonatos.

A formação foi subdividida por Barbosa & Gomes (1958) em membros Taquaral (Inferior) e Assistência (Superior). O **Membro Taquaral** é constituído por mudstones cinzas a negros e siltitos, pobre em carbono orgânico (HOLZ *et al*., 2010; CRIVELLANI, 2017). O **Membro Assistência** é formado por *mudstones* intercalados com folhelhos negros ricos em matéria orgânica (HOLZ *et al*., 2010; XAVIER *et al*., 2018). O conteúdo paleontológico do Membro Assistência é representado por répteis mesosauridius, crustáceus *pygocephalomorpha* e peixes paleonisciformes desarticulados e em alta concentração, que segundo Xavier *et al*. (2018) ocorrem associados com estruturas típicas de ação de ondas de tempestades, como estratificação cruzada *hummocky*, além de conglomerados intraclastos e *grainstones* na região de São Gabriel no Rio Grande do Sul atribuído a este membro. Calças (2008) também registram estromatólitos e lenhos silicificados no estado de São Paulo.

Atualmente há uma relativa concordância quando ao ambiente de formação dos depósitos Irati, depositada em um mar epicontinental raso com conexão restrita com o oceano Pantalassa (ARAÚJO, 2001; HOLZ *et al*., 2010; XAVIER *et al*., 2018). O início da deposição é marcado por *mudstones* cinzas a negros e siltitos que definem o Membro Taquaral, seguida por *mudstones* ricos em matéria orgânica e folhelhos negros

pirobetuminosos intercalados com carbonatos depositados em rampa interna, intermediária a distal inclinada para sudoeste, com restrita circulação da água em relação ao Membro inferior, Taquaral (HACHIRO, 1991; HOLZ *et al*., 2010).

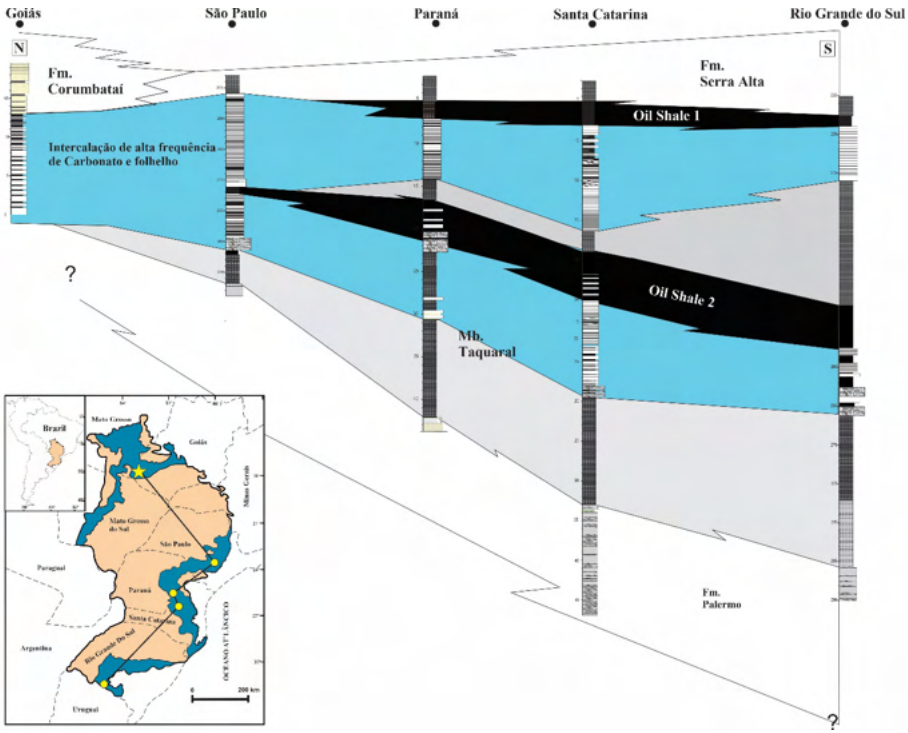

Figura 01. Distribuição lateral dos depósitos da Formação Irati com ênfase nos intervalos *Oil shale* 1 e 2. Note que os intervalos apresentam um suave espessamento na região de Santa Catarina com aunhamento em direção aos estados de São Paulo e Goiás. No Canto inferior esquerdo encontra-se o mapa com a localização dos poços na Bacia utilizados na confecção da figura. Os poços de SP e PR são compilados de Lages (2014) e o do RS de Xavier *et al*. (2018).

3 I MEDODOLOGIA

O alto potencial econômico da Formação Irati tem atraído ao longo dos anos pesquisas por empresas privadas e a academia. Esta última tem produzido e disponibilizados em trabalhos acadêmicos (TCCs, dissertações e teses) um considerável volume de dados organogeoquímicos focados nos folhelhos geradores do Membro Assistência. São estudos focados principalmente nos poços Paleosul-05-SM-PR no Paraná e HV-31-RS no estado do Rio Grande do Sul. Apesar de serem normalmente pontuais, sua integralização e correlação com novos dados provenientes do estado de Santa Catarina permite ampliar o conhecimento dos parâmetros e suas variações ao longo da Bacia do Paraná.

As amostras de poços oriundas de Santa Catarina foram cedidas pela empresa IRATI PETRÓLEO E ENERGIA LTDA. As análises de Pirólise Rock-Eval foram realizadas pelos

laboratórios Weatherford, no Canadá. As análises de biomarcadores foram executadas pelo Laboratório de Geoquímica Orgânica da UFPI (LAGO), usando a metodologia padrão com extração em sohxlet, fracionamento em coluna cromatográfica (CC) e análise da fração saturada em CG-EM, comccromatógrafo da Shimadzu, modelo GCMS-QP2010 SE.

4 I QUANTIDADE E QUALIDADE DA MATÉRIA ORGÂNICA

As características, principalmente química, da matéria orgânica presente na Formação Irati vem sendo discutidas desde a década de 1960, quando Pádula (1969) apresentou teores de COT próximos de 30%. No entanto, como já foi colocado anteriormente por Alferes *et al*. (2011) e Reis *et al*. (2018) os depósitos da Formação Irati apresentam uma estratificação química com variações no tipo e teor de matéria orgânica. Os intervalos de *oil shale* apresentam altos teores de carbono orgânico nos três estados da região sul do país (tabela 01). Da mesma forma, alta qualidade e potencial para produção de hidrocarbonetos. Os teores de COT variam de 17,5 a 21,5% para o estado do Paraná, 8,8 a 19,3 no Rio grande do Sul e os mais altos valores são registrados em Santa Catarina para ambos os intervalos (20,5 a 25,0%).

Oil shale 2 (O-S2) compreende essencialmente folhelhos negros betuminosos localizados na base do Membro Assistência (figura 01). A organofácies é marcada na base por argilitos a siltitos maciços a laminados de com de cor cinza a cinza escuro. É a organofácies com os maiores valores de COT (25 %) e potencial gerador (180 mgHC/gRocha) da Formação Irati. Os dados geoquímicos apresentam aumento dos valores convergentes para SC. Os maiores picos de COT foram 19,30% (RS), 21.5% (PR) e 25% (SC). *Oil shale* 2 é composta por querogênio tipo I e II (*oil-prone*) com aumento da contribuição de querogênio tipo I convergindo para Santa Catarina. A temperatura máxima de pirólise está em média 436°C no RS, 437°C em SC e 435°C no PR. A figura 02 apresenta os cromatogramas representativos do intervalo O-S2 para Santa Catarina, com destaque para a razão positiva de Pr sobre Ph, assim como para a presença de gamacerano, cujos valores oscilam ao longo da seção.

	Paraná		Santa Catarina	Rio Grande do Sul		
	O-S1	O-S2	O-S1	O-S2	O-S1	O-S2
COT (%)	17,5	21,5	20,7	25,0	8,8	19,30
Tmax (°C)	432	435	430	437	430	436
HI (mgHC/g COT)	400	650	830	800	680	750
S2 (mgHC/g Rocha)	40	100	90	180	52	95
Botryococcus (%)	> 0,1	> 0,1	-	-	0,0	7,0
Gamacerano	0,87	0,87	0,56	-	> 0,1	> 0,1
Pr/Ph	1,64	1,26	0,6	1,19	1,13	0,40
Hopano/Esterano	7,70	7,18	3,57	6,13	4,60	1,64

Tabela 01. Valores máximos registrados nas organofácies O-S1 e O-S2 ao longo dos três estados da região sul. de Carbono orgânico total (COT), temperatura máxima de pirólise (Tmax), índice de hidrogênio (HI), razão pristano/fitano (Pr/Ph). Os dados dos parâmetros de biomarcadores do Rio Grande do Sul foram compilados poço SC-20-RS de Reis *et al.* (2018) e do Paraná do poço 05-SM-PR de Bastos *et al.* (2021).

O intervalo *Oil shale* 1 (O-S1) consiste no intervalo com o segundo maior potencial gerador, assim como teor de carbono orgânico (figura 01). Semelhante ao O-S2 é representada por folhelhos negros betuminosos. O intervalo registra um aumento progressivo da base para o topo dos valores de COT. No entanto, os dados dessa organofácies não apresentam picos com forma em cunha como em O-S2. Nos perfis do RS a forma cilíndrica dos dados é levemente côncava, cujos valores máximos são COT (8,8%), S2 (62 mgHC/gRocha) e IH (712 mgHC/gCOT). Para os perfis de Santa Catariana a forma do gráfico assemelha-se a um funil com os valores máximos registrado no topo da fácies (COT: 20,7%; S2: 132 mgHC/gRocha; HI: 850 mgHC/gCOT). No estado do Paraná há uma alta oscilação dos valores, todavia, o aumento progressivo para o topo persiste em alguns poços na porção nordeste do estado. Na porção sudoeste, os gráficos de Rock-Eval S1, S2 e IH apresentam forma negativa com decréscimo dos valores para o topo. O IO, ao contrário, registra altos picos, chegando a 107 mg CO_2/g COT. Novamente, semelhante a fácies anterior, há uma tendência no aumento dos valores de COT para norte, todavia no geral, o estado de Santa Catariana registra os maiores valores de COT e potencial gerador (Figura 03).

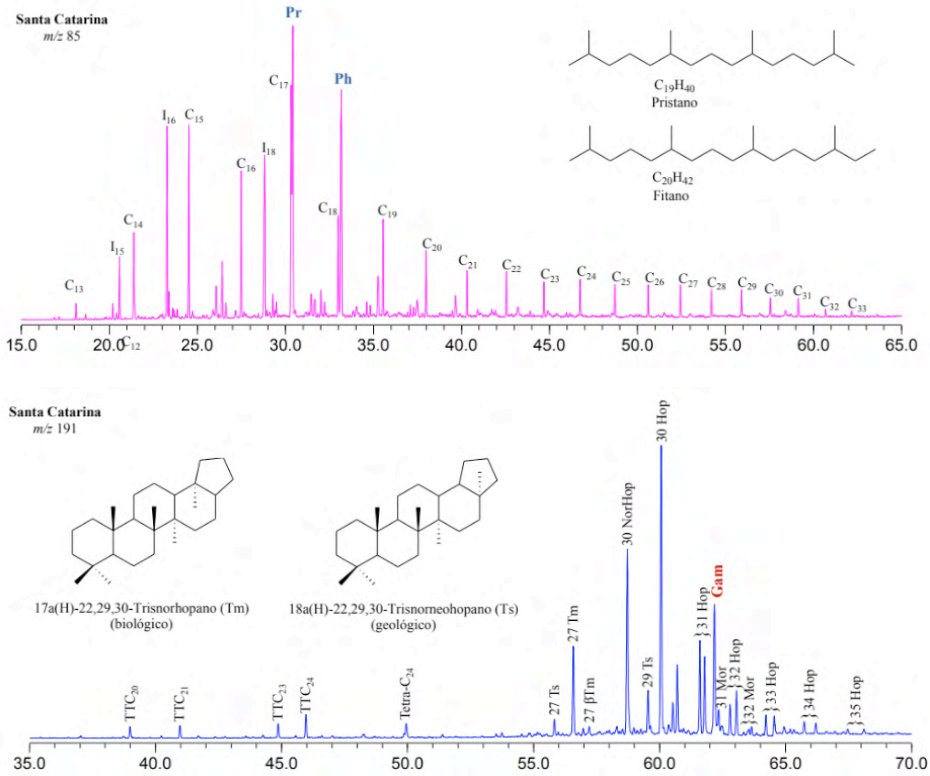

Figura 02. Perfil cromatográfico de monitoramento dos fragmentos *m/z* 85 e 191 representativo do intervalo *Oil shale* 2. Notar no *m/z* 85 a razão positiva de Pr/Ph que predomina da Formação Irati. No *m/z* 191destaque para o pico poeminete de gamacerano (Gam).

Ambos os intervalos nos três estados apresentam querogênio tipo I e II em sua composição. A matéria orgânica tipo I é aquela rica em hidrogênio (IH > 600 mg de Hc/g COT (com alta razão de H/C) 1,5 e pobre em oxigênio (baixa razão O/C <0,1) (PETERS *et al*., 2005). É comumente formado em lagos ou lagunas constituída por algas com alta contribuição de lipídios e a liptinita é o maceral dominante o que lhe confere o maior potencial para geração de óleo e gás. O querogênio tipo II apresenta menor proporção de hidrogênio que o tipo I (IH = 300-600 mg HC/g COT e H/C = 1,2-1,5) e baixa razão de O/C (KILLOPS; KILLOPS, 2005; TISSOT; WELTE, 1984). É comum em ambiente marinho, formada a partir de algas e plâncton. A liptinita também é o maceral dominante. Apesar de menores proporção de hidrogênio, querogênio tipo II possui alto potencial para geração de hidrocarboneto.

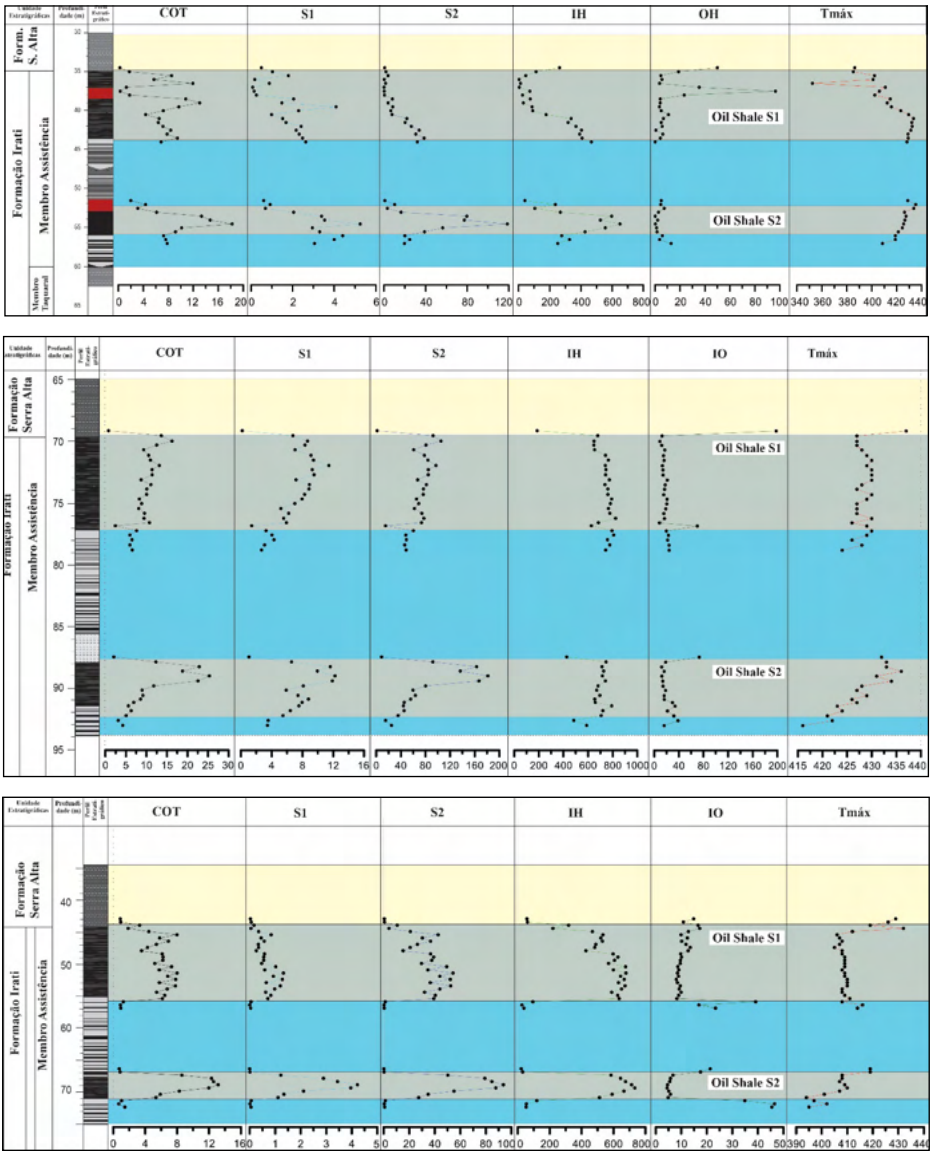

Figura 03. Variação quimoestratigráfica dos teores de carbono orgânico (COT) e parâmetros de pirólise Rock-Eval nos estados do Paraná, Santa Catarina e Rio Grande do Sul, respectivamente. S1: hidrocarbonetos livres, S2: potencial gerador, IH: índice de hidrogênio, IO: índice de Oxigênio.

5 I CONSIDERAÇÕES FINAIS

Os dados obtidos a partir de três poços nos estados do Paraná, Santa Catarina e Rio Grande do Sul permitiu espacializar, assim como compreender as variações laterais dos teores de carbono orgânico e da qualidade da matéria orgânica presente nos intervalos de *Oil shales* da Formação Irati. Apesar da ampla distribuição das organofácies, por mais

de 1.000 km, estas permanecem com as características organoquímicas lateralmente constantes. Predominam em ambos os intervalos querogênio tipo I e II, cuja matéria orgânica apresenta-se imatura, a exceção dos pontos afetados por intrusões ígneas. Contudo, consistem em intervalos com excelente qualidade para geração de hidrocarboneto. Os novos dados mostram que os intervalos mais promissores para a produção de élo estão no estado de Santa Catarina.

REFERÊNCIAS

ALFERES C.L., RODRIGUES, R., PEREIRA E. Geoquímica orgânica aplicada à Formação Irati, na área de São Mateus do Sul (PR), Brasil. **Geochimica Brasiliensis***,* 25(1): 47-54. 2011.

AMARAL S.E. Geologia e Petrologia da Formação Irati (Perminano) no estado de São Paulo. PhD Thesis, Universidade de São Paulo, São Paulo, 81 p. 1967.

ARAÚJO L.M., RODRIGUES, R., SCHERER C.M.S. Sequências deposicionais Irati: arcabouço quimioestratigráfico e inferências paleoambientais. **Ciência, Técnica, Petróleo***,* 20: 193-202. 2001.

BARBOSA O. and GOMES F.A. Pesquisa de petróleo na bacia do rio Corumbataí, Estado de São Paulo. **Divisão de Geologia Mineral – DNPM,** Boletim, vol. 171 40 p. 1958.

BASTOS, Lucas Pinto Heckert *et al*. The birth and demise of the vast epicontinental Permian Irati-Whitehill sea: Evidence from organic geochemistry, geochronology, and paleogeography. **Palaeogeography, Palaeoclimatology, Palaeoecology**, v. 562, p. 110103, 2021.

BRANCH, T., RITTER, O., WECKMANN, U., SACHSENHOFER, R.F. and SCHILLING, F. The Whitehill Formation–a high conductivity marker horizon in the Karoo Basin. **South African Journal of Geology**, 110, 465-476. 2007.

CALÇA C.P. Microbiota fóssil em sílex da Formação Assistência (subgrupo Irati, Permiano, Bacia do Paraná) no Estado de São Paulo. MS Dissertation, Instituto de Geociências, Universidade de São Paulo, São Paulo, 82 p. 2008.

CRIVELLANI K. Análise de parametros geoquímicos de rochas, óleos e betumes em afloramentos das formações Irati e Pirambóia na borda leste da bacia do Paraná, São Paulo, Brasil. MS Dissertation, Instituto de Geociências, Universidade Federal da Bahia, Salvador, 85 p. 2016.

HACHIRO, J. Litotipos, associações faciológicas e sistemas deposicionais da Formação Irati no Estado de São Paulo. Tese de Doutorado. Universidade de São Paulo. 1991.

HOLZ M., FRANÇA A.B., SOUZA P.A., IANNUZZI R. and ROHN R. A stratigraphic chart of the Late Carboniferous/Permian succession of the eastern border of the Paraná Basin, Brazil, South America. **Journal of South American Earth Sciences**, 29, 381-399. 2010.

KILLOPS, S.; KILLOPS, V. **Introduction to Organic Geochemistry**, 2nd edn (paperback). Blackwell Publishing company, 2005. 393 p.

LAGES L.C. A formação Irati (grupo passa dois, permiano, bacia do Paraná) no furo de sondagem FP-01-PR (Sapopema, PR). MS Dissertation, Instituto de Geocincias e Ciências Exatas, Universidade Estadual Paulista, Rio Claro, 117p. 2004.

MEZZALIRA S. Contribuição ao conhecimento da geologia de subsuperfície e da paleontogia da Formação Irati no Estado de São Paulo. In: **Simpósio de paleontologia**, Rio de Janeiro, Anais..., v.43, p. 273-336. 1971.

PÁDULA V. T. Estudos geológicos da Formação Irati, sul do Brasil. Boletim Técnico da PETROBRÁS, V.11, n3, p. 407-430. 1968.

PETERS, K. E.; WALTERS, C.C.; MOLDOWAN, J.M. (2nd ed.). **The biomarker guide**: Volume 1, Biomarkers and isotopes in the environment and human history. Cambridge university press, 2005.

REIS D.E.S., RODRIGUES R., MOLDOWAN J.M., JONES C.M., BRITO M., CAVALCANTE D.C., Portela H.A. Biomarkers stratigraphy of Irati Formation (Lower Permian) in the southern portion of Paraná Basin (Brazil). **Marine and Petroleum Geology**, 95: 110-138. 2018.

WELTE, D. H.; TISSOT, P. B. Petroleum formation and occurrence. Springer-verlag, 1984.

XAVIER P.L.A., SILVA A.F., SOARES M.B., HORN B.L.D., SCHULTZ C.L. Sequence stratigraphy control on fossil occurrence and concentration in the epeiric mixed carbonate-siliciclastic ramp of the Early Permian Irati. **Journal of South American Earth Sciences**, 88: 157-178. 2018.

CAPÍTULO IX

9. ANÁLISE DE BIOMARCADORES NEUTROS EM SEDIMENTO DA FORMAÇÃO SERRA ALTA PERMIANO (BACIA DO PARANÁ)

ANALYSIS OF NEUTRAL BIOMARKERS IN SEDIMENT OF THE SERRA ALTA FORMATION PERMIAN (PARANÁ BASIN)

Lorena Tuane Gomes de Almeida

Programa de Pós-Graduação em Química-PPGQ, Centro de Ciências da Natureza–CCN, Universidade Federal do Piauí-UFPI

Teresina – Piauí

http://lattes.cnpq.br/7505926250231164

Ailton da Silva Brito

Programa de Pós-Graduação em Geologia e Geoquímica-PPGG, Universidade Federal do Pará-UFPA

Belém–Pará

http://lattes.cnpq.br/9873489431846769

Sidney Gonçalo de Lima

Programa de Pós-Graduação em Química-PPGQ, Laboratório de Geoquímica Orgânica-LAGO, Centro de Ciências da Natureza–CCN, Universidade Federal do Piauí-UFPI.

Teresina – Piauí

http://lattes.cnpq.br/1655930426274093

Data de submissão: 11/10/2021

Capítulo do livro Fósseis moleculares e aplicações em geoquímica orgânica (2021)

CAPÍTULO 2

ANÁLISE DE BIOMARCADORES NEUTROS EM SEDIMENTO DA FORMAÇÃO SERRA ALTA - PERMIANO (BACIA DO PARANÁ)

Data de aceite: 01/01/2022
Data de submissão: 11/10/2021

Lorena Tuane Gomes de Almeida
Programa de Pós-Graduação em Química-PPGQ, Centro de Ciências da Natureza–CCN, Universidade Federal do Piauí-UFPI
Teresina – Piauí
http://lattes.cnpq.br/7505926250231164

Ailton da Silva Brito
Programa de Pós-Graduação em Geologia e Geoquímica-PPGG, Universidade Federal do Pará-UFPA
Belém–Pará
http://lattes.cnpq.br/9873489431846769

Sidney Gonçalo de Lima
Programa de Pós-Graduação em Química-PPGQ, Laboratório de Geoquímica Orgânica-LAGO, Centro de Ciências da Natureza–CCN, Universidade Federal do Piauí-UFPI.
Teresina – Piauí
http://lattes.cnpq.br/1655930426274093

RESUMO: A Formação Serra Alta faz parte da seção do Permiano Superior da Bacia do Paraná, ocorre imediatamente sobreposta à Formação Irati, definidas no estado de São Paulo com espessura de 60 m. É considerada uma das unidades litoestratigráficas menos estudadas da Bacia do Paraná, principalmente devido ao seu baixo potencial para hidrocarbonetos. O objetivo principal deste trabalho é caracterizar o paleoambiente deposicional e o grau de evolução térmica da Formação Serra Alta por meio de biomarcadores presentes no extrato de rocha. A matéria orgânica foi extraída em sistema ultrassom, cromatografado em gel de sílica, modificada com nitrato de prata, e analisado por GC-MS. A distribuição geral dos *n*-alcanos e isoprenóides, e alguns parâmetros moleculares sugeriram um abiente ambiente subóxico, baixa maturidade e paleoambiente deposicional marinho com contribuição de matéria orgânica terrestre.

PALAVRAS-CHAVE: biomarcadores, ambiente deposicional, Formação Serra Alta, Bacia do Paraná.

ANALYSIS OF NEUTRAL BIOMARKERS IN SEDIMENT OF THE SERRA ALTA FORMATION – PERMIAN (PARANÁ BASIN)

ABSTRACT: The Serra Alta Formation is part of the Upper Permian section of the Paraná Basin, occurring immediately superimposed on the Irati Formation, defined in the state of São Paulo with a thickness of 60 m. It is considered one of the least studied lithostratigraphic units in the Paraná Basin, mainly due to its low potential for hydrocarbons. The main objective of this work is to characterize the depositional paleoenvironment and the degree of thermal evolution of the Serra Alta Formation through biomarkers present in the rock extract. The rocks were crushed and subjected to ultrasound-assisted extraction. The organic matter was chromatographed on silica gel, modified with silver nitrate, and analyzed by GC-MS. The general distribution of *n*-alkanes and isoprenoids and some molecular

parameters suggested a sub-oxic, low maturity, aquatic depositional paleoenvironment with the contribution of terrestrial organic matter.
KEYWORDS: biomarkers, depositional environment, Serra Alta Formation, Paraná Basin.

1 I INTRODUÇÃO

A Bacia intracratônica do Paraná situa-se no centro-leste porção da América do Sul, e sua história evolutiva consiste em ciclos de subsidência acelerada induzida por eventos orogênicos (ZALÁN *et al.,*1990). Como consequência desses ciclos, as incursões marinhas no paleocontinente permitiu a deposição de sedimentos orgânicos em um mar epicontinental anóxico (NASCIMENTO *et al.,* 2021).

Gordon Jr. (1947) e Schneider *et al*. (1974), que subdividiram o Grupo Passa Dois nas Formações Irati, Serra Alta, Teresina e Rio do Rasto (membros Serrinha e Morro Pelado) na porção central e sul da bacia do Paraná e nas Formações Irati e Corumbataí nos estados de São Paulo, Goiás e Mato Grosso. No entanto, muitos autores ainda utilizam a designação "Formação Estrada Nova" referindo-se as Formações Serra Alta, Teresina e o Membro Serrinha ou parte destas unidades (NEREGATO, 2007).

A Formação Serra Alta faz parte da seção do Permiano Superior da Bacia do Paraná, ocorre imediatamente sobreposta à Formação Irati, possuindo uma das maiores extensões, definidas no estado de São Paulo com espessura de 60 m, além de ser caracterizada por folhelhos cinza escuros com algumas intercalações muito delgadas de carbonatos e *bone beds* de peixes (NEREGATO, 2007). É considerada uma das unidades litoestratigráficas menos estudadas da Bacia do Paraná, principalmente devido ao seu baixo potencial para hidrocarbonetos.

Águas relativamente calmas e distantes da costa e com fundo pouco oxigenado caracterizam seu ambiente deposicional, pois os icnofósseis são praticamente ausentes, porém próximo à base de formação são encontrados bivalves da Zona *Barbosaia angulata*, evidenciando águas um pouco mais rasas e condições de fundo oxidantes, no entanto ainda não há evidências suficientes que indiquem uma possível origem marinha (ROHN, 2001; MEGLHIORATTI, 2006).

O estudo dos biomarcadores fósseis (produtos naturais que podem ser associados a uma origem biossintética específica), permitem a caracterização de petróleo, extratos de rochas ou sedimentos e inferir correlações óleo-óleo, óleo-rocha geradora; os precursores da matéria orgânica presente em sedimentos; maturidade térmica; avaliação da migração de hidrocarbonetos e o grau de biodegradação nos reservatórios; determinação das condições do ambiente deposicional além de informações sobre o período de deposição da rocha geradora (WANG *et al.,* 2007; BROCKS e SUMMONS 2014).

Neste sentido, esse trabalho tem por objetivo caracterizar o ambiente paleodeposicional e grau de maturação térmica da Formação Serra Alta – Bacia do Paraná

por meio da análise de biomarcadores identificados através de Cromatografia a Gás acoplada à Espectrometria de Massas (CG-EM).

1.1 A Bacia do Paraná

A Bacia do Paraná (Figura 1) situa-se na parte centro-leste do continente sul-americano, cobrindo cerca de 1.500.000 km², completamente desenvolvida sobre a crosta continental e preenchida por rochas sedimentares e ígneas (ZÁLAN *et al.,* 1990). Foi dividida por Milani e Ramos (1998) em seis supersequncias: 1) Rio Ivaí; 2) Paraná (Devoniano); 3) Godwana I (Carbonifero-Eotriássico); 4) Godwana II (Meso a Neotriássico); 5) Godwana III (Neojurássico-Eocretáceo) e 6) Bauru (Neocretáceo).

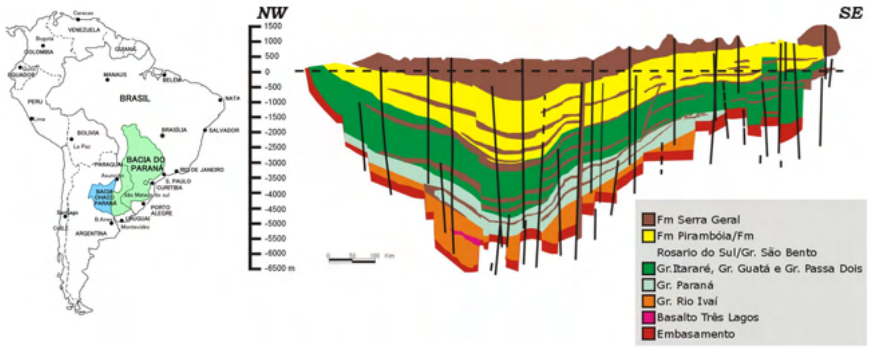

Figura 1. Localização e seção geológica esquemática da Bacia do Paraná. (Fonte: Modificado de ANP, 2010).

As três primeiras (Rio Ivaí, Paraná e Godwana I) estão associadas a sucessões sedimentares que definem ciclos transgressivo-recessivo ligados a oscilações do mar no período paleozoico enquanto as demais representam a deposição de sedimentos continentais com rochas ígneas associadas (MILANI *et al.,* 2007).

A sequência mais antiga, Rio Ivaí (Ordoviciano-Siluriano), foi depositada em um golfo imenso que era preenchido pelas águas do Panthalassa e é constituída por três formações geológicas: Form. Alto Garças que possui espessura máxima de aproximadamente 300 m sendo também a mais antiga; Form. Iapó onde apresenta depósitos relacionados a glaciação Ordoviciana, sendo sobreposta pela formação geológica Vila Maria composta por uma espessa camada argilosa rica em fósseis (BARTORELLI, 2005; MARQUES *et al.,* 2005; MILANI, 2005).

A supersequência Paraná teve sua origem no período Devoniano, quando a bacia passava por um ciclo transgressivo-regressivo, e compreendem as Formações Furnas e Ponta Grossa, seção predominantemente argilosa e uma das potenciais geradoras de petróleo (MILANI *et al.,* 2007).

Do período Carbonífero superior ao Triássico inferior foram acumulados os sedimentos que formam a sequência Godwana I que devido ao longo período de deposição possui duas características marcantes: 1) sua porção basal é um importante registro da Glaciação Karoo, cujo pico aconteceu no Carbonífero inferior e a deglaciação no período Carbonífero superior até o Permiano inferior gerou extensos depósitos glaciais; 2) no Permiano médio há o aparecimento da flora *Glossopteris* e com o declínio das condições glaciais trouxe como consequência direta uma transgressão marinha (LAVINA e LOPES, 1986) e o início da deposição de folhelhos, arenitos e siltitos que constituem as formações Palermo e Tatuí, enquanto a Formação Irati é representada por calcários e folhelhos betuminosos depositados em ambiente marinho restrito (SILVA *et al.,* 2006).

A supersequência Godwana II foi depositada no início do Triássico e possui ocorrências restritas ao território do Rio Grande do Sul e norte do Uruguai, é formada pela deposição de sedimentos de origem fluvial e lacustre, indicando ausência de subsidência durante este período (MILANI, 2005).

A sequência Jurássica-Eocretácica (supersequência Godwana III) compreende o período em que se posicionam os sedimentitos eólicos da Formação Botucatu relacionado à grande desertificação do continente Godwana, e os magmatitos da Formação Serra Geral, associado ao mais volumoso episódio de extravasamento de lavas do planeta resultando no empilhamento de até 2000 m de basalto sobre os sedimentos da Bacia do Paraná (SILVA *et al.,* 2006; MILANI *et al.,* 2007).

A supersequência Bauru corresponde aos grupos Bauru e Caiuá e é constituída por depósitos de arenitos e conglomerados alúvio-fluviais depositados em ambiente continental a desértico, esta sequência ocupou a depressão superficial originada pelos derrames vulcânicos (SILVA *et al.,* 2006).

1.1.1 A Formação Serra Alta

A Formação Serra Alta aparece de forma definitiva como unidade independente no trabalho realizado por Schneider *et al*. (1974), uma revisão litoestratigráfca da Bacia do Paraná, sendo integrada aos estratos basais do Grupo Passa Dois (MENDES 1967; WARREN *et al.,* 2015).

Washburne (1930), Mendes (1952), Barbosa e Gomes (1958), Landim (1970), Fulfaro (1970), Soares e Landim (1973), Suguio *et al*. (1974), Zaine (1980), Petri e Coimbra (1982), Sousa (1985) e Andreis e Carvalho (2001). Sousa *et al*. (1991) são os principais autores que publicaram perfis litológicos para a Formação Serra Alta, porém essas publicações representam perfis idealizados mostrando as relações entre fáceis e suas interpretações (MEGLHIORATTI, 2006).

A Formação Serra tem sua base associada ao desaparecimento dos folhelhos betuminosos e/ou calcários dolomíticos da Formação Irati e aparecimento de siltitos cinza

escuros maciços, às vezes caracterizados pela presença de níveis constituídos por restos de peixes e coprólitos (Lages, 2004). Na borda leste da Bacia do Paraná, a formação geralmente apresenta espessuras inferiores a 100 m (MEGLHIORATTI, 2006).

A presença *mesossauros* nas Formações Irati e Whitehill (África do Sul) permite a correlação entre essas unidades e atribuir a idade Artinskiana para deposição de ambas, por volta de 275 Ma (LAGES, 2004). Rocha-Campos *et al.* (2011), obteve idade por volta de 275 Ma para camada de cinza presentes no topo da Formação Irati, indicando que a sedimentação da Formação Serra Alta é mais recente que 275 Ma, nas unidades sobrepostas à Formação Serra Alta, Rocha-Campos obtiveram idades de 267 ± 17 Ma para a Formação Teresina e de 266,3 ± 4,6 Ma para a Formação Rio do Rasto. Esses dados permitem posicionar a deposição da unidade na época Guadalupiana (WANKE, 2000; HOLZFOERSTER, 2002).

A correlação entre dados palinológicos e as biozonas definidas para os vertebrados fósseis restringem um intervalo próximo a 3 Ma para a deposição dos extratos que compõem a Formação Serra Alta, delimitado entre as idades Capitaniana inferior (265 Ma) e Wordiana inferior (268 Ma), pertencentes a porção intermediária a superior da Época Guadalupiana (DAEMON e QUADROS 1970; BARBERENA *et al.* 1985; LAGES, 2004; LÓPEZ-GAMUNDÍ, 2006; SANTOS *et al*. 2006; ROCHA-CAMPOS *et al.* 2011).

O contato entre as Formações Serra Alta e Teresina é considerado transicional, materializando mudança gradual de ambiente profundo pouco oxigenado para ambiente de águas cada vez mais rasas e agitadas (MENDES 1984, WARREN *et al.,* 2015).

O contato inferior com a Formação é tradicionalmente descrito como transicional, sendo caracterizado pelo desaparecimento de folhelhos e carbonatos e surgimento gradual de siltitos laminados cinzas, próprios da Formação Serra Alta (MAACK, 1947; BEURLEN, 1954; CASTRO, *et al*. 1993).

Schneider *et al*. (1974) considera que a sedimentação das camadas da Formação Serra Alta teria ocorrido em condições similares às do Membro Taquaral da Formação Irati, ou seja, em águas calmas abaixo do nível de base de ondas, em áreas fisiograficamente restritas de um grande corpo d'água interior.

2 | METODOLOGIA

Coleta das amostras

As amostras de poços oriundas de Papanduva-SC foram cedidas pela empresa IRATI PETRÓLEO E ENERGIA LTDA. A amostra analisada corresponde a uma profundidade de 15 m deste poço.

Extração da matéria orgânica

A amostra pulverizada foi mantida em dessecador com $CaCl_2$ e Pentóxido de Fosfóro (P_2O_5) para retirada do excesso de umidade durante 24 horas antes da extração. Cerca de 30 g de amostra foi submetida à extração em banho ultrassom durante 30 min com 50 mL de uma mistura azeotrópica (diclorometano:metanol 12%), 3 vezes. Foi adicionado ao extrato cerca de 500 mg de cobre metálico em pó e levou-se ao ultrassom por 30 min com aquecimento de 60 °C para a retirada do enxofre, as frações foram filtradas, o solvente evaporado sob pressão reduzida e acomodadas em frasco de vidro.

Coluna Cromatográfica

O extrato obtido foi fracionado através de cromatografia em coluna (CC) utilizando como fase estacionária sílica: 10% $AgNO_3$, em uma proporção 1:70 (amostra: fase estacionária). O sistema de eluente empregado foi hexano (Saturados); hexano: acetato de etila 20% (Aromáticos); acetato de etila: metanol 5% (resinas e asfaltenos-NSO) (MOURA *et al.,* 2016).

Condições de análise no CG-EM

A análise da fração saturada por CG-EM foi realizada em um cromatógrafo da Shimadzu, modelo GCMS-QP2010 SE, equipado com auto injetor AOC-5000, seguindo as seguintes condições de análise: injetor 290 °C, razão split de 1:10, temperatura inicial do forno de 60 °C (1 min), apresentando uma rampa de aquecimento de 4 °C/min até 315 °C permanecendo por 15 minutos. Para cromatografia dos componentes foi empregada uma coluna SLB-5MS, 30 m × 0,25 mm, espessura do filme interno de 0,25 μm, usou-se He2 como gás de arraste com fluxo de 1,0 mL/min.

A temperatura de interface e da fonte de íons foram 320 °C e 230 °C, respectivamente. O analisador de massas utilizado foi do tipo quadrupolo operando por impacto eletrônico (70 eV) e os fragmentos detectados na faixa de 57 a 600 Da. A identificação dos biomarcadores foi feita por comparação das ordens de eluição, tempos de retenção e espectros de massas com dados da literatura.

3 | RESULTADOS E DISCUSSÕES

Biomarcadores ou marcadores biológicos são compostos cujas estruturas podem ser interpretadas em termos de sua origem biológica, são considerados fósseis moleculares constituídos de carbono, hidrogênio e outros elementos. Podem ser encontrados em rochas, sedimentos ou carvões e apresentam pequena ou nenhuma mudança estrutural em relação às moléculas orgânicas originais presentes nas membranas plasmáticas dos organismos vivos (procarióticos ou eucarióticos), (PETERS e MOLDOVAN, 2005).

Para a avaliação das informações geoquímicas da Formação Serra Alta foram realizados cálculos de parâmetros de maturação térmica e ambiente deposicicional, de acordo com a sua abundância relativa. A Figura 2 apresenta o perfil cromatográfico do monitoramento dos fragmentos *m/z* 85, 191 e 217, característicos para *n*-alcanos, terpanos e esteranos, respectivamente.

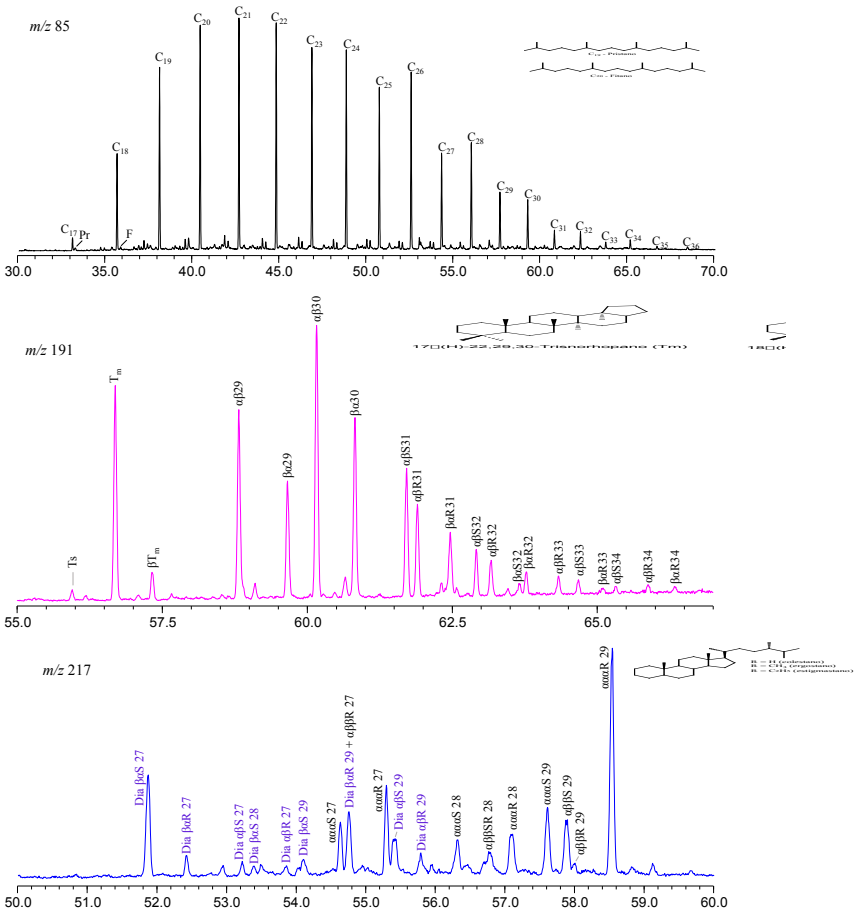

Figura 2. Perfil cromatográfico do monitoramento dos fragmentos *m/z* 85, 191 e 217.

A série de *n*-alcanos variou de C_{15}-C_{35}, com predominância de C_{19}-C_{26}, indicativo de matéria orgânica de origem marinha com contribuição terrestre, os parâmetros CPI e OEP (Tabela 1) mostram preferência par sobre ímpar, e distribuição unimodal com máximos em C_{21}, apresentando alta abundânica de *n*-alcanos.

A relação P/F, usada como parâmetro redox, apresentou valor próximo a 1,44 indicando ambiente deposicional óxico. Na geoquímica orgânica estes valores são geralmente aplicados para a avaliação da oxidação do ambiente deposicional, apesar das

suas muitas limitações, uma vez que pode ser rápida e facilmente medido. Considera-se que os valores destas razões acima de 1,0 indicam o ambiente de deposição óxido, enquanto valores <1,0 indicam condições anóxicas (KELLY *et al.,* 2011; TAO *et al.,* 2015).

Parâmetros	Amostra FSA-15
[1]**CPI-I**	0,61
[2]**CPI-II**	0,80
[3]**OEP-I**	0,95
[4]**OEP-II**	0,68
[5]**TAR**	0,90
[6]**P/F**	1,44
[7]**P/(P+F)**	0,59
[8]**P/*n*-C_{17}**	0,30
[9]**F/*n*-C_{18}**	0,03
[10]**Ts/Tm**	0,05
[11]**Ts/(Ts+Tm)**	0,04
[12]**C_{30} βα/(αβ+βα)**	0,40
[13]**C_{31} αβ 22S/(22S+22R)**	0,57
[14]**C_{32} αβ 22S/(22S+22R)**	0,54
[15]**C_{31} 22R Hop/C_{30}Hop**	0,29
[16]**C_{27}/C_{29} Est**	0,35
[17]**C_{27} S/(20S+20R)**	0,38
[18]**C_{29} 20S/(20S+20R)**	0,26
[19]**Hop/Ester**	12,09

Tabela 1. Parâmetros de biomarcadores de maturidade térmica, origem e ambiente deposicional da matéria orgânica presente na Formação Serra Alta.

1 CPI-I: $0,5*[C_{25}+ C_{27}+ C_{29}+ C_{31}+ C_{33})/(C_{24}+ C_{26}+ C_{28}+ C_{30}+ C_{32}) + (C_{25}+ C_{27}+ C_{29}+ C_{31}+ C_{33})/(C_{24}+ C_{26}+ C_{28}+ C_{30}+ C_{32})]$

2 CPI-II: $2x(C_{23}+C_{25}+C_{27}+C_{29})/[C_{22}+2(C_{24}+C_{26}+C_{28})+C_{30}]$

3 OEP-I: $(C_{21}+6C_{23}+C_{25})/(4C_{22}+4C_{24})$

4 OEP-II: $(C_{25}+6C_{27}+C_{29})/(4C_{26}+4C_{28})$

5 TAR: $(C_{27}+C_{29}+C_{31})/(C_{15}+C_{17}+C_{19})$

6 P/F: Pristano/Fitano

7 P/(P+F): Pristano/(Pristano+Fitano)

8 Pr/*n*-C_{17}: Pristano/*n*-heptadecano (C_{17})

9 Ph/*n*-C_{18}: Fitano/ *n*-octadecano (C_{18})

10 Ts/Tm: C_{27}-18α(H)-22,29,30-trisnorneohopano/C_{27}-17α(H)-22,29,30-trisnorhopano

11 Ts/(Ts+Tm): C_{27}-18α(H)-22,29,30-trisnorneohopano/[(C_{27}-18α(H)-22,29,30-trisnorneohopano+C_{27}-17α(H)-22,29,30-trisnorhopano)]

12 C_{30} *βα/(αβ+βα):* C_{30}-17β, 21α-moretano/(C_{30}-αβ- hopano + C_{30}-17β, 21α-moretano)

13 C_{31} *αβ 22S/(22S+22R):* C_{31}- 17α, 21β-homohopano 22S/(C_{32}- 17α, 21β-homohopano 22S + C_{32}- 17α, 21β-homohopano 22R)

14 C_{32} *αβ 22S/(22S+22R):* C_{32}-17α, 21β-bishomohopano 22S/(C_{32}- 17α, 21β-bishomohopano 22S + C_{32}- 17α, 21β-bishomohopano 22R)

15 C_{31} 22R Hop/C_{30}Hop: C_{31}-17α, 21β-homohopano 22R/ C_{30}-17α, 21β- hopano

16 C_{27}/C_{29} Est: C_{27} 5α,14α,17α(H)-colestano R/ C_{29} 5α,14α,17α(H)-estigmastano R

17 C_{27} S/(20S+20R): C_{27} 5α(H),14α(H),17α(H)-colestano S/(C_{27} 5α(H),14α(H),17α(H)-colestano S + C_{27} 5α(H),14α(H),17α(H)-colestano R)

18 C_{29} 20S/(20S+20R): C_{29}5α(H),14α(H),17α(H)-estigmastano S/(C_{29} 5α(H),14α(H),17α(H)-estigmastano S + C_{27} 5α(H),14α(H),17α(H)-estigmastano R)

19 Hop/Ester: C_{30} 17α,21β-hopano RIC *m/z* 191)/(C_{27} 20S 5α,14α,17α(H)-colestano 20R+20S *m/z* 217)

A presença de hopanos em óleos e sedimentos tem sido relacionada à atividade bacteriana e a contribuição de algas tornando-se um importante parâmetro de maturação, fonte e salinidade (JIANPING *et al.,* 1997; HAUSER *et al.,* 1999; SILVA *et al.,* 2008). Este grupo de compostos compreendem três tipos de diasteroisômeros: 17α, 21β(H)-hopanos *(αβ* hopanos) e 17β, 21α(H)-hopanos *(βα* hopanos ou moretanos) bem como seus diasteroisômeros bioquímicos como 17β, 21 β(H)-hopanos *(ββ* hopanos).

O 18α(H)-trisneohopano (Ts) é mais resistente a degradação térmica do que o 17α(H)-trisnorhopano (Tm), com isso espera-se que os valores da razão Ts/Tm aumente com o aumento da maturação. A razão destes isômeros expressa como Ts/Tm e Ts/(Ts+Tm), apresentaram valores de 0,05 e 0,04, respectivamente, sugerindo amostras imaturas. O C_{27} 17β (H) -22,29,30-trinorhopano (βTm) também foi identificado, este composto é característico de rochas geradoras imaturas, conforme aumenta a maturação térmica, espera-se que a concentração relativa de βTm diminua porque é termicamente instável quando comparada a Ts e Tm (HONG *et al.,* 1986).

A análise do perfil cromatográfico representativo dos esteranos monitorados a partir do fragmento *m/z* 217 indicou a predominância do esterano C_{29} (estigmastano) em relação aos esteranos C_{27} (colestano) e C_{28} (ergostano), normalmente esta predominância é dada em função de uma maior contribuição de vegetais superiores (BECHTEL *et al.,* 2012).

Com o aumento da maturação térmica também é observado a isomerização dos esteranos regulares no C_{20}-5α(H),14α(H),17α(H) de configuração R formando uma mistura de configurações R (epímero biológico), e S (epímero geológico), espera-se que a razão C_{29} 20S/(20S+20R) atinja valores de equilíbrio entre 0,52 e 0,55 (PAN *et al.,* 2008). As razões 20S/(20S+20R) foram 0,38 e 0,26, respectivamente, para C_{27} e C_{29}, corroborando com os valores de Ts/Tm e Ts/(Ts+Tm).

4 | CONCLUSÕES

A análise geoquímica da matéria orgânica da amostra da Formação Serra Alta foi

realizada por meio parâmetros moleculares, com base em *n*-alcanos, terpanos e esteranos.

A distribuição geral de hidrocarbonetos e/ou parâmetros de biomarcadores sugeriram que a amostra apresenta baixa evolução térmica, paleoambiente deposicional subóxico e ambiente marinho com contribuição de matéria orgânica terreste (CPI e OEP mostram preferência par sobre ímpar), corroborado pela razão C_{27}/C_{29} esterano. Entre os esteranos, predominam àqueles de estereoquímica ααα20R em relação ααα20S, que é característica de amostras pouco evoluídas termicamente.

AGRADECIMENTOS

Os autores agradecem à empresa IRATI PETRÓLEO E ENERGIA LTDA pelas amostras cedidas e à UFPI, LAGO, PETROBRAS e FAPEPI pelo suporte financeiro.

REFERÊNCIAS

ANDREIS, R. R.; CARVALHO, I. S. A Formação Corumbataí (Permiano SuperiorTriássico Inferior, Bacia do Paraná) na pedreira de Pau Petro, Município de Taguaí, São Paulo, Brasil: Análise paleoambiental e das pegadas fósseis. **Rev. Bras. De Paleontologia**, 2: 33 - 46, 2001.

ANP, 2010. **Décima Rodada de Licitações: Bacia do Paraná.** Disponível em: http://rodadas.anp.gov.br/arquivos/Round10/arquivos_r10/seminarios/STA_6_Bacia_do_Parana_portugues.pdf. Acesso em: 13 de março de 2021.

BARBERENA, M.C.; ARAUJO, D.C.; LAVINA, E.L. Late Permian and Triassic tetrapods of Southern Brazil. **National Geographic Research**, 1:5-20, 1985.

BARBOSA, O.; GOMES, F. A., **Pesquisa de petróleo na bacia do rio Corumbataí, Estado de São Paulo, Brasil.** Bol. DNPM-DGM, Rio de Janeiro, 171, p.40, 1985.

BARTORELLI, A. Origem das grandes cachoeiras do planalto basáltico da Bacia do Paraná: evolução quaternária e geomorfologia. In: MANTESSO NETO, V.; BARTORELLI, A.; CARNEIRO, C. D. R.; BRITO-NEVES, B. B. **Geologia do Continente Sul-Americano: Evolução da Obra de Fernando Flávio Marques de Almeida.** São Paulo, Brasil: Beca, p. 95-111, 2005.

BECHTEL, A.; JIA, J.; STROBL, S. A. I.; REINHARD, SACHSENHOFER, R. F.; ZHAOJUN, L.; REINHARD, G.; PÜTTMANN, W. Paleoenvironmental conditions during deposition of the Upper Cretaceous oil shale sequences in the Songliao Basin (NE China): Implications from geochemical analysis. **Organic Geochemistry**, v. 2012, p. 76-95, 2012.

BROCKS, J. J. e SUMMONS, R. E. **10.3 - Sedimentary Hydrocarbons, Biomarkers for Early Life A2** - Holland, Heinrich D. Treatise on Geochemistry (Second Edition). K. K. Turekian. Oxford, Elsevier: p. 61-103, 2014.

CASTRO, J.C.; MACIEL, U.; ALVES, C.F.C.; GRECCHI, R.C. O Grupo Guatá na margem nordeste da Bacia do Paraná: uma revisão. In: **I Simpósio sobre a cronoestratigrafa da Bacia do Paraná, Rio Claro.** Boletim de Geociências, p. 55-56, 1993.

DAEMON, R.F.; QUADROS, L.P. Bioestratigrafa do Neopaleozóico da Bacia do Paraná. In: 24º Congresso Brasileiro de Geologia, Brasília. Anais, p. 359-412, 1970.

FÚLFARO, V. J. Contribuição à geología da região de Angatuba, Estado de São Paulo. **Div. Geol. Miner. DNPM-DGM**, Rio de Janeiro, Bol., v.254, p. 83, 1970.

GORDON JR., M. Classificação das formações gonduânicas do Paraná, Santa Catarina e Rio Grande do Sul, Brasil. **Div. Geol. Min. D.N.P.M. Not. Prel. Est.,** 38**,** Rio de Janeiro, 20 p., 1947.

HAUSER, A.; DASHTI, H.; ZHAN, Z. H. Identificação of biomarker compounds in seletcted Kuwait crude oils. **Fuel,** v.78, p.1483-1488, 1999.

HOLZFOERSTER, F. Sedimentology, stratigraphy and synsedimentary tectonics of the Karoo Supergroup in the Huab and Waterberg-Erongo areas, N-Namibia. **Beringeria,** v. 30,1-144, 2002.

HONG, Z.-H., LI, H.-X., RULLKÖTTER, J., MACKENZIE, A.S. Geochemical application of sterane and triterpane biological marker compounds in the Linyi Basin. **Organic Geochemistry,** v.10, 433-439, 1986.

JIANPING, B. 25-norhopane series in the unbiodegraded oil and the source. **Chinese Science Bulletin**, v.42, n. 16, p. 1388-1391, 1997.

KELLY, A. E.; LOVE, G. D.; ZUMBERGE, J. E.; SUMMONS, R. E. Hydrocarbon biomarkers of Neoproterozoic to Lower Cambrian oils from eastern Siberia. **Organic Geochemistry**, v. 42, p. 640-654, 2011.

LAGES, L.C. A Formação Irati (Grupo Passa Dois, Permiano, Bacia do Paraná) no furo de sondagem FP-01-PR (Sapopema, PR). MS Dissertation, Instituto de Geociências e Ciências Exatas, Universidade Estadual Paulista “Júlio de Mesquita Filho”, Rio Claro, p. 117, 2004.

LANDIM, P. M. B., O Grupo Passa Dois (Permiano) na bacia do Rio Corumbataí, São Paulo. **Bol. DNPM-DGM**, v. 252: 1-103, 1970.

LAVINA, E. L.; LOPES, R. C. **A transgressão marinha do Permiano Inferior e a evolução paleogeográfica do Supergrupo Tubarão no Estado do Rio Grande do Sul.** Paula Coutiana, Porto Alegre, n. 1, p. 51-103, 1986.

LÓPEZ-GAMUNDÍ O. Permian plate margin volcanism and tuFFs in adjacent basins of west Gondwana: age constraints and common characteristics. **Journal of South American Earth Sciences**, v.22, p.227-238, 2006.

MAACK, R. Breves notícias sobre a geologia dos estados do Paraná e Santa Catarina. **Arquivos de Biologia e Tecnologia (IBPT)**, v.11, p.63-154, 1947.

MARQUES, L.S.; ERNESTO, M. **O magmatismo toleítico da Bacia do Paraná.** In: MANTESSO NETO, V.; BARTORELLI, A.; CARNEIRO, C.D.R.; NEVES, B.B.B. (Eds.). Geologia do continente sul americano evolução da obra de Fernando Flávio Marques de Almeida. São Paulo, Brasil: Beca, p. 245-263, 2005.

MEGLHIORATTI, T. Estratigrafia de seqüências das Formações Serra Alta, Teresina e Rio do Rasto (Permiano, Bacia do Paraná) na porção nordeste do Paraná e centro-sul de São Paulo. 147 f. Dissertação (Mestrado em Geologia). Universidade Estadual Paulista, Rio Claro-São Paulo, 2006.

MENDES, J.C. A Formação Corumbataí na região do Rio Corumbataí (estratigrafa e descrição dos lamelibrânquios). **Boletim da Faculdade de Filosofa, Ciências e Letras da Universidade de São Paulo (Série Geologia)**, v.145(8), p.1-119, 1952.

MENDES, J.C. **The Passa Dois Group.** In: Bigarella J.J., Becker R.D., Pinto I.D. (eds.). Problems in Brazilian Gondwana geology, Curitiba, Instituto de Geologia, p.119-166, 1967.

MENDES, J.C. Sobre os paleoambientes deposicionais do Grupo Passa Dois. **Revista do Instituto Geológico**, v. 5(1-2), p.15-24, 1984.

MILANI, E. J**. Comentários sobre a origem e a evolução tectônica da Bacia do Paraná.** In: MANTESSO NETO, V.; BARTORELLI, A.; CARNEIRO, C.D.R.; NEVES, B.B.B. (Eds.). Geologia do continente sulamericano evolução da obra de Fernando Flávio Marques de Almeida. São Paulo, Brasil: Beca, p. 264279, 2005.

MILANI, E. J.; MELO, J. H. G.; PAULO ALVES DE SOUZA, P. A.; FERNANDES, L. A.; FRANÇA, A. B. Bacia do Paraná. In: Cartas Estratigráficas. **Boletim de Geociências**, Petrobras, Rio de Janeiro, v. 15, n. 2, p. 265-287, 2007.

MILANI, E. J.; RAMOS, V. A. Orogenias Paleozóicas no domínio sul-americano do Gondwana e os ciclos de subsidência da Bacia do Paraná. **Revista Brasileira de Geociências**, v. 28, n. 4, p-473-484, 1998.

MOURA, A.K.S., SANTOS, A.L.S.; CITÓ, A. M. G. L. Otimização de Metodologia para Fracionamento Cromatográfico da Matéria Orgânica de Óleo Cru e Extratos de Rochas. **XIII Congresso De Geoquímica dos países de Língua Portuguesa**, p. 1, 2015.

NASCIMENTO, C. A.; SOUZA, E. S.; MARTINS, L. L.; RIBEIRO, H. J. P. S.; SANTOS, V. H.; RODRIGUES, R. Changes in depositional paleoenvironment of black shales in the Permian Irati Formation (Parana´ Basin, Brazil): Geochemical evidence and aromatic biomarkers. **Marine and Petroleum Geology**, v. 126, p. 104917, 2021.

NEREGATO, R. Estudo palinológico das Formações Serra Alta, Teresina e Rio do Rasto nos furos de sondagem SP-23-PR e SP-58-PR, centro-norte do Paraná (Permiano, Bacia do Paraná). 107 f. Dissertação (Mestrado em Geociências). Universidade Estadual Paulista, Rio Claro-São Paulo, 2007

PAN, C.; PENG, D.; ZHANG, M.; YU, L.; SHENG, G.; FU, J. Distribution and isomerization of C_{31}-C_{35} homohopanes and C_{29} steranes in oligocene saline lacustrine sediments from Qaidam Basin, Northwest China. **Organic Geochemistry**, v.39, p. 646-657, 2008.

PETERS, K. E.; WALTERS, C. C.; MOLDOWAN, J. M. **The Biomarker Guide. Biomarkers and Isotopes in the Environment and Human History**. v.1, Ed. 2nd, Cambridge University Press. 2005.

PETRI, S.; COIMBRA, A M. Estruturas sedimentares das Formações Irati e Estrada Nova (Permiano) e sua contribuição para a elucidação dos seus paleoambientes geradores, Brasil. In: **Actas 5º Congr. Latino-Americano de Geologia**, v.2: p.353-371, 1982.

ROCHA-CAMPOS, A.C.; BASEI, M.A.; NUTMAN, A.P.; KLEIMAN, L.E.; VARELA, R.; LLAMBIAS, E.; CANILE, F.M.; ROSA, O.C.R. 30 million years of Permian volcanism recorded in the Choiyoi igneous province (W Argentina) and their source for younger ash fall deposits in the Paraná Basin: SHRIMP U-Pb zircon geochronology evidence. **Gondwana Research**, v.19, p 509-523, 2011.

ROHN, R. A Estratigrafia da Formação Teresina (Permiano, Bacia do Paraná) de acordo com furos de sondagem entre Anhembi (SP) e Ortigueira (PR). **Ciência-Técnica-Petróleo, Seção: Exploração de Petróleo**, v. 20, p. 209- 218, 2001.

SCHNEIDER, R. L.; MULHMANN, H.; TOMMASI, E., MEDEIROS, R. A., DAEMON, R. F., NOGUEIRA, A. A. Revisão estratigráfica da Bacia do Paraná. In: **Congresso Brasileiro de Geologia**, Porto Alegre. Porto Alegre: Sociedade Brasileira de Geologia, v.1, p. 41-65, 1974.

SILVA, D. R. A.; MIZUSAKI, A. M.; ANJOS, S. M. C.; CONCEIÇÃO, R. V. O Método Radiométrico Rb-Sr Aplicado em Rochas Sedimentares o Exemplo da Bacia do Paraná, Brasil. **Pesquisa de Geociências**, v. 33, n.1, 83-100, 2006.

SILVA, T. F.; AZEVEDO, D. A.; RANGEL, M. D.; FONTES, R. A.; NETO, F. R. A. Effect of biodegradation on biomarkers released from asphaltenes. **Organic Geochemistry**, v. 39, p. 1249-1257, 2008.

SOARES, P.C.; LANDIM, P. MB., Aspectos regionais da estratigrafia da Bacia do Paraná no seu flanco nordeste. In: **Anais 27º Cong. Bras. Geologia**, Aracaju, v.1, p. 243-296, 1973.

SOUSA, S. H. M.; SUGUI, K. e CASTRO, J. C., 1991. Sedimentary fácies of de Estrada Nova and Corumbataí Formation (Late Peleozoic of the Paraná Basin) in the State of São Paulo, Brazil. In: 7 International Gondwana Symposium, São Paulo, 161-172.

SOUSA, S.H.M. Fácies sedimentares das Formações Estrada Nova e Corumbataí no Estado de São Paulo. São Paulo, SP. (Dissertação de Mestrado), IG-USP, p. 142, 1985.

SUGUIO, K.; SALATI, E.; BARCELOS, J.H., Calcários oolíticos de Taguaí (SP) e seu possível significado paleoambiental na deposição da Formação Estrada Nova. **Rev. Brasil. Geoc**., v.4, p.142-166, 1974.

TAO, S.; WANG, C.; DU, J.; LIU, L.; CHEN, Z. Geochemical applications of tricyclic and tetracyclic terpanes biomarkers in crude oils of NW China. **Marine and Petroleum Geology**, v. 67, p. 460-467, 2015.

WANG, C. YANG, E. A. L. **Petroleum biomarker for oil spill characterization and source identification.** Z. Wang, S. Stout (Eds.), Oil Spill Environmental Forensics, Academic Press, Oxford, 2007.

WANKE, A. Karoo-Etendeka unconformites in NW Namibia and their tectonic implications. PhD Thesis, Würzburg University, Würzburg, p.116, 2000.

WARREN, L.C.; ASSINE, M.L.; SIMÕES, M. G.; RICCOMINI, C.; LUÍS EDUARDO ANELLI, L.E. A Formação Serra Alta, Permiano, no centro-leste do Estado de São Paulo, Bacia do Paraná, Brasil. **Brazilian Journal of Geology**, 45(1), p.109-126, 2015.

WASHBURNE, H. R., **Petroleum geology of the State of São Paulo**. São Paulo, p. 272, 1930.
ZAINE, M. F., Uma barreira geográfica no Paleozóico Superior na região de Fartura, SP. Universidade de São Paulo (Dissertação de mestrado), p.89, 1980.

ZÁLAN, P. V.; WOLF, S.; ASTOLFI, M. A.; VIEIRA, I. S.; CONCEIÇÃO, J. C. J.; APPI, V.; SANTOS NETO, E. V.; CERQUEIRA, J. R.; MARQUES, A. The Paraná Basin, Brazil. In: LEIGHTON MW, KOLATA DR, OLTZ DF e EIDEL JJ (Eds.). Interior cratonic basins. **American Association of Petroleum Geologists Memoir**, v. 51: p. 681-708, 1990.

CAPÍTULO X

10. PRESERVAÇÃO DE GEOPOLÍMEROS NO REGISTRO ESTRATIGRÁFICO E SUAS IMPLICAÇÕES PALEOAMBIENTAIS

GEOPOLYMERS PRESERVATION IN THE STRATIGRAPHIC RECORD AND ITS PALEOENVIRONMENTAL IMPLICATIONS

Ailton da Silva Brito

Universidade Federal do Pará, Programa de Pós-Graduação em Geologia e Geoquímica (PPGG-UFPA), Belém-Pá

http://lattes.cnpq.br/9873489431846769

Data de submissão: 13/07 /2021

Capítulo do livro Fósseis moleculares e aplicações em geoquímica orgânica (2021)

CAPÍTULO 14

PRESERVAÇÃO DE GEOPOLÍMEROS NO REGISTRO ESTRATIGRÁFICO E SUAS IMPLICAÇÕES PALEOAMBIENTAIS

Data de aceite: 01/01/2022
Data de submissão: 13/07/2021

Ailton da Silva Brito
Universidade Federal do Pará, Programa de Pós-Graduação em Geologia e Geoquímica (PPGG-UFPA), Belém-Pá
http://lattes.cnpq.br/9873489431846769

RESUMO: Geopolímeros são produtos das transformações de biopolímeros sintetizadas por plantas terrestres, planctônicas e bentônicas. Aqueles presentes nos sedimentos e rochas que passaram por pequenas alterações ao longo do tempo geológico, onde houve a preservação do esqueleto carbônico, são conhecidos como fósseis moleculares. Com o advento da cromatografia gasosa e espectrometria de massa (CGEM), equipamentos analíticos que permitem a identificação dos fósseis moleculares, houve uma revolução no estudo das sucessões estratigráficas. A fração solúvel extraída das rochas sedimentares ricas em matéria orgânica permite a identificação e caracterização do ambiente deposicional. Assim como, das condições ambientais reinantes durante a formação de cada estrado sedimentar que preservou carbonato orgânico suficientemente analisável ao longo da coluna geológica. As interpretações paleoambientais são possíveis devido as transformações das cadeias carbônicas serem dependentes das condições do meio ambiente, tais como salinidade, disponibilidade de oxigênio livre, temperatura, profundidade e fauna característica de cada ambiente (marinho, lago, continente). Da mesma forma, é possível fazer inferências sobre a idade da rocha a partir de marcadores característicos sintetizados por flora com biozona de baixa amplitude. Tornando-se úteis na identificação do período de formação das rochas geradoras de hidrocarbonatos.

PALAVRAS-CHAVE: Folhelho rico em carbono orgânico, Matéria orgânica sedimentar, Biomarcadores, Interpretações paleoambientais.

GEOPOLYMERS PRESERVATION IN THE STRATIGRAPHIC RECORD AND ITS PALEOENVIRONMENTAL IMPLICATIONS

ABSTRACT: Geopolymers are formed from biopolymers synthesized by terrestrial, planktonic and benthic plants. When it is present within sediment or rock that usually underwent to small changes across the geological time, with the carbon skeleton preservation are called molecular fossils. Since the arrival of gas chromatography and mass spectrometry (GCMS), an analytical equipment that allow identification of molecular fossils, there was a revolution in the study of stratigraphic record. The soluble fraction extracted from sedimentary rocks rich in organic matter allows the identification and characterization of the depositional environment. Furthermore, the environmental conditions prevailing during the formation of each sedimentary bed that preserved enough organic carbon throughout the geological section. The paleoenvironmental interpretations are possible due to the transformations of carbon chains depends on the environmental conditions, such as salinity, free oxygen, temperature, depth

and characteristic fauna of each environment (marine, lacustrine, terrestrial). Likewise, characteristics biomarkers synthesized by flora with low amplitude biozone, limited to a given geological time interval, it is possible to make inferences about the rock age. A useful tool in identifying the period of formation of the source rock.
KEYWORDS: Organic-rich shales, Sedimentary Organic Matter, Biomarkers, Paleoenvironment Interpretation.

1 | INTRODUÇÃO

As rochas sedimentares representam cerca de 75% das rochas que capeiam a crosta terrestre. Dentre estas, aproximadamente 60 % são rochas siliciclásticas finas (folhelhos, argilitos, siltitos). A decantação de partículas finas com predominância de granulometria inferior a 4 μm tende a formar finas laminações. Estas são compostas por argilominerais, separadas por lentes de grãos siliciclásticos tamanho silte (quartzo, feldspatos) ou marcadas apenas por diferenças texturais, formando os folhelhos. A granulometria fina nos folhelhos consequentemente baixa permeabilidade é o fator primário que os permitem preservar matéria orgânica no registro estratigráfico ao longo da colunar geológica. A formação das rochas siliciclásticas finas está condicionada a predominância de baixa energia no ambiente deposicional subquoso suficiente para que haja decantação das partículas em suspenção. Em ambientes onde além da baixa energia predominam condições anóxicas < 0.1ml/l de O_2 conforme Rhodes e Morse (1971), os folhelhos se tornam excelentes meios de preservação, gerando os folhelhos ricos em carbono orgânico, conhecidos simplesmente pelo termo folhelho negro (*black shales*).

Black shales são os principais geradores de hidrocarbonatos em um sistema pretrolífero convencional e não-convencional. São alvos de pesquisas tanto acadêmicas quanto do setor privado relacionado as empresas petrolíferas. A grande parte das informações obtidas são a partir dos fósseis moleculares nelas presente. Fósseis moleculares são moléculas sintetizadas por plantas terrestres, planctônicos e bentônicos (algas, bactérias) encontrados em sedimentos, rochas sedimentares e petróleo que não sofreram alteração ou passaram por pequenas alterações ao longo do tempo geológico, onde houve a preservação do esqueleto carbônico (TISSOT; WELTE 1984; PETERS *et al.,* 2005a). O estudo da matéria orgânica sedimentar permite investigar o potencial para geração de hidrocarboneto de uma rocha geradora, tornando-se crucial para caracterização do sistema petrolífero.

Nesse contexto, os fósseis químicos tornam-se excelentes marcadores moleculares que permitem compreender o caminho da migração do óleo da rocha geradora a reservatório (correlação óleo-óleo e óleo-rocha geradora) e avaliar a evolução e o grau de maturação térmica. Por outro lado, o estudo acadêmico dessas rochas também permite investigar i) a flora precursora a matéria orgânica sedimentar; ii) o ambiente deposicional (Lago, Estuário, Marinho); iii) as condições ambientais (hipersalino, anóxico ou oxidante); iv) os processos

diagenéticos, e; v) até mesmo inferir a idade da rocha geradora ou petróleo. Por exemplo, o oleanano é um biomarcador característico das flores das angiospermas encontrado apenas em óleos e rochas do Neógeno e Cretáceo Superior (PETERS *et al.,* 2005a)

2 | ORIGEM DA MATÉRIA ORGÂNICA SEDIMENTAR

Matéria orgânica sedimentar (MOS) refere-se a todo material presente nos sedimentos e rochas derivados de organismos. As principais fontes de matéria orgânica nos sedimentos são fitoplâncton, plantas superiores, bactérias e zooplâncton (KILLOPS; KILLOPS, 2005). Fitoplâncton e bactérias são responsáveis por cerca de 50 a 60 % da produção da matéria orgânica mundial (TISSOT; WELTE, 1984). Esses autores afirmam que fitoplâncton, principalmente diatomáceas, dinoflagelados, cyanophyceae e nanoplâncton são as principais fontes de matéria orgânica nos sedimentos marinhos, contudo, em alguns ambientes de águas rasas com luz suficiente para a fotossíntese os fitobentos podem se tornar a fonte principal. Fungos aparentemente não tem contribuição significativa para a matéria orgânica sedimentar (KILLOPS; KILLOPS, 2005). Os organismos supracitados são constituídos essencialmente por carboidratos, proteínas e lipídios. (TISSOT; WELTE, 1984), sendo os lipídios os principais compostos químicos fontes de fósseis moleculares.

A produção, acumulação e preservação da matéria orgânica incorporada nos sedimentos são importantes parâmetros para a ocorrência de rocha sedimentar rica em matéria orgânica, porventura, geradora de hidrocarboneto. Rochas geradoras são rochas sedimentares de granulação fina ricas em matéria orgânica que apresenta quantidade, qualidade e maturação térmica adequada (PETTERS; CASSA, 1994; PETERS *et al*., 2005b). Normalmente uma rocha sedimentar apresenta teores de carbono orgânico total (COT) inferior a 1,0%. Para ser considerada rocha geradora, os folhelhos devem conter no mínimo 1,0% de carbono orgânico total, enquanto calcários apresentam em torno de 0,6% (TISSOT; WELTE ,1984). Conforme Libes (2009), o teor de carbono orgânico de rocha geradora que origina uma grande quantidade de petróleo é de 0,5 a 5%. Todavia, o valor mínimo de COT para uma rocha sedimentar ser considerada geradora está em função do tipo de matéria orgânica presente na rocha (TISSOT; WELTE, 1984).

A produção orgânica no ambiente subquoso é controlada principalmente pela luz, temperatura e composição química presente na coluna d`água (nutrientes como fosfatos e nitratos). A atividade biológica fotossintética concentra-se na zona eufótica, localizada próxima a superfície. A profundidade total da zona eufótica está em função das condições locais dos fatores supracitados (luz, temperatura e composição química), normalmente situa-se em torno de 200 m da superfície. Contudo, a produção orgânica concentra-se majoritariamente nos primeiros 60 a 80 m da coluna d'água (TISSOT; WELTE, 1984). A matéria orgânica presente nos sedimentos é composta por moléculas derivadas de partes orgânicas, que pode ser de restos de plantas terrestres (lignina, celulose carboidratos) e

de organismos planctônicos e bactérias (lipídios e proteínas) (KILLOPS; KILLOPS, 2005). Quimicamente esses compostos são formados essencialmente por carbono, hidrogênio e oxigênio, além de nitrogênio e enxofre. Carbono e hidrogênio são os principais constituintes do querogênio. Para cada 1000 átomos de carbono, há entre 500 e 1800 átomos de hidrogênio, dependendo do tipo e evolução da matéria orgânica. O oxigênio é o terceiro mais abundante, variando de 25 a 300 átomos. Nitrogênio e enxofre apresentam as menores proporções, 5 a 30 e 10 a 25 átomos para cada 1000 átomos de C, respectivamente (TISSOT; WELTE, 1984).

O tipo e complexidade da matéria orgânica incorporada aos sedimentos ao longo do tempo geológico este em função da complexidade e evolução da vi em si. As principais fontes de hidrocarbonetos até o Devoniano eram representadas por fitoplâncton marinho e bactérias, e por vezes, algas bentônicas e zooplâncton (TISSO; WELTE, 1984). A partir do Devoniano as plantas vasculares do grupo das pteridófitas conquistaram o continente, e passaram a contribuir para a matéria orgânica sedimentar e geração de petróleo. Alta contribuição de plantas superiores em sedimentos marinhos são identificadas nos folhelhos da Formação Pimenteiras (Mesodevoniano) e Longá (Devoniano Superior-Mississipiano) da Bacia do Parnaíba (BRITO *et al.,* 2020; SOUSA *et al.,* 2020).

3 I EVOLUÇÃO E MATURAÇÃO TÉRMICA DOS BIOPOLÍMEROS

O soterramento dos sedimentos promove transformações da matéria orgânica devido a maturação térmica e consequente geração de petróleo. A maturação está em função de dois fatores importantes: a **temperatura** e o **tempo**. O processo de maturação pode ser dividido em três fases com intervalos de temperaturas distintos, nos quais tem-se a matéria orgânica imatura (diagênese), matura (catagênese) e senil ou supermatura (metagênese).

3.1 Diagênese

Diagênese é a fase inicial de transformações físico-químicas que ocorrem nos primeiros milhares de anos após o soterramento sob temperaturas até 50°C (LIBES, 2009). A atividade microbiana é um dos principais agentes de transformação e decomposição da matéria orgânica atuantes desde a sedimentação até o início da diagênese. Lipídios e lignina são mais resistentes à degradação, sendo os lipídios um dos componentes mais importantes no petróleo. O CO_2, amônia e a água são geradas como subprodutos dessas reações (TISSOT; WELTE, 1984).

Os processos físico-químicos atuantes durante a diagênese promovem uma reestruturação do material orgânico em busca de equilíbrio frente as novas condições de temperatura e pressão. Contudo, a estabilidade química do material orgânico lhes confere pouca mudança na sua composição, sendo estas graduais conforme o aumento

da temperatura (DOW, 1977). As mudanças químicas que ocorrem na estrutura dos compostos, como perdas de grupos funcionais e polimerização, levam os biopolímeros (proteínas, carboidratos, lipídios) a serem convertidos em novas estruturas policondensadas mais estáveis – os **geopolímeros** – conhecidos como querogênio (DOW ,1977; TISSOT; WELTE, 1984; TYSON, 1995). O **querogênio** representa a fração insolúvel em solvente orgânico, e o **betume** a fração solúvel (figura 01). Durante esse processo ocorrem algumas moléculas livres de lipídios que sofrem pouca ou nenhuma alteração na composição ou estrutura molecular, pois são compostos mais resistentes a degradação microbiana, essas moléculas são os **fósseis geoquímicos**. As modificações estruturais dos biomarcadores são sistemáticas e sequenciais, o que permite correlacioná-lo com seu precursor biológico (PHILP, 1985). A matéria orgânica resultante dessa primeira etapa ainda é imatura e o hidrocarboneto mais importante formado durante essa etapa é o metano. Nos últimos estágios da diagênese são produzidos CO_2, H_2O e alguns heteroátomos pesados. O fim da diagênese da matéria orgânica sedimentar é marcado por um índice de reflectância da vitrinita de cerca de 0,5 % equivalente ao início da formação da hulha, onde a maioria dos grupos carboxílicos são removidos (TISSOT; WELTE, 1984).

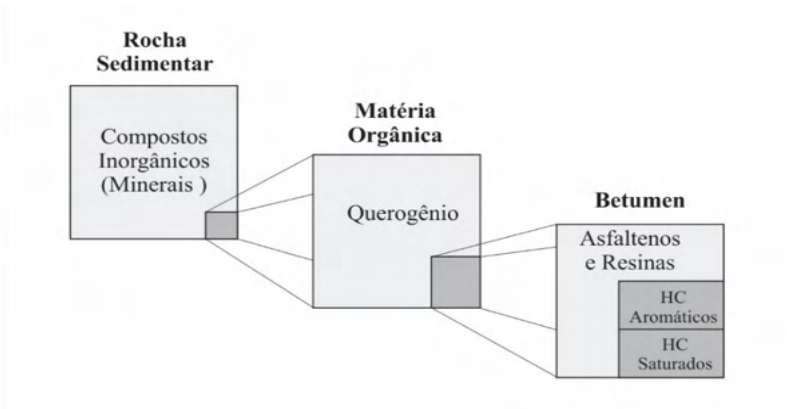

Figura 1. Distribuição da matéria orgânica sedimentar. Os hidrocarbonetos saturados e aromáticos são compostos apenas de C e H, já os asfaltenos contêm C, H, O, S e N. Fonte: modificado de Tissot e Welte (1984).

3.2 Catagênese

A formação de sucessivos novos estratos sedimentares promove o soterramento das camadas sotopostas. A catagênese representa a evolução térmica do querogênio com o aumento do soterramento no intervo de alguns quilômetros de profundidade e temperaturas na ordem de 50° a 150°C (DOW,1977). Na catagênese a matéria orgânica é classificada como matura e o craqueamento térmico é responsável pela geração dos primeiros hidrocarbonetos líquidos (oil window), posteriormente gás seco e condensado (TISSOT;

WELTE, 1984). A quantidade e qualidade de hidrocarboneto formado são controladas pela concentração, tipo e maturidade termal do querogênio presente a rocha fonte (DOW, 1977). O fim da catagênese é marcado pelo desaparecimento das cadeias de carbonos alifáticos do querogênio, corresponde ao índice de vitrinita, em torno de 2.0%. Esse índice equivale ao rank do antracito. A partir deste ponto não há mais geração de petróleo (TISSOT; WELTE, 1984). Os processos operantes sobre a matéria orgânica durante a catagênese são similares aos que ocorrem durante a carbonificação do carvão (DOW, 1977).

3.3 Metagênese

Na metagênese a matéria orgânica encontra-se no mais alto estágio evolutivo da rocha sedimentar, próximo as condições de metamorfismo, com temperaturas que variam de 150 a 200°C (TISSOT; WELTE, 1984). Esse estágio é alcançado apenas em grandes profundidades e representa a última fase significativa de alteração termal do material orgânico (HUNT, 1995). É o intervalo normalmente denominado por alguns geólogos de anquimetamorfismo. Nessa etapa a matéria orgânica é senil, representada apenas por metano (gás seco) e carbono orgânico residual (TISSOT; WELTE, 1984).

4 | FOLHELHOS RICOS EM CARBONO ORGÂNICO

Black shale é o termo comumente usado para as rochas finas ricas em matéria orgânica, que contêm mais de 1,0% de carbono orgânico. Rochas com significativos altos teores de carbono orgânico, como é o caso dos Folhelhos Irati da Bacia do Paraná, cujos teores chegam a 27%, são denominados de folhelhos betuminosos ou *oil shale*. A matéria orgânica é o principal componente responsável pela coloração escura, dando nome a rocha. *Black shale* são finamente laminados formados a partir da decantação de partículas siliciclásticas finas e matéria orgânica em suspensão no ambiente redutor, o que favorece a formação de cristais de pirita disseminados seguindo as laminações. Contudo, nem todo folhelho negro é necessariamente rico em carbono orgânico (WIGNALL; HALLAM, 1992). Assim, como já foi colocado por Spears (1980), é possível folhelho cinza escuro apresentar maior teor de COT que um folhelho negro. Os *black shale* da Formação Pimenteiras na Bacia do Parnaíba registram valores de 0,19 a 0,85%, de carbono orgânico (GONZÁLEZA *et al.,* 2020). Já os folhelhos cinza-escuros denominados Laje Azul da Formação Irati no estado de Santa Catarina chegam a 5%. Dessa maneira, atualmente na literatura estrangeira especializada ao invés do uso simplificado do termo folhelho negro usa-se *organic-rich shale* que englobam ambos os conceitos supracitados.

As condições para a preservação de *organic-rich shale* depende de vários fatores como *input* orgânico, condições oxi-redox do ambiente, circulação da água, produtividade da matéria orgânica, ação microbiana e taxa de sedimentação (DEMAISON; MOORE, 1980; NICHOLS, 2009). Os principais fatores controladores da preservação da matéria orgânica

sedimentar são: i) a produção primária; ii) prevalência de condições anóxicas no meio; iii) elevadas taxas de sedimentação (LEE, 1992; SAGEMAN *et al.*, 2003). A alta produtividade orgânica tem a tendência de criar ambiente com baixa concentração de oxigênio, devido à destruição do material orgânico e conversão para CO_2, seguido pela produção de H_2S por bactérias redutoras de sulfato. A baixa concentração ou ausência de oxigênio livre reduz a taxa de consumo da matéria orgânica (TISSOT; WELTE, 1984). Em ambientes oxidantes altas taxas de sedimentação são cruciais para a preservação da matéria orgânica (RABOUILLE; GAILLARD, 1991; HAY, 1995). Altas taxas de *input* sedimentar eleva a taxa de soterramento do material orgânico.

Outro fator que tem se mostrado relevante é a distância percorrida durante a decantação. Profundidades rasas do ambiente deposicional reduz o *timing* de degradação da matéria orgânica. Mares epíricos são um bom exemplo. As condições transgressivas que predominaram durante o Devoniano Superior favoreceram incursões marinhas sob as regiões cratônicas costeiras do Gondwana, formando mares epicontinentais (ALMEIDA; CARNEIRO, 2004). Esses mares rasos deixaram depósitos de *black shales* nas bacias intracratônicas brasileiras do Amazonas (Formação Barrreirinha), Solimões (Formação Jandiatuba), Parnaíba (Formação Pimenteiras) e Paraná (Formação Ponta Grossa). Os depósitos supracitados compreendem as principais rochas geradoras de hidrocarbonetos das suas respectivas bacias. Na Bacia do Paraná os *organic-rich shale* permianos da Formação Irati compreendem depósitos ditos *oil shales*. Também foram formados em ambiente marinho epicontinental.

5 | FÓSSEIS MOLECULARES

Fósseis moleculares, também conhecidos como biomarcadores e marcadores biológicos, podem fornecer importantes informações sobre as condições ambientais reinantes durante a deposição e diagênese. Ambientes deposicionais são caracterizados por diferentes assembleias de organismos e consequentemente biomarcadores. *n*-Alcanos ímpares de cadeias curtas (C_{15} a C_{21}) são característicos de organismos marinhos e os de cadeias longas (C_{25} a C_{37}) características de plantas terrestres (LIBES, 2009). *Botryococcane* é um biomarcador formado a partir de *Botryococcus braunii*, uma alga típica de ambiente lacustrino. O 24-n-Propilcolestano é um marcador biológico típico de algas marinhas do Devoniano ao Recente (Ver tabela 1). Na ausência de amostras de rocha, biomarcadores presentes no petróleo podem fornecer informações da litologia da rocha fonte. Por exemplo, a ausência de diasteranos indica que o petróleo é de rocha pobre em argila, normalmente formada por carbonatos (PETERS *et al.,* 2005a).

A maturação térmica dificulta as interpretações paleoambientais. Rochas fontes imaturas são ideais para o estudo das condições deposicionais, devido a reduzida taxa de transformações das cadeias carbônicas. Dessa forma, conhecer o grau de maturação

térmica seja em estudo de caracterização do potencial gerador da rocha ou reconstrução paleoambiental é essencial. No estudo de rochas maturas, esse efeito precisa ser levando em consideração durante as interpretações paleoambientais. A determinação da maturidade térmica pode ser realizada com o auxílio de diagramas ternários das frações de hidrocarbonetos saturados, aromáticos e compostos polares (PETERS *et al.,* 2005a). Rochas termicamente imaturas são ricas em compostos polares. O aumento da maturação promove o craqueamento térmico dos compostos e consequente formação de hidrocarbonetos saturados. Assim, o percentual desses compostos aumenta gradativamente com a evolução térmica em relação aos demais compostos.

Ambiente lacustrino apresentam normalmente uma grande variação espacial e temporal de salinidade, condições redox, profundidade, temperatura e *input* de matéria orgânica o que torna o estudo das rochas geradoras de lago, da ótica da geoquímica orgânica, um grande desafio. Nesse ambiente, estudos mostram que petróleo de rocha geradora depositada em águas salobras apresenta alta porcentagem de terpanos tricíclicos em comparação com hopanos, com predominância de 24-metil- e 24-etilcolestano (C_{28} e C_{29}) e algum colestano (C_{27}). Petróleo de rocha geradora depositada sob águas salinas apresentam alta porcentagem de gamacerano, já aquelas depositadas em água doce apresentam baixa concentração de esteranos em relação aos hopanos (PETERS *et al.,* 2005b).

Fósseis moleculares são os principais objetos de estudo da geoquímica orgânica, tornando-se uma ferramenta relativamente recente no estudo da origem, acumulação, migração, exploração de petróleo e no entendimento das condições paleoambientais. Os grupos de biomarcadores e não-marcadores mais utilizados na caracterização de rochas geradoras são os *n*-Alcanos, Isoprenóides acíclicos, terpanos (triclíclicos, tetracíclicos e pentacíclicos), esteranos e hopanos, descrito a seguir.

BIOMARCADOR	**ORIGEM BIOLÓGICA**	**AMBIENTE SEDIMENTAR**
nC_{15}, nC_{17}, nC_{19}	Algas	Lacustre, Marinho
nC_{15}, nC_{17}, nC_{19}	G. prisca, ~Ordoviciano	Marinho tropical
nC_{27}, nC_{29}, nC_{31}	Plantas superiores	Terrígenos
nC_{23}–nC_{31} (ímpares)	Algas não marinhas	Lacustre
C_{12}–C_{24}	Bactérias	Lacustre, Marinho
2,6,10,15,19-pentametilicosano	*Archaea*	Anóxico, hipersalino
Botryococcane	Algas verdes, *Botryococcus*	Lacustre, Salobo

C_{25}–C_{34} alcanos macrocíclicos	Algas verdes, *Botryococcus*	Lacustre salobo
C_{15}–C_{23} alcanos ciclohexil (ímpares)	G. prisca, ~Ordoviciano	Marinho
β-Caroteno	Cianobactérias, algas	Árido, hipersalino
Filocladanos	Coníferas	Terrígeno
4*β*-Eudesmano	Plantas superiores	Terrígeno
C_{19}–C_{30} terpanos tricíclicos	*Tasmanites?*	Marinho, alta latitude
23,24-Dimetilcolestano	Dinoflagelados?, haptophyta	Marinho
C_{30} 24-*n*-propilcolestano	Algas chrysophyta	Marinho
4-Metilesterano	Algumas bactérias, dinoflagelados	Lacustre, marinho hipersalino
Diasterano	Algas, plantas superiores	Rochas marinhas ricas em argilominerais
25,28,30-trisnorhopano	Bactérias	Marinho anóxico
C_{35} 17*α*,21*β*(H)-hopano	Bactérias	Redutor a anóxico
18*α*-Oleanano	Plantas superiores (≥Cretáceo)	——
Gamacerano	Tetraimanol	Hipersalino

Tabela 1. Biomarcadores que em quantidade adequada tornam-se indicadores de ambientes deposicionais. Fonte: Peters *et al.* (2005b) e LIBES (2009).

5.1 Alcanos lineares

Alcanos lineares ou *n*-Alcanos são hidrocarbonetos saturados acíclicos (figura 2) de fórmula C_nH_{2n+2} também conhecido como *n*-parafinas. A série dos componentes homólogos das parafinas é obtida pelo aumento do número de carbonos na fórmula (PETERS *et al.,* 2005a). Apesar de ser aqui a classe dita não-biomarcador, por não está atrelada a um precursor específico, sua distribuição é um importante parâmetro utilizado para diferenciar paleoambientais. A análise dessa classe via CGMS é efetuada através do íon *m/z* 85. A matéria orgânica marinha algálica é comumente indicada pela abundância de *n*-alcanos de cadeias curtas, principalmente *n*-alcanos ímpares (C_{15} a C_{17}), particularmente C_{17} (PETERS *et al.,* 2005a). A matéria orgânica derivada de plantas superiores como folhas e ceras vegetais é caracterizada pela predominância de *n*-alcanos de cadeias longas (>22) e por uma forte predominância de *n*-alcanos ímpares, principalmente de *n*-C_{23} a *n*-$C_{35,}$ especialmente *n*-C_{27}, *n*-C_{29} e *n*-C_{31} (TISSOT; WELTE, 1984; GRICE; EISERBECK, 2014). A predominância de *n*-alcanos de números pares entre *n*-C_{14} a *n*-C_{22} é outro indicador de contribuição de

matéria orgânica originada de plantas terrestres (KUHN *et al.,* 2010). A contribuição de matéria orgânica de origem marinha e continental pode gerar uma distribuição bimodal dos *n*-alcanos (PETERS *et al.,* 2005a). Rochas geradoras de ambientes transicionais também podem apresentar uma bimodalidade com ocorrência de hidrocarbonetos saturados (*n*-alcanos) de baixa (C_{15} a C_{17}) e alta (C_{25} a C_{33}) massa molecular (EGLINTON; MURPHY, 2013).

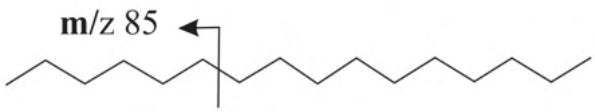

Figura 2. Estrutura do *n*-alcano $C_{16}H_{32}$ com o íon característico da classe.

Deve-se atentar para a maturação térmica que leva a redução dos compostos insaturados de alta massa molecular para formação de hidrocarbonetos saturados de baixo peso molecular, como esteranos e hopanos, ou compostos aromáticos (PETERS *et al.,* 2005a), o que ocasiona o aumento relativo dos *n*-alcanos de baixo peso molecular (C_{15} a C_{17}), comprometendo a interpretação da origem da matéria orgânica (TISSOT; WELTE, 1984).

5.2 Isoprenóides

Isoprenóides são alcanos saturados ramificados formados a partir da união de unidades de isopreno (C_5) e com grupos de metila a cada quatro átomos de carbono da cadeia principal. A unidade isopreno C_5 (figura 3) é formada por cinco carbonos, sendo que a terminação próxima ao grupo metil é chamado de cabeça (*Head*) e a outra de calda (*Tail*). A união desses elementos forma isoprenóides regulares (*head-to-tail*), irregulares (*head-to-head* ou *tail-to-tail*). O pristano (C_{19}) e o fitano (C_{20}) são os isoprenóides mais abundantes em rochas sedimentares fontes de hidrocarbonetos e comumente usados para interpretações das condições paleoambientais.

Pristano e fitano são derivados principalmente do fitol formado a partir da cadeia lateral fitil da clorofila presente em organismos fototróficos. Sob condições redutoras ocorre a clivagem da cadeia lateral fitil, produzindo o fitol, o qual é reduzido para dihidrofitol e, posteriormente para fitano. Em condições oxidantes o fitol é oxidado a ácido fitênico e descarboxilado e reduzido a pristano (PETERS *et al.,* 2005b; LIBES, 2009). A relação entre pristano (Pr) e fitano (Ph) é um excelente indicador do paleoambientes deposicional. Variações nas condições de isoprenóides estão relacionadas às flutuações do potencial redox (Eh) no ambiente, dessa forma essa razão pode ser usada para diferenciar ambientes óxidos e anóxidos. Assim, razões Pr/Ph > 1 indicam ambientes oxidantes, altas razões Pr/Ph (>3) indica matéria orgânica oriunda de fontes terrestres depositadas sob condições

óxidas a subóxidas, já razões Pr/Ph <1 indica ambiente anóxico, quando são razões muito baixas (<0,8) pode indicar ambiente anóxico, comumente salino a hipersalino ou ambiente carbonático (KILLOPS; KILLOPS, 2005).

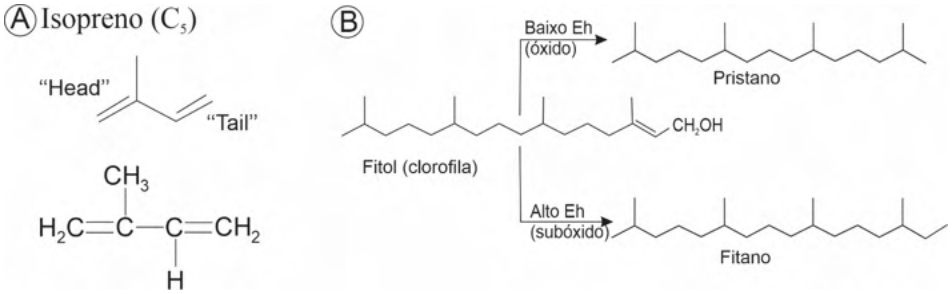

Figura 3. A) Unidade Isopreno. B) Processo de formação do pristano e fitano a partir do fitol derivado da cadeia lateral da clorofila. Fonte: Peters *et al.* (2005b).

5.3 Terpanos

Terpanos (*m/z* 191) é uma classe abrangente de biomarcadores cíclicos (figura 4) presente em rochas geradoras e no petróleo. Sua ampla ocorrência os tornou de grande importância na geoquímica orgânica, aplicados no estudo de maturação, idade geológica e origem da matéria orgânica. Muitos terpanos presentes em petróleo são originados da membrana lipídica de bactérias procariontes que formam várias séries homólogas com componentes acíclicos, bicíclicos, tricíclicos, tetracíclicos e pentacíclicos (PETERS *et al.*, 2005a). Os tricíclicos, tetracíclicos e pentacíclicos são os terpanos mais comuns em óleo e sedimento, especialmente os pentacíclicos.

Os **terpanos tricíclicos** (C_{19} a C_{30}) tem sua origem principal atribuída ao isoprenóide C_{30} presente na membrana de organismos procariontes, estando presentes tanto em ambiente lacustre como marinho (NETO *et al.,* 1982; PETERS *et al.,* 2005b). A distinção do petróleo formado em ambiente marinho e lacustre geralmente pode ser feita usando a razão C_{26}/C_{25} de terpanos tricíclicos (PETERS *et al.,* 2005b). Os terpanos tricíclicos C_{28} e C_{29} são usados na correlação óleo-óleo e óleo-rocha geradora. Os quatro isómeros em C-13 e C-14 (*βα*, *αα*, *αβ* e *ββ*) ocorrem em rocha imatura com predominância de *βα* e *αα*, com o aumento da maturidade o isômero *βα* torna-se predominante (PETERS *et al.,* 2005b). **Terpanos tetracíclicos** (C_{24} a C_{27}) são provavelmente hopanos degradados como é proposto por Peters *et al.* (2005b) e Philp (1985). Este último autor sugeriu que a origem dos tetracíclicos está relacionada à degradação microbiana e termal dos hopanos, onde ocorre a abertura do anel E. Conforme Brassell *et al.* (1993) há uma predominância de terpanos tetracíclicos em ambiente continental como o lacustre e deltas, sugerindo precursores terrestres. A abundância de terpanos tetracíclicos C_{24} em petróleo podem indicar rochas geradora de ambiente deposicional carbonático ou evaporítico (PETERS *et al.,* 2005b).

Os **terpanos pentacíclicos** são os biomarcadores cíclicos mais estudados usados como indicadores da origem da matéria orgânica, ambiente deposicional, evolução térmica e nível de biodegradação (WAPLES; MACHIHARA, 1991; PETERS; MOLDOWAN, 1993). Eles estão presentes em organismos procariontes e plantas superiores e aparentemente ausentes em algas eucariontes (Peters *et al.* 2005b). Os pentacíclicos mais comuns são os hopanóides (hopanos) e os não hopanóides (gamacerano e oleanano). O gamacerano é provavelmente produto da diagênese do tetrahimanol (um álcool triterpanóide) presente em sedimentos marinhos desde o Proterozóico (KILLOPS; KILLOPS, 2005) e sua alta concentração é considerado um indicador de ambiente deposicional hipersalino com estratificação da coluna d'água (PETERS *et al.,* 2005a).

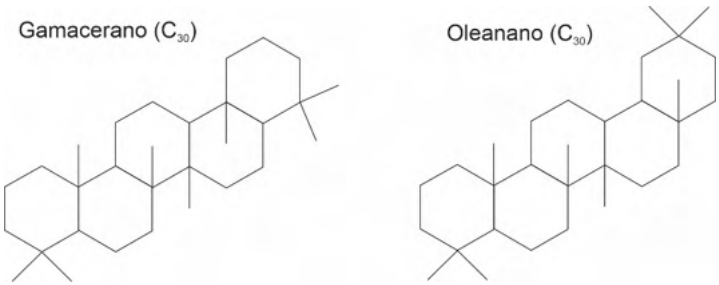

Figura 4. Estrutura do Gamacerano e Oleanano.

5.4 Hopanos

Hopanos são triterpanos pentacíclicos comuns em petróleo e rochas geradoras, formados a partir do bacteriopanotetrol (figura 5A), um composto presente na membrana celular de organismos procarióticos como bactérias e cianobactérias (GRICE; EISERBECK, 2014). Os hopanóides mais frequentemente analisados são C_{27} a C_{35} que formam uma série homóloga com as configurações 17α(H),21α(H)-, 17α(H),21β(H)-, 17β(H),21β(H)- e 17β(H),21α(H)-hopanos (Waples; Machihara 1991). A configuração biológica 17β(H),21β(H)-22R é mais instável termicamente (PETERS; MOLDOWAN, 1993). Assim, durante a diagênese os 17β(H),21β(H)-hopanos são convertidos em hopanos αβ e βα (PETERS; MOLDOWAN, 1993). Os isômeros C_{27} 17α(H)-22,29,30-Trisnorhopano (Tm) e o 18α(H)-22,29,30-Trisnorneohopano (Ts) são amplamente utilizados para caracterização da maturação térmica (figura 5B). Tm é menos estável o que promove sua redução em relação ao Ts durante a evolução térmica. Dessa forma a razão Ts/(Tm+Ts) pode ser usada para inferir o grau de maturação. Já a razão hopano C_{31}/C_{30} é um parâmetro muito útil para distinguir ambiente deposicional marinho e lacustre, principalmente associado a outros parâmetros como a razão C_{26}/C_{25} de terpanos tricíclicos (PETERS *et al.,* 2005).

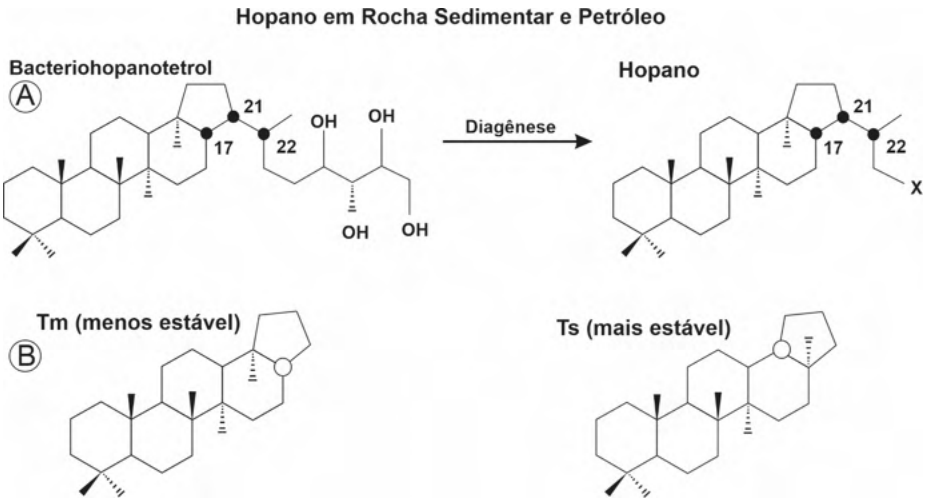

Figura 5. A) Hopano formado a partir do bacteriohopanotetrol presente na membrana lipídica de organismos procariontes. B) estrutura do 17α(H)-22, 29,30-Trisnorhopano (Tm) e o 18α(H)-22,29,30-Trisnorneohopano (Ts). (Fonte: Peters *et al.* (2005b).

5.5 Esteranos

Os esteranos (íon *m/z* 217) são hidrocarbonetos tetracíclicos saturados formados por seis unidades de isopreno. São o produto diagenético dos esteróis, encontrado nas membranas de organismos eucariontes, como algas e plantas superiores (WAPLES; MACHIHARA, 1991; GRICE; EISERBECK, 2014). A principal classe de esteranos presentes no petróleo são os Esteranos regulares (figura 6) – C_{27} (colestano), C_{28} (ergostano) e C_{29} (sitostano) presentes em variados organismos fotossintéticos (PETERS *et al.,* 2005b). A predominância de C_{27} está relacionada a material orgânico derivado de plâncton e zooplâncton, C_{28} a algas lacustres e C_{29} indica a contribuição de plantas superiores (Huang; Meinschein, 1979). A configuração 5α(H),14β(H),17β(H) ou simplesmente αββ, resultado de mudanças na estereoquímica em C-14 e C-17 dos esteróis, é um produto diagenético característico de ambiente hipersalino (WAPLES; MACHIHARA, 1991). A distribuição dos esteranos C_{27}, C_{28} e C_{29} em diagramas ternários pode ser usada para diferenciar ambientes deposicionais (marinho, lacustre, estuário, terrestre). Contudo, o principal uso da distribuição dos esteranos em diagramas ternários é para diferenciar tipos de petróleos das diferentes rochas fontes ou diferenciar as fácies orgânicas de uma mesma rocha geradora (HUANG; MEINSCHEIN, 1979; WAPLES; MACHIHARA, 1991).

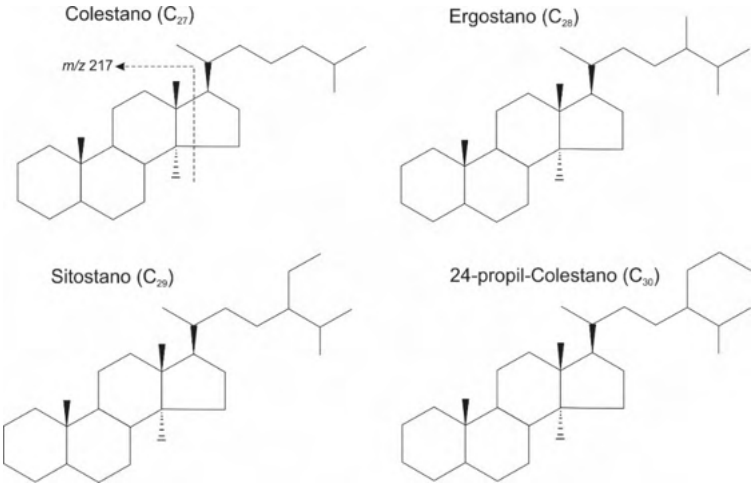

Figura 6. Estruturas dos esteranos de C_{27} a C_{30} com seus principais íons de fragmentação. Fonte: Waples e Machihara (1991).

6 I CONSIDERAÇÕES FINAIS

Ambientes deposicionais são marcados por particular assembleia de organismos, assim como condições físico-químicas. Por conseguinte, os depósitos sedimentares resultantes apresentarão biomarcadores e parâmetros moleculares característicos, devido a relativa resistência a oxidação, biodegradação e a outros processos atuantes durante a sedimentação. As principais classes de organismos produtores de matéria orgânica sedimentar são bactérias, algas e plantas superiores. Os marcadores moleculares por elas geradas, principalmente lipídicos, permitem identificar por exemplo ambiente marinho (predominância de C_{15} e C_{17}, esterano C_{27}, diasterano); sob condições hipersalinas (β-Caroteno, gamacerano); ambiente lacustre (*botryococcane*, esterano C_{28}); dominantemente anóxico (Pr/Ph <1, C_{35} 17α,21β(H)-hopano); ou óxido (Pr/Ph > 1), e; input sedimentar rico em matéria orgânica continental (predominância de *n*-C_{27}, *n*-C_{29} e *n*-C_{31}, esterano C_{29}, Filocladanos).

AGRADECIMENTOS

Ao Programa de Pós-Graduação em Geologia e Geoquímica da Universidade Federal do Pará – PPGG-UFPA.

REFERÊNCIAS

ALMEIDA, F.F.M; CARNEIRO, C. Del Ré. Inundações marinhas fanerozóicas no Brasil e recursos minerais associados. In: Mantesso-Neto V., Bartorelli A., Carneiro C.D.R., Brito Neves B.B (org.). **Geologia do Continente Sul-Americano: evolução da obra de Fernando Flávio Marques de Almeida**. Beca, p. 43-58.

BRASSELL, Simon C. Applications of biomarkers for delineating marine paleoclimatic fluctuations during the Pleistocene. In: **Organic Geochemistry**. Springer, Boston, MA, 1993. p. 699-738.

BRITO, Ailton S. et al. **Postglacial transgressive shales of Upper Devonian–Lower Carboniferous boundary of the Parnaíba Basin**. Journal of South American Earth Sciences, v. 101, p. 102621, 2020.

DEMAISON, G. J; MOORE, G. Tn. **Anoxic environments and oil source bed genesis**. AAPG Bulletin, v. 64, n. 8, p. 1179-1209, 1980.

DOW, W. G. **Kerogen studies and geological interpretations**. Journal of geochemical exploration, v. 7, p. 79-99, 1977.

DE SOUSA, Alek A.C. et al. **Aliphatic and aromatic biomarkers of the Devonian source rocks from the Western Parnaíba Basin Brazil**: Pimenteiras Formation. Journal of South American Earth Sciences, v. 99, p. 102493, 2020.

EGLINTON, Geoffrey; MURPHY, Mary Teresa Joseph (Ed.). **Organic geochemistry: methods and results.** Springer Science; Business Media, 2013.

GONZÁLEZ, Luis D. Caro; MENDONÇA FILHO, João Graciano; MASTALERZ, Maria. **Depositional environment and maturity of Devonian Pimenteira Formation in the São Luís Basin, Brazil**. International Journal of Coal Geology, v. 221, p. 103429, 2020.

GRICE, Kliti; EISERBECK, Christiane. The analysis and application of biomarkers. In: Falkowski P. and Freeman K. (2ª Ed.). **Treatise on geochemistry**. Elsevier Science, 2013. p. 47-78.

HAY, William W. Paleoceanography of marine organic-carbon-rich sediments. In: Huc A.Y. (eds.). **Paleogeography, Paleoclimate, and Source Rocks**, AAPG Studies in Geology, Oklahoma, U.S.A., The American Association of Petroleum Geologists, 1995. p. 21-62.

HUNT, John Meacham. (2ª ed.) **Petroleum geochemistry and geology**. Ed. Freeman, 743 p.1995.

KILLOPS, S.; KILLOPS, V. **Introduction to Organic Geochemistry**, 2nd edn (paperback). Blackwell Publishing company, 2005. 393 p.

Kuhn T.K., Krull E.S., Bowater A., Grice K., Gleixner G. 2010. **The occurrence of short chain n-alkanes with an even over odd predominance in higher plants and soils**. *Organic Geochemistry* 41: 88-95

LEE, Cindy. **Controls on organic carbon preservation**: The use of stratified water bodies to compare intrinsic rates of decomposition in oxic and anoxic systems. Geochimica e Cosmochimica Acta, v. 56, n. 8, p. 3323-3335, 1992.

LIBES, Susan. (2ª ed.) **Introduction to marine biogeochemistry**. Academic Press, 2009. Academic Press, Elsevier, 893 p.

NETO, F.R. Aquino; RESTLE A.; CONNAN, J.; ALBRECHT P.; Ourisson G. **Novel tricyclic terpanes (C19, C20) in sediments and petroleums**. Tetrahedron Letters, v. 23, n. 19, p. 2027-2030, 1982.

NICHOLS, Gary. **Sedimentology and stratigraphy**. John Wiley; Sons, 2009.

PETERS, Kenneth E.; CASSA, Mary Rose. Applied source rock geochemistry. In: Magoon L. B., and Dow W.G. (eds.) **The Petroleum System – From Source to Trap.** American Association of Petroleum Geologists, Tulsa, OK, 1994. p. 93–117.

PETERS, Kenneth E.; WALTERS, Clifford C.; MOLDOWAN, J. Michael. (2nd ed.). **The biomarker guide**: Volume 1, Biomarkers and isotopes in the environment and human history. Cambridge university press, 2005a.

____.____. Volume 1, Biomarkers and isotopes in the environment and human history. Cambridge university press, 2005b.

Peters Kenneth E.; Moldowan J. Michael. (eds.). **The biomarker guide**: interpreting molecular fossils in petroleum and ancient sediments. Prentice-Hall, Englewood Cliffs, NJ 1993.

PHILP, R. P. **Fossil fuel biomarkers**. Applications and spectra. Elsevier Science publisher B. 1985.

RABOUILLE, Christophe; GAILLARD, Jean-François. **Towards the EDGE**: Early diagenetic global explanation. A model depicting the early diagenesis of organic matter, O2, NO3, Mn, and PO4. Geochimica et Cosmochimica Acta, v. 55, n. 9, p. 2511-2525, 1991.

RHOADS, Donald C.; MORSE, John W. **Evolutionary and ecologic significance of oxygen-deficient marine basins**. Lethaia, v. 4, n. 4, p. 413-428, 1971.

SAGEMAN, Bradley B.; MURPHY, Adam E.; Werne, Josef P.; VER STRAETE, charles A.; HOLLANDER, David J.; LYONS, Timothy W. **A tale of shales**: the relative roles of production, decomposition, and dilution in the accumulation of organic-rich strata, Middle–Upper Devonian, Appalachian basin. Chemical Geology, v. 195, n. 1-4, p. 229-273, 2003.

SEIFERT, Wolfgang K.; MOLDOWAN, J. Michael. **The effect of biodegradation on steranes and terpanes in crude oils**. Geochimica et Cosmochimica Acta, v. 43, n. 1, p. 111-126, 1979.

SPEARS, D. A. Towards a classification of shales. **Journal of the Geological Society**, v. 137, n. 2, p. 125-129, 1980.

TISSOT, Bernard P.; WELTE, Dietrich H. (2ºEd.). **Petroleum formation and occurrence.** Berlin, Springer-Verlag, p. 699, 1984.

TUCKER, Maurice E. (3ºEd.). **Sedimentary petrology**: an introduction to the origin of sedimentary rocks. London: Blackwell Scientific Publications. 252 p. 2001.

TYSON, R. V. **Sedimentary organic matter**: organic facies and palynofacies. London, Chapman; Hall, 615 p. 1995.

WAPLES, Douglas Wendle; Machiara Tsutomu. **Biomarkers for geologists**- A practical guide to the application of steranes and triterpanes in petroleum geology. *American Association of Petroleum Geologists Bulletin,* Methods in Exploration, n.9, Oklahoma, Tulsa, 1991.

WIGNALL, Paul B.; HALLAM, A. **Anoxia as a cause of the Permian/Triassic mass extinction**: facies evidence from northern Italy and the western United States. Palaeogeography, Palaeoclimatology, Palaeoecology, v. 93, n. 1-2, p. 21-46, 1992.

CAPÍTULO XI

11. CONSIDERAÇÕES FINAIS

O início do Permiano é marcado pelos pulsos finais da glaciação carbonífera e pelos eventos orogenéticos relacionados a aglutinação das massas continentais do supercontinente Pangeia. Essas mudanças ambientais e climáticas foram registradas na sequência Gondwana I da Bacia do Paraná. Seus depósitos apresentam na base registro glaciais e o progressivo aumento das condições áridas até depósitos eólicos no topo da sequência. A sedimentação responsável pela formação da sucessão mista siliciclástica-carbonática no Cisuraliano se mostrou altamente sensível as variações climáticas desse período. A sucessão estudada engloba os depósitos heterolíticos do topo da Formação Palermo e a sequência mista siliciclástica-carbonática mista da Formação Irati até a base da Formação Serra Alta, compreendendo um total de 120m. O estudo de fácies e microfácies sedimentares somado as análises dos padrões cíclicos, carbono orgânico total, pirólise Rock-Evel e biomarcadores permitiu efetuar a reconstrução paleoambiental, definir os fatores controladores da sedimentação, posicionar a sucessão em relação a curva global do nível do mar, calcular o tempo de duração para cada hierarquia dos padrões cíclicos e espacializar o potencial gerador dos intervalos de *oil shale* da Formação Irati.

A análise faciológica corrobora as interpretações prévias que a sucessão foi gerada em uma plataforma marinha rasa. O baixo conteúdo fossilífero e bioturbações nos folhelhos cinzas a negros do Membro Taquaral depositados sob condições dominantemente subóxidas, somada a sua pouca espessura (~13 m) contudo, amplamente distribuído mostra que o contado com os depósitos heterolíticos altamente bioturbados da Formação Palermo marca o início da restrição do mar Irati com o Oceano Pantalassa. A ocorrências de fósseis tipicamente marinhos como fósseis de dentes de tubarão tipo cladodontes, restos de peixes cartilaginosos tipo *Chondrichthyes* e marcadores biomoleculares são indicativos da ainda ampla conexão oceânica. Os mesmos indicativos de conexão com o Pantalassa também são encontrados nos folhelhos cinzas a negros da base do trato de sistema de mar alto das sequências S3 e S4, indicando que apenas durante as maiores elevações do nível do mar havia conexão com o oceano.

Os folhelhos do topo do Membro Taquaral registram um progressivo aumento da salinidade identificada por marcadores moleculares (ex. Bastos et al., 2021). Essas condições hipersalinas estão relacionadas a saturação da água devido a intensificação do isolamento da bacia o que gerou condições análogas ao atual mar morto. A alta concentração de Ca^{+2}, Mg^{+2},

SO_4^{2-}, CO_3^{2-} favoreceu a precipitação de dolomita e em menor proporção gipso. A precipitação e formação das primeiras camadas carbonáticas marcam o início do Membro Assistência. O intervalo de vigência da sucessão desse membro é marcado pela dominância das condições anóxicas e hipersalinas e sedimentação mista siliciclástica-carbonática gerada até mesmo em microescala. A ausência de evidências de exposição (ex. marcas de raízes, gretas de contração) indicam que a sucessão na região centro-sul a centro-norte da bacia e região noroeste foi depositada na porção distal da bacia. A associação de fácies e microfácies identificou como formada na *mid-outer ramp* a *offshore*, com redistribuição dos sedimentos no *offshore* por correntes de turbidez. As condições de restrições tornam o mar Irati um ambiente com predominância das condições de baixa energia, onde atuação de ondas e geração de laminações cruzadas são raros. Da mesma forma, estruturas produzidas por tempestades não foram encontradas. As condições anóxicas e hipersalinas, com reduzida hidrodinâmica tornaram o ambiente hostil a proliferação biótica, principalmente nectônica e bentônica.

Análises de biomarcadores focados nos folhelhos e margas que ocorrem ciclicamente intercalados as camadas carbonáticas na região norte da bacia também indicam alta produção orgânica, hipersalinidade e anoxia. Quando comparados com as análises da borda sul e região central mostram uma alta similaridade dos parâmetros moleculares, indicando que apesar da abrangência do mar Irati, predominava condições deposicionais relativamente homogênea capaz de gerar padrões cíclicos em todo a sua extensão, da mesma forma, condições necessárias para a alta produção e preservação orgânica.

A sedimentação teve como principal controle deposicional a influência da ciclicidade climática induzida pela oscilação orbital terrestre. A variação climática induzida pela movimentação orbital controlava as oscilações do nível do mar e gerava períodos secos e períodos úmidos. As fases secas eram favoráveis a maior concentração salina, assim como precipitação bioinduzida de carbonato, devido a maior oxigenação do meio. Durante as fases úmidas o influxo de água doce diluía a salinidade, reduzindo a produção carbonática, assim como renovava os nutrientes favorecendo a produção algálica. O *imput* de água doce somado a alta produção orgânica fortalecia a estratificação da coluna d`água e a alta preservação de carbono orgânico. O início da Formação Serra Alta registra os últimos momentos que foram favoráveis a geração de camadas carbonáticas intercaladas aos folhelhos. Com o aprofundamento da bacia, a sedimentação siliciclástica dominou o ambiente.

A ciclicidade climática foi responsável pela geração de 300 pares carbonáticos-siliciclásticos, cujo empilhamento formam 59 ciclos de alta frequência, com uma média de 1 m de espessura. Estes podem ser agrupados em 20 padrões de empilhamentos, que por sua vez

compõem três ciclos de 3ªordem. A identificação da hierarquia dos ciclos foi realizada com base nas idades previamente publicadas de U-Pb SHRIMP em zircões presentes em camadas de cinzas vulcânicas intercaladas aos folhelhos negros. O controle estratigráfico permitiu a correlação da sucessão com a curva global do nível do mar. Dessa forma, os respectivos padrões de empilhamentos compõem ciclos de 3ª, 4ª e 5ª ordem. Da mesma forma, foi possível calcular 8 Ma para a duração do mar Irati e 2,7 Ma para cada ciclo de 3ªordem. O cálculo para os padrões de alta frequência identificaram os ciclos de precessão e excentricidade de curta (± 100 ka) e longa (± 400 ka) periodicidade.

REFERÊNCIAS

Afonso J.C., Cardoso J.N., Schmal M. 1991. Distribution and origin of organic Sulphur compounds in lrati shale oil. *Fuel*, **71**: 409-415.

Afonso J.C., Cardoso J.N., Schmal M. 1994. Hydrocarbon distribuition in the Irati shale oil. *Fuel,* **73**: 363-366.

Alferes C.L., Rodrigues, R., Pereira E. 2011. Geoquímica orgânica aplicada à Formação Irati, na área de São Mateus do Sul (PR), Brasil. *Geochimica Brasiliensis*, **25**(1): 47-54.

Almeida F.F.M. 1980. Tectônica da Bacia do Paraná no Brasil. Relatório da PAULPETRO n° 14091, São Paulo, 187p.

Amaral S.E. 1971. *Geologia e Petrologia da Formação Irati (Perminano) no estado de São Paulo*. PhD Thesis, Universidade de São Paulo, São Paulo, 81 p.

Araújo, L.M. 2001. *Análise da expressão estratigráfica dos parâmetros de geoquímica orgânica e inorgânica nas sequências Irati*. PhD Thesis, Universidade Federal do Rio Grande do Sul. 342 pp.

Araújo L.M., Rodrigues, R., Scherer C.M.S. 2001. Sequências deposicionais Irati: arcabouço quimioestratigráfico e inferências paleoambientais. *Ciência, Técnica, Petróleo,* **20**: 193-202.

Armstroff A., Wilkes H., Schwarzbauer J., Littke R., Horsfield B. 2006. Aromatic hydrocarbon biomarkers in terrestrial organic matter of Devonian to Permian age. *Science Direct*, **240**: 253-274.

Artur P.C. and Soares P.C. 2002. Paleoestrutuas e Petróleo na Bacia do Paraná, Brasil. *Revista Brasileira de Geociências*: **32**(4): 433-448.

Assine M.L., Soares P.C., Milani E.J. 1994. Sequências Tectono-sedimentares Mesopaleozóicas da Bacia do Paraná, Sul do Brasil. *Revista Brasileira de Geociências:* **24**(2): 77-89.

Barbosa O. and Gomes F.A. 1958. Pesquisa de petróleo na bacia do rio Corumbataí, Estado de São Paulo. *Divisão de Geologia Mineral – DNPM*, Boletim, vol. 171 40 p.

Bennett, R. H., O'Brien, N. R., and Hulbert, M. H. 1991. Determinants of clay and shale microfabric signatures: processes and mechanisms. In: Bennett R.H., Bryant W.R., Hulbert M.H., (E.ds.) Microstructure of Fine-Grained Sediments (pp. 5-32). Springer, New York, NY.

Bocardi, L. B., Rostirolla, S. P., Vesely, F. F., & França, A. B. 2009. Diagênese, contexto deposicional e história de soterramento da Formação Rio Bonito, Bacia do Paraná. *Brazilian Journal of Geology*, **39**(3), 465-478.

Calça C.P. 2008. *Microbiota fóssil em sílex da Formação Assistência (subgrupo Irati, Permiano, Bacia do Paraná) no Estado de São Paulo*. MS Dissertation, Instituto de Geociências, Universidade de São Paulo, São Paulo, 82 p.

Caputo M.V. and Crowell J.C. 1985. Migration of glacial centers across Gondwana during Paleozoic Era. *Geological Society of America Bulletin*, **96**: 1020-1036.

Caputo M.V., Melo J.H. G., Streel M., Isbell J.L. 2008. Late Devonian and early Carboniferous glacial records of South America. *Geological Society of America Special Papers*, **441:** 161-173.

Catuneanu O. (eds.). 2006. Principles of Sequence Stratigraphy. Elsevier, 375 p.

Catuneanu, O., Abreu, V., Bhattacharya, J. P., Blum, M. D., Dalrymple, R. W., Eriksson, P. G., C.R. Fielding, W.L. Fisher, W.E. Galloway, M.R. Gibling, K.A. Giles, J.M. Holbrook, R. Jordan m, C.G.St.C. Kendall, B. Macurda, O.J. Martinsen, A.D. Miall, J.E. Neal, D. Nummedal, L. Pomar, H.W. Posamentier, B.R. Pratt, J.F. Sarg, K.W. Shanley, R.J. Steel, A. Strasser x, M.E. Tucker y, C. Winker Winker, C. (2009). Towards the standardization of sequence stratigraphy. *Earth-Science Reviews,* **92**(1-2), 1-33.

Cerri, R. I., Luvizotto, G. L., Tognoli, F. M. W., Warren, L. V., Okubo, J., Morales, N. 2020. Mechanical stratigraphy and structural control of oil accumulations in fractured carbonates of the Irati Formation, Paraná Basin, Brazil. *Brazilian Journal of Geology,* **50**(3): e20190117.

Chahud A. 2007. *Paleontologia de Vertebrados da Transição entre os grupos Tubarão e Passa Dois no Centro-Leste do Estado de São Paulo*. MS Dissertation, Programa de Pós-graduação em Geologia Sedimentar. IGc-USP. São Paulo. 172p

Correa da Silva Z.C. and Cornford C. 1985. The kerogen type, depositional environment and maturity, of the Irati Shale, Upper Permian of Paraná Basin, Southern Brazil. *Org. Geochem.,* **8**: 399-411.

Crivellani K. 2016. *Análise de parametros geoquímicos de rochas, óleos e betumes em afloramentos das formações Irati e Pirambóia na borda leste da bacia do Paraná, São Paulo, Brasil*. MS Dissertation, Instituto de Geociências, Universidade Federal da Bahia, Salvador, 85 p.

Daemon, R. F. 1996. Ensaio sobre a distribuição e zoneamento dos esporomorfos do Paleozóico Superior da Bacia do Paraná. *Boletim Técnico da PETROBRAS*, **9**(2): 211-218.

Dickson, J.A.D. 1966. Carbonate identification and genesis as revealed by staining. *J. Sediment. Petrol.* **36**, 491–505.

Dos Anjos, C. W. D., Meunier, A., Guimarães, E. M., & El Albani, A. 2010. Saponite-rich black shales and nontronite beds of the Permian Irati Formation: sediment sources and thermal metamorphism (Paraná Basin, Brazil). *Clays and Clay Minerals*, **58**(5), 606-626.

Dunham, R. 1962. Classification of carbonate rocks according to deposicional texture. *In:* Ham, W. (ed). Classification of carbonate rocks. Tulsa: AAPG. (Memoir 1). p. 108-121. Embry & Klovan (1971).

Embry, A. Klovan, J. 1971. Late Devonian reef tracts on northeastern Banks Islands, Northwest Territories. *Canadian Petrology and Geology Bulletin*, **19**:730-781.

Espitalié J., Laporte J. L., Madec M., Marquis F., Leplat P., Paulet J., Boutefeu A. 1977. Méthode rapide de caractérisation des roches mètres, de leur potentiel pétrolier et de leur degré d'évolution. *Revue de l'Institut français du Pétrole*, **32**(1): 23-42.

Flügel, E. (ed.) 2004. Microfacies of carbonate rocks: analysis, interpretation and application. London. Springer Verlag. 995p.

Franco, N., Kalkreuth, W. and Peralba, M.D.C.R**.** 2010. Geochemical characterization of solid residues, bitumen and expelled oil based on steam pyrolysis experiments from Irati oil shale, Brazil: A preliminary study. *Fuel*, **89**, 1863-1871.

Gilbert J.M., De Andrade Bruning I.M.R., Nooner D.W., J. Oró. 1975. Predominance of isoprenoids among the alkanes in the Irati oil shale, permian of Brazil. *Chemical Geology*, **15**: 209-215.

Goldberg, K., 2001. *The Paleoclimatic Evolution of the Permian in the Paraná Basin in Southern Brazil*. PhD Thesis. University of Chicago, Chicago, pp. 267p.

Goldberg K. and Humayun M. 2016. Geochemical paleoredox indicators in organic-rich shales of the Irati Formation, Permian of the Paraná Basin, southern Brazil. *Brazilian Journal of Geology*, **46**(3): 377-393**.** DOI: 10.1590/ 2317- 4889201620160001.

Goldhammer, R.K., Lehmann, P.J. and Dunn, P.A. 1993. The origin of high-frequency platform carbonate cycles and third-order sequences (Lower Ordovician El Paso Gp., west Texas): constraints from outcrop data and stratigraphic modelling. *J. Sed. Petrol.*, **63**, 318–359

Golonka, J., and Ford, D., 2000, Pangean (Late Carboniferous–Middle Jurassic) paleoenvironment and lithofacies. *Palaeogeography, Palaeoclimatology, Palaeoecology*, **161:** 1-34.

Goulart E.P., Jardim N.S. 1982. Avaliação geoquímica das Formações Ponta Grossa e Irati - Bacia do Paraná. *In*: *Geologia da Bacia do Paraná: Reavaliação da potencialidade e prospectividade em hidrocarbonetos*, PAULIPETRO - Consórcio CESP IPT, São Paulo, p. 41-74.

Hachiro 1991. *Litotipos, associações faciológicas e sistemas deposicionais da formação Irati no Estado de São Paulo*. MS Dissertation, Instituto de Geociências, Universidade de São Paulo, São Paulo, 191p.

Hofmann, Richard. 2016. The end-Permian mass extinction. *In*: Mángano, M. G., & Buatois, L. A. (Eds.). *The Trace-Fossil Record of Major Evolutionary Events*. Springer, Dordrecht, p. 325-349.

Holz, M., 1997. Early Permian Sequence stratigraphy and paleophisiography of the Paraná Basin in northeastern Rio Grande do Sul state, Brazil. *Anais da Academia Brasileira de Ciências* **69** (4): 521–543.

Holz, M., 1998. The Eo-Permian coal seams of the Paraná Basin in southernmost Brazil: an analysis of the depositional conditions using sequence stratigraphic concepts. *International Journal of Coal Geology* **36**(1– 2): 141– 163.

Holz, M., 2003. Sequence stratigraphy of a lagoonal estuarine system – an example from the lower Permian Rio Bonito Formation, Paraná Basin, Brazil. *Sedimentary Geology*, **162**(3–4): 301–327.

Holz M., França A.B., Souza P.A., Iannuzzi R., Rohn R. 2010. A stratigraphic chart of the Late Carboniferous/Permian succession of the eastern border of the Paraná Basin, Brazil, South America. *Journal of South American Earth Sciences*, **29**: 381-399.

Husinec, A., Basch, D., Rose, B., Read, J. F. 2008. FISCHERPLOTS: An Excel spreadsheet for computing Fischer plots of accommodation change in cyclic carbonate successions in both the time and depth domains. *Computers & geosciences*, **34**(3): 269-277.

Jarvie D.M. 1991. Total Organic carbono (TOC) analysis. In: Merril R.K. (ed) Source and Migration Processes and Evaluation Techniques, Treatise of Petroleum Geology. American AssociationofPetroleumGeologists, Tulsa, p. 113-118.

Jasper A., Menegat R., Guerra-Sommer M., Cazzulo-Klepzig M., Souza P.A. 2006. Depositional cyclicity and paleoecological variability in an outcrop of Rio Bonito formation, Early Permian, Parana´ Basin, Rio Grande do Sul, Brazil. *Journal of South American Earth Sciences*, **21**: 276-293.

Kiehl, J.T. and Shields C.A. 2005. Climate simulation of the latest Permian: Implications for mass extinction. *Geology*, **33**(9):757–760.

Kuehl, S.A., Hariu, T.M., Sanford, M.W., Nittrouer, C.A., Demaster, D.J., 1991. Millimeter scale sedimentary structure of fine-grained sediments: Examples from continental margin environments, *In*: Bennett, R.H., Bryant, W.R., and Hulbert, M.H., (eds.) *Microstructure of Fine-Grained Sediments*: New York, Springer-Verlag, p. 33–45.

Kutzbach, J.E., and Gallimore, R.G., 1989. Pangaean climates: Megamonsoons of the megacontinent: *Journal Geophysical Research*, **94**: 3341- 3357.

Lages L.C. 2004. *A formação Irati (grupo passa dois, permiano, bacia do Paraná) no furo de sondagem FP-01-PR (Sapopema, PR)*. MS Dissertation, Instituto de Geocincias e Ciências Exatas, Universidade Estadual Paulista, Rio Claro, 117p.

Lisboa A.C. 2006. *Caracterização Geoquímica Orgânica dos Folhelhos Neopermianos da Formação Irati- Borda Leste da Bacia do Paraná, São Paulo*. MS Dissertation, Universidade Federal do Rio de Janeiro, 171 p.

López-Gamundi, O. R., & Rossello, E. A. 1993. Devonian-Carboniferous unconformity in Argentina and its relation to the Eo-Hercynian orogeny in southern South America. *Geologische Rundschau*, **82**(1): 136-147.

Magoon L.B. and Dow W.G. (eds.). 1991. *The Petroleum SystemFrom Source to Trap*. AAPG Bulletin-American Association of Petroleum Geologists, United States, **71**, 639 p.

Meyer, K.M., Kump, L.R., Ridgwell, A. 2008. Biogeochemical controls on photic-zone euxinia during the end-Permian mass extinction. *Geology*, **36**(9):747-750.

Mezzalira S. 1971. Contribuição ao conhecimento da geologia de subsuperfície e da paleontogia da Formação Irati no Estado de São Paulo. *In:* Simpósio de paleontologia, Rio de Janeiro, *Anais...*, v.43, p. 273-336.

Milani, E.J. 1997. *Evolução tectono-estratigráfica da Bacia do Paraná e seu relacionamento com a geodinâmica fanerozóica do Gondwana sul-ocidental*. PhD Thesis, Universidade Federal do Rio Grande do Sul, Porto Alegre.

Milani E.J. 2004. Comentários sobre a origem e a evolução tectônica da Bacia do Paraná. *In*: Mantesso Neto V., Bartorelli A., Carneiro C.D.R., Brito Neves B.B. (eds). *Geologia do continente sul-americano: evolução da obra de Fernando Flávio Marques de Almeida*. São Paulo, Beca, p. 265-279.

Milani E.J., Assine M.L., Soares P.C., Daemon R.F. 1995. A sequência Ordovício-siluriana da Bacia do Paraná. *Boletim de Geociências da PETROBRÁS*, **9**(2/4): 301-320.

Milani E. J., França A. B., Schneider R. L. 1994. Bacia do Paraná. *Boletim de Geociências da PETROBRÁS*, **8**: 69-82.

Milani, E.J., Melo, J.H.G., Souza, P.A, Fernandes, L.A. and França A.B 2007a. Bacia do Paraná. *B. Geoci. Petrobras*, Rio de Janeiro, **15**, 265-287.

Milani E.J. and Ramos V.A. 1998. Orogenias paleozóicas no domínio sul-ocidental do Gondwana e os ciclos de subsidência da Bacia do Paraná. *Revista Brasileira de Geociências*, **28**(4): 473-484.

Milani, E. J.; Faccini, U. F.; Scherer, C. M. S.; Araújo, L. M.; Cupertino, J. A. 1998. Sequences and stratigraphic hierarchy of the Paraná Basin (Ordovician to Cretaceous), Southern Brazil. Boletim IG-USP, São Paulo, p. 125-173. (Série Científica, n. 29).

Milani E.J., França A.B., Medeiros R.A. 2007b. Rochas geradoras e rochas-reservatório da Bacia do Paraná, faixa oriental de afloramentos, Estado do Paraná. *Boletim de Geociências da PETROBRÁS*, **15**: 135-162.

Neto C.C. 1983. Geochemistry of Brazilian Oil Shales. *American Chemical Society*, **230**: 13-35.

Neto, C. C., Furtado, E. G., Concha, F. J. M., Cardoso, J. N., Quadros, L. P. 1978. Anomalies in the stratigraphic distribution of hydrocarbons in the Irati oil-shale. *Chemical Geology*, ***23***(1-4): 181-192.

Netto, R.G. 1994. *A paleoicnologia como ferramenta de trabalho na sequência sedimentar Rio Bonito/Palermo*. PhD Thesis, Universidade Federal do Rio Grande do Sul, Instituto de Geociências, Porto Alegre-Brasil, 272 p

Nomura S.F., Sawakuchi A.O., Bello R.M.S., Méndez-Duque, Fuzikawa K. 2014. Paleotemperatures and paleofluids recorded in fluid inclusions from calcite veins from the northern flank of the Ponta Grossa dyke swarm: Implications for hydrocarbon generation and migration in the Paraná. *Marine and Petroleum Geology*, **52:** 107-124.

Ogg, J. G., Ogg, G., & Gradstein, F. M. 2016. A concise geologic time scale: 2016. Elsevier.

Padula V.T. 1968. Estudos geológicos da formação Irati-sul do Brasil. *Boletim de técnico da PETROBRÁS*, **11**(3): 407-430.

Parrish, J.T., 1993. Climate of the Supercontinent Pangea: The Journal of Geology, **101**:215-233.

Potter, P. E., Maynard, J. B., & Pryor, W. A. 1980. Sedimentology of shale: study guide and reference source. Springer Science & Business Media. 327p.

Quintas M.C.L., Mantovani M.S.M., Zalán P.V. 1999. Contribuição ao estudo da evolução mecânica da Bacia do Paraná. *Revista Brasileira de Geociências*, **29**(2): 217-226.

Ramos, A.S., Rodrigues, L. F., de Araujo, G. E., Pozocco, C. T., Ketzer, J. M., Heemann, R., Lourega, R. V. 2015. Geochemical characterization of Irati and Palermo formations (Paraná Basin–Southern Brazil) for shale oil/gas exploration. *Energy Technology*, **3**(5): 481-487.

Reis D.E.S., Rodrigues R., Moldowan J.M., Jones C.M., Brito M., Cavalcante D.C., Portela H.A. 2018. Biomarkers stratigraphy of Irati Formation (Lower Permian) in the southern portion of Paraná Basin (Brazil). *Marine and Petroleum Geology*, **95**: 110-138. DOI: https://doi.org/10.1016/j.marpetgeo.2018.04.007

Ribas L., Neto J.M.R., França A.B., Porto Alegre H.K. 2017. The behavior of Irati oil shale before and after the pyrolysis process. Journal of Petroleum Science and Engineering, **152**: 156-164. DOI: http://dx.doi.org/10.1016/j.petrol.2017.03.007

Rohn R., Lages L.C., Penattr J.R.R. 2003. Litofácies da formação Irati no furo de sondagem FP-01-PR (Permiano, borda leste da Bacia do Paraná). *In:* Congresso Brasileiro de P&D em Petróleo & Gás. Rio Janeiro, v. 2, p. 1-6.

Rohn R. 2007. The Passa Dois group (Paraná Basin, Permian): investigations in progress. *In*: Ianuzzi, R., Boardman, D.R. (Eds.), *I Workshop - Problems in Western Gondwana Geology, South America - Africa Correlations*: Du Toit Revisited. Petrobrás, Gramado, pp. 151–157.

Sadler, P. M., Osleger, D. A., & Montanez, I. P. 1993. On the labeling, length, and objective basis of Fischer plots. *Journal of Sedimentary Research*, **63**(3): 360-368.

Santos R.V., Dantas E.L., Olveira C.G., Alvarenga C.J.S., Anjos C.W.D., Guimarâes E.M., Oliveira F.B. 2009. Geochemical and thermal effects of a basic sill on black shales and limestones of the Permian Irati Formation. *Journal of South American Earth Sciences*, **28**: 14-24.

Santos, R. V., Souza, P. A., de Alvarenga, C. J. S., Dantas, E. L., Pimentel, M. M., de Oliveira, C. G. and de Araújo, L. M. 2006. Shrimp U–Pb zircon dating and palynology of bentonitic layers from the Permian Irati Formation, Paraná Basin, Brazil. *Gondwana research*, **9:** 456-463.

Santos Neto, E.V., Cerqueira, J.R., 1993. Aplicação da Geoquímica Orgânica na cronoestratigrafia e paleogeografia da Formação Irati. *In*: Simpósio Sobre Cronoestratigrafia da Bacia Do Paraná, 1, vol. 1. UNESP, pp. 71 Rio Claro. *Anais*…Rio Claro.

Schieber, J. 2011. Reverse engineering mother nature: shale sedimentology from an experimental perspective: *Sedimentary Geology*, **238:** 1–22.

Schieber, J., Sur, S. and Banerjee, S. 2007. Benthic microbial mats in black shale units fromthe Vindhyan Supergroup, Middle Proterozoic of India: the challenges of recognizing the genuine article. In: Atlas of Microbial Mat Features Preserved within the Clastic Rock Record (Eds. Schieber, J., et al.). *Elsevier, Amsterdam*, pp. 189–197.

Schieber, J., Southard, J.B. and Schimmelmann, A. 2010. Lenticular shale fabrics resulting from intermittent erosion of muddy sediments - comparing observations from flume experiments to the rock record. *Journal of Sedimentary Research* **80:** 119–128

Schneider, R.L., Muhlmann H., Tommasi E., Medeiros R.A., Daemon, R.A., Nogueira, A.A 1974. Revisão estratigráfica da Bacia do Paraná. *In:* Congresso Brasileiro de Geologia, 28 Porto alegre. *Anais...* v.1, p 41-65.

Schwarzacher, W. 2000. Repetitions and cycles in stratigraphy. Earth-Science Reviews, **50**(1-2): 51-75.

Soares P.C., Soares A.P., Bettú D.F. 2014. Formação da sequência triássico-jurássica na Bacia do Paraná. *Boletim de Geociências da Petrobrás*, **22**(1): 135-160.

Stanley S. M. (eds.). 2009. Earth System History, third edition. New York, W. H. Freeman and Company, 580p.

Stow, D. V., & Piper, D. W. 1984. Fine-grained sediments: deep-water processes and facies: Proceedings and discussion of the International workshop, held Halifax, Canada, in August 1982. Special Publication-Geological Society of London, (15).

Strasser, A., Hilgen, F. J., & Heckel, P. H. 2006. Cyclostratigraphy–concepts, definitions, and applications. *Newsletters on Stratigraphy*, **42**(2): 75-114.

Thomaz Filho, A., Mizusaki, A. M. P., & Antonioli, L. 2008. Magmatism and petroleum exploration in the Brazilian Paleozoic basins. *Marine and Petroleum Geology*, **25**(2): 143-151.

Tognoli, F.M.W.; Netto, R.G. 2003. Ichnological signature of Paleozoic estuarine deposits from the Rio Bonito-Palermo succession, eastern Paraná Basin, Brazil. *In:* Buatois, L.A. (ed.) Mángano, M.G. Icnología: Hacia una convergencia entre Geologia y Biologia. Asociación Paleontológica ArgentIna, Publicación Especial 9: 141-155.

Turner, S., Regelous, M., Kelley, S., Hawkesworth, C., Mantovani, M. 1994. Magmatism and continental break-up in the South Atlantic: high precision ^{40}Ar-^{39}Ar geochronology. *Earth and Planetary Science Letters*, **121**(3-4): 333-348.

Walker R.G. and James N.P. (eds.). 1992. *Facies Models Response to sea level change*. Ontario, Geological Association of Canada, 409 p.

Wicander, R., & Monore, J. S. 2010. Historical Geology: Evolution of Earth and Life Through Time: Brook. Cole, Cengage Learning, Belmont. 463p.

Wiens, F. Estratigrafia fanerozoica resumida del Paraguay. Asunción: Geoconsultores, 1990. 6 p.

Xavier P.L.A., Silva A.F., Soares M.B., Horn B.L.D., Schultz C.L. 2018. Sequence stratigraphy control on fossil occurrence and concentration in the epeiric mixed carbonate-siliciclastic ramp of the Early Permian Irati. *Journal of South American Earth Sciences*, **88**: 157-178.

Zacharias, A. Á. (2004). *Preenchimento de vales incisos por associações de fácies estuarinas, Formação Rio Bonito, Nordeste do Paraná*. MS Dissertation. Instituto de Geociências e Ciências Exatas , UNESP - Universidade Estadual Paulista, 112p.

Zacharias A.A. and Assine M.L. 2005. Modelo de preenchimento de vales incisos por associações de fácies estuarinas, formação Rio Bonito no norte do estado do Paraná. *Revista Brasileiro de Geociências*, **35**(4): 573-583.

Zalán, P. V. 1991. Influence of pre-Andean orogenies on the Paleozoic intracratonic basins of South America. AAPPG Bulletin.

Zalán, P. V., Wolff, S., Astolfi, M. A. M., Vieira, I. S., Conceição, J. C. J., Appi, V. T., Santos Neto, E. V., Cerqueira, J. R. and Marques, A. 1990. The Paraná Basin, Brazil. *In:* Leighton, M. W., Kolata, D. R., Oltz, D. F., Eidel, J. J. (Eds.) Interior cratonic basins. Tulsa: American Association of Petroleum Geologists. AAPG. Memoir, 51. pp. 681-708.

APÊNDICE A

Supplementary Material

12. Biomarker Profile of Organic-Rich Shale from the Permian Irati Formation, Paraná Basin: Statistical and Paleoenvironment Implications of High Organic Matter Production within a Shallow and Cyclic Carbonate-Shale Sequence

Table 1. TOC content and pyrolysis analysis parameters from rocks of Irati Formation.

Parameters	**Samples**													
	SCb-01	**SCb-02**	**SCb-03**	**SCb-04**	**SCb-05**	**SCb-06**	**SCb-07**	**SCb-08**	**SCb-09**	**SCb-10**	**SCb-11**	**SCb-12**	**SCb-13**	**SCb-14**
Distance from diabase intrusion (m)	*0.20*	*1.00*	*1.68*	*2.55*	*2.93*	*3.43*	*3.49*	*3.99*	*4.14*	*4.56*	*5.58*	*6.72*	*7.21*	*8.41*
TOC	0.59	0.95	1.66	2.97	2.51	1.49	3.18	0.78	2.22	1.85	0.92	2.80	1.47	1.80
S_1	0.03	0.07	3.15	3.27	2.95	2.98	5.49	1.33	3.67	2.14	1.04	4.19	2.54	2.28
S_2	0.03	0.22	5.55	5.97	4.52	4.19	12.45	2.00	4.54	2.72	1.97	6.06	2.99	2.54
S_3	0.22	0.19	0.29	0.32	0.24	0.12	0.24	0.16	0.25	0.42	0.18	0.28	0.25	0.50
Tmax	607	403	356	336	325	332	355	328	318	302	329	303	302	300
PI	0.50	0.24	0.36	0.35	0.39	0.42	0.31	0.40	0.45	0.44	0.35	0.41	0.46	0.47
HI	5	23	334	201	180	281	392	257	205	147	213	216	203	141
OI	37	20	17	11	10	8	8	21	11	23	20	10	17	28
Bitumen	0.02	0.03	0.90	1.52	1.18	0.56	1.55	0.24	0.89	0.92	0.57	1.14	0.44	0.82
HC	0.014	0.016	0.11	0.19	0.16	0.15	0.24	0.15	0.21	0.19	0.22	0.14	0.13	0.12
Bitumen/TOC	0.03	0.03	0.54	0.51	0.47	0.38	0.49	0.31	0.40	0.50	0.62	0.41	0.30	0.46

TOC: Total Organic Carbon (wt%); **S_1:** free hydrocarbon (HC) content; (mg HC/g rock); **S_2:** remaining HC generative potential; (mg HC/g rock); **S_3:** oxygen content. (mg HC/g rock); **PI:** Production Index=$S_1/(S_1+S_2)$; **HI:** Hydrogen Index = S_2 x 100/TOC (mg HC/g rock); **OI:** Oxygen Index = S_3 x 100/TOC (mg HC/g rock); **Bitumen:** dichloromethane: methanol 12% extract %; **HC:** total hydrocarbon (wt%).

Table 2. Biomarker parameters of thermal maturity of the organic matter organic matter extracted from rocks of Irati Formation.

Parameters	Samples													
	SCb-01	**SCb-02**	**SCb-03**	**SCb-04**	**SCb-05**	**SCb-06**	**SCb-07**	**SCb-08**	**SCb-09**	**SCb-10**	**SCb-11**	**SCb-12**	**SCb-13**	**SCb-14**
CPI	0.77	1.02	0.67	0.65	0.77	0.68	0.68	0.56	0.63	0.63	0.45	0.53	0.67	0.61
OEP	1.16	1.09	0.77	0.65	0.64	0.75	0.66	0.65	0.70	0.68	0.61	0.60	0.74	0.67
T_s/T_m	0.23	0.41	0.11	0.05	0.08	0.08	0.10	0.04	0.07	0.16	0.31	0.06	0.32	0.15
$T_s/(T_s+T_m)$	0.18	0.39	0.10	0.04	0.07	0.08	0.09	0.03	0.07	0.14	0.24	0.05	0.25	0.17
C_{30} βα/(αβ+βα)	0.19	0.10	0.26	0.29	0.29	0.21	0.27	0.21	0.25	0.23	0.23	0.24	0.21	0.20
C_{31} αβ S/(S+R)	0.37	0.55	0.47	0.43	0.41	0.33	0.29	0.37	0.31	0.30	0.29	0.26	0.26	0.27
C_{32} αβ S/(S+R)	0.39	0.55	0.50	0.42	0.41	0.41	0.39	0.37	0.38	0.38	0.31	0.32	0.45	0.44
C_{35} αβ S/(S+R)	0.33	0.55	0.50	0.43	0.42	0.41	0.36	0.39	0.40	0.38	0.38	0.30	0.40	0.42
C_{27} S/(S+R)	0.20	0.33	0.24	0.21	0.30	0.20	0.18	0.24	0.17	0.19	0.19	0.15	0.17	0.14
C_{29} S/(S+R)	0.20	0.36	0.31	0.23	0.23	0.21	0.18	0.19	0.17	0.20	0.11	0.14	0.12	0.12
C_{29} ββS/(αββ+ααα)	0.27	0.24	0.27	0.25	0.27	0.28	0.29	0.23	0.26	0.27	0.25	0.26	0.30	0.31
MA(I)/MA(I+II)	-	-	0.04	0.05	0.05	0.10	0.05	0.20	0.12	0.09	0.16	0.09	0.16	0.05
TA(I)/TA(I+II)	-	-	0.12	0.56	0.09	0.49	0.12	0.50	0.27	0.38	0.42	0.28	0.64	0.33
RMP	2.78	1.84	1.88	2.37	1.55	1.32	1.52	1.34	1.71	1.37	1.21	1.32	1.22	1.11
MPI-1	0.92	0.39	0.72	0.81	0.65	0.31	0.60	0.80	0.67	0.75	0.82	0.37	0.43	0.28
MPI-2	1.09	0.46	0.82	0.92	0.74	0.37	0.70	0.89	0.77	0.85	0.91	0.43	0.50	0.34
MPI-3	2.54	1.37	1.21	1.36	1.14	1.12	1.14	1.13	1.26	1.11	1.06	0.91	0.98	0.85

CPI: 2x(C_{23}+C_{25}+C_{27}+C_{29})/[C_{22}+2(C_{24}+C_{26}+C_{28})+C_{30}] in TIC; **OEP:** (C_{21}+6C_{23}+C_{25})/(4C_{22}+4C_{24}) in TIC; **T_s/T_m:** C_{27} 18α(H)-22,29,30-trisnorneohopane/C_{27} 17α(H)-22,29,30-trisnorhopane in *m/z* 191; **$T_s/(T_s+T_m)$:** C_{27} 18α(H)-22,29,30-trisnorneohopane/[(C_{27} 18α(H)-22,29,30-trisnorneohopane + C_{27} 17α(H)-22,29,30-trisnorhopane)] in *m/z* 191; **C_{30} βα/(αβ+βα):** C_{30}-17β(H),21α(H)-moretane/(C_{30}-17α(H),21β(H)- hopane + C_{30}-17β(H),21α(H)- moretane) in *m/z* 191; **C_{31} αβ S/(S+R):** C_{31}- 17α(H),21β(H)-homohopane 22S/(C_{31}- 17α(H),21β(H)-homohopane 22S + C_{32}-17α(H),21β(H)-homohopane 22R) in *m/z* 191; **C_{32} αβ S/(S+R):** C_{32}- 17α(H),21β(H)-bishomohopane 22S/(C_{32}- 17α(H),21β(H)-bishomohopane 22S + C_{32}- 17α(H),21β(H)-bishomohopane 22R) in *m/z* 191; **C_{35} αβ S/(S+R):** C_{35}- 17α(H),21β(H)- pentakishomohopane 22S/(C_{35}- 17α(H),21β(H)- pentakishomohopane 22S + C_{35}- 17α(H),21β(H)- pentakishomohopane 22R) in *m/z* 191; **C_{27} S/(S+R):** C_{27} 5α(H),14α(H),17α(H)-cholestane R/ C_{29} 5α(H),14α(H),17α(H)-stigmastane R in *m/z* 217; **C_{29} S/(S+R):** C_{27} 5α(H),14α(H),17α(H)-cholestane S/(C_{27} 5α(H),14α(H),17α(H)-cholestane S + C_{27} 5α(H),14α(H),17α(H)-cholestane R) in *m/z* 217; **C_{29} ββS/(αββ+ααα):** C_{29} 5α(H),14α(H),17α(H)-stigmastane S/(C_{29} 5α(H),14α(H),17α(H)-stigmastane S + C_{27} 5α(H),14α(H),17α(H)-stigmastane R) in *m/z* 217; **MA(I)/MA(I+II):** C_{21}-Monoaromatic sterane + C_{22}-Monoaromatic sterane)/(C_{27}- Monoaromatic sterane + C_{28}-Monoaromatic sterane + C_{29}-Monoaromatic sterane) in *m/z* 253; **TA(I)/TA(I+II):** C_{20}-Triaromatic sterane + C_{21}-Triaromatic sterane)/(C_{26}- Triaromatic sterane + C_{27}-Triaromatic sterane + C_{28}-Triaromatic sterane) in *m/z* 231; **RMP:** 2-MP/1-MP, *m/z* 192; **MPI-1:** 1,5(2-MP+ 3-MP)/(P + 1-MP + 9-MP), *m/z* 192; **MPI-2:** 1,89(2-MF+3-MP)/[P+1,26(1-MP+9-MP), *m/z* 192; **MPI-3:** (2-MP+3-MP)/(1-MP+9-MP), *m/z* 192.

Table 3. Biomarker parameters of biological source and depositional environment of the organic matter extracted from rocks of Irati Formation.

Parameters	Samples													
	SCb-01	**SCb-02**	**SCb-03**	**SCb-04**	**SCb-05**	**SCb-06**	**SCb-07**	**SCb-08**	**SCb-09**	**SCb-10**	**SCb-11**	**SCb-12**	**SCb-13**	**SCb-14**
TAR	1.18	1.08	0.99	0.65	0.65	0.44	0.40	0.11	0.22	0.29	0.22	0.33	0.20	0.28
C_{13-18}	16.35	14.53	20.47	27.87	28.90	35.80	32.26	53.81	37.78	34.56	45.58	30.75	44.85	38.16
C_{19-24}	39.02	49.42	33.60	35.95	33.98	30.44	37.20	31.68	38.76	37.76	30.98	38.21	35.03	34.05
C_{25-33}	44.63	36.05	45.93	36.18	37.13	33.76	30.54	14.51	23.46	27.68	23.44	31.04	20.13	27.80
Pr/Ph	0.76	0.68	0.62	0.65	0.65	0.70	0.66	0.70	0.74	0.72	0.70	0.44	0.65	0.53
Pr/(Pr+Ph)	0.43	0.40	0.38	0.40	0.39	0.41	0.40	0.41	0.43	0.42	0.41	0.31	0.39	0.35
Pr/*n*-C_{17}	1.49	2.00	2.85	2.22	1.47	2.36	1.93	0.74	1.72	1.77	1.31	1.45	1.38	1.37
Ph/*n*-C_{18}	2.62	2.60	6.85	6.57	5.84	6.72	8.80	2.50	5.65	5.48	2.63	8.25	4.34	5.48
***i*G**	41.55	33.24	61.39	61.95	49.58	24.23	44.77	105.52	28.96	25.01	38.17	73.75	29.16	43.28
C_{31}R/C_{30}Hop	0.33	0.09	0.60	0.57	0.58	0.43	0.49	0.31	0.43	0.44	0.43	0.39	0.12	0.31
Hop/Ster	1.97	3.01	1.20	1.88	2.28	1.43	1.51	1.98	1.38	0.88	1.29	1.49	2.42	0.84
C_{27}/C_{29}	1.42	1.58	0.98	1.31	0.50	1.50	1.36	1.59	1.35	1.56	1.34	1.55	1.24	1.36
DBT/P	0.06	0.46	1.03	0.51	1.87	1.09	1.51	1.26	1.32	1.34	0.20	2.11	2.06	1.65

TAR: (C_{27}+C_{29}+C_{31})/(C_{15}+C_{17}+C_{19}) in TIC; **C_{13-18}:** Relative percentage of *n*-alkanes in the range of *n*-C_{13-18} in TIC; **C_{19-24}:** Relative percentage of *n*-alkanes in the range of *n*-C_{19-24} in TIC; **C_{25-33}:** Relative percentage of *n*-alkanes in the range of de *n*-C_{25-33} in TIC; **Pr/Ph:** Pristane/Phytane in TIC; **Pr/(Pr+Ph):** Pristane/(Pristane+Phytane) in TIC; **Pr/*n*-C_{17}:** Pristane/*n*-heptadecane (C_{17}) in TIC; **Ph/*n*-C_{18}:** Phytane/ *n*-octadecane (C_{18}) in TIC; ***i*G:** 100 × [Gammacerane/ Gammacerane + C_{30} 17α(H),21β(H)-hopane)] in *m/z* 191; **C_{31}R/C_{30}Hop:** C_{31}- 17α(H),21β(H)-homohopane 22R/ C_{30} 17α(H),21β(H)-hopane)] in *m/z* 191; **Hop/Ster:** (C_{30} 17α(H),21β(H)-hopane in *m/z* 191)/(C_{27} 20S 5α(H),14α(H),17α(H)-cholestane 20R+20S) in *m/z* 217; **C_{27}/C_{29}**: C_{27} 5α(H),14α(H),17α(H)-cholestane R/ C_{29} 5α(H),14α(H),17α(H)-stigmastane R in *m/z* 217; **DBT/P:** dibenzothiophene in *m/z* 184/phenanthrene in *m/z* 178.

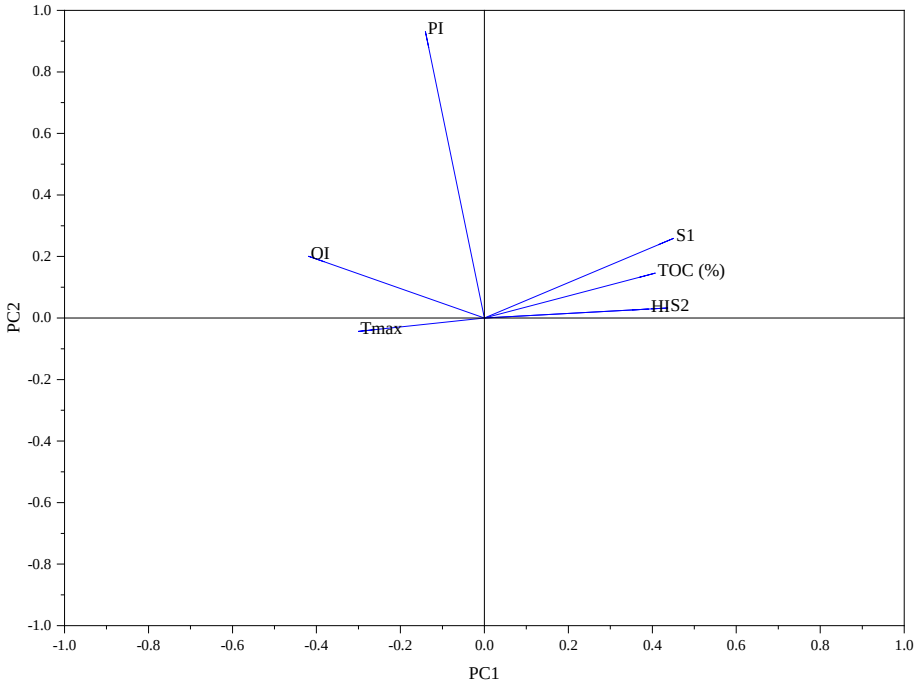

Figure 1. Factor loadings for the PCA (TOC, S1, S2, HI, OI, PI and Tmax).

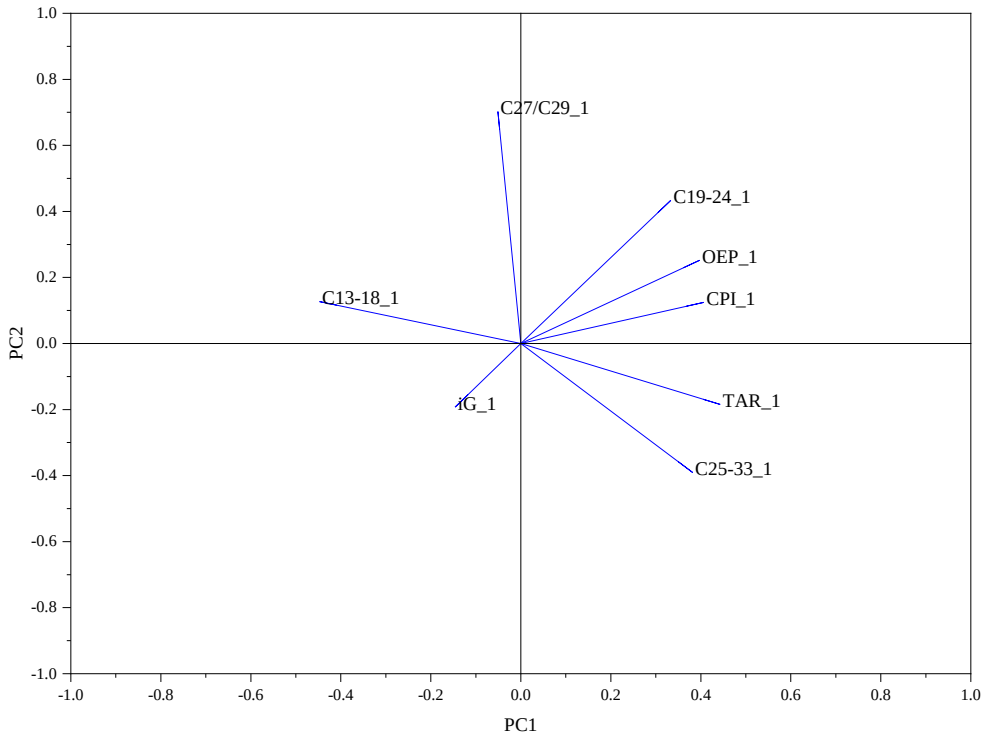

Figure 2. Factor loadings for the PCA (CPI, OEP, TAR, $C_{13\text{-}18}$, $C_{19\text{-}24}$, $C_{15\text{-}33}$, *i*G and C_{27}/C_{29} sterane ratio).

APÊNDICE B

Supplementary Material

Permian organic-rich shale within a mixed carbonate-siliciclastic system from an epicontinental sea in the West Gondwana, Paraná Basin, Southern Brazil: Paleoenvironmental and geochemical reconstruction

Table of contents

Table 01. Geochemical data of the P3B-12-001 (P001), P3B-12-043 (43), and P3B-12-047 (P47).

HOLE	DEPTH	S1	S2	S3	TOC	Tmax(°C)	HI	OI	PI	CARB(%)
P3B-12-001	69,19	0,18	1,41	1,50	0,76	437,00	186,26	198,15	0,11	8,68
P3B-12-001	69,59	6,76	92,40	1,73	13,62	427,00	678,31	12,70	0,07	6,92
P3B-12-001	70,03	8,66	105,17	1,49	16,22	427,00	648,28	9,18	0,08	6,86
P3B-12-001	70,35	8,33	80,86	1,52	12,50	427,00	646,88	12,16	0,09	5,61
P3B-12-001	70,73	7,04	60,82	1,60	9,31	428,00	653,07	17,18	0,10	24,84
P3B-12-001	71,18	9,12	78,16	1,60	10,54	429,00	741,49	15,18	0,10	8,53
P3B-12-001	71,57	9,44	84,00	1,76	10,98	430,00	765,24	16,03	0,10	7,16
P3B-12-001	72,00	11,43	97,08	1,74	13,12	429,00	739,77	13,26	0,11	6,41
P3B-12-001	72,34	9,27	84,61	1,62	11,36	430,00	745,07	14,27	0,10	8,65
P3B-12-001	72,75	9,51	84,50	1,64	11,39	430,00	742,07	14,40	0,10	5,07
P3B-12-001	73,16	7,17	67,24	1,86	8,70	430,00	772,78	21,38	0,10	7,66
P3B-12-001	73,55	8,90	81,62	1,98	11,08	428,00	736,64	17,87	0,10	7,55
P3B-12-001	73,90	8,85	76,66	1,70	10,08	427,00	760,52	16,87	0,10	12,27
P3B-12-001	74,34	8,28	76,43	1,56	10,05	430,00	760,80	15,53	0,10	14,57
P3B-12-001	74,71	7,95	65,39	1,73	8,26	429,00	791,55	20,94	0,11	11,82
P3B-12-001	75,08	7,00	69,13	1,81	8,85	427,00	781,57	20,46	0,09	7,39
P3B-12-001	75,48	5,20	62,06	1,53	8,11	427,00	765,32	18,87	0,08	15,80
P3B-12-001	75,86	6,21	74,05	1,49	9,53	427,00	776,78	15,63	0,08	10,36
P3B-12-001	76,27	5,56	77,45	1,57	9,40	430,00	824,02	16,70	0,07	6,35
P3B-12-001	76,62	5,93	73,50	0,92	10,74	426,00	684,23	8,56	0,07	4,06
P3B-12-001	76,87	1,41	15,12	1,69	2,41	429,00	626,61	70,04	0,09	75,72
P3B-12-001	77,27	3,27	60,38	1,50	7,60	430,00	794,06	19,73	0,05	23,50
P3B-12-001	77,62	4,03	48,09	1,38	5,95	429,00	807,96	23,19	0,08	30,10
P3B-12-001	78,00	4,30	49,09	1,41	6,48	426,00	757,44	21,76	0,08	18,84
P3B-12-001	78,42	3,08	46,25	1,44	5,96	428,00	776,27	24,17	0,06	42,75
P3B-12-001	78,83	2,68	48,68	1,59	6,55	424,00	742,75	24,26	0,05	10,79
P3B-12-001	87,47	1,05	8,70	1,49	2,04	432,00	426,89	73,11	0,11	5,96
P3B-12-001	87,87	6,58	91,88	2,30	12,32	433,00	746,02	18,67	0,07	1,92
P3B-12-001	88,26	11,62	163,00	2,76	22,86	433,00	713,13	12,08	0,07	2,06
P3B-12-001	88,61	9,94	136,48	3,05	18,79	436,00	726,23	16,23	0,07	5,24
P3B-12-001	89,00	12,23	181,32	3,12	25,32	431,00	716,14	12,32	0,06	2,95
P3B-12-001	89,41	11,88	166,98	3,16	22,55	434,00	740,45	14,01	0,07	2,96
P3B-12-001	89,81	8,11	80,18	1,69	11,77	428,00	681,17	14,36	0,09	4,69
P3B-12-001	90,15	5,89	59,78	1,65	8,92	427,00	670,03	18,49	0,09	4,65
P3B-12-001	90,58	7,42	63,70	1,48	9,15	429,00	695,95	16,17	0,10	3,09
P3B-12-001	90,88	8,78	55,99	1,40	8,56	426,00	654,01	16,35	0,14	3,94
P3B-12-001	91,14	7,96	45,41	2,05	6,90	427,00	658,02	29,71	0,15	27,58
P3B-12-001	91,42	7,55	44,22	1,90	5,59	423,00	791,62	34,01	0,15	30,03
P3B-12-001	91,81	6,43	45,19	1,35	6,28	424,00	719,93	21,51	0,12	10,40
P3B-12-001	92,21	5,47	35,63	1,61	5,04	421,00	706,38	31,92	0,13	16,63
P3B-12-001	92,60	3,55	15,11	1,21	3,13	422,00	483,37	38,71	0,19	22,24
P3B-12-001	93,00	3,46	24,88	0,68	4,23	416,00	588,32	16,08	0,12	1,46

P3B-12-043	11,21	2,32	0,93	1,65	0,50	429	187,50	332,66	0,71	NA
P3B-12-043	11,61	3,88	35,52	1,79	4,91	432	723,42	36,46	0,10	NA
P3B-12-043	12,00	10,09	88,63	2,84	12,60	430	703,41	22,54	0,10	NA
P3B-12-043	12,41	9,11	85,74	2,38	12,40	432	691,45	19,19	0,10	NA
P3B-12-043	12,81	10,90	101,96	2,32	14,60	429	698,36	15,89	0,10	NA
P3B-12-043	13,22	11,07	85,03	2,45	11,60	427	733,02	21,12	0,12	NA
P3B-12-043	13,57	9,05	74,02	1,91	8,94	429	827,96	21,36	0,11	NA
P3B-12-043	14,02	11,05	91,34	2,45	11,75	431	777,36	20,85	0,11	NA
P3B-12-043	14,42	10,40	98,65	2,34	10,40	432	948,56	22,50	0,10	NA
P3B-12-043	14,82	10,56	94,98	2,25	12,30	433	772,20	18,29	0,10	NA
P3B-12-043	15,20	9,81	88,96	2,47	10,20	432	872,16	24,22	0,10	NA
P3B-12-043	15,60	6,99	61,20	1,93	7,91	425	773,70	24,40	0,10	NA
P3B-12-043	16,00	10,49	90,65	2,35	10,75	431	843,26	21,86	0,10	NA
P3B-12-043	16,42	10,54	83,15	2,05	9,69	430	858,10	21,16	0,11	NA
P3B-12-043	16,80	7,35	65,73	2,21	6,42	430	-	34,42	0,10	NA
P3B-12-043	17,22	7,12	70,04	2,44	6,60	432	-	36,97	0,09	NA
P3B-12-043	17,61	7,80	72,12	2,13	8,03	429	898,47	26,54	0,10	NA
P3B-12-043	17,96	8,92	78,67	2,58	8,51	430	924,44	30,32	0,10	NA
P3B-12-043	18,31	7,98	86,72	2,49	8,45	427	-	29,47	0,08	NA
P3B-12-043	18,68	6,48	67,13	2,24	7,78	428	862,85	28,79	0,09	NA
P3B-12-043	19,08	6,45	46,33	2,09	5,92	429	782,60	35,30	0,12	NA
P3B-12-043	19,50	4,41	53,07	3,01	6,17	429	860,13	48,78	0,08	NA
P3B-12-043	19,91	5,94	51,35	2,65	5,78	430	888,41	45,85	0,10	NA
P3B-12-043	28,70	3,04	4,33	1,48	1,72	427	251,74	86,05	0,41	NA
P3B-12-043	29,14	7,81	116,84	2,48	9,75	435	-	25,44	0,06	NA
P3B-12-043	29,55	10,87	122,77	2,64	18,30	434	670,87	14,43	0,08	NA
P3B-12-043	29,93	10,69	119,34	2,74	18,00	429	663,00	15,22	0,08	NA
P3B-12-043	30,34	10,30	129,82	2,21	18,80	431	690,53	11,76	0,07	NA
P3B-12-043	30,74	8,29	98,04	2,60	14,50	430	676,14	17,93	0,08	NA

P3B-12-043	31,15	9,49	65,83	2,32	8,23	431	799,88	28,19	0,13	NA
P3B-12-043	31,50	9,03	63,18	2,87	8,76	430	721,23	32,76	0,13	NA
P3B-12-043	31,87	9,17	50,25	2,64	7,31	426	687,41	36,11	0,15	NA
P3B-12-043	32,24	9,63	29,42	2,92	4,73	426	621,99	61,73	0,25	NA
P3B-12-043	32,61	9,42	35,77	2,96	5,73	430	624,26	51,66	0,21	NA
P3B-12-047	10,02	4,02	17,94	1,80	3,67	427	489,23	49,09	0,18	NA
P3B-12-047	10,42	9,04	86,30	2,61	13,29	435	649,26	19,64	0,09	NA
P3B-12-047	10,82	10,03	95,78	2,32	14,14	431	677,37	16,41	0,09	NA
P3B-12-047	11,25	10,00	81,38	2,84	12,88	431	631,88	22,05	0,11	NA
P3B-12-047	11,66	8,90	77,40	2,21	10,60	436	730,53	20,86	0,10	NA
P3B-12-047	12,05	5,72	53,08	2,35	7,37	430	720,22	31,89	0,10	NA
P3B-12-047	12,45	11,11	92,86	2,61	10,82	431	858,23	24,12	0,11	NA
P3B-12-047	12,86	10,65	94,12	2,54	11,60	431	811,31	21,89	0,10	NA
P3B-12-047	13,27	11,06	95,61	2,39	11,67	434	819,07	20,47	0,10	NA
P3B-12-047	13,68	10,38	74,43	2,17	9,71	431	766,21	22,34	0,12	NA
P3B-12-047	14,05	9,79	76,24	2,03	9,72	432	784,77	20,90	0,11	NA
P3B-12-047	14,40	8,08	80,03	2,24	9,81	433	815,88	22,84	0,09	NA
P3B-12-047	14,79	7,45	75,02	2,25	8,60	431	872,02	26,15	0,09	NA
P3B-12-047	15,21	8,63	60,01	2,45	8,13	433	738,31	30,14	0,13	NA
P3B-12-047	15,58	8,84	70,88	2,92	9,07	436	781,13	32,18	0,11	NA
P3B-12-047	15,96	7,13	73,62	2,34	8,88	429	829,43	26,36	0,09	NA
P3B-12-047	16,34	6,92	81,67	2,64	9,41	435	868,28	28,07	0,08	NA
P3B-12-047	16,76	5,41	54,10	2,26	6,81	430	794,07	33,17	0,09	NA
P3B-12-047	17,16	5,73	64,06	2,07	8,81	428	726,88	23,49	0,08	NA
P3B-12-047	17,49	6,09	40,17	2,41	5,58	431	720,54	43,23	0,13	NA
P3B-12-047	17,90	2,73	36,79	0,65	5,30	423	694,15	12,26	0,07	NA
P3B-12-047	26,59	0,36	2,03	0,17	0,86	430	237,43	19,88	0,15	NA
P3B-12-047	26,94	5,26	91,01	0,33	12,60	426	722,30	2,62	0,05	NA
P3B-12-047	27,35	8,40	167,56	0,51	21,85	428	766,86	2,33	0,05	

										NA
P3B-12-047	27,77	7,19	124,95	0,49	17,60	425	709,94	2,78	0,05	NA
P3B-12-047	28,15	7,54	154,20	0,73	21,40	424	720,56	3,41	0,05	NA
P3B-12-047	28,53	7,16	146,60	1,93	19,20	425	763,54	10,05	0,05	NA
P3B-12-047	28,88	4,58	74,96	0,75	10,75	424	697,30	6,98	0,06	NA
P3B-12-047	29,20	4,37	62,68	0,30	8,89	423	705,06	3,37	0,07	NA
P3B-12-047	29,56	4,79	52,71	0,19	7,03	423	749,79	2,70	0,08	NA
P3B-12-047	29,90	5,80	32,63	0,42	5,35	421	609,91	7,85	0,15	NA
P3B-12-047	30,29	3,35	26,55	4,25	6,04	422	439,93	70,42	0,11	NA
P3B-12-047	30,66	4,93	34,60	0,32	5,68	420	609,15	5,63	0,12	NA
P3B-12-047	31,06	4,08	34,45	0,26	5,98	418	576,09	4,35	0,11	NA
P3B-12-047	31,42	3,56	26,59	0,37	5,14	415	517,32	7,20	0,12	NA

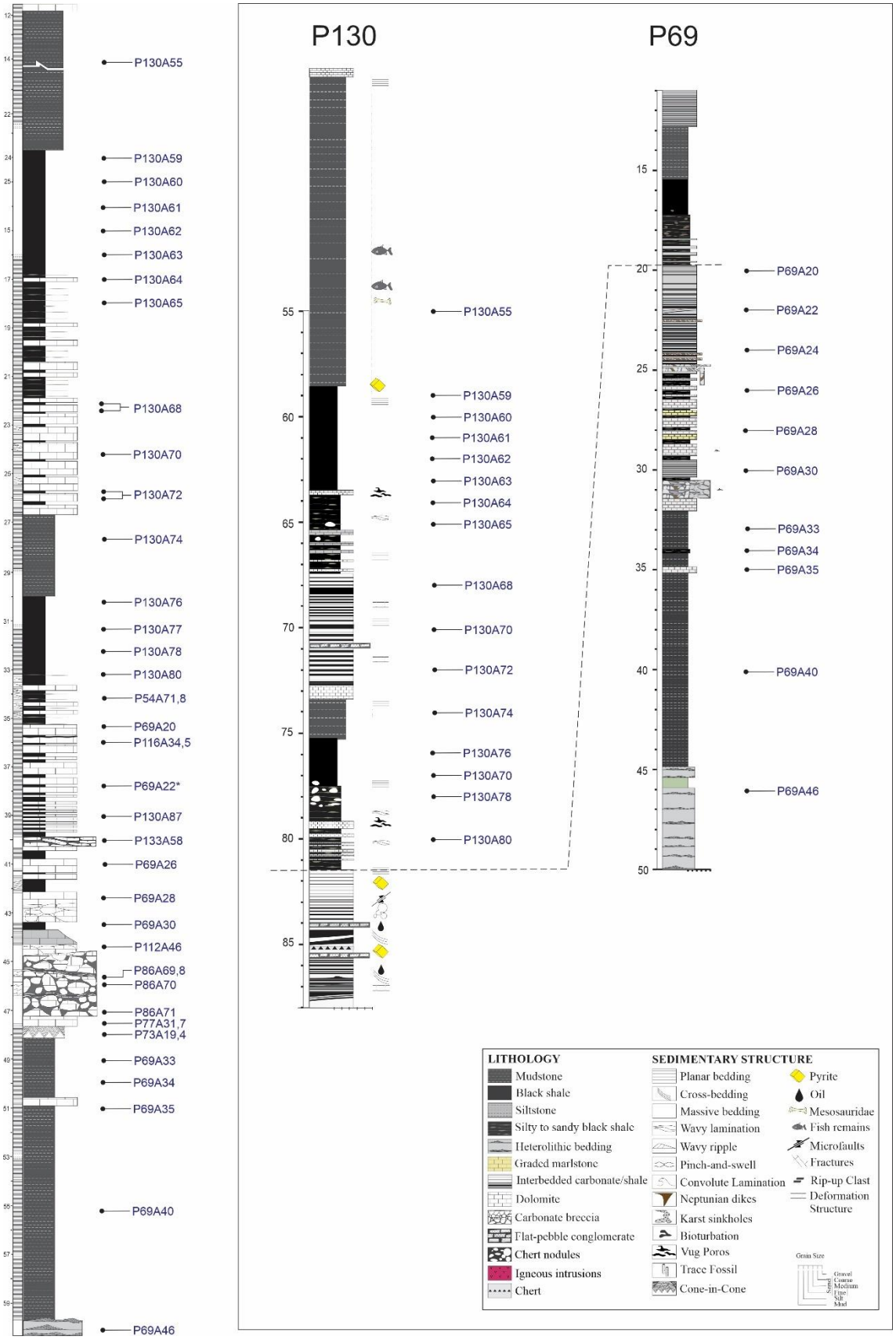

Figure 01. The stratigraphic position of the samples analyzed using XRD and SEM/EDS.

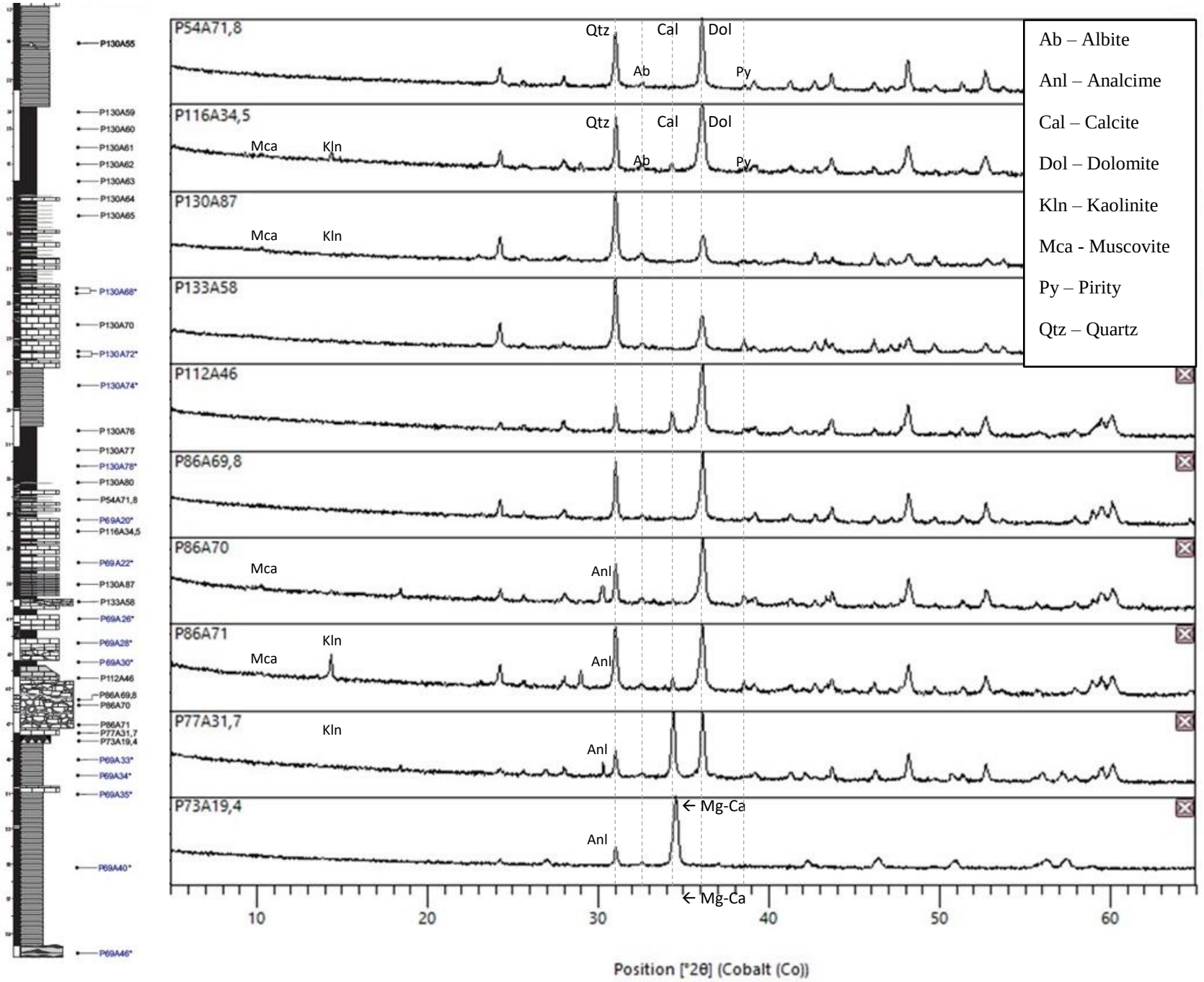

Figure 02. Difference in the mineralogical composition of the studied mixed succession.

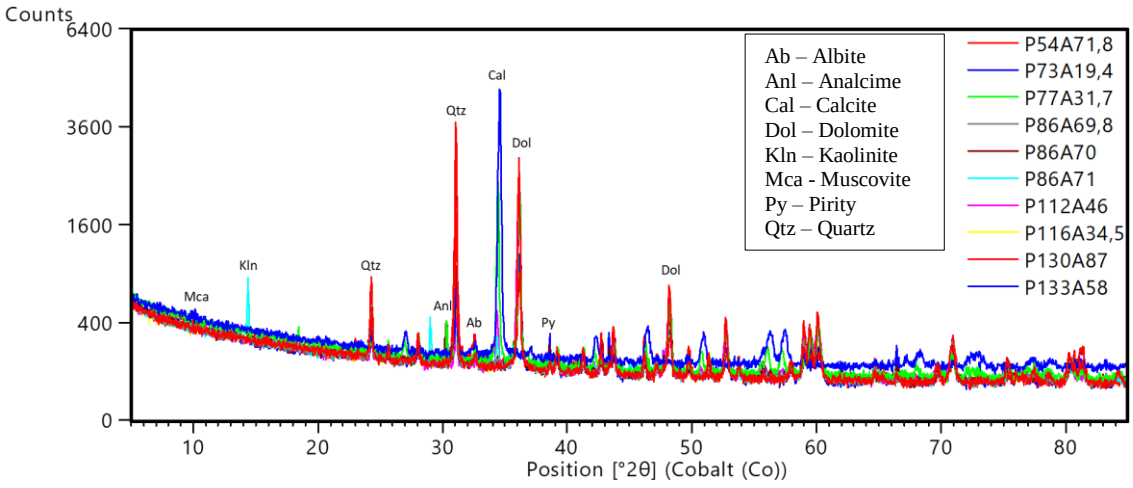

Figure 03. Mineralogical composition of the main analyzed samples.

UNIVERSIDADE FEDERAL DO PARÁ
INSTITUTO DE GEOCIÊNCIAS
PROGRAMA DE PÓS-GRADUAÇÃO EM GEOLOGIA E GEOQUÍMICA

PARECER

Sobre a Defesa Pública da Tese de Doutorado de AILTON DA SILVA BRITO

A banca examinadora da Tese de Doutorado de **AILTON DA SILVA BRITO** orientando do Prof. Dr. **Afonso César Rodrigues Nogueira** (**UFPA**), composta pelos professores doutores **Juliana Charão Marques** (**UFRGS**), **Alexandre de Andrade Ferreira** (**CENPES/PETROBRAS**), **Joelson Limas Soares (UFPA)** e **José Augusto Martins Corrêa** (**UFPA)**, após apresentação da sua tese intitulada "**RECONSTITUIÇÃO PALEOAMBIENTAL E POTENCIAL PETROLÍFERO DA SUCESSÃO SILICICLÁSTICA-CARBONÁTICA PERMIANA DA BACIA DO PARANÁ**", emite o seguinte parecer:

O candidato realizou sua apresentação de modo claro e bem organizado, dentro do tempo estipulado. Na arguição mostrou domínio da temática abordada e respondeu às perguntas formuladas pela banca. A banca destaca que o volume e a qualidade dos dados obtidos são uma importante contribuição para a geologia da Bacia do Paraná, em especial da Formação Irati. Por outro lado, merecem uma atenção os seguintes pontos: revisão da descrição dos métodos aplicados na geoquímica orgânica, melhor detalhamento da geoestatística, revisão das fácies, da ordem e do tempo de duração dos ciclos.

De modo geral, o trabalho caracteriza-se pelo elevado detalhamento, volume e qualidade de dados geoquímicos, estratigráficos e petrográficos obtidos.

Finalmente, a banca examinadora decidiu por unanimidade aprovar a tese de doutorado.

Belém, 15 de fevereiro de 2022.

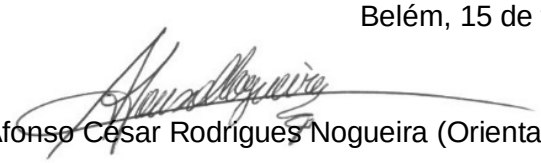

Prof. Dr. Afonso César Rodrigues Nogueira (Orientador – UFPA)

Prof.ª Dr.ª Juliana Charão Marques (UFRGS)

Prof. Dr. Alexandre de Andrade Ferreira (PETROBRAS)

Prof. Dr. Joelson Lima Soares (Membro-UFPA)

Prof. Dr. José Augusto Martins Corrêa (Membro-UFPA)